A VERTICAL AXIS WIND TURBINE GENERATOR BASED ON THE TANGENTIAL WALL - JET ACTION

BY

GURUGE ELMO LAKSHMAN PERERA MSc (Hons)

A Thesis Submitted To The Council For National Academic Awards In Partial Fulfilment Of The Requirements For The Award Of Doctor Of Philosophy.

DEPARTMENT OF MECHANICAL AND PRODUCTION ENGINEERING,
THE POLYTECHNIC,
HUDDERSFIELD.

IN COLLABORATION WITH,
THE CENTRAL ELECTRICITY RESEARCH LABORATORIES OF CEGB,
LEATHERHEAD.

MAY 1988

A VERTICAL AXIS WIND TURBINE GENERATOR BASED ON THE TANGENTIAL WALL-JET ACTION

ABSTRACT

G E L Perera

Introduction of a tangential wall-jet at an appropriate location on an octagonal cylinder results in a high lift force. Theoretical investigation is undertaken;

(i) To determine the aerodynamic lift and drag due to the boundary layer modification caused by the tangential wall-jet.

(ii) To evaluate the power out-put of a vertical axis wind turbine generator working on the aerodynamic lift due to the tangential wall-jet.

Mathematical analysis for two types of two-dimensional models have been developed to represent the flow conditions due to the tangential wall-jet. The flow is divided into "Main Flow" and a "Boundary Layer Flow". Stream lines representing the "Main Flow" around the octagonal cylinder have been plotted for evaluating the two mathematical models and for studying the flow conditions created by the tangential wall-jets.

The "Main Flow" is determined by the potential flow theory and is corrected for the 'circulation' by a super-position technique, making use of the experimental values of the lift coefficient. Both the laminar and the turbulent flow conditions have been considered within the "Boundary Layer Flow". Momentum Integral equation has been used to determine both the laminar and the turbulent boundary layer development and surface shear stress for correcting the measured pressure components of the lift and the drag coefficients.

The instantaneous net power generated by the octagonal cylinder is integrated to determine the power out-put of the wind turbine generator. Power required for the formation of the wall-jets and the effect of the jet height on the jet-momentum coefficient are also estab-lished.

The possibility of pressure recovery within the region enclosed by the orbiting cylinders of the wind machine results in a modification of the flow stream tube of the air flow past the machine. A modified Betz limit is derived by allowing for the pressure variation associated with a given shape of the stream tube.

Wind tunnel tests have been carried out on a stationary octagonal cylinder subjected to tangential wall-jet for the measurement of static pressure distribution on the surface. The pressure components of the lift and the drag forces are evaluated. The circulation due to the tangential wall-jet is calculated from the magnitude of the pressure component of the lift forces assuming the validity of the Joukovski's theorem. A wind tunnel model of the proposed wind machine was fabricated and the feasibility of the application of the lift generated by tangential wall-jet is established.

ACKNOWLEDGEMENT

I Would like to express my gratitude to all those who gave me guidance and assistance during the completion of this thesis.

I am especially indebted to Dr. H V Rao, Director of studies, for his invaluable advice and the patient professional attention which he has given me unstintingly over the years, and for supervising me and providing active encouragement towards completion of my work.

My thanks are also due to my supervisors Professor J Patterson from the Department of Mechanical Engineering of Huddersfield Polytechnic and to Dr. J F Ainslie of Central Electricity Research Laboratories of CEGB, for their professional advice and encouragement. Specially to Dr. J F Ainslie for making arrangements on my behalf for wind tunnel studies at Central Electricity Research Laboratories, Leatherhead. I also wish to acknowledge the advice and help rendered by Mr. Ken Richards and many others in CERL, Leatherhead.

I am also grateful to Dr. W Weston Head of the Department of Mechanical Engineering and to Dr. A Allsopp former Acting Head of the Department of Mechanical Engineering for further encouragement and support for the work.

I am also grateful to the Academic Support Group (Computing) of the Polytechnic, specially to Mr. Dave Richards and Mr. Peter Dewell for their unreserved help, and to Mr. Garry Cook of computer operations for his excellent work in physical preparation of the computer graphics.

I am very grateful to all the technicians of the Department of Mechanical Engineering for their excellent work in physical preparation of Test Rigs specially to Mr. W Bickerstaff, Mr. P Norman, Mr. M Quarmby, Mr. E Nield and Mr. B Smith and to the former technician Mr. P Knowels for their unreserved practical help over the years.

Finally I am grateful to my parents and to my wife for their sustained encouragement and interest through out the research work.

DECLARATION

Whilst registered as a candidate for the degree for which the submission is hereby made, I have not been a registered candidate for another award of the CNAA or of any other degree awarding body. No material contained within this thesis has been used in any other submission for an academic award.

TABLE OF CONTENTS

		Page
LIST OF TABLES		
LIST OF FIGURES		
ACKNOWLEDGMENT		
DECLARATION		
ABSTRACT		
NOMENCLATURE		i-iv
INTRODUCTION		1
CHAPTER 1	**LITERATURE SURVEY**	
1.1	Introduction	8
1.2	Vertical Axis Wind Turbine Generators	8
1.3	Different Wind Power Generator Concepts	12
1.4.1	Madaras Rotor Concept	14
1.4.2	Background Theory to the Magnus Effect	15
1.5.1	Previous Work on the Tangential Wall-jet Principle	16
1.5.2	Aerodynamic Forces Due to the Tangential Wall-jet	22
1.6	Numerical Methods for the Determination of the Flow Past Symmetrical Bluff Bodies	28
1.7	Numerical Methods for the Determination of the Aerodynamic Lift Due to the Tangential Wall-jet	34
1.8	Aerodynamic Theory of Wind Turbine Generators	38

CHAPTER 2 THEORETICAL ANALYSIS - POWER OF A VERTICAL AXIS WIND TURBINE GENERATOR DUE TO AERODYNAMIC LIFT ON ORBITING CYLINDERS

2.1 Background 40

2.2 Instantaneous Power Generated in Madaras Concept 41

2.3 Instantaneous Power Generated by the Aerodynamic Forces Utilising Wall-jet effect on Octagonal Cylinder 45

2.4 Switch-over Angles for a Wind Turbine Generator Working on Aerodynamic Lift 48

2.5.1 Tangential Wall-jet Principle for the Madaras Rotor Concept 52

2.5.2 Comparison of Theoretical C_p of the Madaras Rotor Concept with Concept of Wall-jets 55

2.6.1 The Concept of a New Vertical Axis Wind Turbine Generator 56

2.6.2 The Octagonal Cylinder Wind Machine 57

2.6.3 Number of Wall-jets, End Plate Diameter Ratio and Aspect Ratio 60

2.6.4 Calculation of the Momentum Coefficient and the Power Required for Air Supply to the Nozzle 62

2.7 Maximum Possible Power Coefficient of a Wind Turbine Generator 65

2.7.1 Betz-type Limit for Coefficient of Performance Allowing for the Pressure Variation - The Flow Model 66

2.7.2 The Coefficient of Performance 68

2.7.3 The Effect of Pressure Variation 69

CHAPTER 3 THEORETICAL ANALYSIS - FLUID FLOW PAST AN OCTAGONAL CYLINDER WITH TANGENTIAL WALL-JETS

3.1	Basic Principle of High Lift Generation Due to the Modified Boundary Layer	79
3.2	Mathematical Models for Fluid Flow	80
3.2.1	Two-dimensional Model with an Octagonal Cross-section with a Wall-jet and a Location of Air Withdrawal (Model-1)	85
3.2.2	Two-dimensional Model with an Octagonal Cross Section with a Wall-jet (Model-2)	87
3.3.1	Boundary Layer Flow and the Main Flow	93
3.3.2	Differential Equations for Stream Function	94
3.4.1	Boundary Conditions for the Model-1	95
3.4.2	Approximations in prescribing the boundary conditions on contours for the Model-1	97
3.4.3	Computation of the Coordinates of Nodal Points and Evaluation of the Stream Function at the Nodal Points for the Model-1	98
3.5.1	Computation of the coordinates of the nodal points and evaluation of the stream at the Nodal Points for the Model-2	100
3.5.2	Approximations Prescribing the Boundary Conditions on the Contours, for the Model-2	104

3.6.1 Use of the NAG D03EAF routine for slip stream velocities and stream functions 105

3.6.2 Determination of the Stream Function Using the NAG D03EAF Routine 106

3.6.3 Accuracy of the NAG D03EAF and Selection of the Segment Points 107

3.6.4 Slip Stream Velocities on the Octagonal Cylinder with a Tangential Wall-jet 108

3.6.5 Computer Time for Determining the Stream Function of the "Main Flow" 110

3.6.6 Stream Lines Around the Octagonal Cylinder 111

3.6.7 Comparison of the Fluid Flow Model-1 and Model-2 116

3.6.8 Circulation Due to the Boundary Layer Modification 123

3.7 Boundary Layer Flow 126

3.7.1 Governing Equations for the Laminar Boundary Layer 129

3.7.2 Basic Assumptions Made for the Laminar Flow 132

3.7.3 Boundary Layer Flow in the Presence of Pressure Gradient 134

3.7.4 Initial conditions for the Integration of Momentum Integral Equation 143

3.7.5 Method of Solution for the Laminar Boundary Layer 147

3.7.6 Evaluation of Λ for Given K 153

3.8.1 Turbulent Boundary Layer 157

3.8.2 Momentum Integral Equation for the Determination of the Turbulent Boundary Layer 158

3.8.3 Preliminary Investigation of the effect on the dV/dX of the Turbulent Boundary Layer Growth 161

3.8.4 Evaluation of the Non-dimensional Surface Shear Stress Based on the Parabolic Velocity Profile within the Laminar Sub-layer 166

3.8.5 Typical Behaviour of Turbulent Boundary layer Growth 169

3.8.6 Computation of the Surface Shear Stress for the Laminar and Turbulent Boundary Layer 177

3.8.7 Lift and Drag Coefficients 179

CHAPTER 4 EXPERIMENTAL STUDIES - AERODYNAMIC LIFT DUE TO WALL-JET ARRANGEMENT FOR WALL-JETS ORBITING OCTAGONAL CYLINDERS

4.1 Aim and Programme of the Experimental Work 185

4.2.1 Details of Wind Tunnels and Compressed Air Supply Used in the Experimental Work 186

4.2.2 Major Measuring and Recording Instruments Used in the Experimental Work 188

4.3.1 Exploratory Wind Tunnel Studies with the NACA 0018 Aerofoil 189

4.3.2 Investigation of Lift and Drag for the Octagonal Cylinder in the Presence of Wall-jet 191

4.3.3 The Jet Momentum Coefficient and the Jet Mean Velocity 200

4.4.1 Feasibility of the Engineering Application of the Tangential Wall-jets principle - Axial Rotary Valve 201

4.4.2 Octagonal Cylinders for the Model 202

4.4.3 Air Supply and Switch-on and off Jets. 203

4.4.4 Arrangement of the Bearing Between the Outer Shaft and the Inner Shaft 204

4.4.5 Wind Tunnel Tests on the Model 204

CHAPTER 5 RESULTS AND CONCLUSIONS

5.1 Pressure Components of Lift and Drag Coefficients 215

5.2 Lift and Drag Coefficients 216

5.3 Effective Circulation 218

5.4 Stream Lines for the Main Flow 220

5.5 Coefficient of Performance for the Proposed Wind Turbine Generator 229

5.6 Major Parameters for a Three Bladed 100 kW Machine 230

5.7 Conclusions 236

REFERENCES 240

APPENDICES

		Page
Appendix 1A	Lift and Drag Coefficients Due to Magnus Effect (Extract from Ref 13)	1-1
Appendix 2A	Lift and Drag Forces Due to Magnus Effect	2-1
Appendix 2B	Lift and Drag Forces Due to Tangential Wall-jet and the Power Required to Form the Jet	2-5
Appendix 3A	Non-dimensional Conversions Used in the Document	3-1
Appendix 3B	Determination of the Boundary Conditions at the Jet Entrance	3-2
Appendix 3C	Slip Stream Velocities at the Contour C2	3-6
Appendix 3D	Momentum Integral Equation With $(\partial\phi/\partial y)_\delta = UR/\delta$	3-8
Appendix 3E	Initial Values of Z and (dZ/dX) at the Stagnation Point	3-12
Appendix 3F	Initial Conditions for the Stagnation Point for $R \neq 0$	3-16
Appendix 3G	Initial Conditions for the Leading Edge	3-23
Appendix 3H	Momentum Integral Equation for the Turbulent Boundary Layer	3-25
Appendix 3I	Parabolic Velocity Profile for the Laminar Sub-layer	3-29
Appendix 3J	Turbulent Boundary Layer Thickness and the dV/dX	3-34
Appendix 3K	A Solution for the Flow Around a Circular Cylinder Using the NAG DO3EAF Routine	3-38

Appendix 3L	Set of Typical Values of the Slip Velocities Around the Octagonal Cylinder	3-40
Appendix 4A	Major Measuring and Recording Instruments Used for the Wind Tunnel Tests	4-1
Appendix 5A	Flow Chart of the Computer Programmes and the FORTRAN Computer Programme PART4N	5-1
Appendix 5B	Main Flow Chart and the FORTRAN Computer Programme STTUR1	5-19
Appendix 5C	FORTRAN Computer Programme CLCDT	5-29
Appendix 5D	FORTRAN Computer Programme POWERG1	5-34
Appendix 5E	FORTRAN Computer Programme GRID1	5-38
Appendix 5F	FORTRAN Computer Programme PART2	5-42
Appendix 5G	FORTRAN Computer Programme PART3	5-46
Appendix 5H	FORTRAN Computer Programme CPMAX	5-48

LIST OF TABLES

		Page
Table 3-1	Number of Segments for the Model-1	86
Table 3-2	Number of Segments for the Model-2	92
Table 3-3	Initial Conditions -Determination of the Turbulent Boundary Layer Growth With the Laminar Sub-layer with a Parabolic Profile	171
Table 4-1	Initial Conditions for the Wind Tunnel Tests with the Octagonal Cylinder	194 195
Table 4-2	Initial Conditions and the Results for the Wind Tunnel Model of the Wind Machine	206
Table T-J1	Turbulent Boundary Layer Growth With out the Laminar Sub Layer	3-37
Table T-K1	Flow Past a Circular Cylinder	3-38
Table T-L1	Slip Velocities around a octagonal Cylinder $\theta = 45°, C_\mu = 0.4$	3-40

LIST OF FIGURES

Fig 2.1	Aerodynamic Lift Due to Tangential Wall-jet / Magnus Effect	42
Fig 2.2	Resultant Forces and Switching-over Angles	50
Fig 2.3	Change-over angle Vs Angular (Axi-al) Velocity	51
Fig 2.4	Proposed Concept of the VAWTG with Tangential Wall-jets	59
Fig 2.5	Jet Nozzle	62
Fig 2.6	Flow Model and Static Pressure Variation	72
Fig 2.7	Shape of Stream Tubes for K=0, K=0.1	73
Fig 2.8	Shape of Stream Tubes for K=0.16, K=1.0	74
Fig 2.9	$\phi - \psi$ Relationship	75
Fig 2.10	$C_p - \psi$ relationship	76
Fig 2.11	$U_{min} - K$ Relationship	77
Fig 2.12	$C_p, A_d/A_w, A_\infty/A_d$ Against K for C_p Max	78
Fig 3.1	Flow Past an Octagonal Cylinder with out a tangential wall-jet	82
Fig 3.2	Flow Past an Octagonal Cylinder with a tangential wall-jet	83
Fig 3.3	Two-dimensional Flow Model for the Flat Plate with a Tangential Wall-jet	84
Fig 3.4	Two-dimensional Flow Model for the Octagonal Cross-section with a Jet and Air Withdrawal (Model-1)	88

Fig 3.5	Two-dimensional Flow Model for the Octagonal Cross-section with a Tangential Wall-jet (Model-2) (Left-contour)	89
Fig 3.6	Two-dimensional Flow Model for an Octagonal Cross-section with a Tangential Wall-jet (Model-2) (Right Contour)	90
Fig 3.7	Segments and Nodal Points on an Octagonal Side	91
Fig 3.8	Slip Stream Velocities Around the Octagonal Cylinder	103
Fig 3.9	Shapes of the Contour C2 for Preliminary Investigation	114
Fig 3.10	Stream Lines Around the Contour C2	115
Fig 3.11	Stream Lines Around the Contour C2 Using Model-1 $C_\mu = 0.55, \theta = 125°$	118
Fig 3.12	Stream Lines Around the Contour C2 Using Model-2 $C_\mu = 0.25, \theta = 135°$	119
Fig 3.13	Stream Lines Around the Contour C2 Using Model-2 $C_\mu = 0.40, \theta = 135°$	120
Fig 3.14	Stream Lines Around the Contour C2 Using Model-2 $C_\mu = 0.55, \theta = 135°$	121
Fig 3.15	Stream Lines Around the Contour C2 Using Model-2 $C_\mu = 0.40, \theta = 145°$	122
Fig 3.16	Boundary Layer Flow and the Main Flow	133
Fig 3.17	Shapes of the Velocity Profiles for the Method of Pohlhausen	156
Fig 3.18	Shape Factor Vs K and the Method of Calculation of Λ	156
Fig 3.19	Prandtl's Turbulent Velocity Profile and the Laminar Sub-layer	172
Fig 3.20	Proposed Laminar Sub-Layer Profile	172

Fig 3.21	Boundary Layer Growth without the Laminar Sub-layer	173
Fig 3.22	Turbulent Boundary Layer Growth Using the Parabolic Profile for the Laminar Sub-layer dV/dX>0	174
Fig 3.23	Turbulent Boundary Layer Growth Using the Parabolic Profile for the Laminar Sub-layer dV/dX<0	175
Fig 3.24	Turbulent Boundary Layer Growth Using the Parabolic Profile for the Laminar Sub-layer dV/dX=0	176
Fig 3.25	Lift and Drag Coefficients on the Contour C2 (Model-2)	184
Fig 4.1	NACA 0018 Aerofoil With a Tangential Wall-jet	196
Fig 4.2	Aerodynamic Lift Due to the Tangential Wall-jet	197
Fig 4.3	Arrangement of the Tangential Wall-jet	198
Fig 4.4	Calibration of the Pressure Gauges for Velocity Measurements	198
Fig 4.5	Octagonal Cylinder with Pressure Tappings	199
Fig 4.6	Gauge Pressure Vs Mean Jet Velocity	207
Fig 4.7	Tests on the Octagonal Cylinder with End Plates	208
Fig 4.8	Wind Tunnel Model of the VAWTG	209
Fig 4.9	Centre Column of the Wind Machine	210
Fig 4.10	Outer Shaft (Cylinder) With End Caps	211
Fig 4.11	Tangential Wall-jets - (Air Nozzles)	212
Fig 4.12	Air Distribution System	213

Fig 4.13	Centre Column and the Taper Roller Bearings	214
Fig 5.1	Effect of the Jet Angle on Lift and Drag Coefficients	221
Fig 5.2	Lift and Drag Coefficients against Jet-momentum Coefficient $Re_0 = 2.8 \times 10^4$	222
Fig 5.3	Lift and Drag Coefficients against Jet-momentum Coefficient $Re_0 = 4.3 \times 10^4$	223
Fig 5.4	Lift and Drag Coefficients against Jet-momentum Coefficient $Re_0 = 5.8 \times 10^4$	224
Fig 5.5	Lift and Drag Coefficients against Jet-momentum Coefficient $Re_0 = 7.3 \times 10^4$	225
Fig 5.6	$C_L(\mathrm{Max}), C_L(\mathrm{Max})/C_D$ against Jet Angle	226
Fig 5.7	Γ_{n-d} against $V_j/W, Nr/W$	227
Fig 5.8	Coefficient of Performance of the Proposed VAWTG	228
Fig 5.9	Stream Lines for $C_\mu = 0.25, \theta = 125°$	231
Fig 5.10	Stream Lines for $C_\mu = 0.40, \theta = 125°$	232
Fig 5.11	Stream Lines for $C_\mu = 0.55, \theta = 125°$	233
Fig 5.12	Stream Lines for $C_\mu = 0.40, \theta = 135°$	234
Fig 5.13	Stream Lines for $C_\mu = 0.55, \theta = 145°$	235
Fig 1A.1	Lift and the Drag Coefficients Due to the Magnus Effect (Extract from Ref 13)	1-1
Fig 2A.1	Magnus Effect	2-1
Fig 2B.1	Cylinder With a Tangential jet	2-6
Fig 3B.1	Velocity Profile at the Jet Entrance	3-2

NOMENCLATURE

A	Cross-sectional area of the stream tube (m^2)
b	Height of the jet (m)
B	Number of cylinders / Blades
C_μ	Jet Momentum Coefficient defined as $\frac{1}{2}\frac{b}{r}\frac{V^2}{W_r}$
C_P	Performance Coefficient defined as $\frac{P}{\rho H R W^2}$
C_L	Lift Coefficient
C_D	Drag Coefficient
D	Modelled Infinity (n-d)
F_x	x Component of the resultant force (n-d)
F_y	y Component of the resultant force (n-d)
f	Friction Factor (n-d)
F	External force on the fluid within the controlled volume defined by the stream tube
Fj_{xn}	X component of the force due to the jet momentum (3.8-24)
Fj_{xn}	Y component of the force due to the jet momentum (3.8-25)
H	Height of the cylinder (m)
J	Defined in the equation 3.7-25
K	Mean pressure variation coefficient (Chapter 2)
K	Defined in equation 3.7-40 (Chapter 3)
K_n	Pressure variation coefficient for upstream of the actuator disc (Chapter 2)
K_{do}	Pressure variation coefficient for the down stream of the actuator disc
k_a	Gas constant of air

L_x, L_{xn}	X Component of the lift force due to the tangential wall jet / Magnus effect (n-d)
L_y, L_{xn}	Y Component of the lift force due to the tangential wall jet / Magnus effect (n-d)
l	Length of the octagonal side (m)
$\dot{m}$	Mass flow rate of air through the stream tube
N_r	Defined in equation 2.2-8
N	Radian angular velocity of VAWTG
n	Non-dimensional distance measured normal to the octagonal surface
P	Static pressure $\left(N/m^2\right)$
P'	Instantaneous power (n-d)
P_ω	Dissipated power due to the viscous action (n-d)
P'_{net}	Net Power produced by the VAWTG / Madaras Rotor Concept
P_∞	Atmospheric pressure $\left(N/m^2\right)$
Q	Defined in equation 3.7-24
r	Circumferential radius of the octagonal cylinder (m)
R	Radius of the orbit (m)
R	Defined in equation 3.7-27
Re	Reynolds number (See Appendix 3A)
Re_o	Reynolds number (See Appendix 3A)
s	Solidity ratio
s	Distance measured along the surface in the down stream direction
S	$\equiv s/l$
T_a	Atmospheric air temperature (K)

t	Non-dimensional jet height used in the equation 2.6-1
U	Velocity at the edge of the boundary layer (m/s)
U_j	Jet air velocity (m/s)
V_x	x component of the non-dimensional free stream velocity
V_y	y component of the non-dimensional free stream velocity
V_j	Wall-jet air velocity (n-d)
V_m	Maximum value of V
V	Velocity of air used in the C_p analysis
$\overline{V}$	Mean value of V_j
W	Wind velocity (m/s)
W_r	Wind velocity relative to the orbiting cylinder / blade
x	Co-ordinates in the x- direction
X	$\equiv \frac{x}{l}$
y	Co-ordinates in the y- direction
Y	$\equiv \frac{y}{l}$
Z	Defined in equation 3.7-31
$i, \hat{j}, \hat{k}$	Unit Vectors as defined in section 2.3
α	$\equiv (4-K)/(2-K)$ in section 2.7.1
α	Defined in equation 3.8-7 (Chapter 3)
β	$\equiv (K)/(2-K)$ in section 2.7.1
β	Defined in equation 3.8-5 (Chapter 3)
Γ	Effective circulation $\left(m^2/s\right)$
Γ_{n-d}	Non-dimensional Effective circulation (See Appendix 3A)

δ	boundary layer thickness (m)
δ^*	Displacement thickness
Δ	Non-dimensional boundary layer thickness
η	Defined as y/δ in Chapter 3
η_E	Nozzle isentropic expansion efficiency
θ	Momentum thickness
θ, θ_j	Angle between the jet axis and the free stream velocity
Λ	Shape factor defined by the equation 3.7-21
μ	Viscosity of air $(kg/m \cdot s)$
ρ	Density of air $\left(kg/m^3\right)$
ν	Kinematic viscosity $\left(m^2/s\right)$
σ	Solidity Ratio
τ	Surface shear stress $\left(N/m^2\right)$
τ_{n-d}	Non-dimensional surface shear stress
ϕ	Stream function $\left(m^2/s\right)$
ϕ	In section 2.7.1 defined as V_ω/V_∞
Φ	Non-dimensional stream function
ψ	in Section 2.7.1 defined as V_d/V_∞
ω, ω_z	Axial rotational speed (rad/sec)
Ω, Ω_z	Orbital speed (rad/sec)

INTRODUCTION

Motivation

It is estimated that there is a technical potential for generation of power around 45 Twh/year from land-based wind energy conversion systems, equivalent to 17 % of current electricity demand of UK. Wind energy is considered to be the most promising renewable energy source for electricity generation. The cost of electricity generation by the use of wind power is predicted to be in the range of 2.5 to 3.2 p/kWh, by the year 2000 A.D. This figure compares very favourably with the corresponding cost of 3.0 to 4.7 p/kWh predicted for electricity generation by coal. This makes it extremely attractive to consider large scale expansion of wind power utilisation. Hence research and development activities for improving existing types of wind machines and exploring new ideas will be useful. The principle of tangential wall-jets for high lift generation, and its utilisation to a vertical axis wind turbine generator is investigated in this Thesis, for possible application to medium/ large scale wind turbine generators.

Background

Kinetic energy of natural wind may be exploited in a wind energy conversion system for generating electric power or for directly operating devices requiring mechanical work. Such systems may broadly be categorised into (i) Wind turbines operating with lift generated by aerofoil sections, (ii) Wind turbines operating with aerodynamic lift generated by the boundary layer modification.

The research and development work on the first of the above two categories has been in progress for considerable time and systems have been constructed for generating electric power with magnitudes of the order of a few hundreds of kilo-Watts. These machines where designed utilising the principles of aerodynamics achieve high efficiencies of operation. The research and development work on the second category of the devices progressed only to a limited extent. This is due to inadequate theoretical studies and practical difficulties encountered in actual operation. The Madaras Rotor Concept belongs to this category and utilises the Magnus effect created by axially rotating cylinders. Detailed studies on the Madaras Rotor Concept have shown that the theoretical advantages of the Magnus Effect are unable to find a successful application in a Wind Energy Conversion System. Boundary layer theory shows that the flow field around

an axially rotating cylinder can be simulated with an introduction of a tangential wall-jet at an appropriate location of the surface of a non-rotating cylinder. Pressure distribution around the cylinder created by the boundary layer flow modification results in an aerodynamic lift. Such a lift may successfully be utilised to a Vertical Axis Wind Turbine Generator.

Theoretical Work

In the present work theoretical investigation is undertaken for evaluating the performance of a wind machine using the wall-jet principle. This work is divided into the following two categories;

(i) Evaluation of the power out-put of the vertical axis wind turbine generator working on the aerodynamic lift due to the tangential wall-jet.

(ii) Determination of the aerodynamic lift and drag due to the boundary layer modification caused by the tangential wall-jet on an octagonal cylinder.

The work carried-out under category (i) is presented in chapter 2 of the Thesis. Here the instantaneous net power generated by the octagonal cylinder due to the aerodynamic lift is used to determine the power out-put of the wind turbine generator. Power required for the formation of the wall-jets and the effect of the non-dimensional jet height, on the momentum coefficient are also established. In the new concept of vertical

axis wind turbine generator the lift generated by the boundary layer modification due to the tangential wall-jet is aerodynamically similar to the Magnus effect. In order to compare the application of the lift generation by both of these principles the theoretical power out-put of the traditional Madaras Rotor Concept is compared with a concept having fixed cylinders with tangential wall-jets.

The proposed VAWTG has orbiting octagonal cylinders which allows for the pressure recovery within the elements of the wind machine and results in a modification of the flow stream tube of the air flow past the machine. This lead to the re-examination of the Betz limit, the traditional theoretical limit of the power coefficient. Basic assumptions of the traditional derivation, are found to be inconsistent with the steady flow energy equation for inviscid flow. Therefore, by allowing for a pressure variation and the associated shape of the stream tube through the introduction of a coefficient "K", a modified Betz limit is derived.

Lift and the drag coefficients on an octagonal cylinder due to the tangential wall-jet required for the prediction of the power out-put of the proposed wind machine are determined by considering a two-dimensional steady flow model in chapter 3. The two types of two-dimensional mathematical models have been developed to represent the flow conditions due to the tangential

wall-jet. The flow is divided into "Main Flow" and a "Boundary Layer Flow". Governing partial differential equations have been set-up and solutions have been obtained. For the evaluation of the two mathematical models and to understand the flow conditions created by the tangential wall-jets, stream lines representing the "Main Flow" around the octagonal cylinder have been plotted.

The "Main Flow" which was determined by the potential flow theory as above, was corrected for the circulation by a super-position technique making use of the experimental studies of the lift/drag coefficients. Both the laminar and the turbulent flow conditions have been considered with in the "Boundary Layer Flow". Momentum Integral equation has been used to determine both the laminar and the turbulent boundary layer development within the "Boundary Layer Flow". For the laminar flow conditions Pohlhausens approximate method has been used. The traditional 1/7 th Power Law turbulent velocity profile was modified by including a parabolic sub-layer profile which on using of the Blasius formula for pipe wall shear-stress enabled the determination of the turbulent boundary layer development.

The theoretical static pressure variation around the octagonal cylinder, determined for the "Main Flow" velocity field using the Bernoulli's equation has been

used to calculate the pressure components of the aerodynamic lift and the drag due to the tangential wall-jet. These components of lift and drag forces together with the jet momentum force at the jet entrance and the forces due to surface shear stress, obtained from the "Boundary Layer Flow" gave the Lift and the drag forces.

Experimental Work

Experimental investigation, consisting of wind tunnel studies may be divided into two parts:

(i) Measurement of the pressure components of the lift and drag forces for an octagonal cylinder subjected to tangential wall-jet.

(ii) Practical application of the aerodynamic lift due to the tangential wall-jet in a new concept of a vertical axis wind turbine generator.

Wind tunnel tests have been carried-out on a stationary octagonal cylinder having sides of the octagon measuring 42 mm and having a height of 600 mm. Static pressure distribution on the surface of the octagonal cylinder has been measured and the pressure components of the lift and the drag forces produced by the tangential wall-jet are evaluated. The circulation due to the tangential wall-jet is calculated from the experimentally determined magnitudes of the pressure

component of the lift forces for the octagonal cylinder, assuming the validity of the Joukovski's theorem.

A wind tunnel model of the proposed wind machine was fabricated. The feasibility of the engineering application of the tangential wall-jet for a wind turbine generator and the working of a rotary axial valve through which jet air supply occurs were tested.

The first part of the experimental work indicated was carried out in the wind tunnel at Huddersfield Polytechnic and the second part of the experiment was carried out in the wind tunnel at Central Electricity Research Laboratories in Leatherhead. In the first part of the work electronic data logging facilities have been used. The programme of the experimental work is fully discussed in the chapter 4 of the Thesis.

Theoretical and experimental investigation clearly indicates the potential for the use of Tangential Wall-Jet principle for a Vertical Axis Wind Turbine Generator. Prototype testing will however be required to obtain data on performance coefficients and evaluate the practical operating problems.

CHAPTER 1

1. LITERATURE SURVEY

1.1 Introduction

Conventional wind energy conversion system has been the leader in harnessing the energy from the wind. Since the discovery of the primary advantage of the Vertical Axis Wind Turbine Generator (VAWTG) design, unlike Horizontal Axis Wind Turbine Generators (HAWTG), they do not require a yaw control to turn the machine into or away from the wind, VAWTG has been regarded as a replacement to the Horizontal Axis Wind Turbine Generator. Hence considerable amount of research and development has been done on the existing, VAWTG and also into the new types of Wind Turbine Generators with the hope that from the dark-horse pack a big winner is going to emerge.

1.2 Vertical Axis Wind Turbine Generators

Among many different types of VAWTG **Darrieus concept** has drawn greater attention in research and development in the recent years (1). This by no means a new design. Almost 45 years after its patent in USA, it was rediscovered by National Research Council, Ottawa,

Canada, during the early 1970's (2). In 1974 engineers at Sandia Laboratories, Albuquerque, N.M also started work on the Darrius concept.

Its blade is shaped much like an aircraft wing with a leading edge. Therefore the aerofoil drives the blade into the wind regardless of its direction. Each Darrieus blade is curved in the symmetrical shape a rope would take if spun around a vertical axis. A major advantage of this design is the blades do not require a variable -pitch mechanism to protect them from damage in the high winds. To strike the balance between the cost and the performance, wind machines are designed to obtain power from winds with in the operational wind speeds. When the Darrieus machine exceeds the maximum that the machine is designed to operate, the propeller feathers. Because of the aerodynamic characteristics, the Darrieus blades go into a stall in high winds. But while the Darrieus machine has this positive no-pitch characteristic, it will not self start like a HAWTG. (Typical Darrieus blades will not create lift until brought upto speed) Hence in one of the latest Sandia machines, the electric generator doubles as a starter motor. The machine also delivers mechanical power to the base of the shaft allowing heavy power generating equipment to be placed and supported near to the ground line. But one of the main disadvantages is low rotational speeds

and hence costly transmissions. The predictions about the Darrieus machine is that the coefficient of performance (Cp) is as that of the HAWTG. (2).

A machine which has several advantages over a Darriues concept has been developed. This **Cyclogyro vertical axis wind turbine generator** has straight, variable pitch blades. This is a self starting machine and pitch control permits the extraction of a greater amount of power. Wind tunnel studies have indicated, at low rotational speeds Cyclogyro has better power coefficients, than the Darrieus type machines (1). The straight Cyclogyro blades are also comparably cheaper to manufacture.

Circulation-controlled vertical axis wind turbine generator has the same basic configuration as the Cyclogyro, but the rotors are designed to take advantage of a STOL (Short Take-Off and Landing) aircraft-wing design as the circulation control wing. In the concept the trailing edge is rounded instead of having the knife-edge configuration. High pressure air is blown over the trailing edge. The air adheres to the trailing edge, then shoots off sideways. In the case of an aircraft this acts like a flap, causing the air to flow down-wind, giving increased lift. The use of same configuration on vertical axis Cyclogyro rotor will both increase the torque at a given speed and

allow the turbine to operate at a lower optimum speed. Since it can operate at low speeds to create high efficiencies, it cuts-down the centrifugal forces greatly, resulting in an easy structural design. Predicted theoretical limit of the coefficient of performance was 40-50 percent, operating at about half the speed of a conventional blade horizontal axis wind turbine generator (3,4). This shows the circulation controlled machines has a high inherent coefficient of performance. The Darrieus machine, has a coefficient of performance in the range of 20 to 40 percent (1). The propeller types generally operates in the 40 to 45 range.

Another machine which may be the possible successor to the Darrieus wind turbine generator is the **Variable Geometry Vertical Axis Wind Turbine Generator.** It has been designed originally to retain all the advantages of vertical axis operation while eliminating the complex blades of the Darrieus machine, replacing them with straight, un-tapered, untwisted aerofoils. Designers of this machine also claim that this machine has a power and structural load control and the resilience to the cyclic stalling. The first prototype testing has been completed in 1976 and a coefficient of performance of 0.35 has been obtained. Since 1986 a

test and monitoring programme has been under taken by the Department of Energy, on a 25 m machine in Carmarthen Bay, South Wales, UK (5,6).

1.3 Different Wind Power Generator Concepts

Tornado wind turbine generator is a augmentor machine. Which uses the idea of getting more out of the propeller, which enables the propeller to shrunk in size, reducing costs. However, in this type of machine additional static structures are needed to increase the wind speeds to the propeller (7). Tornado concept designed by Dr. James Yen of Grunnan Aerospace Corporation, Bethpage, N. Y. predicts the power in the wind to be increased by a factor of upto 1000 (8). This system consists of a tower with operable vertical vents. The vents on the side toward the wind would open while those opposite the flow would close. As the wind blows into the tower it would spiral towards the top, creating a vortex (A miniature tornado). In the centre of this vortex is a low pressure area, which causes the outside air to be sucked in through openings around the base of the tower. As this is sucked to fill the low pressure void, it would drive rotor blades

near the bottom of the tower. One of the major draw-backs in this system is the necessity of a huge tower.

Electro Fluid Dynamic concept (EFD) is one of the most theoretically promising concepts. This wind power generator concept has no moving parts. EFD reproduce nature's way of producing a thunderstorm, causing the charged rain drops accumulating in the cloud and giving rise to an electric field and consequent discharge leading to lightning. On this basic principle EFD wind power generator has been developed. In this concept wind blows water droplets through a highly charged grids evenly causing the droplets to become charged. The wind would then blow these particles towards another charged grid. The mechanical energy of the wind does work in overcoming electro static repulsion, and the energy is translated into electric current (9,10).

As the EFD concept, **Humid Air Wind Machine** is also based on the principles of nature. About one-third of the solar energy that reaches the surface of the earth goes into evaporating the moisture. The idea of the device is to capture this energy. It is the natural-draft tower in which humid air would be brought in at the bottom. The wet air, being lighter than dry air, would rise and expand, causing its temperature to

drop. The cooling of air results in condensation of moisture and the latent heat in the humid air would be given off to the now drier air. The warmer air would have increased buoyancy and would continue to rise upto the tower, passing a wind turbine on its way out. Again the major draw back of the system has been the height of the tower. A mechanized expansion-compression cycle to boost this natural process and reduce the tower height has been considered. But the energy required for the expansion-compression machines are considerable compared with total power out-put of the concept (11).

1.4.1 Madaras Rotor Concept

Madaras rotor power plant (12,13) was originally proposed by Julius D Madaras in 1929 for generation of power on a large scale. This system utilises the Magnus Effect of rotating cylinders vertically mounted on flat cars form an endless train around a closed track and alternators geared to the wheels of each car generate the electric power. Analytical, wind tunnel and full-scale aerodynamic studies of the wind powered, Madaras concept were conducted between 1929 and 1934 (14). Since then there was little progress of the originally proposed "Madaras Concept" in the absence of

pressing need for wind energy systems owing to the then cheap fossil fuels. In 1970's a detailed study of the "Madaras Concept" was undertaken by the Dayton University Research Institute, Ohio, USA. This study indicated several practical problems in using the "Magnus Effect" especially for medium / Small scale power generation as detailed below.

(i) The complexity of using large rotating cylinders and the energy losses during angular acceleration and deceleration.

(ii) The disadvantage of additional frictional losses during the motion of the rather heavy supporting cars along the race track.

(iii) The requirement of essentially unidirectional wind for a race track configuration.

(iv) The difficulties in adjusting and controlling the operating parameters for optimum performance.

1.4.2 Background Theory to The Magnus Effect

The boundary layer theory shows that the lift force on a rotating cylinder in a fluid flow is due to the modification in the boundary layer flow resulting from the reduced difference between the velocities of the

fluid and the solid wall. Where the angular velocity of the rotating cylinder is adequate, separation is completely eliminated on that side of the cylinder where the fluid and the surface of the cylinder move in the same direction, but on the other side of the cylinder where the direction of the fluid motion is opposite to that of the solid wall, separation occurs over a considerable region, towards the trailing side. The flow pattern produced in the above situation approximates to that of the two-dimensional non-viscous fluid flow past a circular cylinder with a superimposed circulation. For such a case potential flow theory establishes the "Magnus Effect" i.e., The presence of a high lift force (15).

1.5.1 Previous Work on The Tangential Wall-Jet Principle

In the presence of a tangential wall-jet on one side of a body, reduces the pressure distribution and modifies the boundary layer separation. Use of such a boundary layer control to alter the lift and drag forces on a bluff body in an air stream goes back to the beginning of the centenary. In 1904 Prandtl demonstrated lift generation on a circular cylinder by suction on the upper surface, which was mainly due to the unsymmetri-

cal pressure distribution around the cylinder (15). Similarly the injection of fluid as a tangential jet at the upper surface of a cylinder will also create an unsymmetrical pressure distribution giving rise to the lift force. This is mainly due to the boundary layer separation delay, brought about by the energy input of the jet. The delay of the boundary layer separation has been widely used to increase the lift to drag ratio and is usually referred to as the "Circulation Control" (17).

Due to the wide practical application of this principle, the tangential wall-jet has drawn attention (4) of many researchers in the past. Such investigations on boundary layer control by blown air through narrow tangential slots dates back to 1921 (17). Since then there are many reported investigations on wall-jets in the absence of external stream, while only few considered the detailed aspects of the velocity profile and pressure distribution, in the presence of an external stream.

The work on measurements on skin friction in a plane turbulent wall-jet (18) by Sigalla refers several studies in 1930's including the work on turbulent jet expansion (19) by Forrthmann in 1934. Bradshaw (20) refers to these little known work as "Scattered Literature" on the subject. However published work by

Glauert (21) in 1956 on theoretical solution for the wall-jet was supported by the experiments of Bakke (22) in 1957 and Sigalla (23) in 1958. Further analysis of the laminar jet by Tetervin (24) has obtained results in good agreement with Glauert (21). However these works carry only little practical interest in view of the extremely low critical Reynolds numbers of the mixing layer flows. The work on turbulent wall-jets with and without an external stream by Bradshaw (20) produces some useful results. In his work Bradshaw (20) make a fair criticism on previous workers for neglecting in their calculation the shear-stress between the postulated fluid layers. Bradshaw (20) developed theoretical model including the effect of the shear-stress based on concepts of mixing lengths and eddy viscosity profile as given below;

$$\frac{\tau_0}{0.5\rho U_j^2} = 0.0315 \frac{\left(U_j \delta_j\right)^{-0.182}}{\nu}$$

$$\left(3000 < \frac{U_j \delta j}{\nu} < 15000\right)$$

Although, the theory due to Glauert (21) gives a good general description of the flow, Bradshaw (20) has achieved better results for the surface shear-stress where Glauert (21) has underestimated the shear-stress by about 25 % by using the Blasius's pipe flow formula.

Literature survey shows that the most of the work (4,20) has been concentrated on tangential wall-jet blowing over a curved surface in the absence of external stream. The attachment of the jet to the surface is the well-known "Coanda Effect". In these studies mainly the overall features of the flow had been dealt with, although there was little reference to the shear-stress distribution.

Carriere and Eichelbrennen (25) give results of mean velocity profile traverses in a jet blowing tangentially beneath the boundary layer on a wind tunnel wall and on the deflected flap of an aerofoil, and also present a step-by-step calculation method in which the profile is divided in to layers between the velocity extremum, where each layer was treated independently by empirical formulas for both the eddy viscosity and the shear-stress.

Carrriere and Eichelbrennen (25) also established theory of the flow attachment by tangential air jet discharging against a adverse pressure gradient. This work also discusses a series of (i) basic experiments and (ii) overall calculations of the boundary layer, down stream of a tangential wall-jet.

Theoretical investigation into circulation control by slot blowing, applied to a circular cylinder by Dunham (17) discusses the theory developed on the basis of

Spalding's unified boundary layer theory (17). Dunham has used this work for calculating the wall-jet momentum and velocity to delay the boundary layer separation until a specified point in a given pressure distribution. This has enabled, estimates to be made of the lift generated, on a circular cylinder with narrow tangential slots on the upper surface for boundary layer control. He also highlighted the distinction between the circulation control and the jet-flap. The circulation control uses a small amount of slot air to energize the boundary layer where the jet-flap uses as much as ten times the quantity of air forming a jet sheet to the inviscid flow as lift (17). A jet-flap generates thrust as well as lift. The calculation of two-dimensional flow field around a cylinder or aerofoil of given shape and incidence is indeterminate until the circulation around an aerofoil with a sharp trailing edge is fixed by the Kutta-Joukowski condition. In the case of a rounded trailing edge, this condition is replaced by the generalized condition, that the boundary layer on the upper surface separates at almost exactly the same pressure as does the boundary layer on the lower surface. And the circulation could be increased by delaying the separation on the upper surface. Dunham (17) has also confirmed experimentally, that the pressures at which the upper and lower surface

separation occurs remain equal, even on a circulation controlled cylinder. This provides the the link for matching the boundary layer calculations with the inviscid flow calculations. In his theoretical model Dunham has used a high Reynolds number to ensure the turbulent boundary layer separation. In this theoretical model Dunham has used a numerical step-by-step procedure for calculation of the velocity distribution within the boundary layer around the surface, including the down stream of a jet, by the method developed by Spalding (1964) , until the separation criteria was satisfied. The results of these theoretical investigation were in good agreement with their own experimental results.

Cheeseman (1966, 1967) (3,4) has proposed the application of circular controlled helicopter rotors. He devised a novel parkable rotor with blades of circular cross-section on which lift would be generated by circulation control. The scope for moving the effective rear stagnation point and hence generating lift was obviously maximized by choosing a circular cylinder, though Cheesman explained other important reasons for this choice such as reducing the gust sensitivity of the rotor in a rotating wing aircraft by using a bluff body with a blown-jet. In his work (3,4) Cheesman described the generation of the lift by the circulation control technique and results obtained by

testing of a scale model "Hingeless Rotor" (4), at the National Gas Turbine Establishment. In particular he has shown that the operating rotors at high values of thrust coefficient per blade which has lead to high induced power factors, to be used in Vertical Take-Off and Landing (VTOL) circulation control stopped rotor aircraft.

1.5.2 Aerodynamic Forces Due to Tangential Wall-jets

Furuya and Yoshino (26) have investigated the aerodynamic forces acting on a circular cylinder with tangential jet of air. This investigation was carried-out to establish the characteristics of flow surrounding a circular cylinder with tangential injection of air immersed in a uniform flow. As a result it was found, that the separation has taken place where the radius of curvature of the the cylinder was discontinuously increased even if the wall itself was smoothly connected. A systematical investigation was carried-out on aerodynamic forces acting on two-dimensional circular cylinder and on velocity profiles of mixing region of jet when the station of a jet and intensity of jet were varied at rather small Reynolds numbers.

Furuya and Yoshino (28) have established the characteristics of the jet by conducting the experiments in the absence and in the presence of the main flow. In the absence of the main flow the Reynolds number and the location of the jet, has shown little influence on the boundary layer thickness and velocity profiles. The obtained results were in agreement with the Newman's experimental data of static pressure distribution (61) on the wall in the direction of the flow.

Further the characteristics of the jet in the presence of the main flow have been investigated. In this case the velocity of the jet was seen to be reduced and eventually reversed with respect to the main flow in the vicinity of the main flow (27). Furuya and Yoshino have also observed that the velocity profile of the mixing region of the jet has almost a fixed shape across the whole span, except at the points near to the end plates. The velocity profiles of mixing region and various circumferential stations at the centre of the span in two cases for $C\mu = 0.085$ and 0.0544 were similar in shape. Yoshino and Furuya have also observed that the profiles were seen to preserve its similarity even after the point of separation. In this work pressure distribution has been used to calculate the lift and drag coefficients generated by the wall-jet. The maximum of the lift to drag ratios were all alike for

the jet angle $\theta_j \geq 0°$, while the maximum of C_L/C_D and the value of the $C\mu$ at that maximum increase as θ_j increases for $\theta_j < 0°$. In this case $C_L/C_D = 10$ *and* $C_L = 3.3$ were obtained at $C\mu = 0.4 \cdot$ $C_L/C_D > 10$ were also obtained as $C\mu$ was further increased and C_L/C_D had reached the maximum somewhere at $C\mu > 0.4$.

Furuya and Yoshino (28) both theoretically and experimentally investigated the static pressure distribution and velocity profile of jet about a circular cylinder. Following are the major conclusions that may be drawn on their reported work;

a) On the Jet

(i) Velocity profiles of the mixing region of the jet are throughout geometrically similar in shape even after passing the point of separation of the flow.

b) On the Lift and Drag Coefficients

i) The case of small $C\mu < 0.1$) for the $\theta_j \leq -20°$ the $C_L > 0$ and C_L once decreases and increases after passing through the point of minimum as $C\mu$ increases. In the mean time C_D decreases after passing through the local minimum. For $\theta_j > 0°$ the boundary layer control like $\theta < \theta_{sep} < 90° + \theta_j$ is impossible.

ii) In the case of large $C\mu (> 0.1)$, the rate of increase of C_L with an increase of $C\mu$ is nearly constant regardless of θ_j. Greater the θ_j is, greater the C_L is,

when the C_μ is maintained constant. On the other hand, the rate of increase of C_D with an increase of C_μ increases as θ_j increases.

Further investigations on the aerodynamic characters of the circular cylinder with the tangential blowing with the effect of a side-wall has been carried-out by Yoshino, Waka et. al. (27). In this study, the span-wise distributions of characteristic values such as lift and drag coefficients of a circular cylinder with tangential blowing immersed in a uniform flow have been measured. From the obtained results, the variation in these coefficients due to the presence of the side-wall of a wind tunnel has been determined. This range of variation has become narrower when the location of the slot for introducing the jet-air farther downstream. The induced angle of attack and trailing vortices has also been calculated. Yoshino et. al. have given the importance to systematic investigation of the overall "Wing" characteristics, such as span-wise distribution of them, characteristics at the mid-span and so forth, and the flow around the cylinder in the wind tunnel. This kind of investigation has a greater importance in the industrial application, not limited to the circular cylinder. For instance this method is applicable for a problem of a separated flow near the wing root of an axial flow machine or for meeting the demand of "designers"

requiring the two-dimensional characteristics of an aerofoil with the separated flow. However these methods have very limited application for the theoretical and experimental investigation for the aerodynamic lift in the present problem.

However, further work by Waka, Yoshino et. al. (27) on the aerodynamic characteristics at the mid-span of a circular cylinder with tangential blowing has some importance to the present work on wall-jets. In their work, three different methods have been devised to determine the induced angle of attack as a function of lift coefficient at the mid-span of a circular cylinder with tangential blowing immersed in a uniform flow. The lift and drag coefficients on the circular cylinder have been corrected to give data for two-dimensional flow conditions by making use of the induced angle of attack thus obtained. The circumferential static pressure distribution on the surface of the cylinder has also been calculated by modified Parkinson-Jandali method to apply to an asymmetric flow around the cylinder with blowing.

Waka et al. have carried-out experiments by varying aspect ratio of the cylinder, angular location of the jet, and the jet momentum coefficient under the conditions of constant $Re = 2.1 \times 10^5$. Then the calculated pressure distributions for symmetric $(C\mu = 0)$ and

asymmetric ($C\mu > 0$) flow with respect to the x-axis have been compared with the Dunhams (17) calculated pressure distributions. Further the relationship between the lift coefficient and the drag coefficient and the momentum coefficient have been established. Results show that as C_L increases, C_D decreases once and takes a minimum value, after that C_D increases again. C_D is mainly given by the sum of the profile drag coefficient C_{D0} and the induced drag coefficient C_{Di} for the considered Reynolds number. As the C_L increases, C_{D0} decreases and C_{Di} increases. When C_L is small, the decrement of C_{D0} is greater than the increment of C_{Di}, so that as whole, C_D decreases. As C_L attains greater values, however, the increment of C_{di} comes to exceed the decrement of C_{D0}, so that C_D begins to decrease (28). The ratio of the increase of C_D to that of C_L is larger and is in the same order of aspect ratio of 4, 6, 8 and the values of C_D becomes to the values of the same order. Hence the influence of the aspect ratio on lift and drag coefficient relation appears clearly with an increase of the lift coefficient.

1.6 Numerical Methods For The Determination of The Flow Past Symmetrical Bluff Bodies

Work by Parkinson and Jandali (34) describe a way of predicting the important features of flows past bluff bodies whose shapes cause flow separation and the formation of a broad wake. A two-dimensional incompressible potential flow was considered for the flow external to a symmetrical bluff body and with its wake. In this work the desired flow separation points were made the critical points of a conformal transformation to a complex plane in which surface "sources" in the wake create stagnation conditions at the critical points. The stagnation stream lines have then transformed to tangential separation stream lines in the physical plane, with separation at the desired pressure. The position and length of the sources have been determined by the requirement of separation position and the coefficient of pressure. The flow inside the separation stream lines was ignored and base pressure was assumed to be constant at the separation point. This work also gives features of the theoretical model which includes a finite wake width, a pressure distribution on the separation stream lines decreasing asymptotically towards the free stream value at infinity and simple analytical expression for the pressure distribution on the body. Comparison of the

theory with the experimental data and with other theories were also presented for the normal plate, the circular cylinder, the 90° wedge and the elliptical cylinder. Parkinson and Jandali's theory appears to be in good agreement with their own experimental results (34).

Head and Patel (37) in 1968, presented a integral method for the calculation of two-dimensional incompressible turbulent boundary layer. In this method entrainment has increased when the rate of growth of the layer was less than that of the corresponding equilibrium layer and has decreased it when the rate of growth was greater. This variation of entrainment was in accordance with observation, and a simple physical explanation has been proposed to account for it. In this work the comparisons with measured boundary layer developments show the general accuracy of the method. They have increased the accuracy of the predictions by taking to account the effects of the convergence and the divergence of the flow.

Further work by Patel and Celik (61) presented a method for the calculation of the mean flow past a circular cylinder. It utilizes the interactive procedure that couples a boundary layer calculation method, by which the location of separation and the displacement thickness of the boundary layer were predicted, and the

two-parameter irrotational flow model, which predicts the pressure distribution. The displacement effect of the boundary layer was explicitly taken into account in the irrotational flow model. The point of separation, drag coefficient, and pressure distribution parameters has been predicted at high Reynold numbers of 10^8. This work shows the importance of boundary layer in a critical flow regime. This was presumed to be a result of the rapid thickening of the boundary layer in the intensive pressure- rise in this regime. They also have observed the continuity of the Reynold number dependence even upto $Re = 10^8$ This was due to the way in which the available minimum pressure coefficient data has been extrapolated to high Reynolds numbers, or may be due to the increased influence of surface roughness with increased Reynolds number which was not considered in their model.

El-sharawi, El-Refai and El-Bedeawi (29) have developed a finite deference method for solving the boundary layer equations governing the laminar flow about a rotating sphere which was subjected to a uniform stream in the direction of the axis of rotation. Although the work deals with a special case of this problem; namely, the flow around a sphere rotating about its axis and simultaneously subjected to a stream in the direction of the axis of rotation, method of solution and results carry a greater interest. This work shows that large

gradients exist near the stagnation point and also near the separation point. For the chosen Re=10000 El-Sharawi and others give the position separation point θ as a function of the rotational speed. And also their results show for the investigated range of rotational speed (0 - 10000) the separation point always lies equational plane (29) and shifts forward as the value of the rotational speed increases. This is in agreement with the conclusions of Schlichting (15), that the displacement of the separation point is due to the effect of centrifugal forces which, behind the equational plane (52). This has the effect of an additional pressure increase in flow direction and therefore cause the separation point to shift forward.

Investigation into aerodynamics of a circular cylinder in cross-flow, by Bychkov and Kovalenko (30) discuss the aerodynamic forces, the distribution of pressure and its fluctuations. These tests have been carried-out in a low-turbulence subsonic wind-tunnel at $10^5 \leq Re \leq 5 \cdot 10^5$. In these investigations for different turbulence level of the flow and cylinder surface roughness they have observed "sign-variable" lift (30) with a variable drag. In the case of low-turbulence flow at critical values of Reynolds number, over a smooth cylinder, suggesting asymmetric and unsteady position of boundary layer separation. Pressure fluctuations on the cylinder surface have attained a

maximum in the pre-separation region. Greater the turbulence of the free stream and higher the roughness of the cylinder surface stabilize the positions of the separation point and also results in a greater symmetry of the flow over the cylinder.

Buchkov and Kovalenko have extended this work to aerodynamic forces on a smooth rotating cylinder (31). These experiments have also been carried-out in the same low-turbulence subsonic wind tunnel at $10^5 \leq Re \leq 6 \cdot 10^5$. In these investigations Buchkov and Kovalenko have observed significant changes in the location of asymmetric points of the boundary layer separation. They also have showed that at the critical Reynolds number, rotation stabilizes and the flow about the cylinder and reduces the fluctuations of the aerodynamic forces. Turbulent flow have also produced a smoother variation in aerodynamic forces, due to the more stable location of separation points.

Buchkov and Kovalenko have investigated further on aerodynamic forces on a rough cylinder in cross-flow (32). These experiments have also been carried-out in the same low turbulence wind tunnel at the same Reynolds numbers (31). During these tests they have established that the magnitude and the nature of variation in aerodynamic forces of a rotating rough cylinder which differed significally from the case of

the smooth cylinder. This was due to properties of the flow in the wall-region and the location of the points of the separation of the boundary layer. They also have found that the higher turbulence level did not have any significant effect on the aerodynamic forces of the rough cylinder in the critical range of the Reynolds numbers.

Another detailed investigation has been carried-out by Zubarev (33) on the same phenomenon but on a "moving surface". This study has been made of the boundary layer on a cylinder with a "moving surface" while the cylinder was travelling with a constant velocity in an incompressible fluid. Zubarev (33) have obtained expressions for the distributions of the frictional stress on the surface of the cylinder and the coordinate of the singular point in the solution of the boundary layer equations that indicates the appearance of a region of a reverse flow for different values of the relative velocity of the motion of the cylinder. In this work numerical calculations have also been made of the work of the forces of friction associated with displacement of the cylinder.

1.7 Numerical Methods For The Determination of The Aerodynamic Lift Due To The Tangential Wall-jet

Presence of a tangential wall-jet at an appropriate location on a curved surface, in a main stream creates an unsymmetrical pressure distribution. Among published literature only very few have concentrated in reaching a possible analytical / numerical solution to the problem.

Waka and Yoshino (28) have calculated the circumferential static pressure distribution by extending the Parkinson Jandali (34) which can be applied to two-dimensional flow around a symmetrical bluff body with a broad wake. Assuming frictionless flow and a imaginary plane (t-plane (28)) they have managed to transfer points from the original T-plane using a transformation equation;

$$t \equiv f(t) = e^{-i\gamma}\left(T - \cos\delta - \frac{1}{T - \cot\delta} \right)$$

Where, $T = X + iZ$, $t = x + iz$

$i = imaginary\ \ unit$

γ - angle between the incident flow and the X-axis, δ angle between the stagnation point and the T- plane. Waka and Yoshino have transformed a complete circle

with radius R the centre of which is at the origin, to a circular arc slit, in the t- plane. This slit mapped from the circle is not symmetric with respect to the X-axis. It has also been considered the complex potential of a flow around a circle with radius R immersed in a uniform flow U_∞ the direction of which is inclined by the angle γ with respect to the X-axis in the T-plane. Along with this were the two sources of different strengths 2Q1 and a Q2 at symmetric angular positions E and -E on the circumference of the circle respectively, a sink of strength (Q1 +Q2) at the origin and a circulation of strength Γ around the circle. By using the total complex potential of the asymmetric flow in the T-plane and separation velocities which were obtained by using empirical pressure coefficients, circumferential static pressure distribution has been calculated. Since Waka and Yoshino have adopted a method of transformation of a circle into a slit, limits the use of the given method for different configurations. They also have ignored the skin friction and hence the surface shear stress.

A modified finite element method for solving the time dependent incompressible Navier-Stokes equations has been developed by Gresho and others (35). This has been achieved by utilizing the Galerkin finite element (36) and the simplest approximate isoparametric element for modelling the Navier-Stokes equations. The

approximation has been modified in two ways in the interest of cost effectiveness. After appending and "hour-glass" connection (35) term to the diffusion matrixes, the modified equations have been integrated in time using the forward Euller method (51) in a special way to compensate for that portion of the time truncation error. However in the absence of the correction due to the shear-stress and owing to the complicity of introducing such a factor to the equations finite element technique introduced by Gresho was not considered in obtaining a numerical solution to the problem.

Turbulent wall-jets by Rajarathnam (38) gives a detail account of the behaviour of the plane turbulent wall-jets. A plane jet coming out of a nozzle tangentially to a smooth flat plate which is submerged in a semifinite expanse of the same fluid. As the jet leaves the nozzle due to the velocity discontinuity, a shear layer develops on the fluid side and a boundary layer develops on the wall side. If the surrounding fluid is also in motion in the same direction, phenomenon is referred as the plane turbulent compound wall-jet.

A detail study on compound wall-jets has been undertaken by Eskinazi and Kruka (39) in 1962. Their first work on mixing of a wall-jet into a free-stream

has been done with a zero pressure gradient. Experiments have been carried-out for various ratios of jet to free-stream velocities and have obtained results in agreement with the Blasius's frictional law (49). And also the non-dimensional shear-stresses have found to be in agreement with Fortmann's (19) results which were computed from the momentum considerations. Since this work was carried-out only for the zero pressure gradient, comparisons with the results of the present work can not be made. However the work give a good general understanding of the compound wall-jet and the mixing layers which enabled to formulate the present problem.

In their further work Kruka and Eskinazi (40) have carried-out experimental investigations on a plane, steady, turbulent wall-jet in a free-stream of air. Here they have considered a negligible longitudinal pressure gradient. In that investigation Kruka and Eskinazi have observed that the inner layer has constantly lost its momentum caused by the frictional stresses at the wall while the outer layer has preserved its momentum. These analysis have been carried-out by using empirical equations.

1.8 Aerodynamic Theory of Wind Turbine Generators

Betz limit (55,56) for the performance coefficient is one of the factors useful in evaluating the aerodynamic design of a wind turbine generator. However the "Betz limit" does not represent the maximum possible performance coefficient for a wind energy conversion system (57).

Loth (58,59) has carried-out series of investigations on the power coefficient of wind turbine generators. For the work on optimization of Darrieus turbine, with upwind and downwind momentum model (58) a generalised Betz limit has been derived. In this work an arbitrary number of actuator discs in series has been used. A momentum-type velocity model has been introduced with separate cosine -type interference coefficients for the upwind and downwind half of the rotor. The values for the optimum rotor efficiency, solidity, and correspond-ing interference coefficients have been obtained in a closed -form analytical solution by maximizing the power extracted from the downwind rotor half as well as from the entire rotor.

Further work by Loth and McCoy (59) on wind power limitations associated with vortices have used the pressure dissipation inside vortices due to viscous shear. The reduced level of the total pressure flux of

the flow inside a vortex has an adverse effect on all vortex ingesting wind machines. The Betz limit and wind turbines ingesting the vortex generated by an aerofoil has been computed.

By introducing number of actuator discs to their models, Loth and McCoy have succeeded in proving that the universal use of the Betz limit for wind power generators is erroneous. However the pressure recovery between the upwind and the downwind sections of a wind turbine generator and the influence of the shape of the stream tube on the "Betz limit" have not been considered.

CHAPTER 2

2. THEORETICAL ANALYSIS - POWER OF A VERTICAL AXIS WIND TURBINE GENERATOR DUE TO AERODYNAMIC LIFT ON ORBITING CYLINDERS

2.1 Background

The performance of conventional wind machine is essentially determined by the ratio of the lift to the drag coefficient obtainable for the particular geometry used for the blading. The achievement of a high lift results in an efficient and compact machine for given power to be generated. One of the methods for developing a very high lift coefficient, far in excess of what is possible with an aerofoil, is to use the "Magnus Effect" in association with a rotating cylinder (13). The basic principle is illustrated in Fig 2.1. There was little progress of the originally proposed "Madaras Rotor Concept" (12,13) as there was at that time no economic advantage compared to the use of fossil fuels or nuclear energy. A detailed study of the "Madaras Rotor Concept" was undertaken by the University of Dayton Research Institute, Ohio, USA. The above study indicated several practical problems in using the "Magnus Effect", especially for medium/small scale power generation, as detailed below;

(i) The complexity of using large rotating cylinders and the energy losses because of the need for reversal of rotation, for the cylinders for each orbital motion.
(ii) The presence of additional mechanical losses due to friction during the motion of the heavy carriages on a track.
(iii) The requirement of essentially unidirectional winds for a race track configuration.
(iv) The difficulties in adjusting and controlling the operating parameters for optimum performance (13).

The major difficulties of employing large rotating cylinders in the "Madaras Concept" as detailed above may be overcome by achieving the aerodynamic lift through the use of a wall-jet on non-rotating orbiting cylinders as shown in the Fig 2.1. (Also see the section 3.1)

2.2 Instantaneous Power Generated in Madaras Rotor Concept

The components of lift force due to the Magnus Effect (15), in non-dimensional form, can be expressed as;

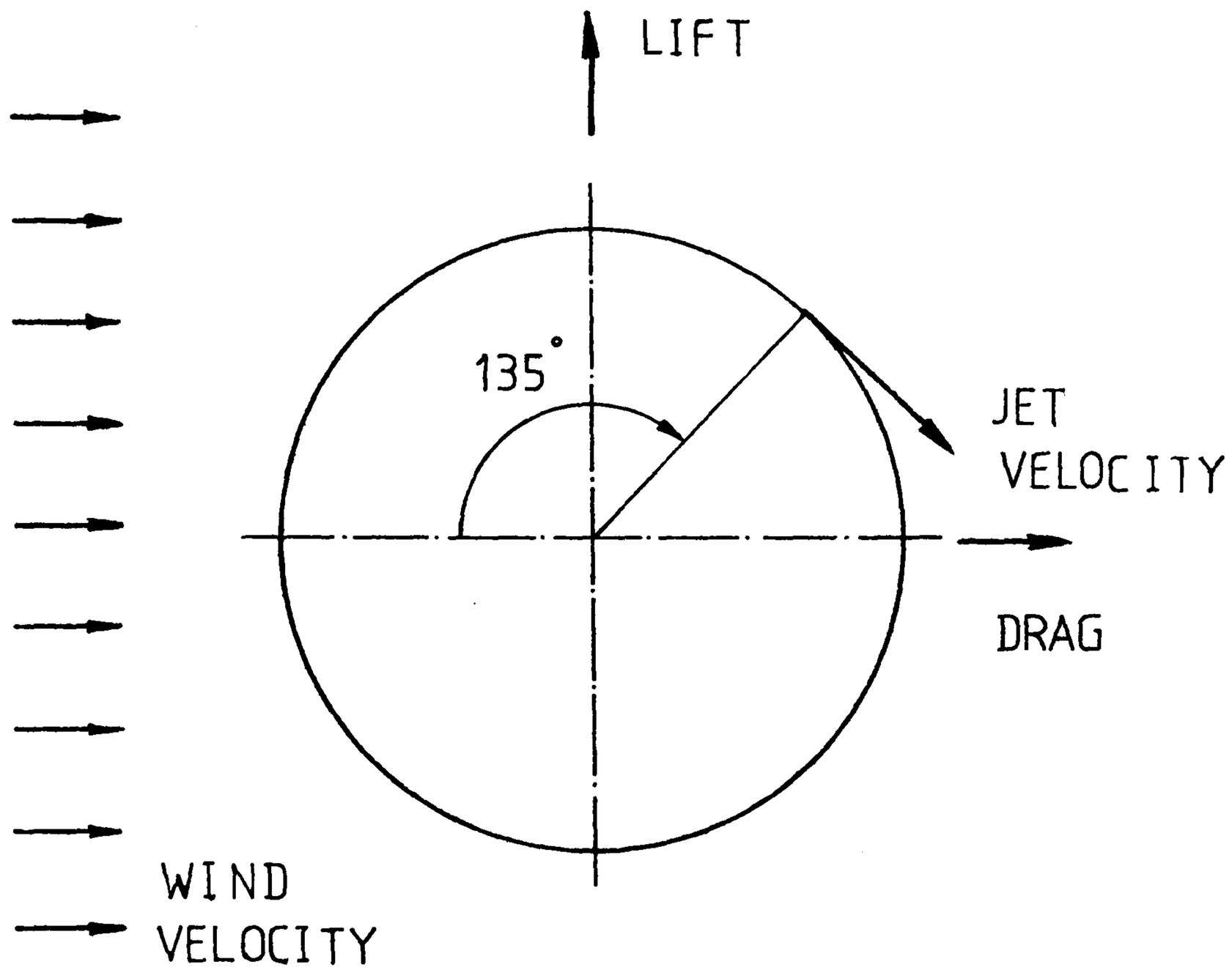

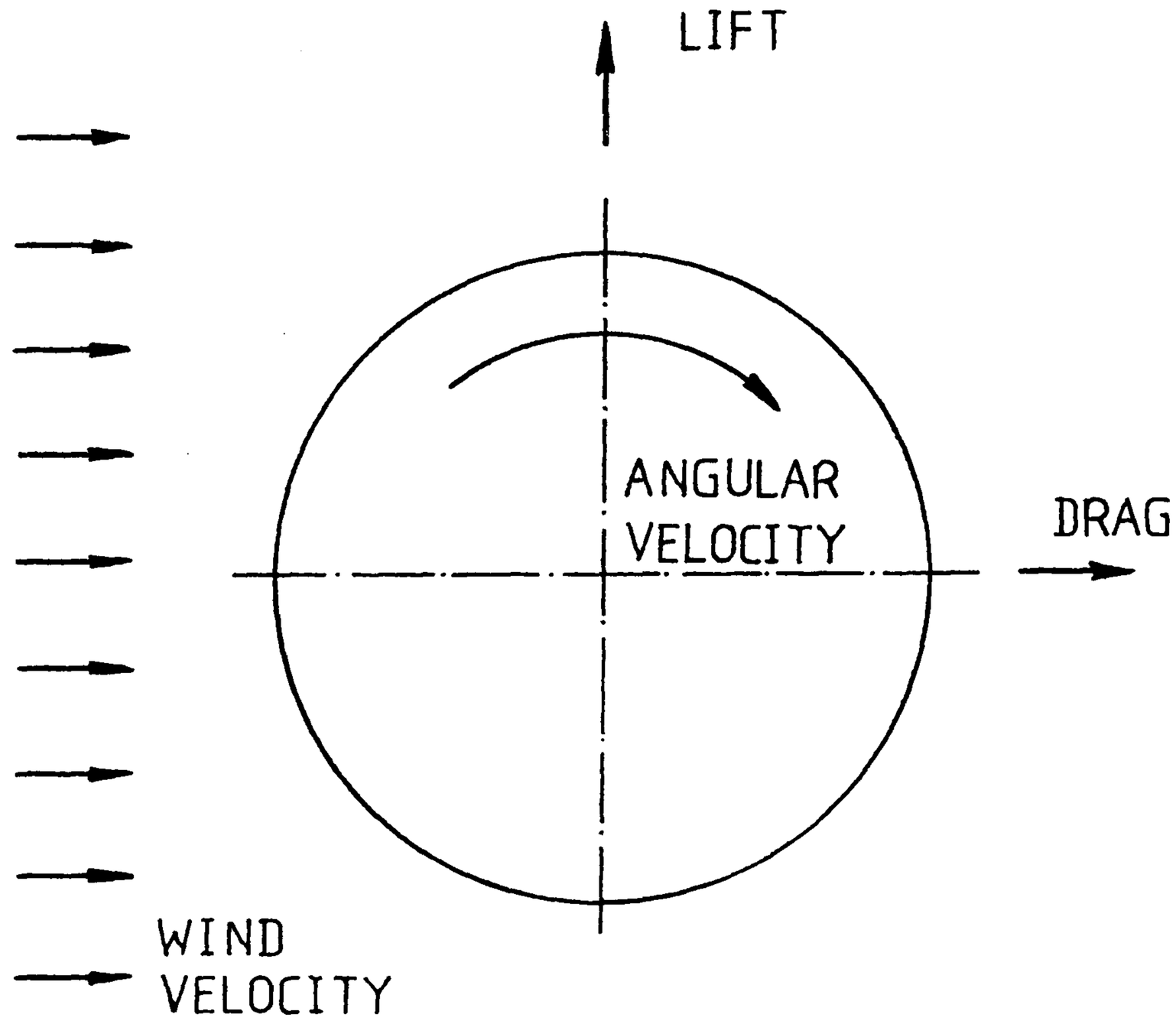

Fig 2.1 Aerodynamic Lift Due to
Tangential Wall-jet/Magnus Effect

2.2-1 $$L_x = 2\Pi\left(\frac{r}{R}\right)\left(\frac{\omega_z}{\Omega_z}\right)\left(\frac{R\Omega_z}{W}\right)V_y$$

$$L_y = -2\Pi\left(\frac{r}{R}\right)\left(\frac{\omega_z}{\Omega_z}\right)\left(\frac{R\Omega_z}{W}\right)V_x$$

(See Appendix 2A)

and the components of drag force in non-dimensional form for the cylinder employed for lift generation using the Magnus Effect is

2.2-2 $$D_x = C_D \cdot U_m \cdot V_x$$

$$D_y = C_D \cdot U_m \cdot V_y$$

(Where the drag coefficient C_d for the Madaras Rotor Concept is taken as 0.4 (13))

The instantaneous power produced in the Madaras Concept due to the orbital motion of the cylinders may be expressed in non-dimensional form as;

2.2-3 $$P' = F_x V_x + F_y V_y$$

where the total component of the forces on the cylinder in non-dimensional form are given by;

2.2-4 $$F_x = L_x + D_x$$

$$F_y = L_y + D_y$$

The Power dissipated due to viscous action for the axial rotation of a cylinder P_ω can be expressed as;

2.2-5 $$P_\omega = \tau(2\Pi r H) r\omega$$

Where;

τ - surface shear stress

The surface shear-stress τ is expressed as;

$$\tau = \frac{\rho f U_s^2}{2}$$

For reasonably large values of radius of a cylinder the friction factor can be taken as for a flat plate with velocity of U_s $(\equiv r\omega)$ (53)

Therefore

$$f = \frac{0.074}{(Re)^{1/5}}$$

$$Re = \Pi r \cdot \frac{U_s \rho}{\mu}$$

and thus the shear-stress τ can be expressed as;

2.2-6 $$\tau = 0.02942\left(r^{1.6}\omega^{1.8}\rho^{0.8}\mu^{0.2}\right)$$

from the equations 2.2-5 and 2.2-6,

2.2-7 $$P_\omega = 0.1849\left(H r^{3.6}\omega^{2.8}\rho^{0.8}\mu^{0.2}\right)$$

The power required for the axial rotation of a cylinder given by the equation 2.2-7, non-dimensionalised on the same basis as P′ of equation 2.2-3, is given below by;

2.2-8
$$P'_{\omega} = 0.1849 N_r^{-0.2} V_M^{2.8} \left(\frac{r}{R}\right)^{2.8} \left(\frac{\omega}{\Omega}\right)^{2.8}$$

Where

$$N_r = \frac{\rho W r}{\mu}$$

$$V_M = \frac{R\Omega}{W}$$

Therefore the net instantaneous power produced in the Madaras Rotor Concept, in the non-dimensional form is;

2.2-9
$$P'_{net} = P' - P'_{\omega}$$

The above equation is used in section 2.5.2 to compare the theoretical power coefficient of the Madaras Rotor Concept with the Concept of using tangential wall-jets.

2.3 Instantaneous Power Generated by the Aerodynamic Forces Utilising Wall-jet Effect on Octagonal Cylinders

In the section 3.1 the basic principle of the lift generation by the tangential wall-jets on non-rotating

cylinders is described. The components of the lift force due to the wall-jet on an octagonal cylinder may readily be obtained by representing the lift force as a two-dimensional vector. To facilitate this, the jet momentum coefficient is expressed as a vectorial equation as follows;

$$\overline{C}_{\mu} = \left(0\hat{i} + 0\hat{j} + \mu_z \hat{k}\right)$$

Where the unit vectors i, j lie in a plane normal to the axis of orbital rotation of the octagonal cylinder and the unit vector $\hat{k}$ is along the axis of orbital rotation.

The lift force vector due to the tangential wall-jet can now be expressed in the non-dimensional form;

2.3-1
$$\vec{L} = -\frac{\rho C_r r^2 H U_m\left(\overline{C}_{\mu}\overline{U}\right)}{\rho W^2 (rH)}$$

$$= -\rho C_r r^2 H U_m \begin{pmatrix} i & j & k \\ 0 & 0 & \mu_z \\ U_x & U_y & 0 \end{pmatrix}$$

Therefore the components of the lift force due to the tangential wall-jet are expressed in the non-dimensional form as;

2.3-2
$$L_x = C_r U_m\left(\mu_z \cdot V_y\right)$$

$$L_y = -C_r U_m\left(\mu_z \cdot V_x\right)$$

Therefore the power produced by the non-rotational cylinder elements may now be obtained in terms of L_x , L_y and also the forces D_x , D_y, given in the equations 2.2-1 and 2.2-2 which are also applicable here with an appropriate value of C_D. The procedure is identical to that developed in the section 2.2 and the equation for the instantaneous power produced is given by the same form of the equation as 2.2-3. i.e.,

2.2-3 $$P' = F_x V_x + F_y V_y$$

Where;

2.2-4 $$F_x = L_x + D_x$$

2.2-4 $$F_y = L_y + D_y$$

The lift to the jet momentum coefficient C_r and the drag coefficient C_D of the above equation are determined in the section 3.8.7.

Power required to form the wall-jet P_j is evaluated in Appendix-2B and the final result is expressed in the non-dimensional form as;

2.3-3 $$P_j' = \left(\frac{b}{r}\right)\frac{V_j}{W^3} C_{pa} T_a \left(\psi^n - 1\right)$$

Where in the equation 2.3-3,

$$\psi^n = \left(\frac{p_a}{p_1'} \right)^n = \frac{T_0}{T_1'}$$

Therefore the net power produced in the non-dimensional form for this case is;

2.3-4 $$P'_{net} = P' - P'_j$$

The above expressions for instantaneous power is used to predict the theoretical power coefficient of the wind machine based on the wall-jet principle of lift generation, in section 2.5.1.

2.4 Switch-over Angles for a Wind Turbine Generator Working on Aerodynamic Lift

For a Vertical Axis Wind Turbine Generator (VAWTG) working on the aerodynamic lift generated by a principle such as the "Magnus Effect", requires directional change of the axial rotation of cylinders at diametrically opposite points of an orbit lying on a line perpendicular to the wind velocity direction (Fig 2.2) considered case of Madaras Rotor Concept for wind power generation. As the cylinder travels around the orbit from points 1 to 4 the net force is a result of components of the lift and the drag forces. During this section of the orbit the drag force also

contributes to generate useful power. However as the machine rotates in the counter clock-wise direction and produces useful power, the axial rotation of the cylinder has to change from the counter clock-wise direction to the clock-wise direction between the points 2 and 3 of the orbit. The orbital angle between these two points is taken as the switch over angle θ_{c1}. From the points 4 to 5 the net force has components such that useful power is produced because of lift due to the "Magnus Effect". As the cylinder reaches the point 6 the axial rotation should again be changed into the clock-wise direction. The angle between points 5 and 6 where the axial rotation changes from the clock-wise direction to the counter clock-wise direction is the second switch-over angle θ_{c2}. However between the points 5 and 6, as the cylinder drives against the wind there is no useful contribution of forces for power generation. Between the points 6 and 1 the forces acting on the cylinder are identical to the forces in between the points 4 and 5.

Fig 2.3 shows the relation ship between the orbital angle and the angular velocity (axial) of a cylinder. For the Madaras Rotor Concept the switch over angles are taken as; $5° \leq \theta_{c1}, \theta_{c2} \leq 10°$

for the purpose of comparison of power coefficients discussed in the section 2.5.2

$$F_2 = L \cos\alpha - D \sin\alpha$$

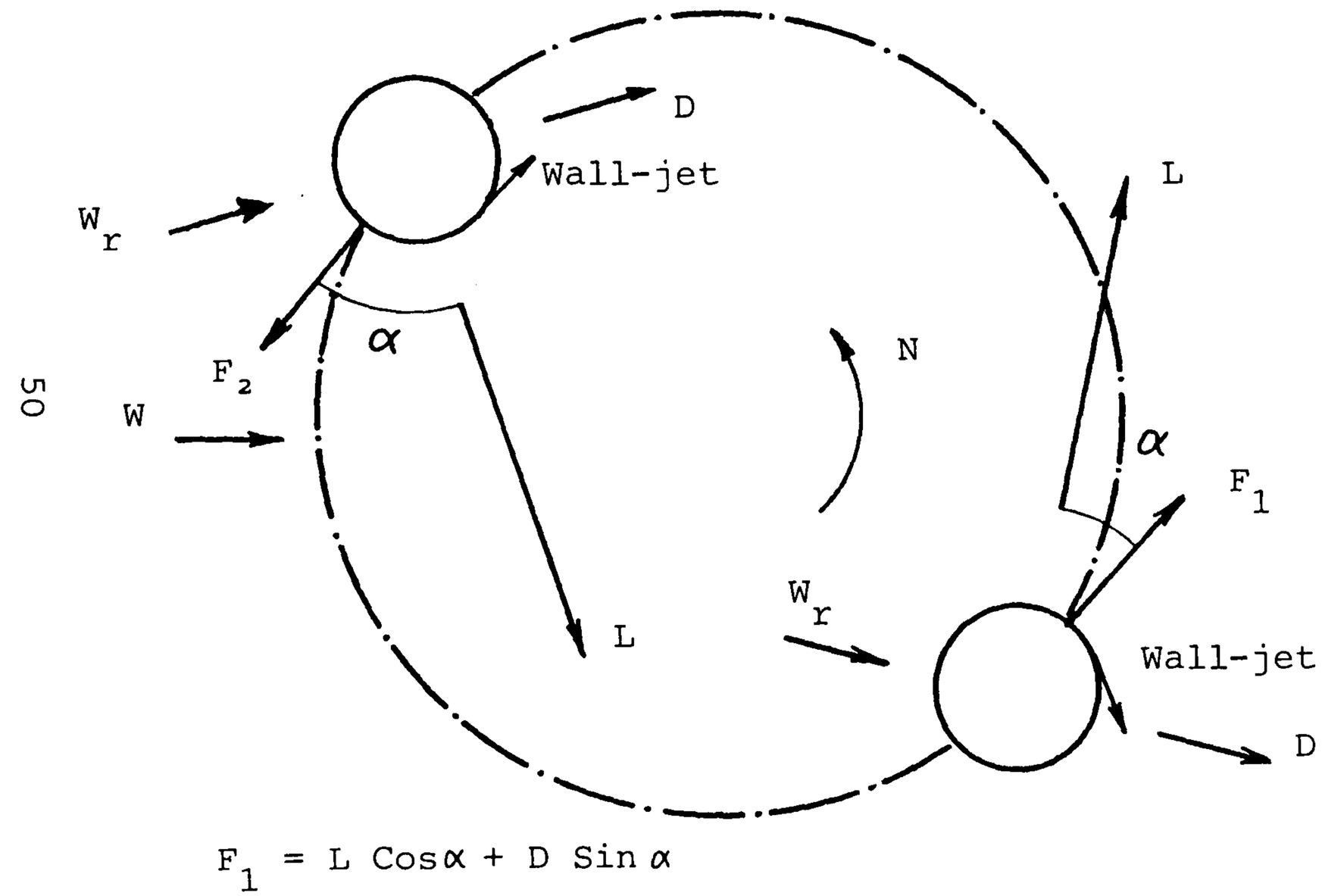

$$F_1 = L \cos\alpha + D \sin\alpha$$

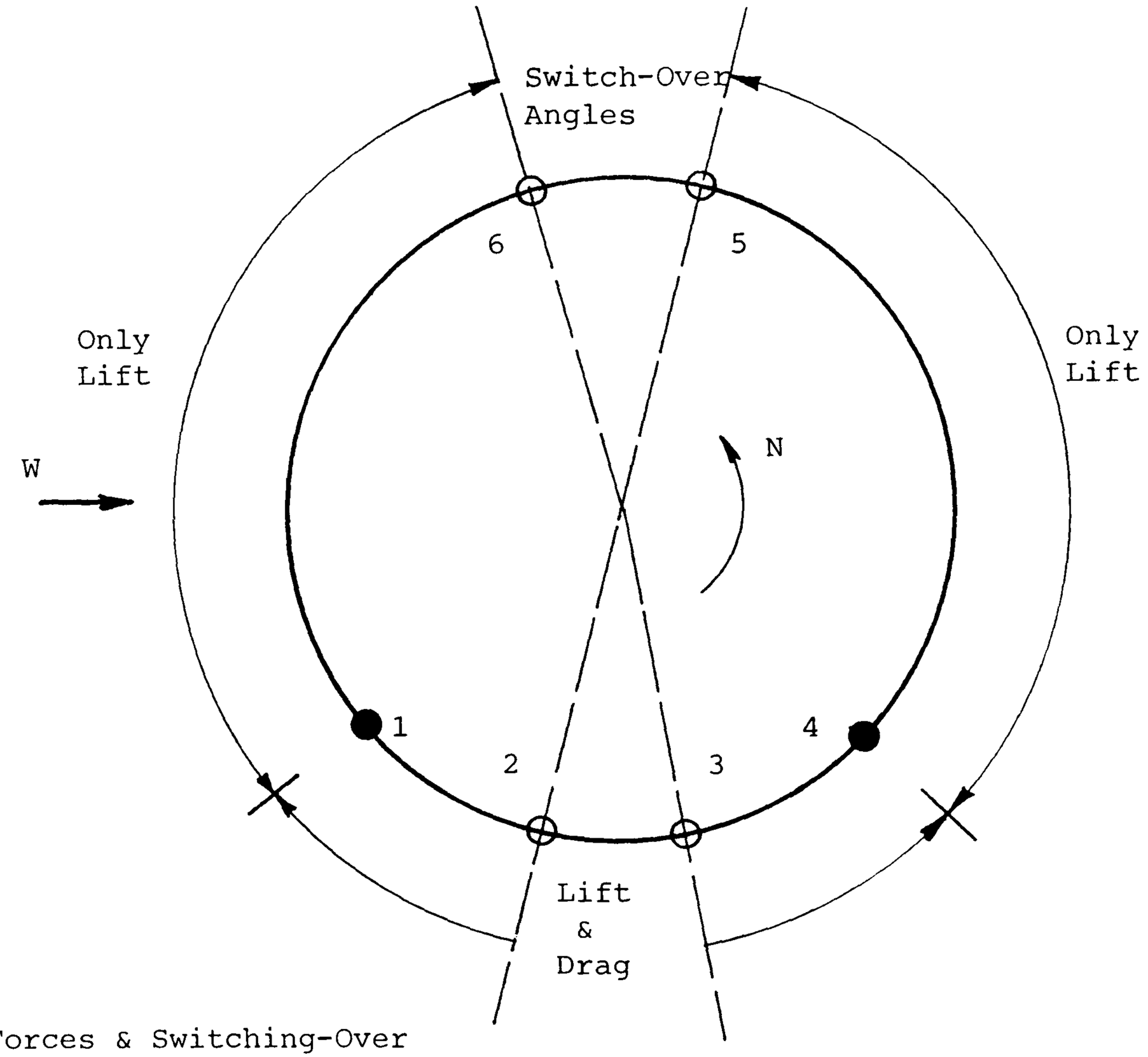

Fig 2.2 Resultant Forces & Switching-Over Angles

During one complete orbit for optimum operating conditions the direction of the net resultant force should always be in the same direction as the orbital motion of the cylinder. However for a given wind velocity and a constant axial rotation achieving this optimization with the Madaras Rotor Concept is impossible.

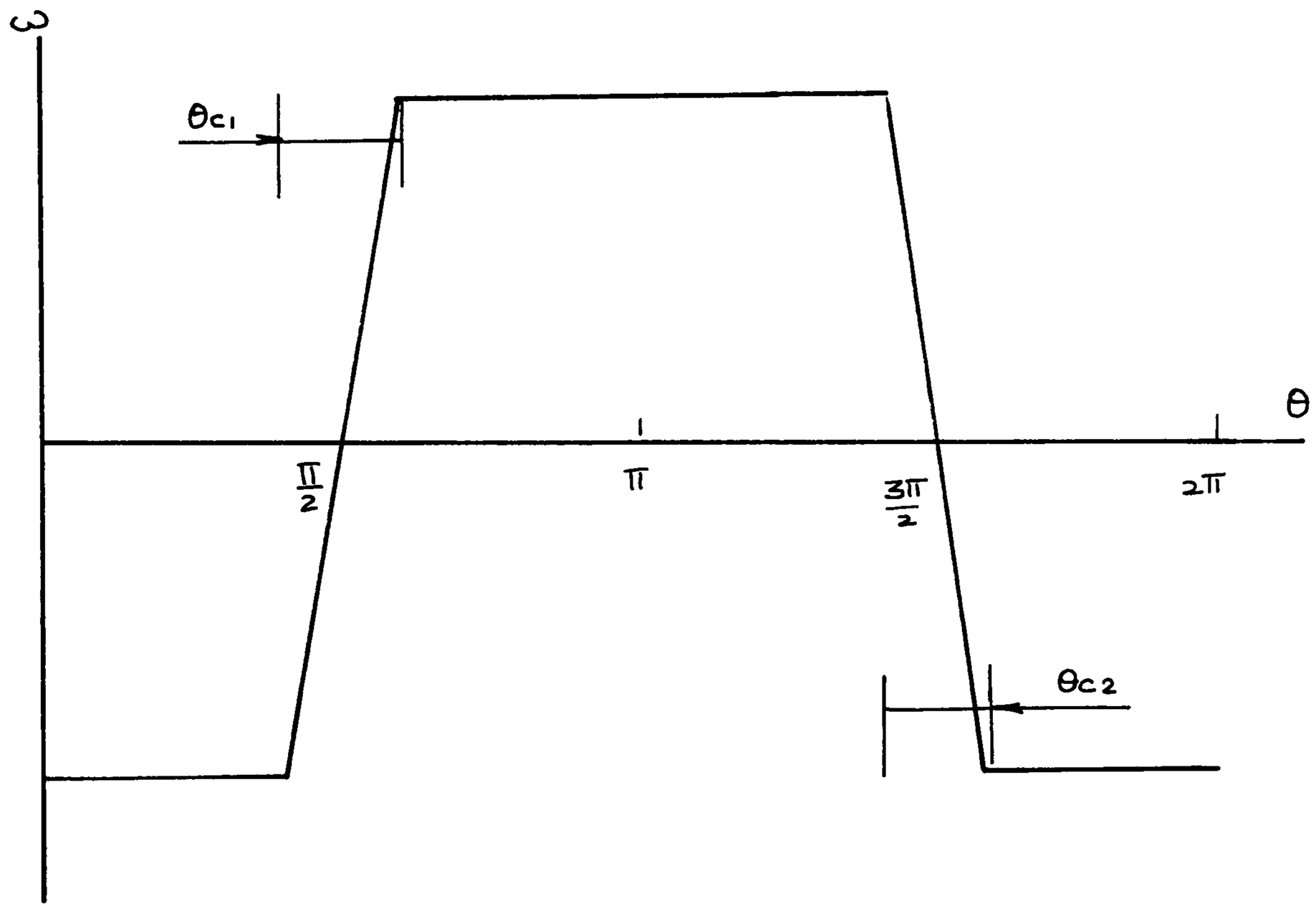

Change Over Angle Vs Angular (Axial) Velocity

Fig 2.3

In the case of a wind machine using the principle of tangential wall-jets (see 3.1) the switch over angles can practically be made zero as this involves only

switching over to a different set of wall-jets at locations considered earlier. In between switch over points it is also possible to optimize the operating conditions of the machine by activating different sets of jets in order to obtain required angle between directions of jet and the relative wind velocity (see paragraph 3 of 4.3.2).

However for the present comparison study discussed in the section 2.5.2 the effectiveness of the optimization of the jet location on octagonal cylinders is not considered, since this study was based only on a fixed jet position.

2.5.1 Tangential Wall-jet Principle for the Madaras Rotor Concept

The wall-jet principle may be applied to achieve aerodynamic lift in the Madaras Rotor Concept instead of using axial rotation of the cylinders (see 3.1). Theoretical power output of a wind machine based on the traditional Madaras Rotor Concept is compared with a machine utilising the concept consisting of cylinders with tangential wall-jets.

The mean power produced by the system during one

complete orbit is;

2.5-1 $$\overline{P} = \frac{1}{T}\int_0^T P\,dt$$

Where

$$T = \frac{2\Pi}{\Omega}$$

Therefore the equation 2.5-1 can also be expressed as;

2.5-2 $$\overline{P} = \frac{\Omega}{2\Pi}\int_{\theta=0}^{\theta=2\Pi} P\left(\frac{d\theta}{\Omega}\right)$$

$$= \frac{1}{2\Pi}\int_0^{2\Pi} P\,d\theta$$

P = Instantaneous power at an angular position θ which is given by; (see 2.2 and 2.3)

$$P = F_t \cdot \left(\frac{\Omega D}{2}\right)$$

F_t = sum of the tangential components of the instantaneous lift and drag forces produced on the cylinder at the position $\theta°$

The power coefficient C_p can be expressed as;

$$C_p \equiv \frac{\overline{P}}{Available\ \ Wind\ \ Power}$$

$$= \frac{\overline{P}}{(1/2\rho W^3)(2RH)}$$

or

2.5-3 $$C_p = \left(\frac{X_p \sigma}{2}\right) \cdot \frac{1}{360} \int_0^{2\Pi} \frac{F_t}{(\rho W^2 r H)} \cdot d\nu$$

Where

$$X_p = \frac{\Omega R}{W}$$

$\sigma \equiv$ solidity ratio

The FORTRAN computer programme which is developed to evaluate the values of C_p for the traditional Madaras Rotor Concept and for the concept utilising the tangential wall jets, is given in the Appendix 5D. The non-dimensional track speed $\Omega R/W$, the ratio of the rotational speed of the cylinder around its axis to the orbital rotational speed of the machine ω/Ω, the ratio of the cylinder to the track radius r/R, the Aspect Ratio of the cylinder H/r, and the switch over angle θ_c are the main input parameters in the POWERG1 programme for the evaluation of the power coefficient of the Madaras Rotor Concept with axially rotating cylinders.

For the evaluation of the Power Coefficient for the case utilising the wall-jets, the non-dimensional jet

velocity V, is used in place of the ratio ω/Ω for the main input parameters in the FORTRAN programme POWERG1.

2.5.2 Comparison of Theoretical C_p of The Madaras Rotor Concept With concept of Wall-Jets

The computer programmes mentioned in the section 2.5.1 are used for the comparison of the traditional Madaras Rotor Concept with the tangential wall-jets. In this study the inertia losses due to angular acceleration and deceleration during switch over angles, of axially rotating cylinders are considered to be negligible. In principle this is only possible where regenerative braking is achieved with 100 % efficiency. In practice these losses will reduce the value of C_p. In spite of this assumption of 100 % regenerative braking, computer simulation studies show that, by using tangential wall-jets in a Madaras Rotor Concept, as much as 30% increase in power output after accounting for the power required for the formation of the wall-jets is possible (62).

Hence these theoretical studies show that by replacing axially rotating cylinders with fixed cylinders provided with tangential wall-jets will enable to design a more efficient Wind Turbine Generator.

However both the original Madaras Rotor Concept and the modified concept proposed by the Dayton University Research Institute have many practical disadvantages over a conventional wind turbine generator (13). Therefore it will not be possible to achieve the optimum utilisation of the wall-jet principle and its advantages, in applying to the Madaras Rotor Concept. The principle of high lift generation may also be utilised to enhance the performance of a conventional wind machine by introducing tangential wall-jets on to the turbine blades (62). A preliminary study indicated that the complexity of the mechanical arrangement, will render this technique impractical in general. Hence a new concept of a Vertical Axis Wind Turbine Generator utilising the principle of wall-jets is proposed (see 2.6.1 and 2.6.2).

2.6.1 The Concept of a New Vertical Axis Wind Turbine Generator

The tangential wall-jets can be applied with several advantages in a new concept of a Vertical Axis Wind Turbine Generator consisting of two or more polygonal cylinders acting as turbine "blades" as shown in Fig 2.4 (41). The performance is optimized by introducing the wall-jets at appropriate locations dependent on the

relative wind direction, as cylinders orbit about the axis of the machine. Both the boundary layer considerations (see 2.6.3) and the wind tunnel studies (4.3.2) showed that it is adequate to use only one tangential wall-jet located at an angular position of about 135° measured from the upstream stagnation point with respect to relative wind velocity. The number of sides of the polygon is decided by the requirement for introducing the wall-jets at an optimum angle of about 135°. Therefore for a Vertical Axis Machine the minimum convenient number of sides required is 8. Hence octagonal cylinders are considered to be "blades" of the new machine. The wind machine using the above concept is referred to as **The Octagonal Cylinder Machine.**

2.6.2 The Octagonal Cylinder Wind Machine

The proposed wind machine (Fig 2.4) is to have octagonal cylinders as turbine blades and following are the major additional advantages over a conventional Vertical Axis Wind Turbine Generator;

(i) The Wall-jets can also be used for aerodynamic braking and speed control.

(ii) The flexible nature of air jets makes it simple

to alter the operating conditions with changes in the wind speed and direction, maintaining optimum performance throughout.

(iii) The structural stability of the octagonal cylinders will result in material savings as critical stress conditions present for traditional "blades" are avoided.

(iv) Less liable for "stalling" as wall-jets stabilise the boundary layer.

(41,62)

The only major disadvantage of the Machine is due to the requirement of the external source of power for the jet air supply. This can overcome by employing a passive air supply through the use of inbuilt centrifugal impellers driven by the wind machine itself as indicated in the Fig 2.4. In this case to start the machine external power has to be supplied either from a separate electric motor or by using the electric generator of the wind machine as a motor. If the generator of the wind machine is not connected to an electric power grid or does not form part of a wind-diesel plant, then a mechanical starter using a Savonius Rotor can be used. However the selection of the starting system has to be decided on the economics and the individual conditions of the operation of the wind turbine generator.

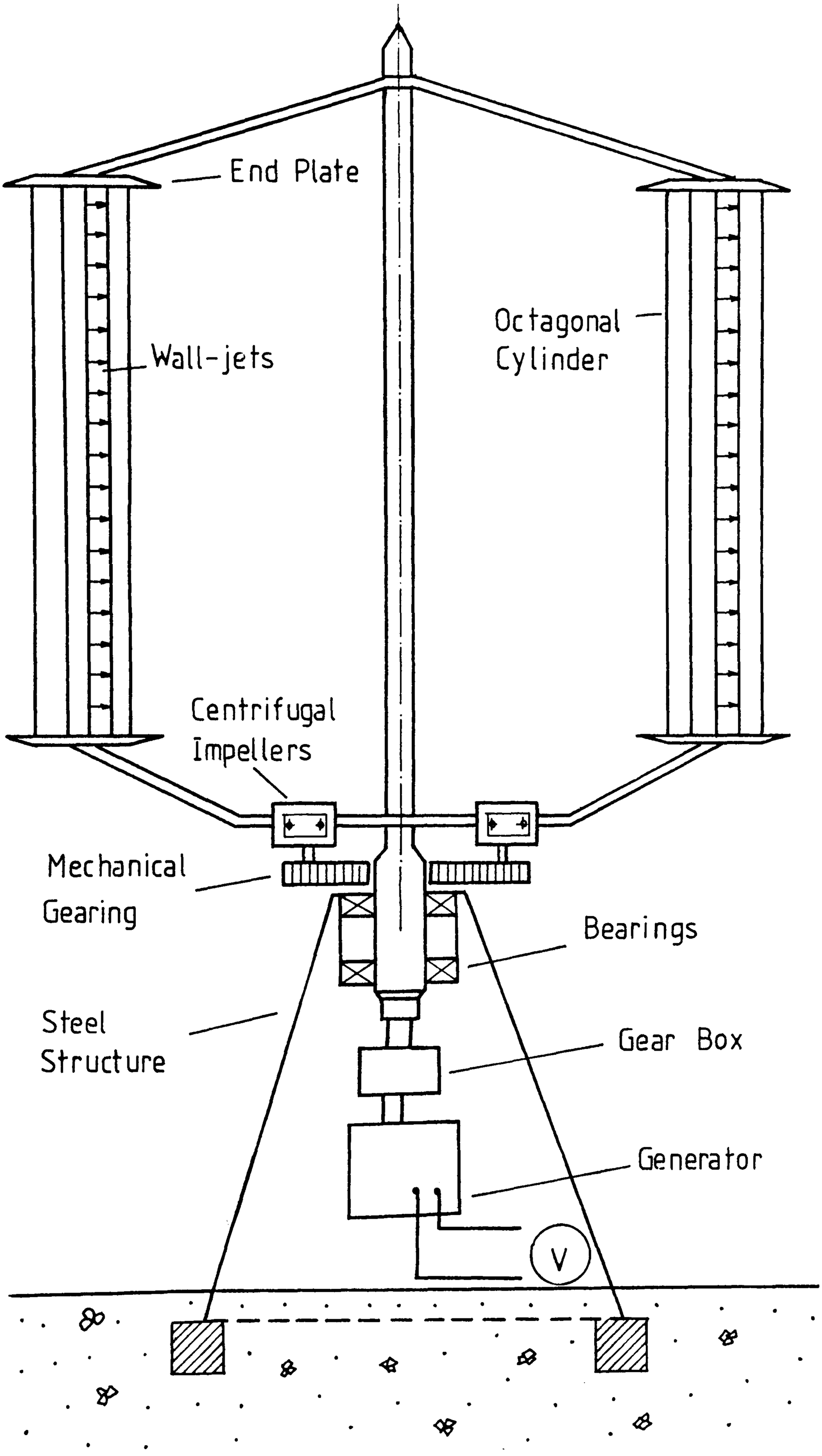

Fig 2.4 Proposed Concept of the VAWTG
with Tangential Wall-jets

2.6.3 Number of Wall-Jets, End Plate Diameter Ratio and Aspect Ratio

Tests were carried carried-out using one, two or three tangential wall-jets to determine the number of wall-jets required to achieve the maximum aerodynamic lift on the octagonal cylinder. The investigation showed that by increasing the number of wall-jets, the obtainable lift force could also be increased. However the power required for the formation of the wall-jets was also increased. Hence the instantaneous net power decreases with greater number of wall-jets. Therefore for the present application, single wall-jet has been selected as sufficient to create the adequate aerodynamic lift. This makes also easier to optimize the the wall-jet angle and hence the switch over of the jets from one set to the other in a complete orbit.

Investigations done by the Dayton University Research Institute (13) on the Madaras Rotor Concept, has proved the effect of the end plate diameter on the aerodynamic lift due to the axial rotation (Magnus Effect) of the cylinder. Since the flow patterns created by both the Magnus Effect and the Tangential Wall-jet are identical in nature, Dayton University findings on the ratio of the end plate diameter to the cylinder diameter was considered. This was qualitatively verified to be

satisfactory with the Octagonal cylinder described in the section 4.3.2. The ratio is taken to be equal to 2.0 for the present work. It was also observed that by increasing the end plate diameter ratio above 2.0 the lift to drag coefficient ratio C_L/C_D increases and eventually has an extremum value. By introducing the end plates to the wind tunnel model of the octagonal cylinder end losses are kept to a minimum value. Also at the mid-span, the flow around the octagonal cylinder becomes closer to a two-dimensional flow. Thus the comparisons of the results of the experimental investigations with the two-dimensional theoretical models are justifiable.

The technical report (13) also shows, that the lift to drag coefficient ratio C_L/C_D does not have any maximum with respect to the cylinder aspect ratio. For increasing values of the aspect ratio C_L/C_D increases and hence, the aspect ratio of the cylinder is decided here with arbitrarily to be 6.

2.6.4 Calculation of The Momentum Coefficient and The Power Required for Air Supply to The Nozzle

Using the non-dimensional jet height $t(\equiv h/r)$ the jet momentum coefficient C_μ can be expressed as;

2.6-1
$$C_\mu = K1 \cdot t \frac{(1-y)}{(1+4y)}$$

and the power required for the formation of the jet by the nozzle can be expressed as;

2.6-2
$$P_N = \frac{K2 \cdot t(1-y)^{3/2}}{y(1+4y)}$$

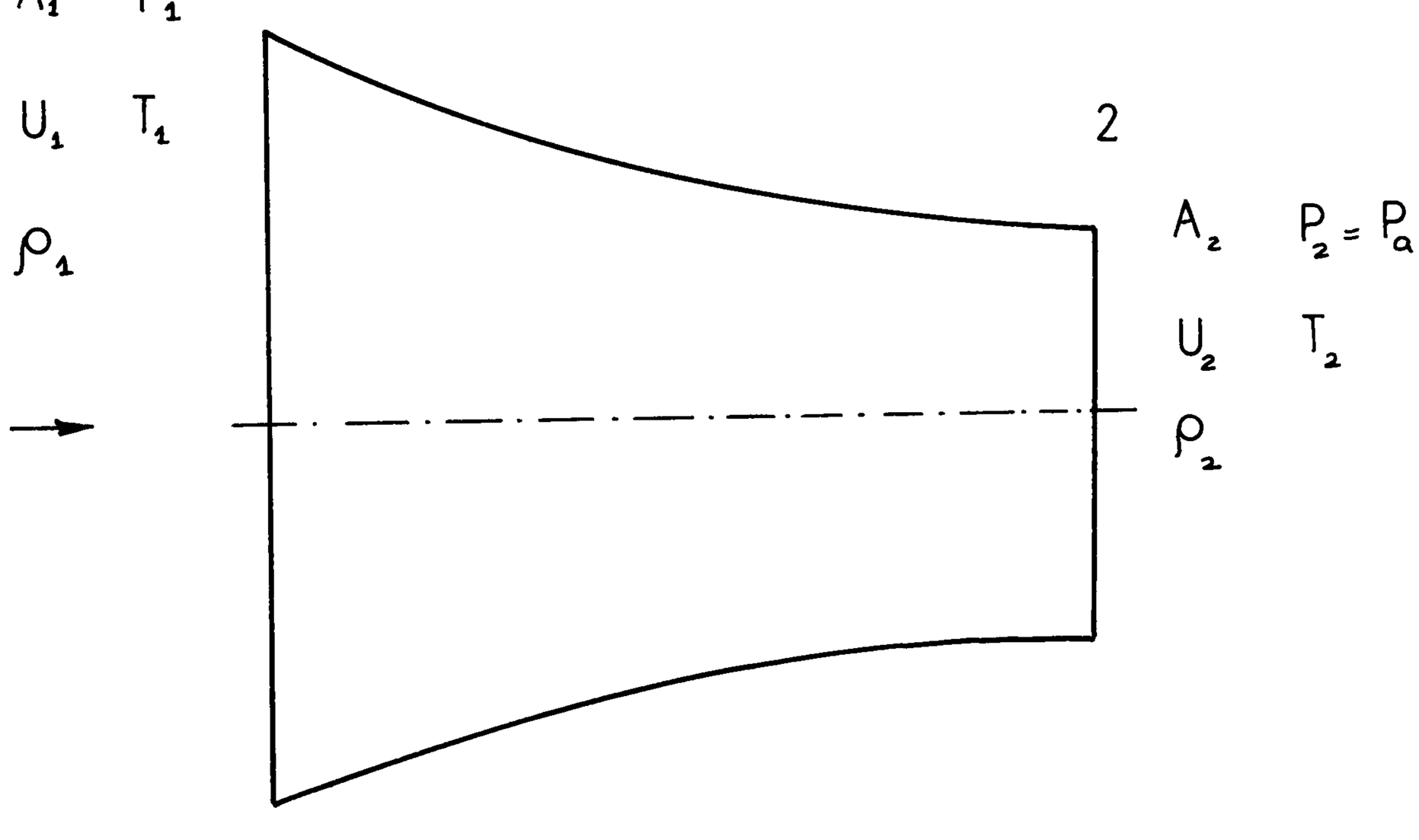

Fig 2.5 Jet Nozzle

In the equations 2.6-1 and 2.6-2 y is defined as;

2.6-3
$$y = r_p^{0.286} \equiv \left(\frac{P_a}{p_1} \right)^{0.286} < 1$$

At the exit of the nozzle the velocity of air U_2 is obtained from the steady flow energy equation, assuming adiabatic flow. We get (62) (Fig 2.5),

$$U_2 = \sqrt{2C_p(T_1 - T_2)}$$

Where T_1 and T_2 are absolute temperatures of air at locations 1 and 2. C_p is the specific heat of the air.

The mass flow rate through the nozzle $\dot{m}$ may now be expressed using the isentropic nozzle efficiency and the velocity U_2 as follows;

2.6-4
$$\dot{m} = p_a \frac{\sqrt{2\eta_E}}{\sqrt{T_a}} \frac{\sqrt{C_p}}{k_a} A_2 \frac{\sqrt{1-x}}{1-\eta_E(1-x)}$$

Where

$$x = \exp\left(1 - \frac{1}{\gamma}\right)$$

η_E is nozzle isentropic expansion efficiency. k_a is the gas constant for air.

The momentum flow rate of air jet through the nozzle is given by;

2.6-5 $\dot{Q}_2 = \dot{m} U_2$

Eliminating y between the equations 2.6-1 and 2.6-2, P_N may be expressed as;

2.6-6
$$P_N = K3 \cdot \frac{\sqrt{(4C_\mu + K1 \cdot t)}}{K1 \cdot t - C_\mu}$$

Where K1, K2 and K3 are constants.

Where the function represented by the equation 2.6-6 does not have an extremum with respect to "t" and within the practical range of values for "t" $dP_N/dt < 0$. From the equation 2.6-6 can be seen that, as the jet height ratio increases the required power for the formation of the jet decreases.

From the equation 2.6-1 for given values of y, as the non-dimensional jet height (t) increases the jet momentum coefficient increases and hence the lift coefficient C_L of the cylinders of the machine increases. Therefore ideally, by increasing the non-dimensional jet height, more lift can be produced. However the magnitude of the jet-height ratio t is limited by the practical arrangement for introducing the two-dimensional wall-jet. It is also observed that the drag coefficient will also increase with greater values of t due to the increased projected area of the octagonal cylinder. Equations 2.6-4 2.6-1 and 2.6-6 are used for calculation of C_μ, $\dot{m}$ and P_N in the design of the wind machine.

2.7 Maximum Possible Power Coefficient of a Wind Turbine Generator

Traditional Betz limit has been identified as the maximum possible power coefficient, for a wind machine operating under ideal flow conditions. However it is known for certain configurations of wind machines theoretical analysis shows that the power coefficient may exceed the traditional Betz limit of 16/27 (58,59). The proposed Vertical Axis Wind Turbine Generator using the wall-jet principle differs from the conventional wind machines and a reappraisal of the applicability of the Betz limit is necessary. The main reason for exceeding the Betz limit arises due to the pressure recovery in the region between the up-wind and the down-wind active elements comprising the wind turbine. Therefore a modified Betz-type limit is derived accounting for the pressure variation within the stream tube, up-stream and down-stream of the actuator disc and the associated shapes for the stream tube (42). The quantitative effect of the pressure variation and the associated shape for the stream tube is expressed through the use of pressure variation coefficient K.

The basic assumptions in the Betz's analysis based on the stream tube for an actuator disc, shown in the Fig. 2.6 may be summarized as follows;

(i) Steady, incompressible, inviscid flow

(ii) Pressures on the surfaces of the stream tube, upstream and down-stream of the actuator disc are equal to p_∞ although the pressures at inlet and outlet of the actuator disc differ from p_∞.

The assumption (ii) is inconsistent with the steady flow energy equation for inviscid flow. This may be reconciled only by assuming that the stream tube changes in area rather abruptly across the actuator disc as shown in the Fig. 2.7 (for $K = 0$).

2.7.1 Betz-Type Limit for Coefficient of Performance Allowing for the Pressure Variation - The Flow Model

Fig 2.6 shows the one-dimensional steady flow model. Mass conservation equation for incompressible fluid flow gives;

2.7-1 $$A_1 V_\infty = A_d V_d = A_w V_w$$

The linear momentum equation for inviscid, incompressible flow for the control volume enclosed by the section 1 and 4 and by the stream tube (Fig 2.6) is given by;

2.7-2 $$F - A_d(p_2 - p_3) = \dot{m}(V_w - V_\infty)$$

The energy equations for the control volume between the sections 1 and 2 , 3 and 4 (Fig 2.6) are given by;

2.7-3 $$\frac{p_2 - p_\infty}{\rho} = \frac{V_\infty^2 - V_d^2}{2}$$

2.7-4 $$\frac{p_3 - p_\infty}{\rho} = \frac{V_w^2 - V_d^2}{2}$$

From the equations 2.7-3 and 2.7-4 on substraction,

2.7-5 $$\frac{p_2 - p_3}{\rho} = \frac{V_\infty^2 - V_w^2}{2}$$

The external force F on the control volume appearing in the linear momentum equation (2.7-2) is obtained by considering the pressure forces on the surface of the control volume. We have,

2.7-6 $$F = p_u\left(A_d - A_1\right) + p_D\left(A_w - A_d\right) - p_\infty\left(A_w - A_1\right)$$

Where the mean pressure p_u and p_D are assumed to be given by;

2.7-7 $$p_u = p_\infty + \frac{K_u\left(p_2 - p_\infty\right)}{2}$$

2.7-8 $$p_D = p_\infty + \frac{K_D\left(p_3 - p_\infty\right)}{2}$$

Assuming that $K_u = K_D = K$, and using the equations (2.7-1), (2.7-7) and (2.7-8) with equation (2.7-6), F may be expressed as;

2.7-9
$$F = \frac{KA}{2}\left[(p_2 - p_3) - \frac{V_d}{V_\infty}(p_2 - p_\infty) - \frac{V_d}{V_w}(p_\infty - p_3) \right]$$

Substituting for $(p_2 - p_\infty), (p_3 - p_\infty), (p_2 - p_3)$ from the equation 2.7-3 to 2.7-5 and for F from the equation 2.7-9 into the equation 2.7-2, we get the relationship between the velocity ratios as follows;

2.7-10
$$\phi^2 - \phi(\alpha\psi - 1) + \beta\psi^3 = 0$$

The relationship between ϕ and ψ corresponding to the traditional Betz's analysis is obtained from the equation 2.7-10 by putting the value of $K = 0$. We get for this, special case,

$$(1 + \phi) = 2\psi$$

2.7.2 The Coefficient of Performance

The coefficient of performance of a wind turbine is given by;

2.7-11
$$C_p = \frac{(V_\infty^2 - V_w^2)/2 \cdot (\rho V_d A_d)}{(\rho A_d V_\infty^3)/2}$$

$$\equiv \quad \psi\left(1-\phi^2\right)$$

The optimum value of C_p is then obtained by maximising the C_p given by the equation 2.7-11 with the constraining relationship between the ϕ *and* ψ given by the equation 2.7-10. Here the value of K is a parameter which is dependent on the shape of the stream tube.

It is readily verified that for $K=0$ the traditional Betz limit for C_p of 16/27 occurs for $\phi=1/3$ *and* $\psi=2/3$.

2.7.3 The Effect of Pressure Variation

The effect of allowing the pressure to change gradually on the surface of the stream tube, which follows from the energy equation for steady inviscid flow, may be studied by taking different values for K_u *and* K_D. The values of K_u *and* K_D are associated with a corresponding shape of the stream tube, up-stream and down-stream of the actuator disc, respectively. In the present simplified analysis, equation 2.7-10 and 2.7-11 are applicable where, $K_u = K_D = K$. The possible shapes of stream tubes for values of K ranging from 0 to 1 are shown in the Fig 2.7 and Fig 2.8. It may be noted that the traditional Betz's analysis corresponding to $K=0$ and the associated stream tube has quite an abrupt

change in cross-sectional area close to the actuator disc. Figs 2.9 and 2.10 show the variation of ϕ and C_p with respect to ψ for values of K ranging from 0 to 1.0, computed from the equations 2.7-10 and 2.7-11. It can be seen in Fig 2.9 that ψ attains a minimum value, ψ_{min} for given K and $\phi-\psi$ graphs may be considered to be in two parts, Viz; a "lower leg" and an "upper leg" corresponding to the lower and the higher values of ϕ for given ψ. The "lower legs" of $\phi-\psi$ graphs for given K in Fig 2.9 correspond to the "higher legs" of the $C_p-\psi$ graph for the same K of Fig 2.10, and vice-versa. From the definition of ϕ and the equation 2.7-1, a higher value of ϕ signifies a lower wake area for the stream tube. Hence the "lower leg" of the $C_p-\psi$ graphs correspond to lower wake areas, which has an obvious physical significance. For values of K in the region of 0. to 0.18, the lower legs of the $C_p-\psi$ graphs exhibit a maximum.

The simple assumption of using the arithmetic mean value of pressures at stations 1 , 2 and 3 , 4 as the constant mean pressure on the stream tube surface between the sections 1 , 2 and 3 , 4 respectively, corresponds to $K=1.0$ However for $K=1.0$ it is noted from the figures 2.9 and 2.10, $\phi=\psi=1$ and $C_p=0$ is the only possible solution.

Fig 2.11 shows the variation of ψ_{min} with respect to K. Fig 2.12 shows the variation of C_p , A_w/A_d , A_∞/A_d with respect to K, for the location of maximum value of C_p on the "lower leg" of the C_p-ψ graphs.

The use of stream tube in the Betz's analysis arises from the requirement that the wind machine operates in the atmosphere, with air intake from atmosphere and air exit back to atmosphere. This is in contrast with the situation encountered in conventional turbo-machines where the handling of the fluid supply and disposal does not directly influence the operating parameters of the machine. Hence Betz limit is meaningful only for the conditions of operation of wind machines and is dependent on the shape of the stream tube past the actuator disc.

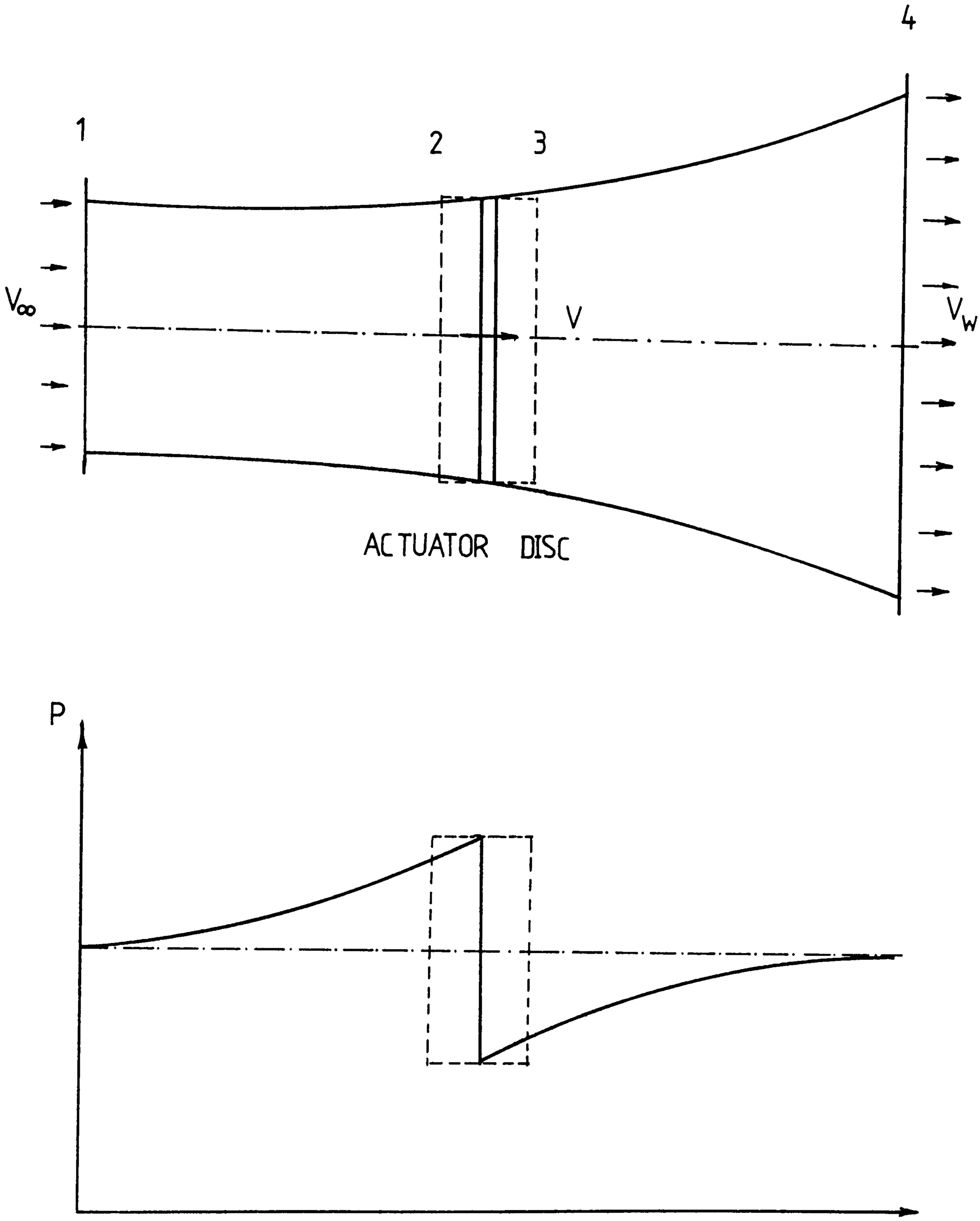

Fig 2.6 Flow Model and the Static Pressure Variation

K = 0

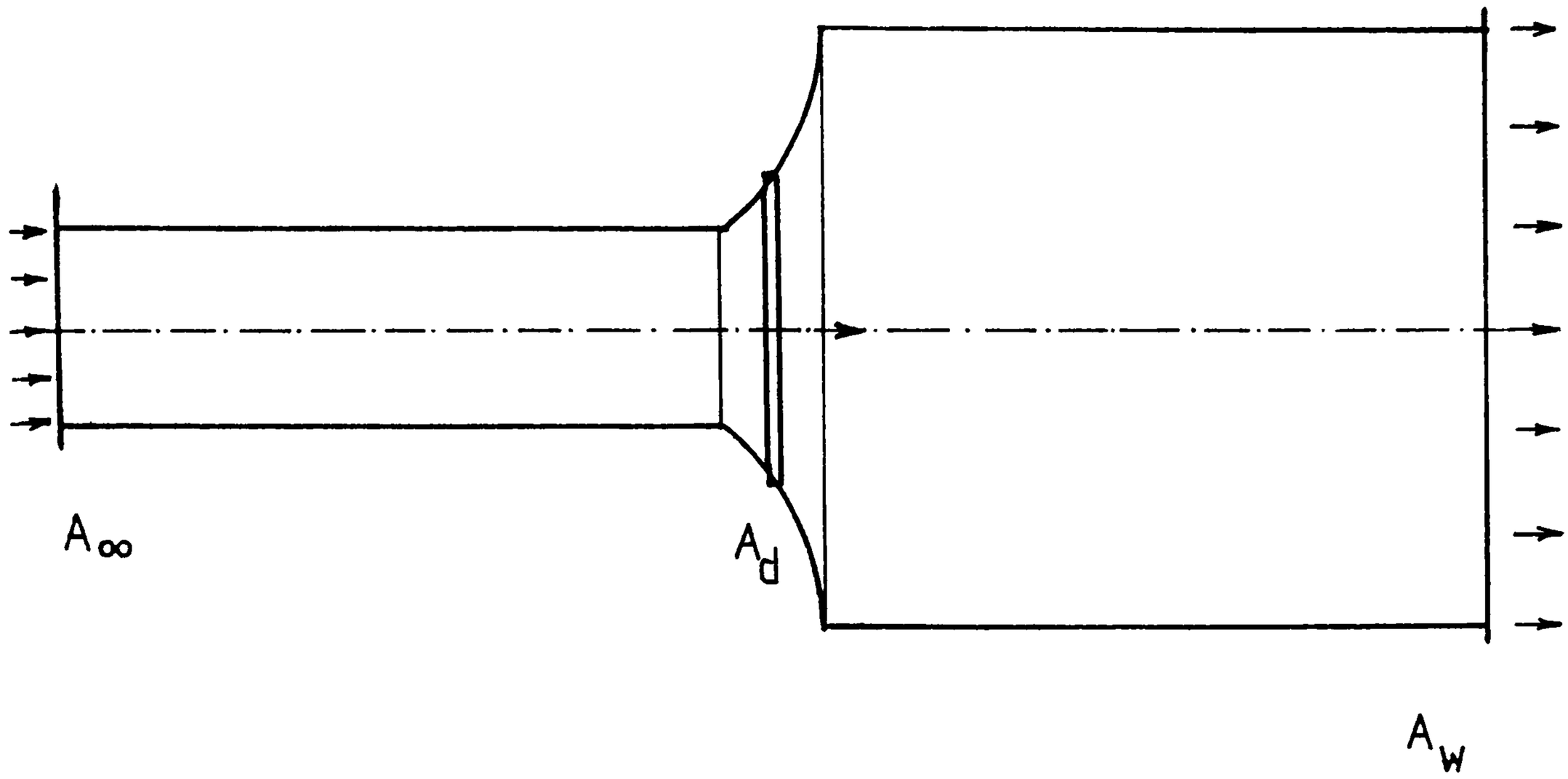

K = 0.1

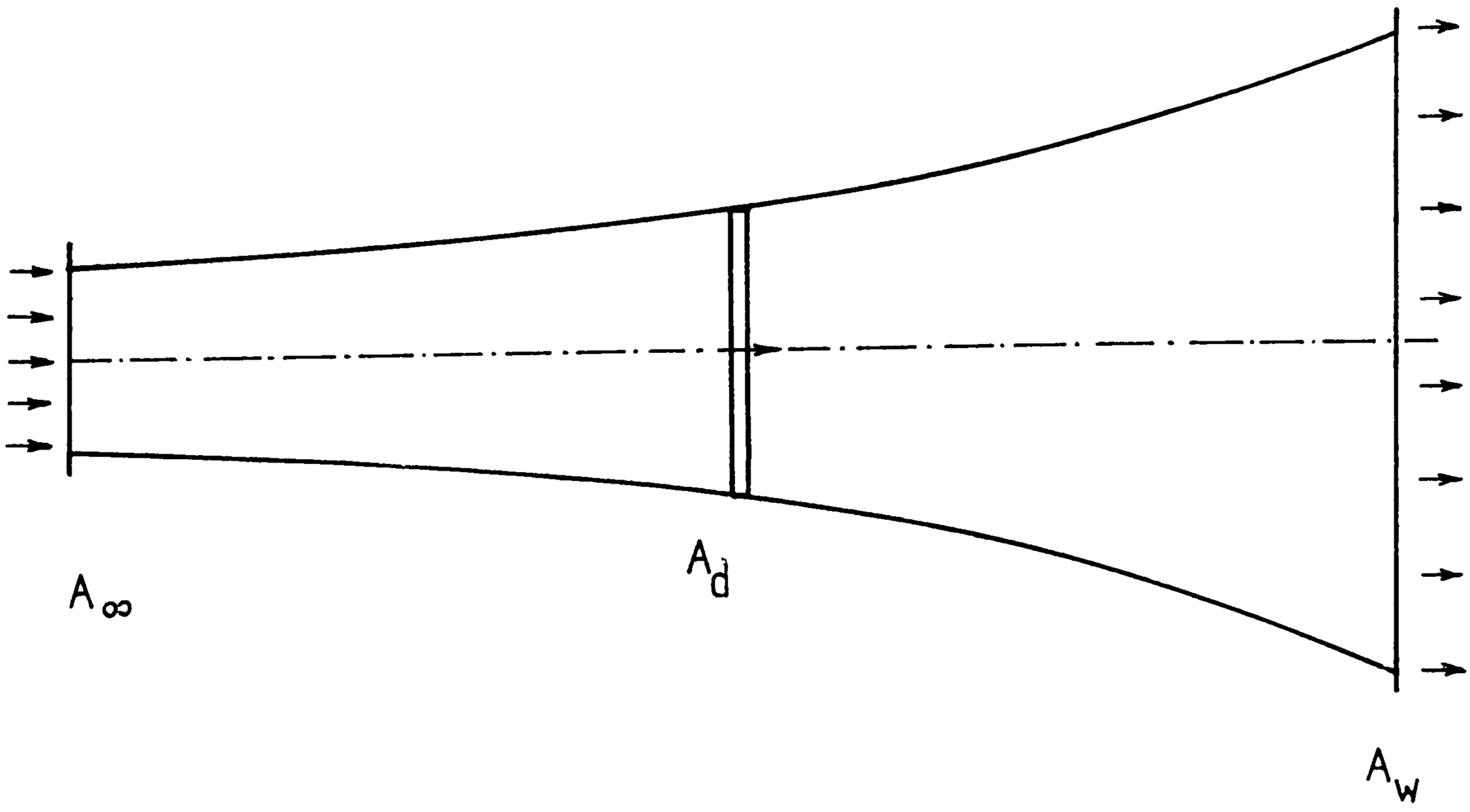

Fig 2.7 Shape of Stream Tubes
for K=0, K=0.1

K= 0.16

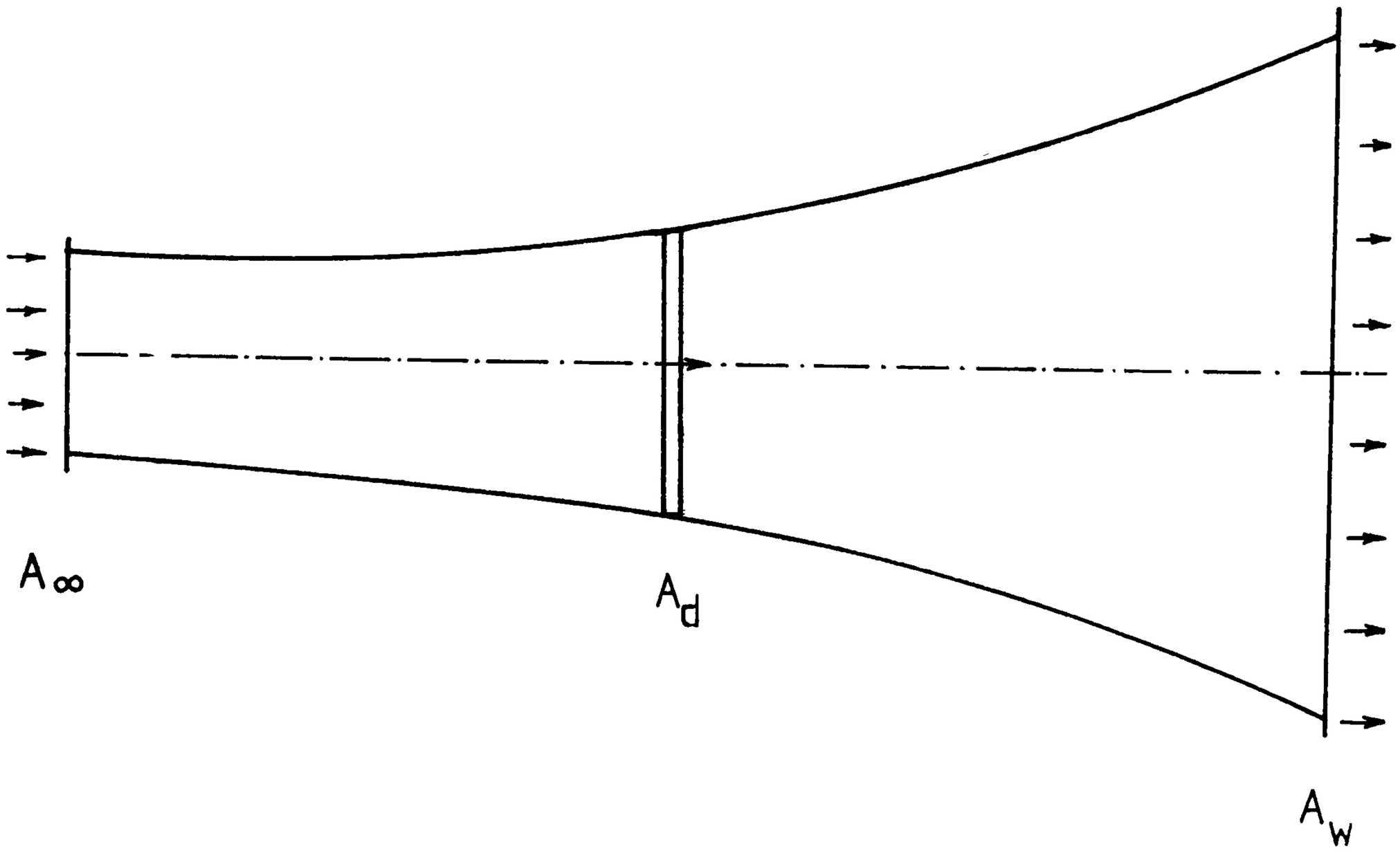

K= 1.0

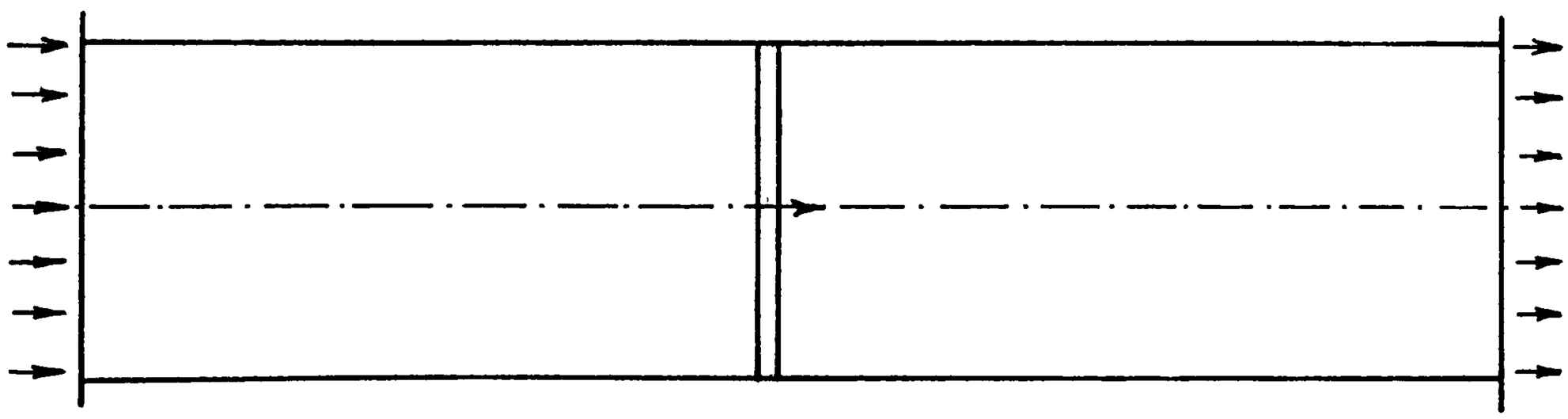

Fig 2.8 Shape of Stream Tubes
for K=0.16, K=1.0

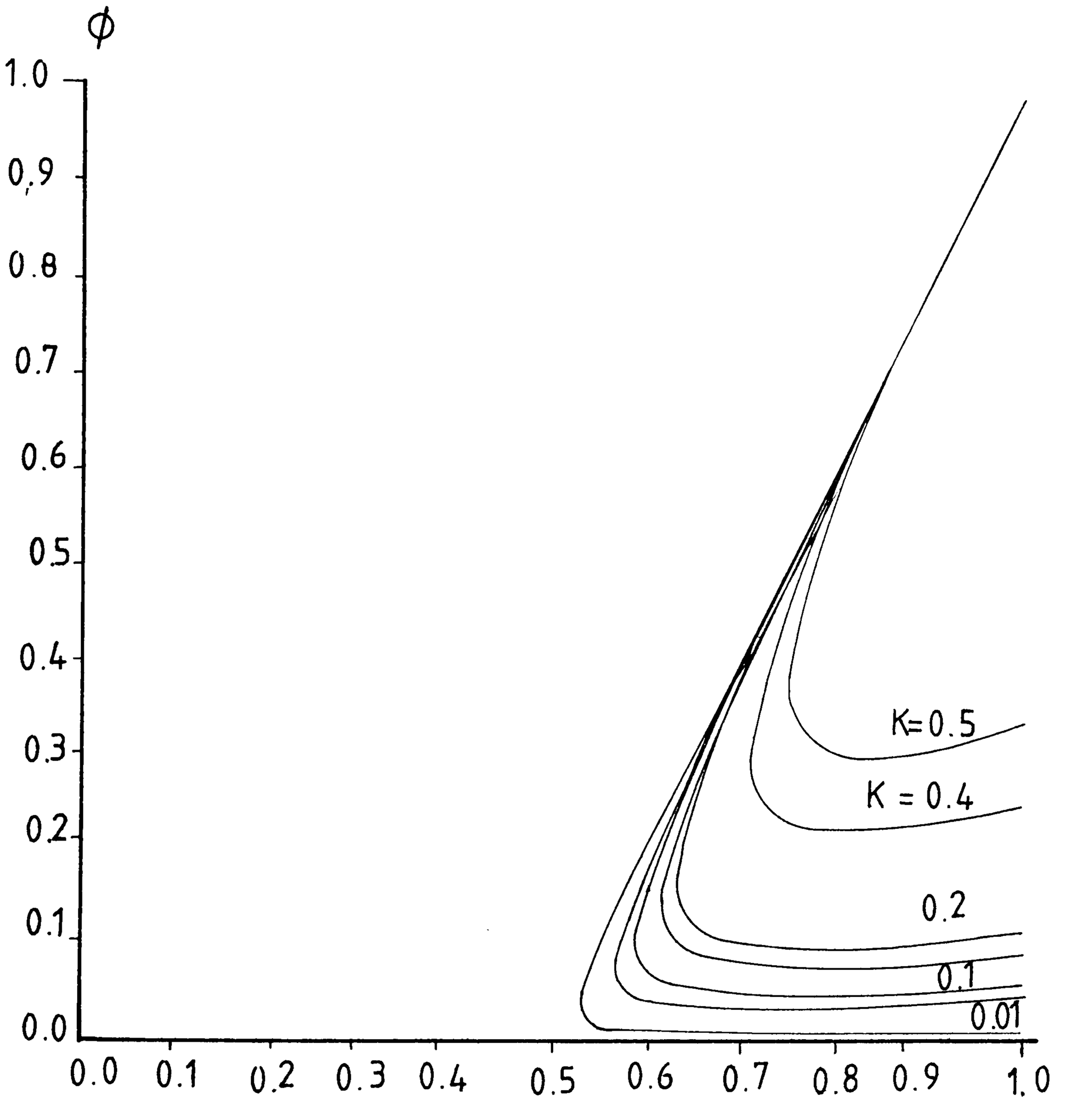

Fig 2.9 ϕ - ψ Relationship

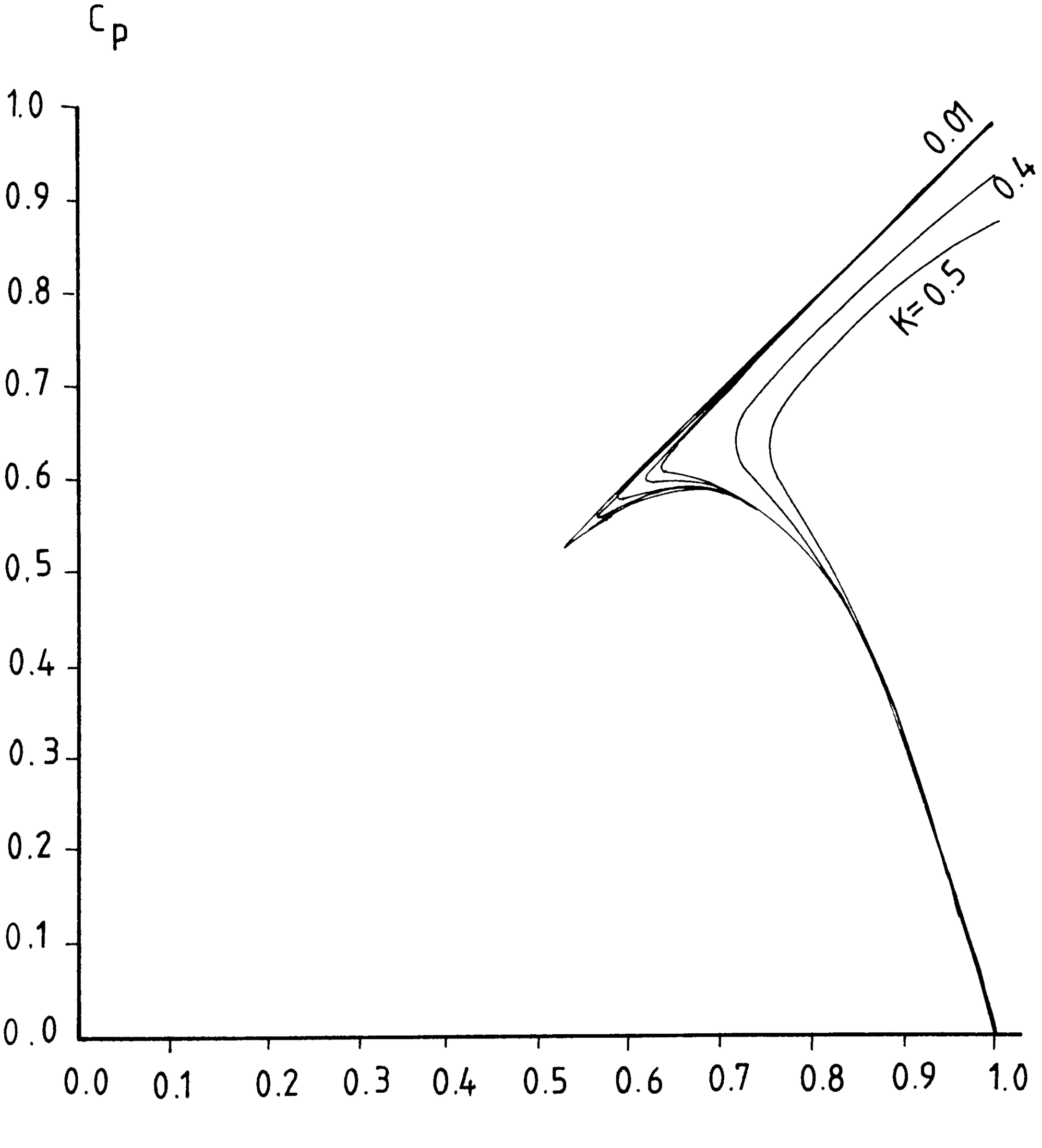

Fig 2.10 C_p - ψ Relationship

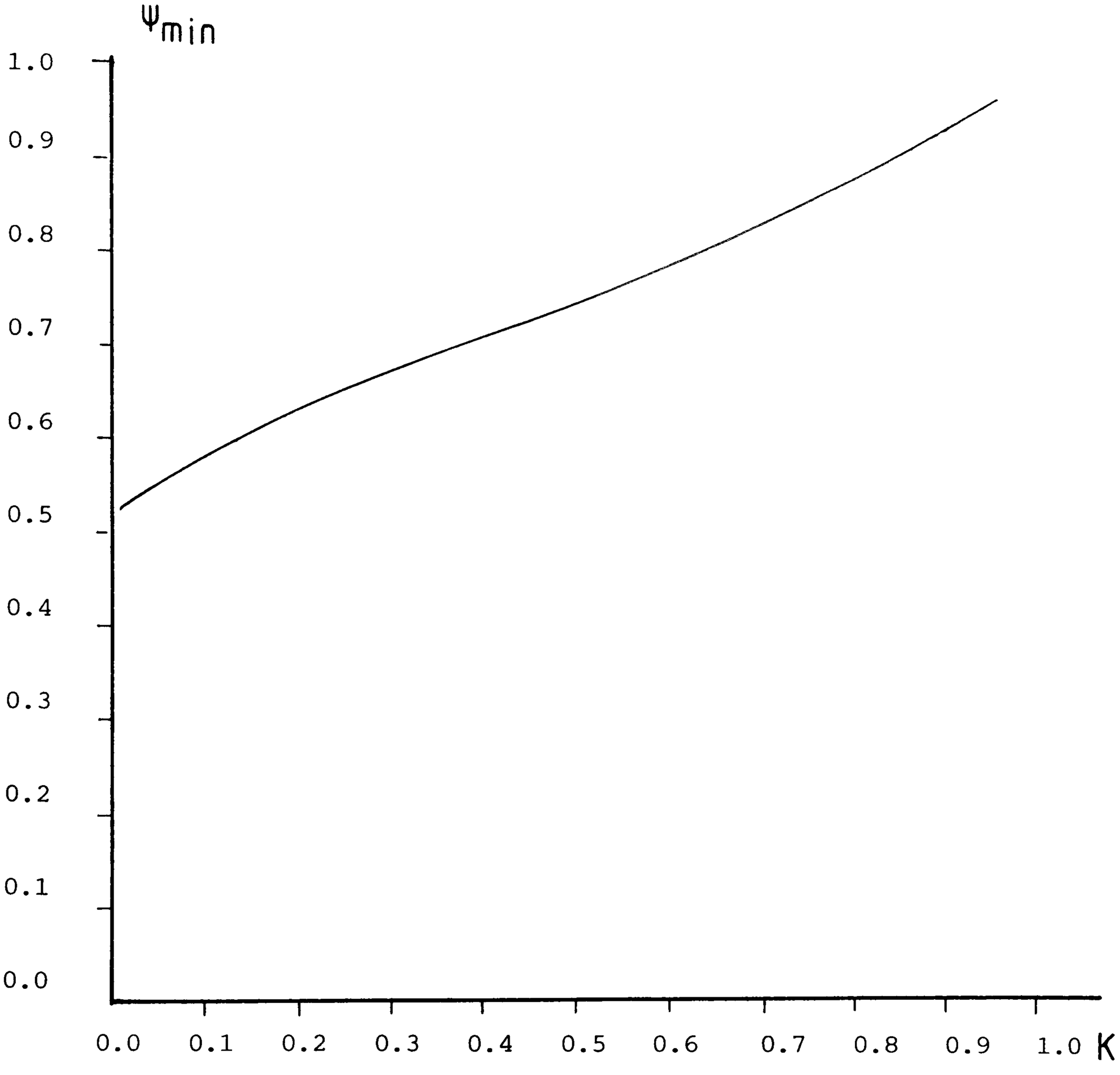

Fig 2.11 U_{min} - K Relationship

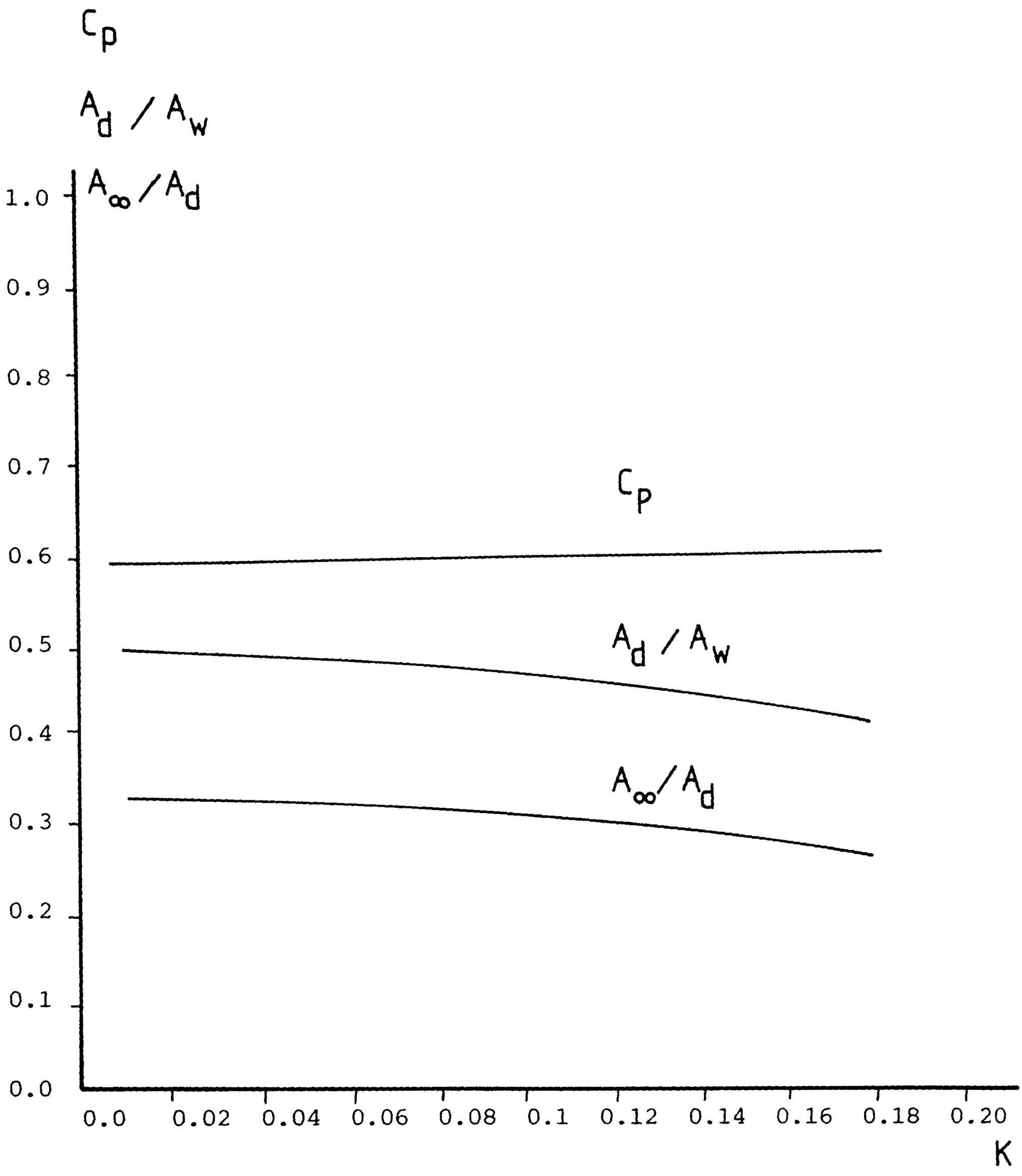

Fig 2.12 C_p, A_d/A_w, A_∞/A_d Against K for C_p Max

CHAPTER 3

3 THEORYRETICAL ANALYSIS - FLUID FLOW PAST AN OCTAGONAL CYLINDER WITH TANGENTIAL WALL-JETS

3.1 Basic Principle of Lift Generation Due to The Modified Boundary Layer

Introduction of a tangential wall jet at an appropriate location on a symmetrically placed bluff body, such as an Octagonal cylinder (i.e. cylinder of octagonal cross-section) in a free stream, gives rise to a high lift force. This is due to the modification of the boundary layer flow, influenced by the tangential wall-jet. A two-dimensional flow past the bluff body is considered as depicted in Fig 3.1. Where the jet momentum is adequate, boundary layer separation is completely eliminated in the down stream region from the point where the jet is introduced upto the down stream separation stream line. On the other side of the cylinder beyond the separation stream line (Fig 3.2), where the jet influence is negligible, separation occurs over a considerable region towards the trailing side. The flow pattern outside the boundary layer produced in the above situation approximates to that of the two-dimensional non-viscous fluid flow past circular cylinder with a superimposed circulation. For a such a case, potential flow theory establishes the

presence of a high lift force (15). The modification in the boundary layer flow for the case of a rotating cylinder in a free stream of cross-flow, resulting from the reduced difference between the velocities of the fluid and the solid wall approximates the boundary layer flow with the wall-jet for a non-rotating cylinder (62) (Fig 2.1).

The use of tangential wall-jet for high lift generation on an octagonal cylinder, has several advantages over the traditional lift generating methods using aerofoil sections (See 2.6.2). In view of this, predictions of the lift and the drag forces due to this phenomenon have been made (2.3). Only a limited information is available on the lift and drag coefficients due to the tangential wall-jets, all of which are on circular cylinders (26,27,28). In order to carry out a comprehensive investigation of the boundary layer modification on the lift and the drag forces for octagonal cylinders, theoretical analysis has been carried out, using mathematical models of fluid flow.

3.2 Mathematical Models for Fluid Flow

Introduction of end plates to the octagonal cylinder considered in the section 2.6.3 has the effect of minimizing the flow in the direction parallel to axis

of cylinder, and hence it is considered sufficient to treat the present problem as a two-dimensional flow. Initially a flat plate with a tangential wall-jet in a free-stream, situated at an angle to the stream was considered as an exploratory model to study the nature of flow on any one of the sides of the octagon. This was a steady flow, over a smooth plate submerged in a semi-finite expanse of the fluid entering with a uniform velocity and subjected to a tangential wall-jet of the same fluid issuing from the nozzle as depicted in the Fig 3.3. In this representation as the jet leaves the nozzle, due to the velocity discontinuity a shear layer develops on the fluid side, and the boundary layer develops on the wall-side. Experience in developing this theoretical model was useful in formulating the two-dimensional mathematical models discussed in the sections 3.2.1 and 3.2.2. For the present problem, in replacing the three-dimensional physical models by two-dimensional models, the solutions have become simpler. However, these being two-dimensional, it is impossible to represent actual three-dimensional fluid flow situation. Therefore two possible representations are proposed (Model-1 and Model-2). Solutions for both the models out-side the boundary layer (see 3.3.1) are evaluated and compared (see 3.6.7).

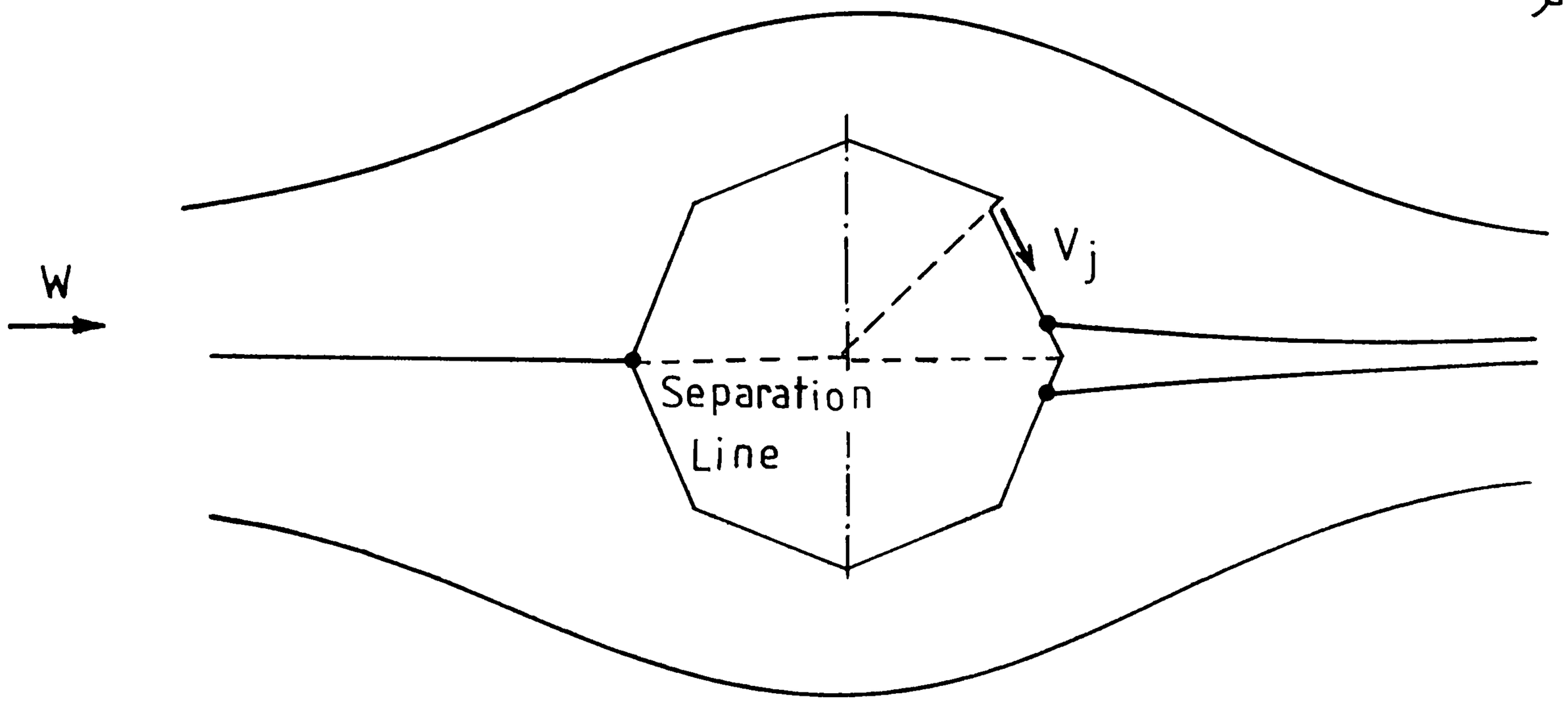

Fig 3.1 Flow Past an Octagonal Cylinder
with out a Tangential Wall-jet

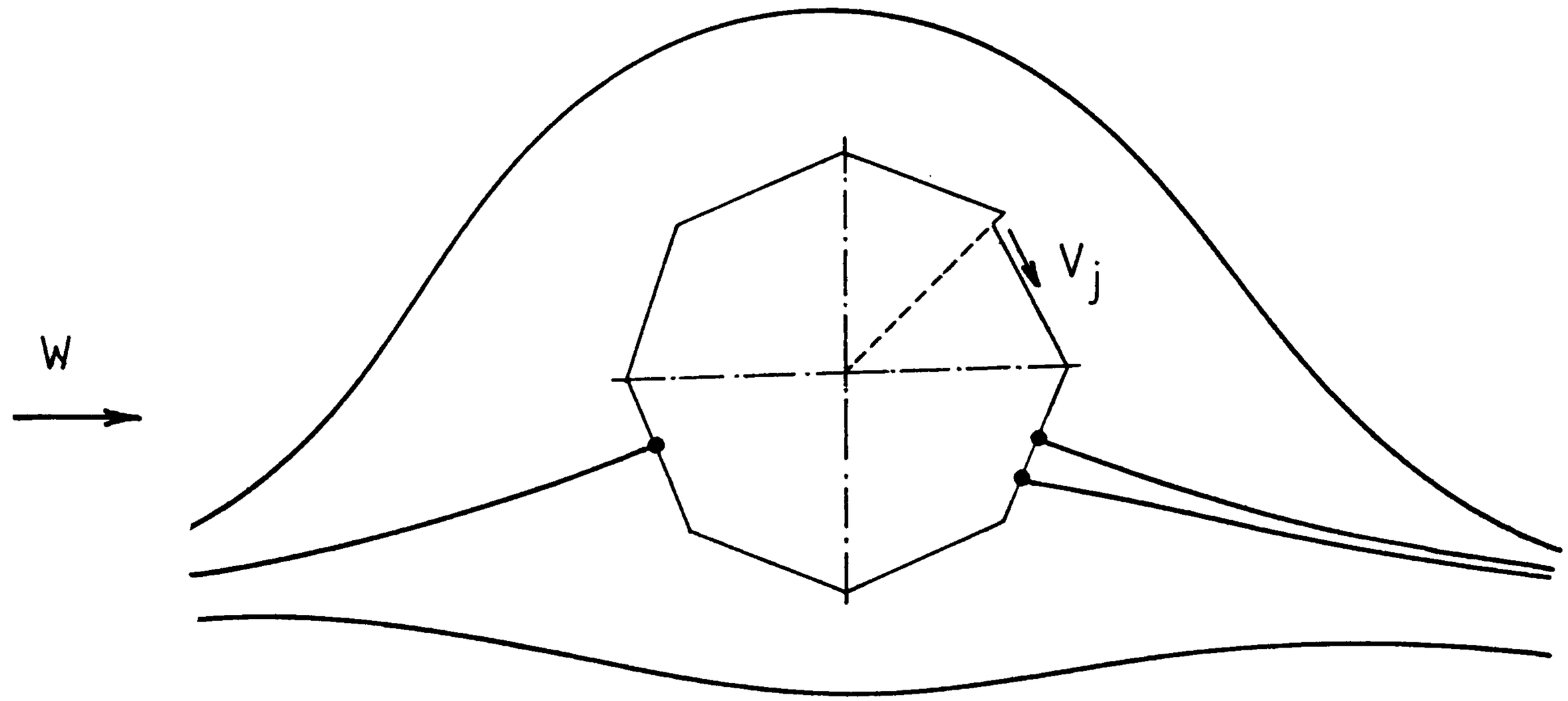

Fig 3.2 Flow Past an Octagonal Cylinder with a Tangential Wall-jet

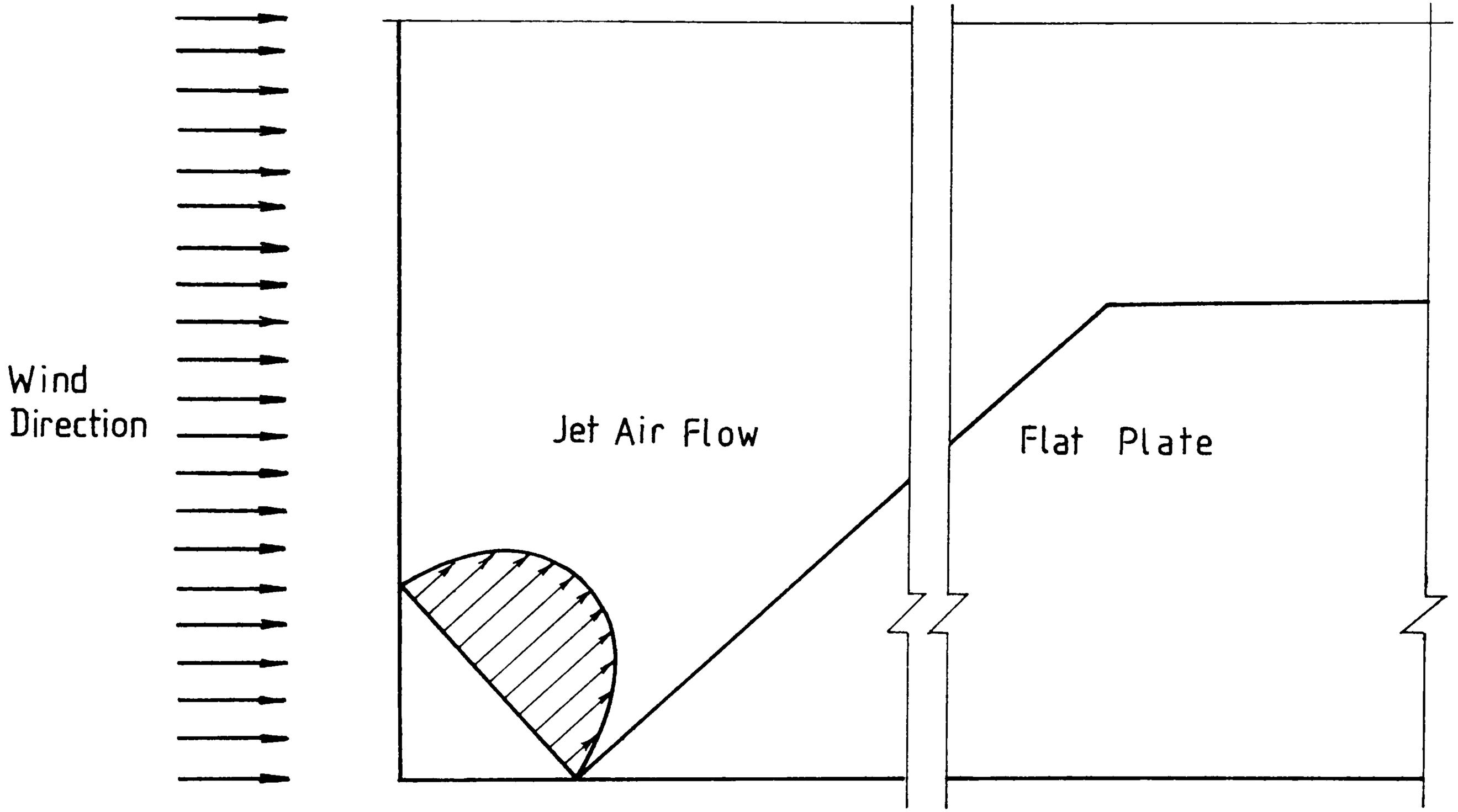

Fig 3.3 Two-Dimensional Flow Model for the Flat Plate with a Tangential Wll-jet

3.2.1 Two-dimensional Model With an Octagonal Cross-section With a Wall-jet and a Location of Air Withdrawal (Model-1)

The first two dimensional steady flow model considered, consists of an octagon placed in an uniform stream of air and subjected to a tangential wall-jet at an appropriate location. The quantity of air which is introduced as the wall-jet is drawn inwards at a diametrically opposite location on the octagon (Fig 3.4). The boundary conditions are prescribed according to the physical situation of the fluid boundaries except those at the point of infinity which are simulated by finite coordinates to create the outer contour and to facilitate numerical integration procedures. The outer contour is defined by the points A'(10,10), B'(-10,10), C'(-10,-10), D'(10,-10). (Fig 3.4). The free stream enters at B'C' and discharges through A'D' and on these boundaries stream function changes linearly with distance measured along the boundaries. It is assumed that there is no flow across boundaries A'B', C'D'.

On the inner contour C2, at the location of the jet entry, AB, the velocity profile is represented by the 1/7 th power law (see Appendix 3B). The stream function along the contour C2 from point B to F is a

constant and equal to the stream function at B, since there is no flow across this part of the contour. The same is true for points G to A and the stream function is having a constant value equal to that at point A. At the location of air withdrawal (F to G) the stream function is assumed to vary linearly over the distance F to G. The zero slip stream line connects the outer contour C1 with the inner contour C2 at point S. Therefore from G to A the stream function has a zero value. The contours C1 and C2 are divided into segments (Fig 3.7) as detailed in the Table 3-1.

Table 3-1

Side	A-B	B-C	C-D	D-E	E-F	F-G	G-H
Number of Segments	6	10	10	10	10	6	10
Side	H-I	I-J	J-A	A'-B'	B'-C'	C'-D'	D'-A'
Number of Segments	10	10	10	4	8	4	8

3.2.2 Two-dimensional Model With an Octagonal Cross Section With a Wall-jet (Model-2)

The second two-dimensional steady flow model considered consists of an octagon placed in an uniform stream of air and subjected to a tangential wall-jet at an appropriate location. The quantity of air which is introduced as the wall-jet is drawn inwards from the axial direction normal to the plane of two-dimensional flow. In order to satisfy the continuity equation in two-dimensional flow arrangement, a "δs" thickness strip which connects the inner contour with the outer contour is introduced (Fig 3.5). The thickness of the strip should be as small as possible to minimize the influence of the strip on the flow pattern around the octagon cylinder and the jet, and in the present case it is selected to have a non-dimensional value of 0.01 and located at the upstream stagnation point. This means the strip is about 1/100 in width compared with the side of the octagon. Further the shape of the strip may be adjusted to follow closely the slip stream line through the stagnation point, by a trial and error procedure.

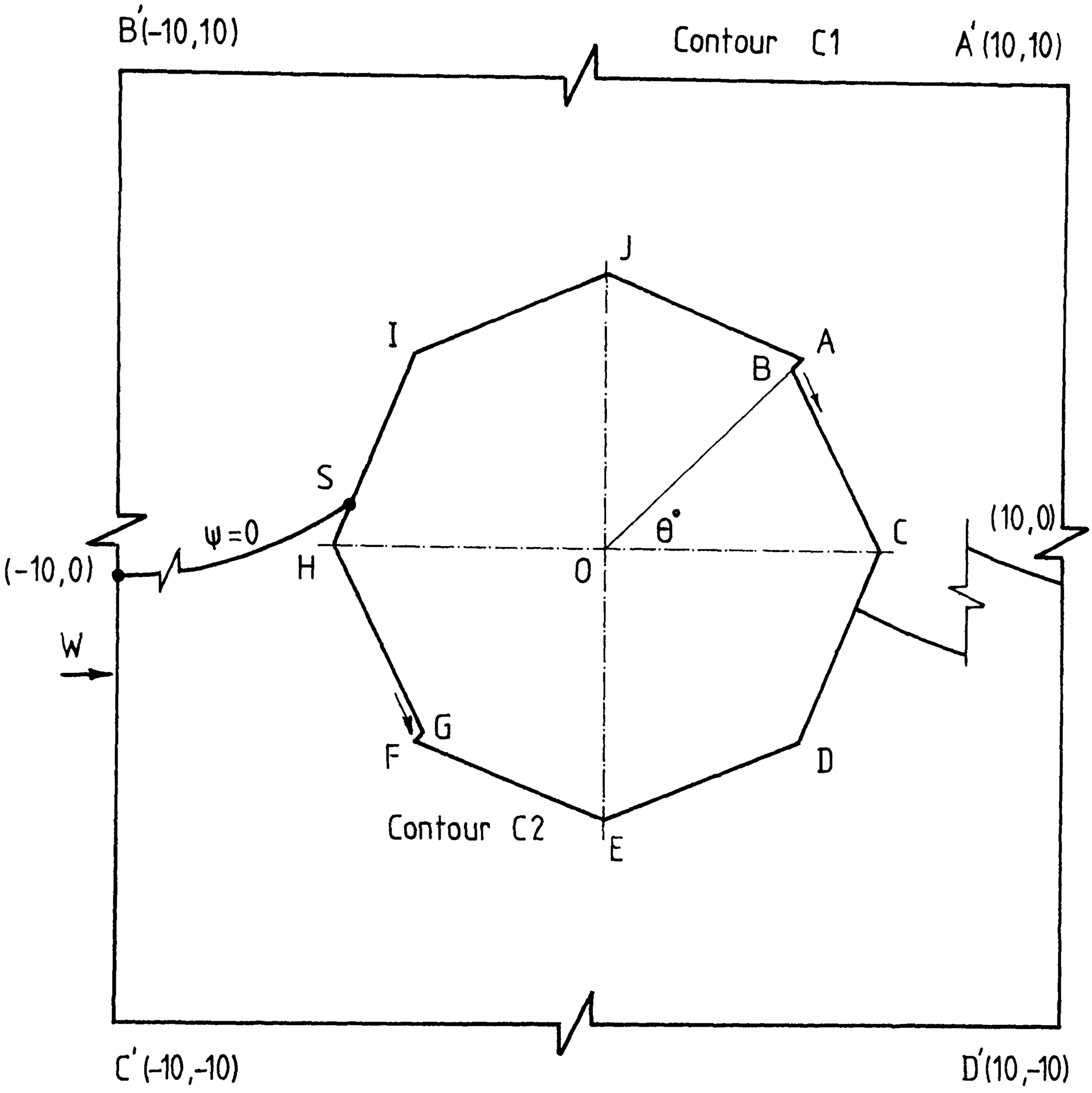

Fig 3.4 Two-Dimensional Flow Model for the Octagonal Cross-section with a jet and a air Withdrawl (Model-1)

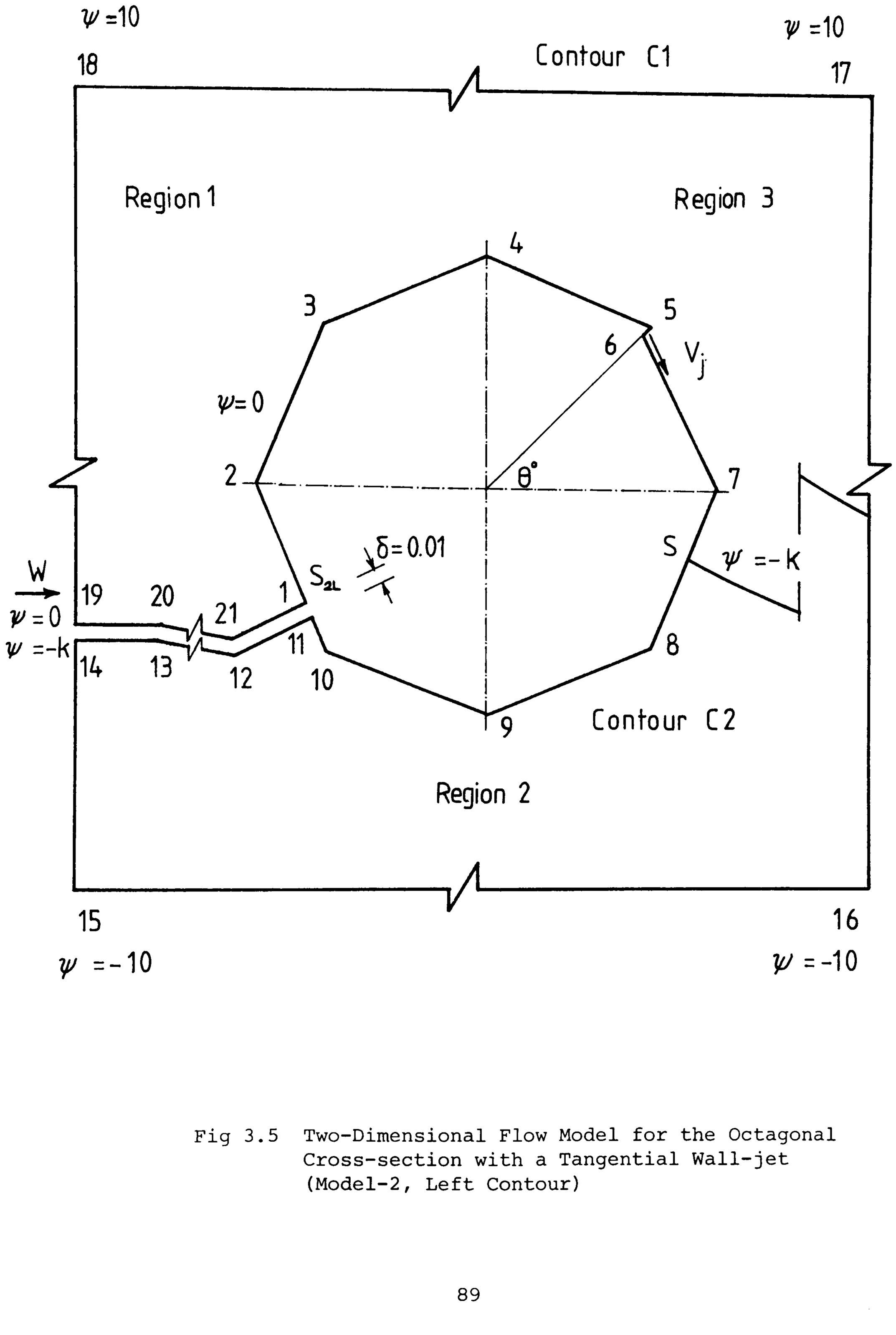

Fig 3.5 Two-Dimensional Flow Model for the Octagonal Cross-section with a Tangential Wall-jet (Model-2, Left Contour)

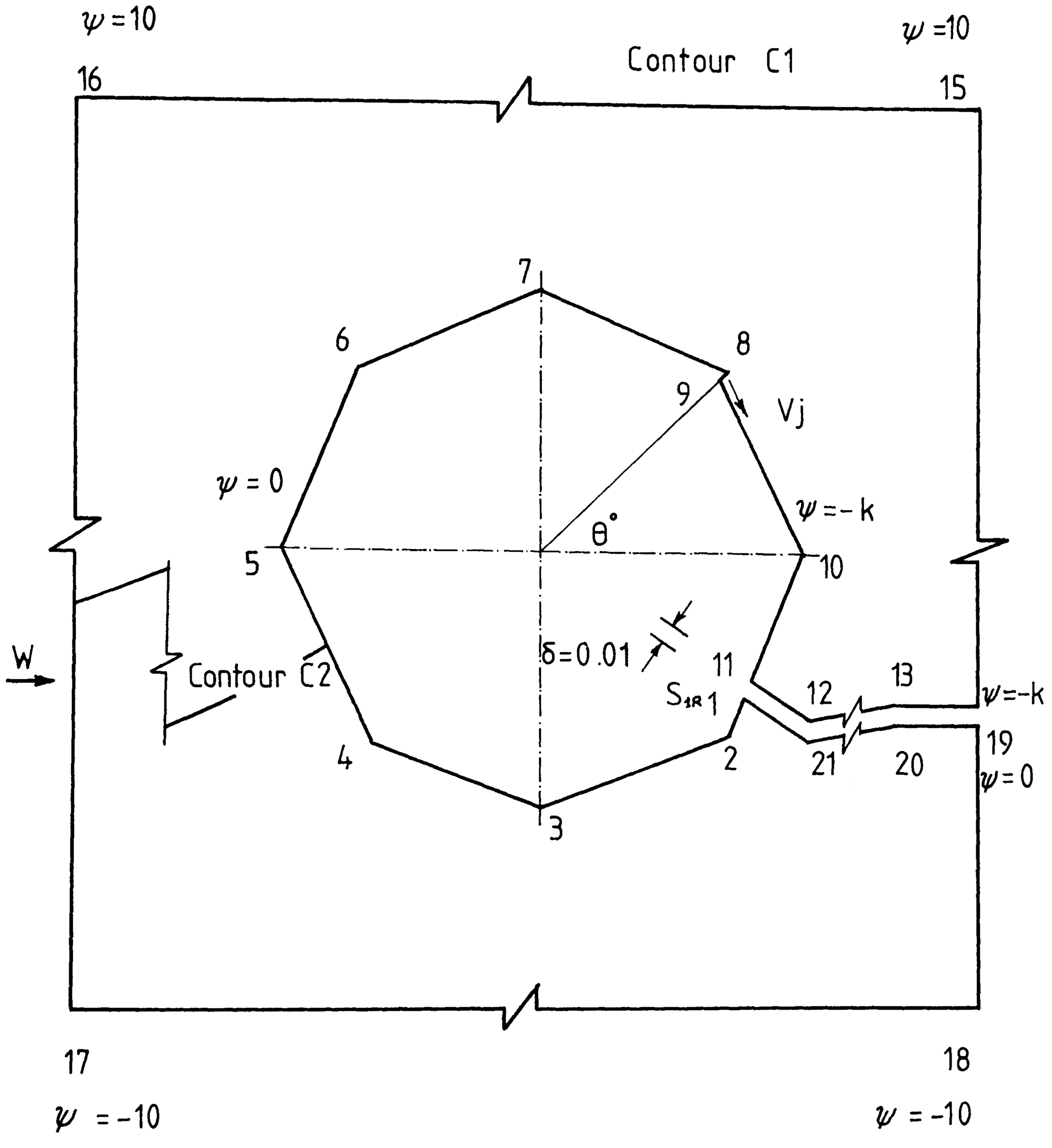

Fig 3.6 Two-Dimensional Flow Model for the Octagonal Cross-section with a Tangential Wall-jet (Model-2, Right Contour)

The method of iteration used to locate the upstream stagnation point, where the strip meets the inner contour C2 is as follows. Initially an arbitrary strip (1,21,20,19,11,12,13,14) (Fig 3.6) on the down stream side is selected. The two-dimensional flow field is now defined by a single contour enclosing a region. This can be seen in the Fig 3.6 following the point numbering from 1 to 21. This flow field is called the "right Hand" flow system (Model-2R). The two-dimen-sioal flow system in the Fig 3.5 will be called as the "Left Hand" flow system (Model-2L) to distinguish the two. The contour of the Right Hand and Left Hand flow systems are divided into segments as indicated in the Table 3-2.

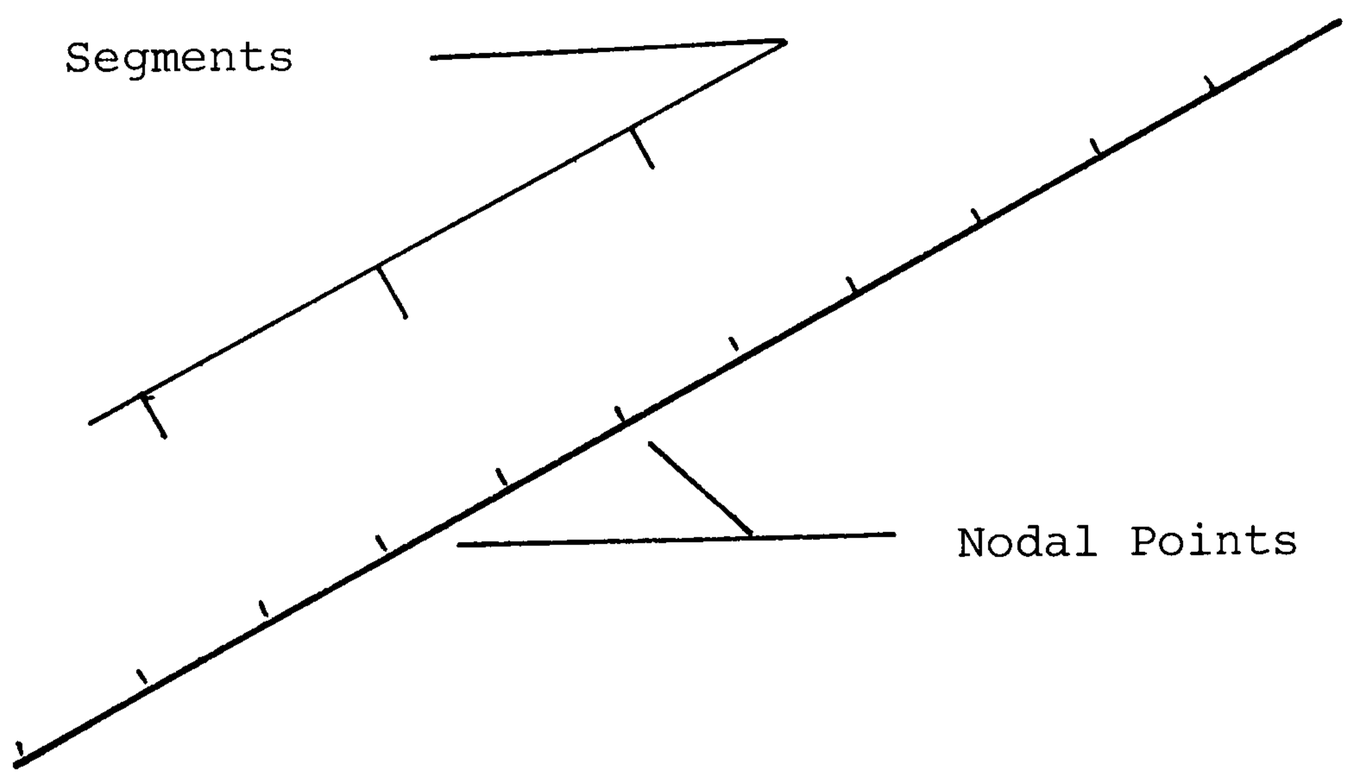

Fig 3.7 Segment and Nodal Points on an Octagonal Side

Table 3-2

Side	Model	1-2	2-3	3-4	4-5	5-6	6-7	7-8
Number of Segments	2R	n *	10	10	10	10	10	10
	2L					6	10	10

Side	Model	8-9	9-10	10-11	11-12	12-13	13-14	14-15
Number of Segments	2R	6	10	10-n *	1	1	1	4
	2L	10	10					

Side	Model	15-16	16-17	17-18	18-19	19-20	20-21	21-1
Number of Segments	2R	4	8	·4	4	1	1	1
	2L							

* Number of segments are decided by the Computer programme PART4N

In the Model-2R (Fig 3.6) as there is no flow across the contour joining the points 19, 20, 21, 1, 2, 3, 4, 5, 6, 7, 8 the stream function Φ has a constant value which is taken to be zero. On the jet (from points 8 to 9) the stream function is determined by considering the velocity profile for the jet in the form of 1/7 th power law (see Appendix 3B). Thus the stream function on the points 9, 10 and 10, 11 are equal to the stream

function at point 9 (=-K). On the slip stream defined by the points 11, 12, 13, 14 the stream function is given by $\Phi = -K$. From points 14 to 15 the stream function changes linearly from -K to +10. On the side joining points 15 and 16 the stream function is equal to +10 and the stream function changes linearly with the Y-coordinate and attains a value of -10 at nodal point 17. From points 17 to 18 the stream function remains a constant. The stream function changes linearly from points 18 to 19 where it attains the zero value at point 19. The above boundary values of the stream function are utilized in formulating the boundary conditions as discussed in the section 3.5.1.

3.3.1 Boundary Layer Flow and the Main Flow

The two-dimensional flow field surrounding the octagon is determined by the traditional method of dividing it into a boundary layer flow and an ideal fluid flow outside the boundary layer. The latter flow is referred to here as the "main flow". Boundary layer flow is determined by the momentum integral equation (3.7-1). The main flow, i.e., the flow outside the boundary layer is assumed to be incompressible and non-viscous so that this part of the flow may be determined by the potential flow theory (15).

3.3.2 Differential Equations for Stream Function

The partial differential equations for velocity and pressure are obtained on the basis of the momentum and the mass conservation equations for the incompressible viscous laminar fluid flow around the octagon cross-section. These are the traditional the Navier-Stokes equations, and can be expressed in the non-dimensional form;

3.3-1
$$U\frac{\partial U}{\partial X}+V\frac{\partial U}{\partial Y}=-\frac{\partial P}{\partial X}+\frac{\mu}{\rho c W}\left(\frac{\partial^2 U}{\partial X^2}+\frac{\partial^2 U}{\partial Y^2}\right)$$

$$U\frac{\partial V}{\partial X}+V\frac{\partial V}{\partial Y}=-\frac{\partial P}{\partial Y}+\frac{\mu}{\rho c W}\left(\frac{\partial^2 V}{\partial X^2}+\frac{\partial^2 V}{\partial Y^2}\right)$$

$$\frac{\partial U}{\partial X}+\frac{\partial V}{\partial Y}=0$$

For the assumed potential flow outside the boundary layer, where $\mu=0$, the equations (3.3-1) on introducing the two-dimensional stream function ϕ lead to Laplace's equation. For ϕ;

3.3-2
$$\nabla^2\phi=\frac{\partial^2\phi}{\partial x^2}+\frac{\partial^2\phi}{\partial y^2}=0$$

The transformation of the Navier-Stoks equation to the form of Laplace's equation for ϕ makes easier to obtain

a solution to the main flow of the present problem. However because of the assumption of potential flow in the transformation, the equation 3.3-2 does not represent a flow with a circulation. Therefore the solutions obtained by using the equation 3.3-2, are to be corrected to account for the circulation using the wind-tunnel data as shown in the section 3.6.8.

3.4.1 Boundary Conditions for the Model-1

For the fluid flow model-1 (3.2.1) the boundary conditions for the Laplace's equation along the contours C1 and C2 are specified by considering a uniform wind velocity across sides B'C' (Fig 3.4). The stream function at the mid-point of B'C' is arbitrarily taken to be zero. By considering the stream line through the stagnation point S, and the mid-point of B'C', the stream function for the point A is found to be zero. Determination of the boundary conditions on the contour C2 are discussed in the Appendix 3B. These give expressions for the stream function, in non-dimensional form (see Appendix 3A) along the contours C1 and C2 and are given by;

along GH, HI, IJ, JA $\Phi = 0$

along BC, CD, DE, EF $\Phi = -2K1K2\left(\frac{h}{2l}\right)^{8/7}$

along AB from A to mid-point AB $\Phi = -2K1K2Z^{8/7}$

along AB, from mid-point of AB to B

$$\Phi = -2K1K2\left(\frac{h}{2l}\right)^{8/7} + K1K2Z^{8/7}$$

along FG $\Phi = \Phi_B\left(\frac{X_G - X}{X_G - X_F}\right)$

along C'D' $\Phi = -10.$

along A'B' $\Phi = +10.$

along A'D' $\Phi = Y$

along B'C' $\Phi = Y$

3.3-3

Where

$$K1 = \frac{8}{7}\sqrt{\frac{C_\mu}{2R/h}}$$

$$K2 = \frac{8}{7}\left(\frac{2l}{h}\right)^{1/7}$$

$$Z = \left(\frac{h}{2l}\right) - \left(\frac{d}{l}\right)$$

3.4.2 Approximations in Prescribing the Boundary Conditions on the Contours for the Model-1

In prescribing the boundary conditions on the contours C1 and C2, the following approximations have been made;

a) Along AB (Fig 3.4) the jet velocity has a profile prescribed by the 1/7 power law (Equation 3B-1) and along FG (Fig 3.4) the air intake has a uniform velocity profile.

b) On the sides A'B' and C'D' the velocity of air at all points is normal to the sides and has a constant value of W.

c) The solution obtained with the infinite size of the outer contour C1, being sufficiently large compared to the dimensions of the inner contour C2, will be close to the solution for the case of finite free stream across the cylinder.

In using the NAG DO3EAF (44) routine on the contours C1 and C2 the following approximations have also been made.

The boundaries of the contours C1 and C2 are divided into n small intervals, in such a way that any corners or abrupt changes in the form of the boundary occur at

points of the sub-divisions. The stream function, Φ, and its normal derivative to the contour, $(\partial\Phi/\partial n)$, are within these intervals and prescribed at the mid-points of the intervals which are called the nodal points of the intervals. If the above values are denoted by Φ_i and Φ_i', $i = 1,2,3,.....n$, then half of them is prescribed as boundary conditions and the other half is evaluated in the mathematical procedure. Thus when Φ is prescribed at the appropriate nodal point of the $i\ th$ interval of the contour C1 or the contour C2, $\partial\Phi/\partial n_i$ is evaluated, at this "nodal" point for this interval (44).

3.4.3 Computation of the Coordinates of Nodal Points and Evaluation of the Stream Function at the Nodal Points for the Model-1

The NAG DO3EAF (43) routine requires the coordinates of segments, the boundary values (the stream function) on nodal points and the coordinates of the nodal points as main parameters in obtaining the solution for the "Main Flow". Here the nodal points are taken to be the mid-points of the segments. For a given jet angle θ and non-dimensional jet height h/l, at all the coordinates A, B, C, D, E, F, G, H, I, J of the octagonal contour (Fig 3.4) are determined. The coordinates of the end points of the segments and the

coordinates of the nodal points are determined according to the number of segments specified to each individual octagonal side as shown in the Table 3-1. Then at these nodal points the value of the stream functions are calculated using the boundary conditions on the contours given in the section 3.4.1.

The coordinates of the end points of the A′, B′, C′, D′ are specified (see 3.2.1) for the outer finite contour C1. Similar to the procedure used for the contour C2 the coordinates of the end points of the segments, the coordinates of the nodal points and the stream functions at nodal points are determined according to the segment specification and the boundary conditions which are given in the Table 3-1 and the section 3.4.1, respectively (Fig 3.7).

FORTRAN programme PART2 and PART3 are developed to compute the required input data for the NAG DO3EAF routine and are given in the Appendix 5F.

On the contour C2 the non-dimensional stream function Φ may be defined in terms of the jet momentum coefficient C_μ as shown in the Appendix 3B. The Jet Momentum Coefficient C_μ, non-dimensional jet height h/l and the jet angle θ are been used as main in put parameters for the FORTRAN programme PART3.

On the outer contour C1 stream function is expressed in terms of the free stream velocity W as shown in the Appendix 3B and leads to specified non-dimensional stream function Φ on this counter.

3.5.1 Computation of the Coordinates of the Nodal Points and Evaluation of the Stream Function at the Nodal Points for the Model-2

The two-dimensional fluid flow representation considered for the Model-2 requires, a δs strip at the upstream stagnation point S_{2L} for the left hand flow system (See 3.2.2 and Fig 3.5). The location of the S_{2L} and the shape of the strip is to be determined. In order to determine the S_{2L}, initially the flow model Model-2R (see 3.2.2 and Fig 3.6) is used. For this Model-2R a similar δs strip at the location S_{1R} has to be specified. Therefore a down stream stagnation point S_{1R} is specified arbitrarily. Considering the slip velocities around the inner contour C2 the upstream stagnation point S_{2L} is determined. This has been done according to the procedure given below;

Stage 1. For the right hand side contour (Fig 3.6) the down stream stagnation point S_{1R} has been taken to be the nearest nodal point to the point of intersection

between the octagonal surface and a radial line through the centre of the octagon which measures an angle of ($\theta + 22.5°$) with the radial line corresponding to the location of the jet.

The angle $\theta + 22.5°$ is chosen here as this will locate the S_{2R} point approximately close to the true down-stream stagnation point for the jet positions θ ranging from $35°$ *to* $55°$, considered in the present work. Using the δs strip as described above with the Model-2R, the velocities around the contour C2 are computed. The upstream stagnation point S_{2L} is then determined.

Stage 2. For the second stage of the procedure at the upstream stagnation point S_{2L}, *the* δs strip is introduced. Now by considering the slip stream velocities around the inner contour C2 the true down stream stagnation point is determined (Fig 3.5 and Fig 3.8).

For the introduction of the δs strip mentioned in Stages 1 and 2 the following procedure has been used;

On one of the sides of the δs strip there are the three straight lines connecting the points 1, 21, 20, 19. In the free stream flow direction these points are taken to be equal distant to each other. At points where the perpendicular lines to sides connecting points 15, 18

and 2, 10 crosses the 1/3 of the measured in the free stream direction and distances are taken as the points 20 and 21 respectively. The second side of the δs strip are the three straight lines connecting the points 11, 12, 13, 14 parallel to the lines connecting points 1, 21, 20, 19 with the distance of δs.

Once the location of the S_{2L} is fixed the geometry of the Model-2L is finalised and the necessary input parameters for the NAG D03EAF are obtained as detailed in the section 3.4.3.

Stagnation points S_1 , S_2, the actual downstream and upstream stagnation points, the coordinates of the ends of the segments, the coordinates of the nodal points (Fig 3.5) and the magnitudes of the stream functions at nodal points are determined by the FORTRAN programme PART4N (see Appendix 5A). Jet momentum coefficient C_μ, angle θ between the jet axis and the free stream velocity, free stream velocity W, and the non-dimensional jet height h/l are the main input parameters, used in this computer programme.

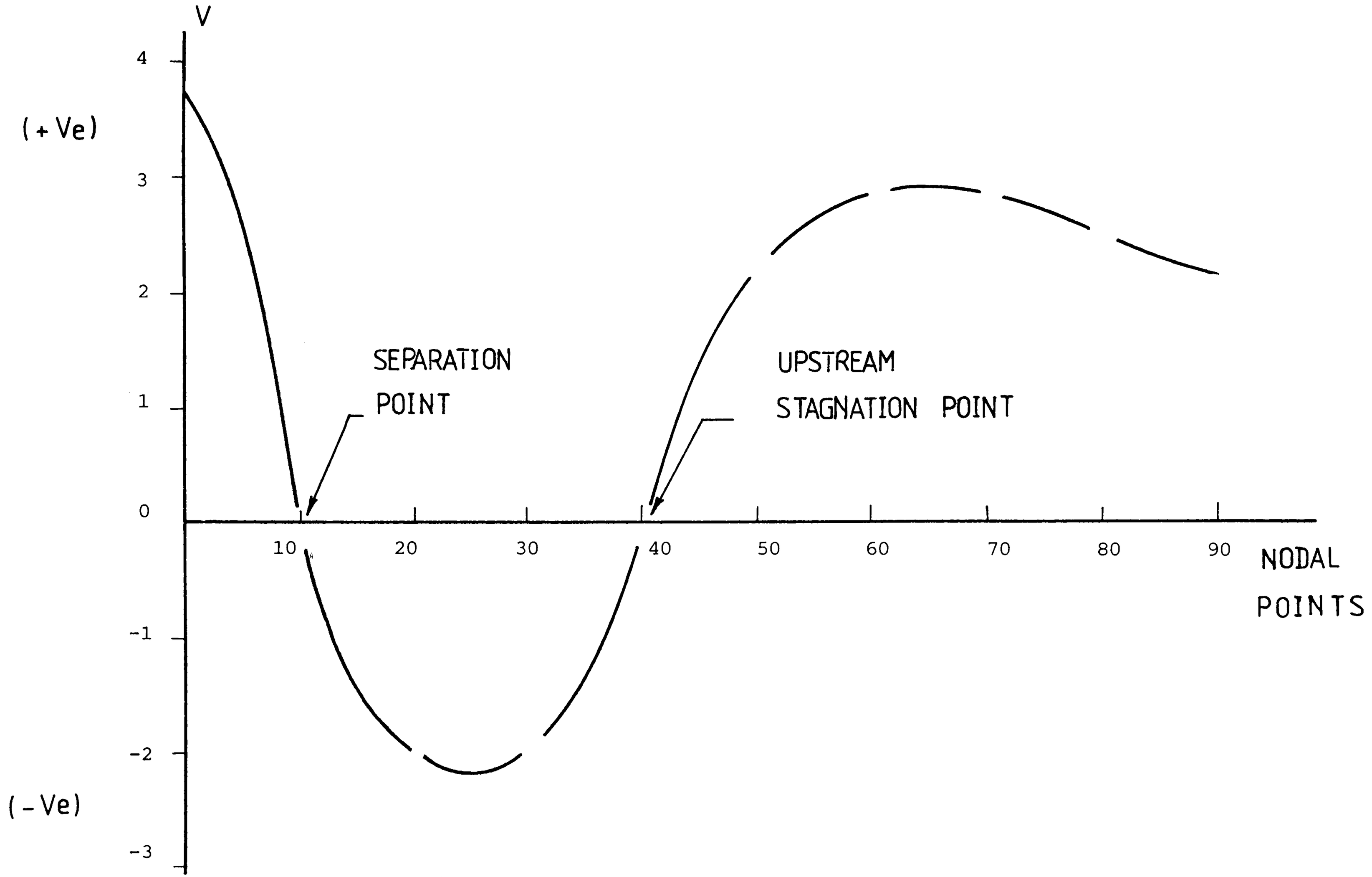

Fig 3.8 Slip Stream Velocities around the Octagonal Cylinder

3.5.2 Approximations Prescribing the Boundary Conditions on the Contours, for the Model-2

In addition to the approximations used in the section 3.4.2, for the model-2 the following assumptions have been made;

(i) The strip consisting of points 1, 21, 20, 19 and 11, 12, 13 14 , makes negligible influence on the position of the upstream stagnation point S_{1R}, for the "right hand flow system" (Fig 3.6). Hence, the upstream stagnation point S_{1R} evaluated with the assumed point for the S_{2R} is used when the flow changes over to the "left hand flow system" (Fig 3.5).

(ii) The upstream stagnation point S_{2L} required in specifying the "left hand flow system", (Model-2L, Fig 3.5) which finally used for the solution, is determined using the "right hand flow system" (Model-2R, Fig 3.6). In specifying the downstream stagnation point S_{1R} for the latter case, its arbitrary location has negligible influence on the position of S_{2L}.

(iii) For both the flow systems ("Right Hand" and "Left Hand") line connecting the points 1, 21, 20, 19 represents the zero slip stream line.

(iv) The δs strip is sufficiently narrow that the main flow field, especially in the vicinity of the octagon, is approximately same as the flow field existing the actual three-dimensional situation present where the jet air is introduced in the axial direction.

3.6.1 Use of the NAG D03EAF Routine for Slip Stream Velocities and Stream Functions

NAG scientific routine D03EAF (43) solves Laplace's equation (3.3-2) in two dimensions for an arbitrary domain bounded by internally or externally by one or more closed contours, given the value of either the unknown function or its normal derivative (into the domain) at each point of the boundary (44,43). This routine uses an integral method, based upon Green's theorem (44,45,46), which yields the solution, Φ, at any point within the domain, in terms of $(\partial\Phi/\partial n)$ and Φ values along the boundary.

The solution is obtained in two stages. The first stage is executed only once to determine the complementary boundary values, i.e. normal derivative $(\partial\phi/\partial n)$ where the stream function ϕ is specified or vice-versa. The second stage is executed repeatedly as many times as the number of points at which the

solution is required. The second stage utilises the computed values obtained in the first stage and the coordinates of the points where the solution is required, as input data. This involves solving a set of simultaneous linear algebraic equations which is achieved by means of auxiliary routines F01BK and F04UAF.

3.6.2 Determination of the Stream Function Using the NAG D03EAF Routine

In the original NAG D03EAF (43) package supplied, the two stages of the routine are computed in a single computer programme. This programme was modified, so that the two stages may be executed independently in applying the package for obtaining the solution to the main flow for the Model-1 and Model-2. This was done to achieve maximum possible accuracy with in the allowable maximum computer execution time. This arises from the fact that the accuracy of the solution depends on the number of nodal points used in the specifying the contours. This is discussed further in the next section 3.6.3. The separation of the programme into independent routines also provides the flexibility to use the intermediate results of the first stage, at a subsequent later time for obtaining solutions, to

evaluate the surface shear-stress of the solid boundary, and the values of the lift and the drag coefficients due to the boundary layer modification on the octagonal cylinder by wall-jet (3.8.7).

3.6.3 Accuracy of the NAG D03EAF and Selection of the Segment Points

The accuracy of the computed solution depends upon how closely stream function ϕ, is approximated by constants in each interval of the boundary, and upon how well the boundary contours, which may be curved, are represented by straight sided polygons whose vertices are at the selected points of the contours. Consequently, the accuracy increases as the boundary is sub-divided into smaller and smaller intervals. Alternatively, since the point of maximum error always lies on the boundary of the domain, an estimate of the error over analytical solution has been obtained by computing the stream function ϕ for the simulated mathematical model consisting of a circular cylinder under cross-flow without a tangential wall-jet. These preliminary investigations show the sensitivity of the solution to the number of segments on the inner contour C2 is higher than the number of segments on the outer contour C1. It was also established that the number of

segments required on the outer contour C1, can be decreased to some extent while increasing the size of the outer contour C1, represented by the modelled infinity, in order to achieve the same accuracy of the solution. Based on these investigations on the outer contour C1, 24 nodal points (24 segments) and on the inner contour C2, 92 nodal points (92 segments) have bee selected. For the modelled infinity the outer contour size of 20 X 20 non-dimensional lengths has been selected. Having selected these contour specifications, the solution using NAG D03EAF routine for a circular cylinder showed only an error of 0.02 %. The detailed computed results are presented in the Appendix 3K.

3.6.4 Slip Stream Velocity on the Octagonal Cylinder With a Tangential Wall-jet

The calculated values of the normal derivatives of the stream function $(\partial\phi/\partial n)$ at nodal points represent the slip stream velocities on the octagonal cylinder (see 3.6.2) (see Appendix 3C). A typical sample of these computed velocities are shown in the Appendix 3L. These results indicate that the velocity variation with respect to the distance measured along the contour of

the octagon, has a wavy nature with an extremum value close to the vertex. This variation of the slip velocity will be referred to here as "Oscillatory nature" for slip velocity. Causes for this behaviour may be explained by two hypothesises;

1. The mathematical /computational limitations of the NAG D03EAF routine in predicting the slip stream velocities at the vertices of the octagonal contour C2, introduce this spurious result.

2. The true behaviour of the flow patterns around the vertices of the octagonal contour C2 has the oscillatory nature.

In order to investigate the above the NAG D03EAF routine has been used to analyse the flow around simple two-dimensional solid boundaries. Here (i) A rectangular cross-section , (ii) A triangular cross-section in a free stream has been considered (Fig 3.9).

The rectangular cross section which was used as the model was placed in the free stream at an angle of attack of 90°. The computed flow field around the rectangular cross-section showed an oscillatory slip velocity around end points of the sides of the contour (Fig 3.9a). However when the model was rotated around its axis to give a smaller angle of attack, the

oscillatory nature for the slip velocity at the vertices of the rectangular cross-section disappeared. Further a similar investigation with the triangular cross-section showed results of a comparable nature. This clearly establishes the cause for the oscillatory nature of the slip stream velocities at corner points of the contour C2. Hence the second of the two hypothesises used to explain the behaviour of the flow around the octagonal cylinder can be identified as the sole reason for such a behaviour of the slip stream velocities.

3.6.5 Computer Time for Determining the Stream Function of the "Main Flow"

The computer time required for the stage one of the NAG D03EAF which is executed only once for a particular problem, is proportional to the square of the number of segments N^2. On the other hand the time taken for the execution of the stage two of the NAG D03EAF routine, to obtain the stream function at a given point of the flow field is proportional to the number of segments (N). By separating the two stages of the original NAG routine into two independent routines it is possible to use the maximum number of segments for the allowable computer time for a single job run, resulting in a high

accuracy. The number of segments for both the model-1 and model-2 have been chosen to be 116 which represents a reasonable compromise between the computer time and of the accuracy of the solution which was discussed in the section 3.6.3.

3.6.6 Stream Lines Around the Octagonal Cylinder

The solution obtained for the "Main Flow" is used to determine the stream lines around the octagonal cylinder in the free stream of air, with the tangential wall-jet. The second stage of the NAG D03EAF routine is used to evaluate the stream function at various points inside the domain bounded by the contour C1 and C2. In the case of Model-1 points lying on lines perpendicular to the octagonal sides through nodal points have been used to create a grid around contour C2 (Fig 3.10). On each of these perpendicular lines, 26 points at intervals of 0.01, 0.02, 0.03, 0.04, 0.05, 0.06, 0.07, 0.08, 0.09, 0.1, 0.12, 0.14, 0.16, 0.18, 0.20, 0.22, 0.24, 0.26, 0.28, 0.30, 0.32, 0.34, 0.36, 0.38, 0.40, have been selected. This forms a total of 2080 (26X80) grid points. The coordinates and the corresponding stream functions at these points are used to determine the stream lines around the octagonal cylinder. This has been done by finding the

coordinates of points on radial lines, at which the stream function attains a specified value of stream function, $\Phi preset$. In this procedure all the 2080 points on the grid are scanned for every $\Phi preset$ value. On each of the radial lines Φmax and the Φmin values are found. If the $\Phi preset$ value is within the range of the Φmax *and* Φmin the coordinates of the points where the stream function has the $\Phi preset$ value, on the radial line are interpolated. All such coordinates for a given $\Phi preset$ value constitute a stream line. If a stream line has the shape, shown by A B C D E F G H in the Fig 3.10, the section A B C, section D E and section E F G are treated as separate stream lines with the same $\Phi preset$ value for the purpose of computer plotting. The scanning process is always started from the first radial line (radial line which goes through the first nodal point of the side connecting the points 1 and 2) (Fig 3.10) and carried-out in the clock-wise direction. In scanning all the grid points if the continuity of the stream function is broken, further points predicted having the same $\Phi preset$ value are treated as another stream line with the same $\Phi preset$ value i.e. stream line P Q R and stream line K L M with $\Phi = K2$. The maximum possible number of points on any one radial line line for a given $\Phi preset$ value is unlikely to be more than 4 and this has been incorporated in the computer programme. The FORTRAN computer programme GRID1

developed to prepare the coordinates of the stream lines in the above mentioned manner is given in the Appendix 5E.

The coordinates for the stream lines generated are used with a simple computer programme which utilises with the GHOST-80 soft-ware routine to obtain computer plotted stream lines. By treating the stream lines with same $\Phi preset$ values, with special conditions attached as mentioned above, enables to plot the stream lines with shapes given in the Fig 3.10 conveniently. Stream lines obtained for typical flow conditions with and without the circulation are given in the section 5.1

The grid points lie on perpendicular lines to the octagonal sides of in the Model-1 (see 3.6.1 1 and 3.6.5) and resulting in large undetermined areas between any two octagonal sides. Hence the stream lines, within these undetermined areas of the main flow have to be approximated by smooth lines. Therefore in developing the Model-2 these perpendicular lines have been replaced by radial lines, from the centre of the octagonal cylinder and through the nodal points as shown in the Fig 3.10, for the purpose of generating the grid points.

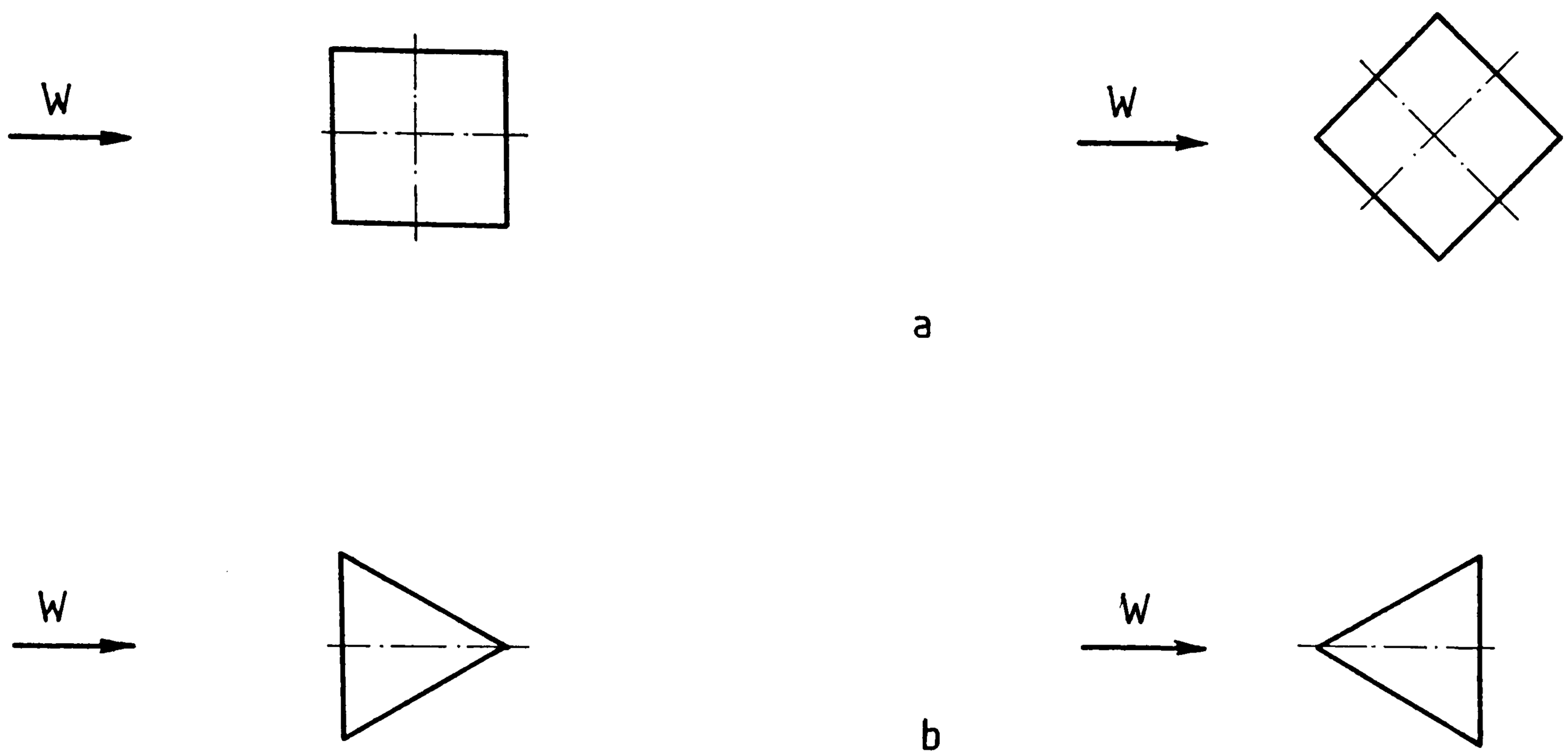

Fig 3.9 Shapes of Contour-C2 for Preliminary Investgation

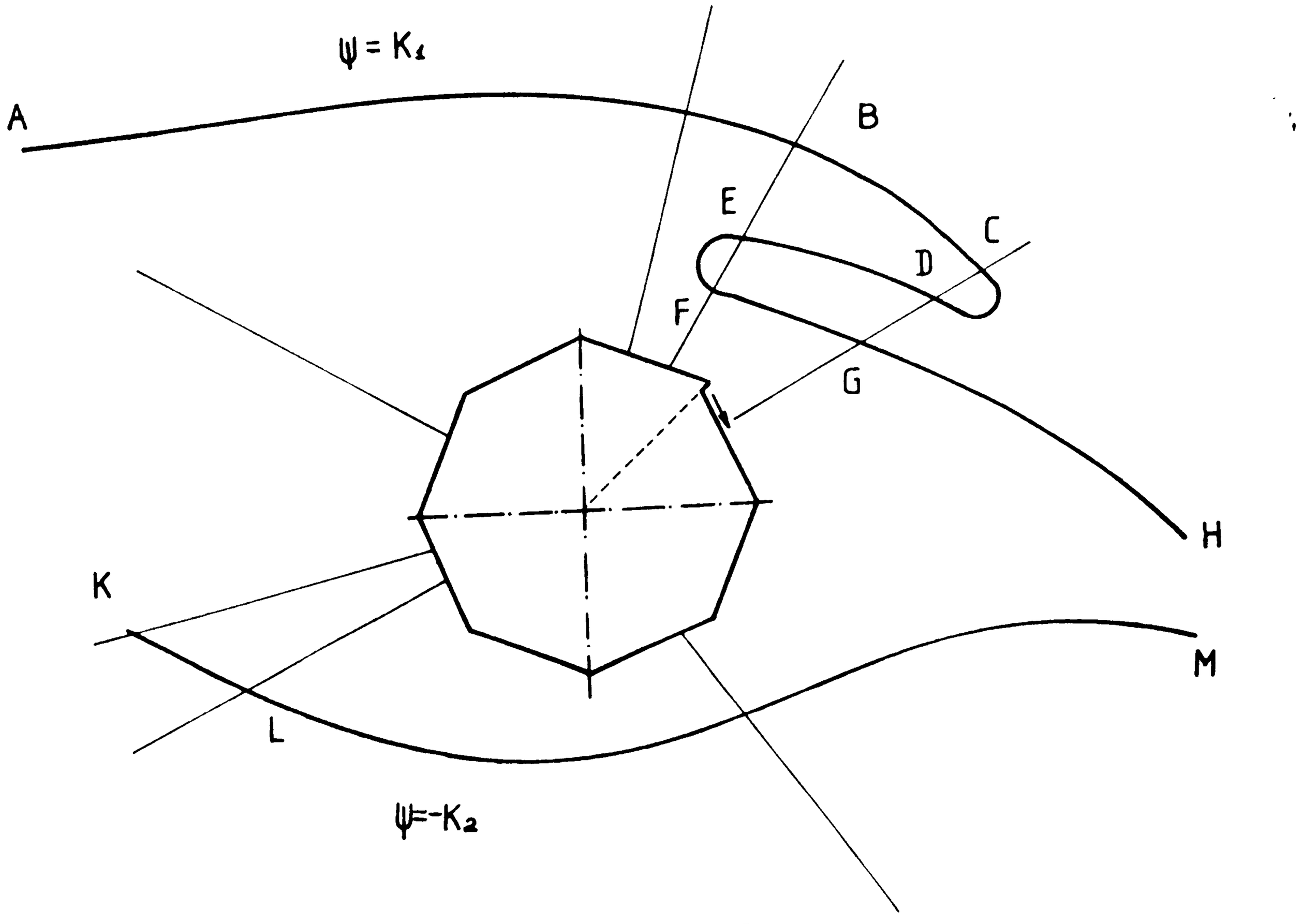

Fig 3.10 Stream Lines around the Contour C2

3.6.7 Comparison of the Fluid Flow Model-1 and Model-2

For the Model-1 on the inner contour C2 the continuity equation for the two-dimensional model has been satisfied by introducing an air intake point on the contour C2. This has been chosen at a diametrically opposite location on the two-dimensional model to minimize the influence of the imposed air intake on the tangential wall-jet. For the Model-1 the stream lines of the "Main Flow", around the octagonal cross-section, for different typical flow conditions are computed and are shown in Fig 3.11 to Fig 3.15. As the momentum coefficient increases, these figures clearly show, the influence of the air intake on the flow conditions around the octagonal cylinder. This is particularly strong towards the bottom half of the flow model. Therefore if the Model-1 is to be used for the prediction of the lift generation due to the boundary layer modification around the octagonal cylinder, a correction has to be made to account for the influence of the air intake, on the over-all pressure distribution,

In the Model-2, to satisfy the continuity equation for the two-dimensional model, the small "δs" strip has been introduced (see 3.2.2) (Fig 3.5). To minimize the influence of the "δs" strip, on the flow field around

the octagonal cylinder, upstream stagnation point S_{2l} where the strip is introduced has been computed. Using the Model-2 stream lines plotted around the octagonal cylinder for the same typical flow conditions are given in the 5.1. These representations involving different momentum coefficients, h/l and θ values show considerable improvement of the flow field. This conclusion is arrived at by the comparison of the stream lines for the case of a rotating cylinder in a cross-flow (15). There is a considerable similarity between the stream lines of the Model-2 and the above. This also shows the negligible influence on the "Main Flow" stream lines due to the selected location of the δs strip at the up-stream stagnation point. It is also possible to eliminate this influence, totally by the method of iteration in determining the the up-stream and down-stream stagnation points and by adjusting the shape of the δs strip to match with the zero slip stream line.

Hence, for further investigations Model-2 has been selected, as it gives a more accurate representation of the flow field

Text cut off in original

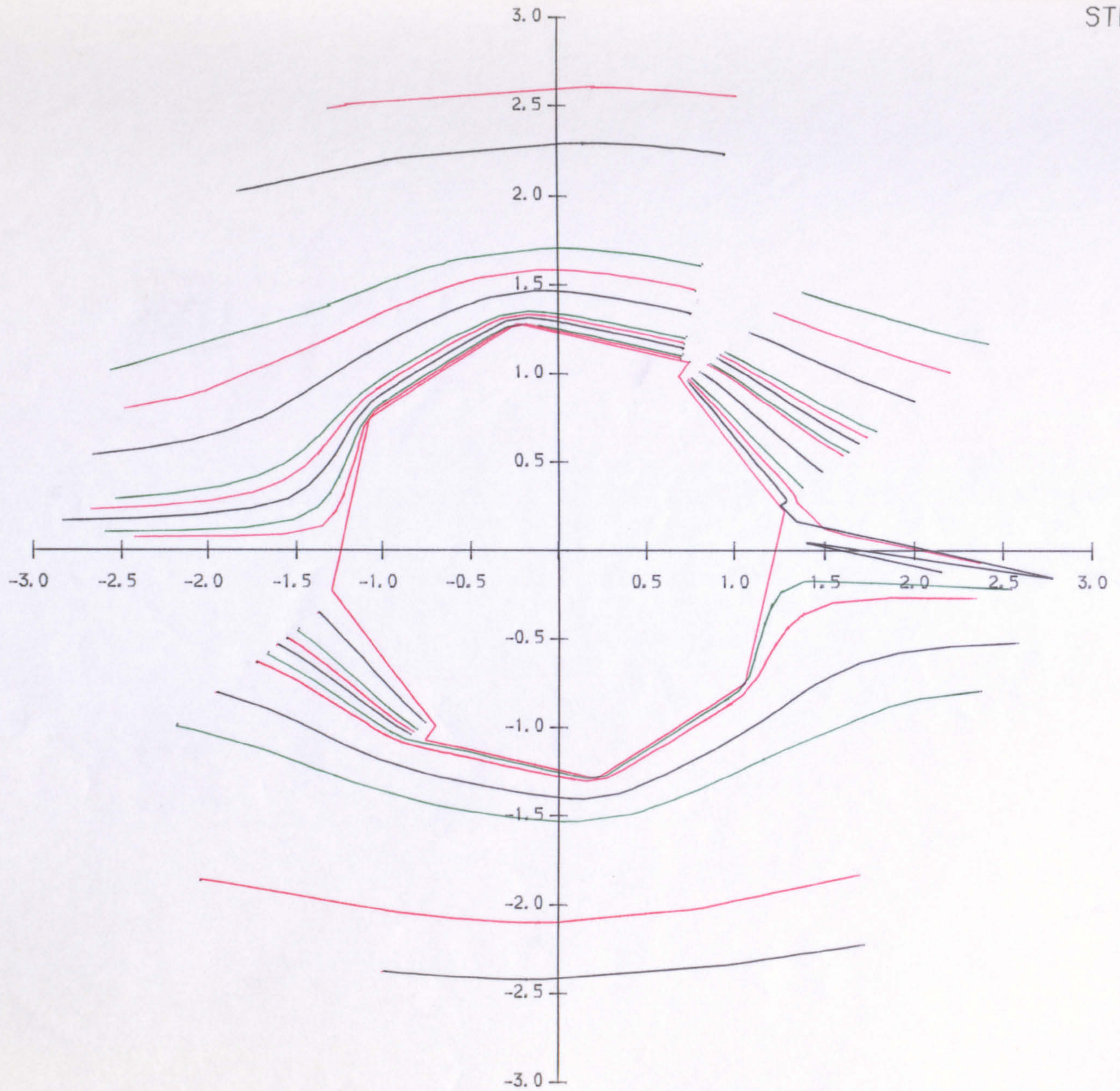

Fig 3.11 Stream Lines Around Contour C2
(Model 1, $\theta=125^{o}$, $C_{\mu}=0.55$

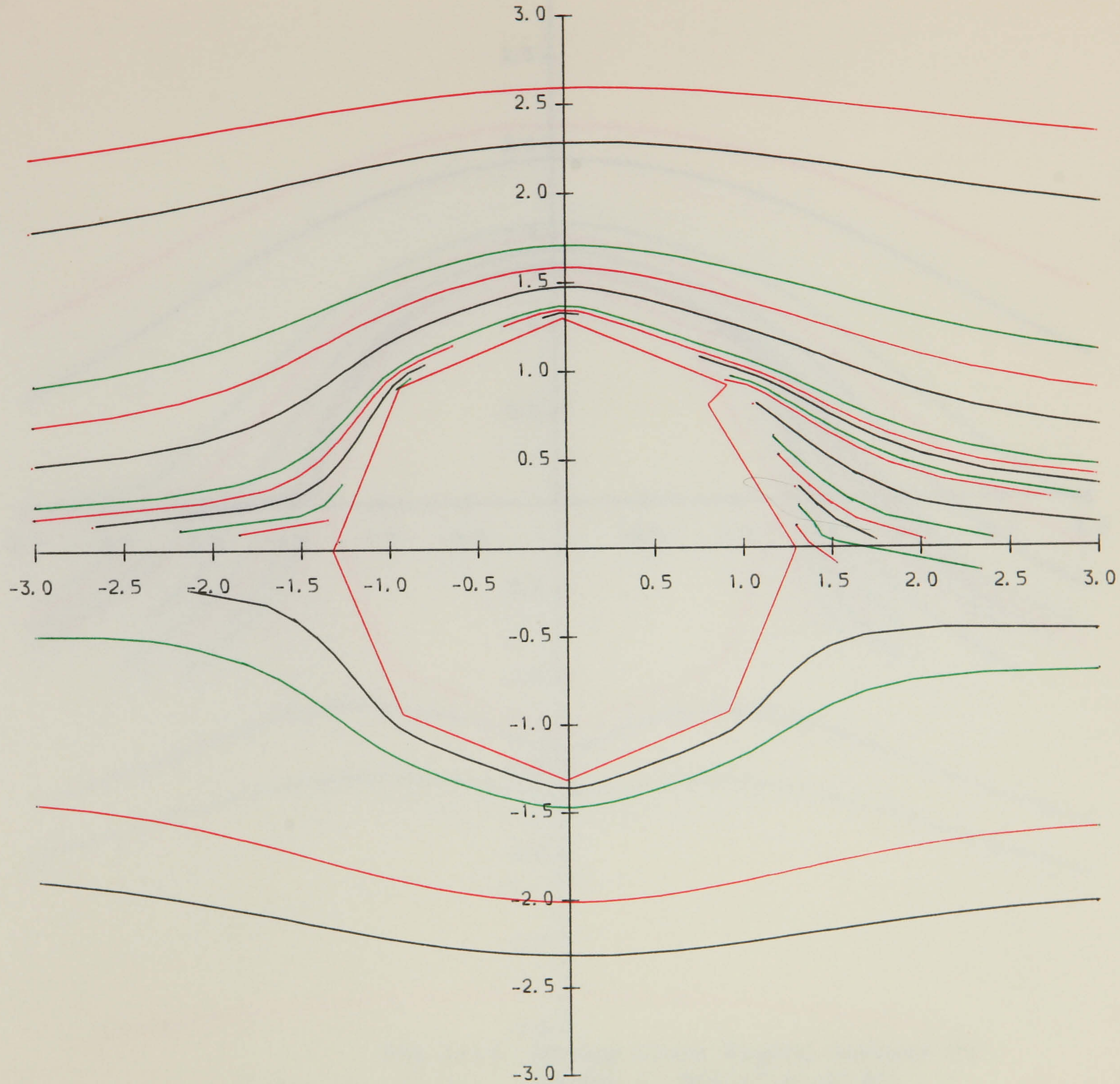

Fig 3.12 Stream Lines Around the Contour C2
(Model 2, $\theta=135^{o}$, $C_{\mu}=0.25$)

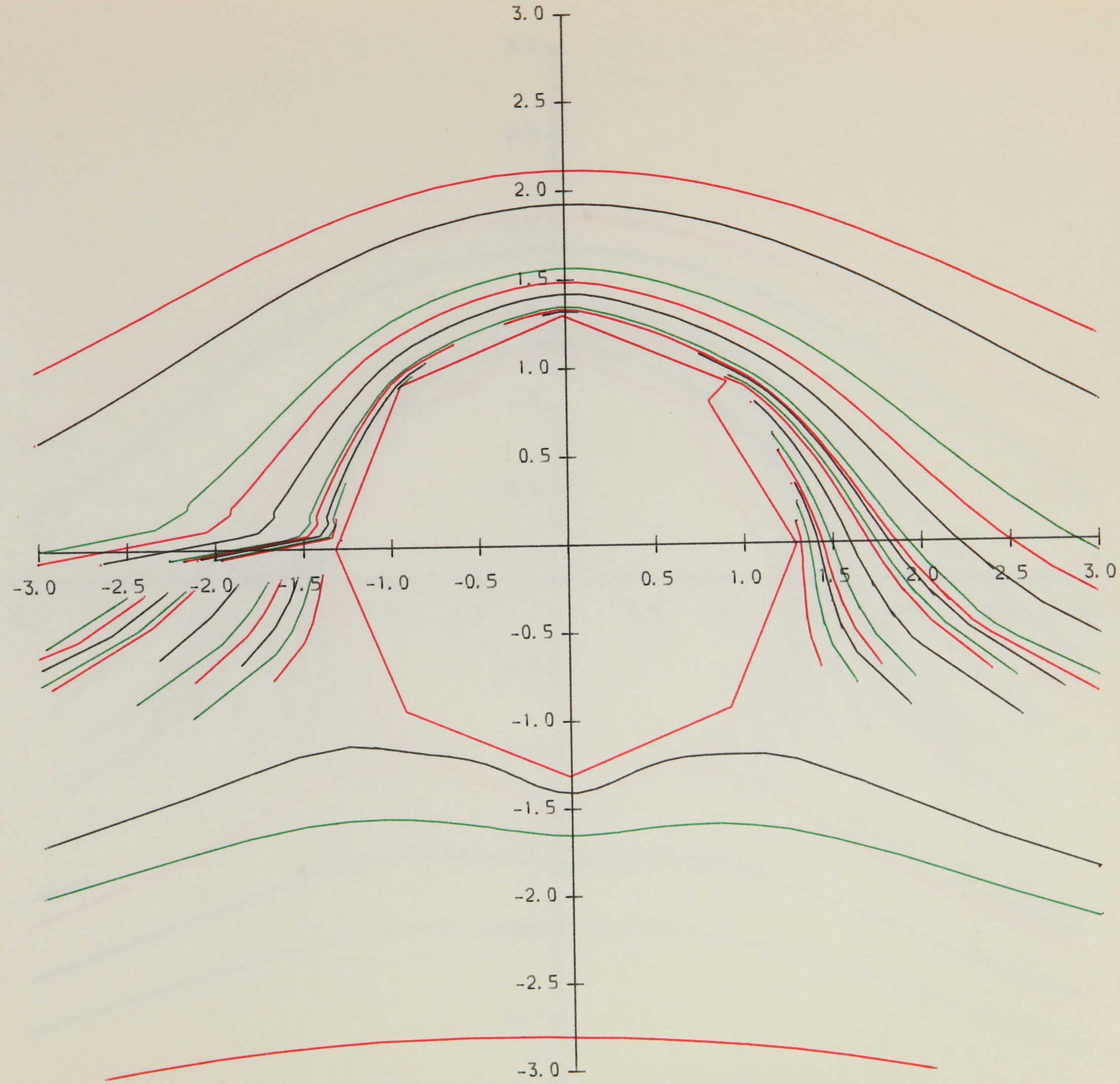

Fig 3.13 Stream Lines Around Contour C2
(Model 2, $\theta=135^{o}$, $C_{\mu}=0.40$)

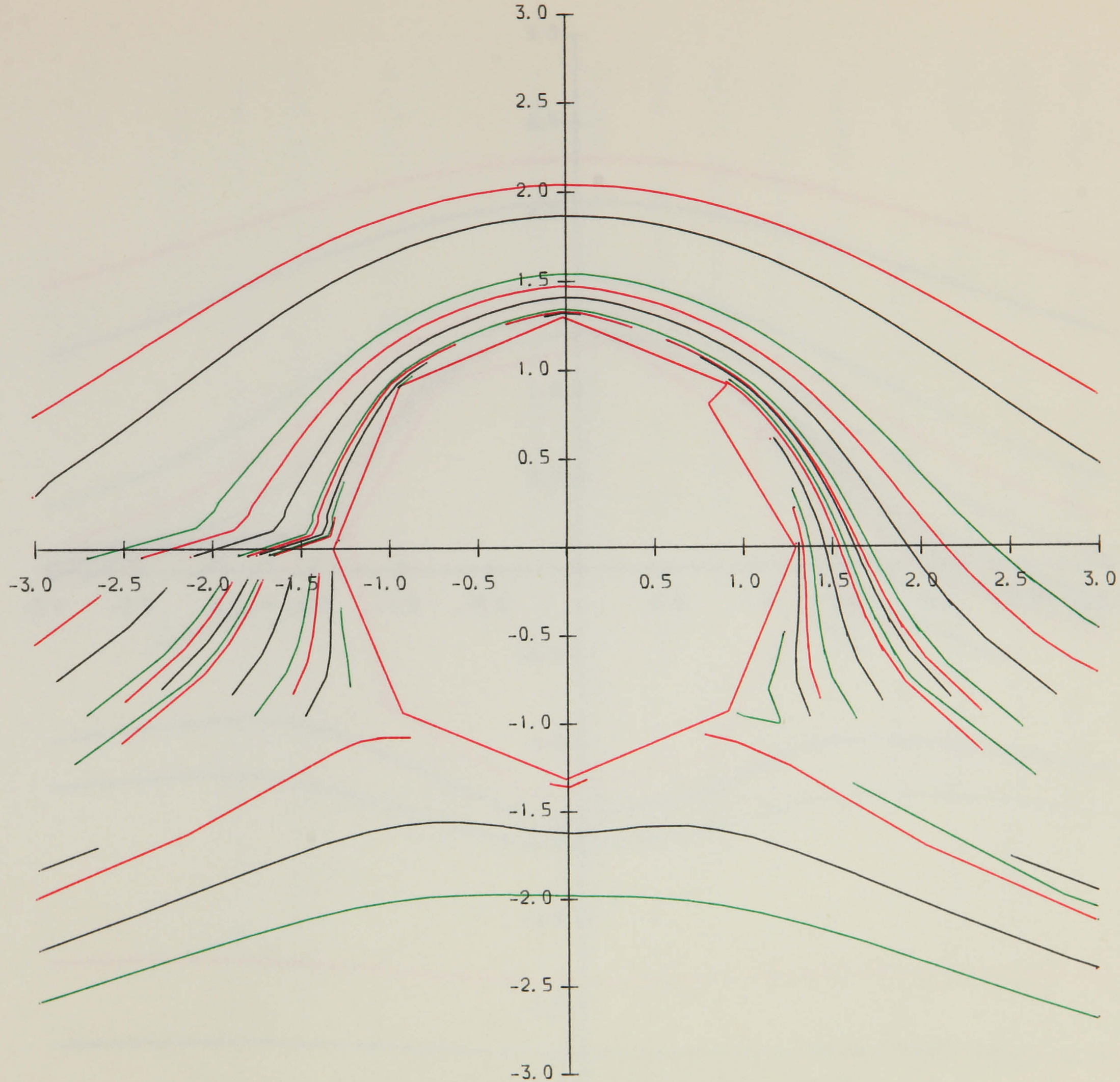

Fig 3.14 Stream Lines Around the Contour C2
(Model 2, θ=135°, C_μ=0.55)

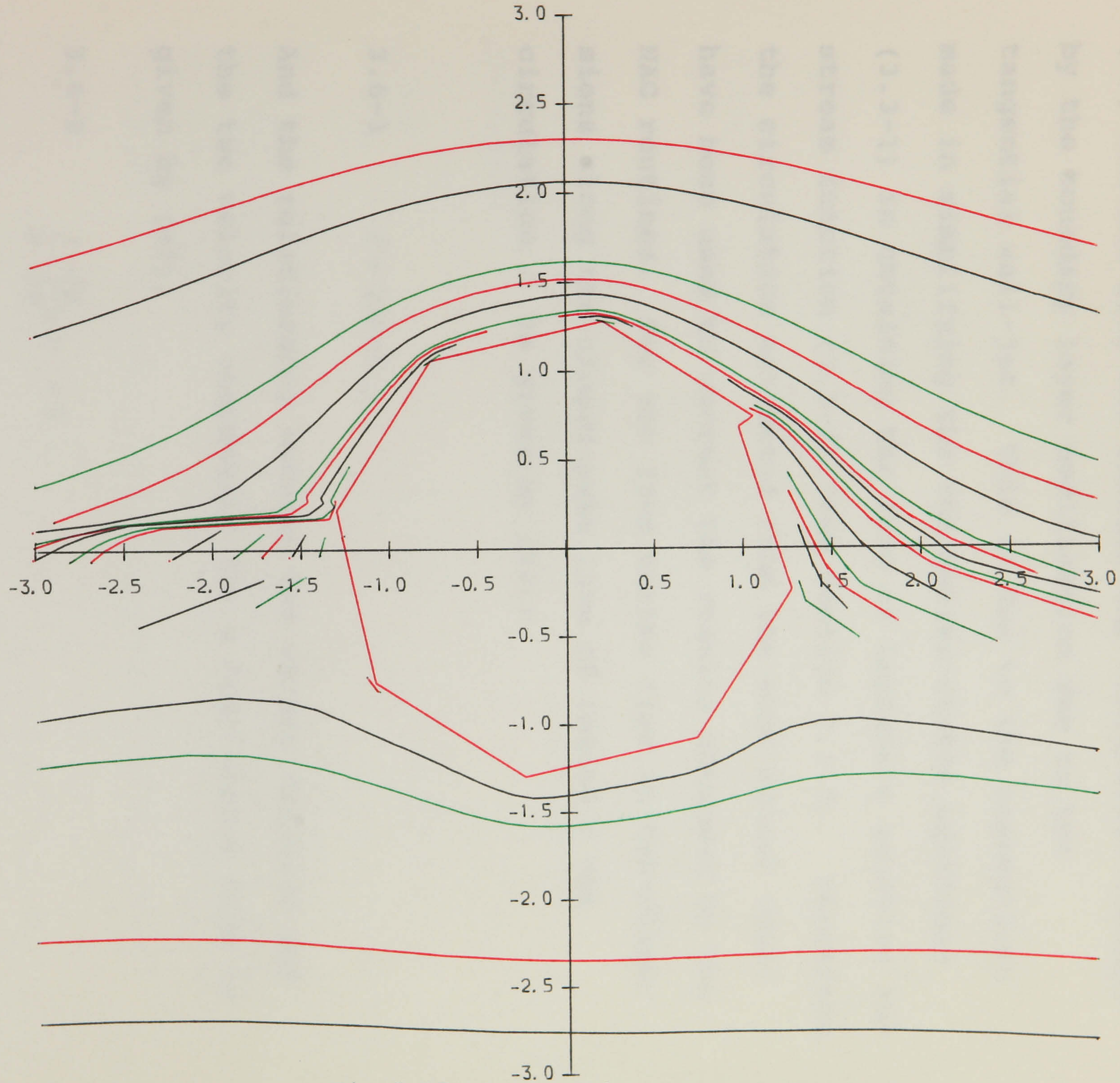

Fig 3.15 Stream Lines Around the Contour C2
(Model 2, $\theta=145^{o}$, $C_{\mu}=0.40$)

3.6.8 Circulation Due to the Boundary Layer Modification

The flow field determined by employing the NAG D03EAF (43) routine does not include the circulation created by the boundary layer modification due to the tangential wall-jet. This is due to the assumptions made in simplifying the the Navier-Stokes equations (3.3-1) in obtaining the form of Laplace's equation for stream function (3.3-2) (See section 3.3.2). Therefore the circulation estimated from the wind tunnel tests have been used to correct the results obtained by the NAG routines. For the free vortex flow in two-dimensions along the closed path line of radius r the circulation Γ is given by (47);

3.6-1 $$\Gamma = 2\Pi r V_{\omega}$$

And the relationship between the stream function and the two velocity components for a free vortex flow is given by (47);

3.6-2 $$\frac{1}{r} \cdot \frac{\partial \phi}{\partial \theta} = V_r = 0$$

and

3.6-3 $$-\frac{\partial \phi}{\partial r} = V_{\omega} = \frac{\Gamma}{2\Pi r}$$

By integrating these equation the stream function ϕ is obtained as;

$$\phi = -\frac{\Gamma}{2\pi}(\ln r + \ Constant)$$

Where, $r = R_0$, $\phi = \phi_0$

$$\phi_0 = -\frac{\Gamma}{2\Pi}(\ln R_0 + \ Constant)$$

or

3.6-4 $$(\phi - \phi_0) = -\frac{\Gamma}{2\Pi} \cdot \ln\left(\frac{r}{R_0}\right)$$

Where $r \geq R_0$

Therefore

3.6-5 $$\Phi_{\Gamma\ n-d} = \frac{\Gamma_{n-d}}{4\Pi} \ln \frac{(X^2 + Y^2)}{(R_0/l)^2}$$

If the computed value of the stream function in the section 3.6.2 is Φ, the corrected value of the stream function Φ_c is given by the super-position principle as;

$$\Phi_c = \Phi_{\Gamma n-d} + \Phi$$

For the considered octagonal cross-section, $R_0 = R$,

$$\frac{R_0}{l} = \frac{R}{l} = \frac{1}{2\sin(22.5)^\circ}$$

and

$$\left(X^2 + Y^2\right) \geq \left(\frac{R}{l}\right)^2$$

Therefore the Γ_{n-d} obtained from the wind tunnel tests (see 4.3.2) have been used to modify the stream function as shown by the equation 3.6-5. The stream lines around the octagonal cross-section are obtained for the main flow after correcting for the circulation, for typical cases and are given in the section 5.1.

Slip velocities for the boundary layer flow were obtained by the first stage of the NAG D03EAF routine (see 3.6.2) which does not take to account the circulation. These slip velocities are also to be corrected for the circulation. If the stream function corrected for the circulation is Φ_c the slip velocity corrected for the circulation can be given by;

$$V_{\omega c} = -\frac{\partial \Phi_c}{\partial r}$$

The lift force L for the octagonal cylinder can now be expressed using the Kutta-Joukowski theorem (47);

3.6-6 $$L = \rho W \Gamma H$$

Therefore the lift coefficient is given by;

$$C_L = \frac{\rho W \Gamma H}{0.5 \rho W^2 (2RH)}$$

and hence the lift coefficient may be given in the alternative form;

3.6-7 $$C_L = \Gamma_{n-d} \cdot \left(\frac{l}{R} \right)$$

3.7 Boundary Layer Flow

Pressure distribution on the surface of the octagonal cylinder obtained from the mathematical fluid flow model for the "Main flow" (See 3.2) and the surface shear forces are required in calculating the theoretical values of the lift and the drag coefficients (see 3.8.7). In order to calculate the surface shear forces the boundary layer flow around the octagonal cylinder is considered. The pressure distribution and the slip velocities at the octagonal surface obtained from the "Main flow" are used to stipulate the boundary conditions. This ensures that the velocity on the edge of the boundary layer

automatically matches with the slip velocities of the "Main flow" at the octagon surface (Fig 3.16). In determining the laminar boundary layer thickness and the wall shear-stress Prandtl's boundary layer equations are used (15). In integration of the above equations, with the required boundary conditions on the boundary layer around the octagonal cylinder is sub-divided into Region-1, Region-2 and Region-3. These are;

Region-1 : from the point 1 to the point 5,

Region-2 : from the point 11 to the point S,

Region-3 : from point the point 6 to the point S

as depicted in the Fig 3.5.

For the general conditions considered in this investigation, from the stagnation point S_1, a laminar layer develops in both the Region-1 and Region-2 and farther down-stream, changes into a "turbulent layer". For the Regions 1 and 2 considered (Fig 3.5) the laminar boundary layer develops with initial conditions stated in the section 3.7.5. It is usual to make simplifying assumptions in setting up the boundary layer equations, for example in the Pohlhausen's method (48), the pressure is assumed to be a constant, in the direction at right angles to the boundary layer, whereas along the wall the pressure is regarded as being "impressed" by the external flow so that it becomes a given function. The resulting omission of

the equation of motion perpendicular to the direction of flow, was interpreted by Pohlhausen, in physical terms, as that the fluid particle in the boundary layer has zero mass, and suffers no frictional drag as far as its motion in the transverse direction is concerned. With such fundamental changes introduced into the equations of motion as in this case considered it is anticipated that their solutions will exhibit certain mathematical singularities and that of a good agreement between observed and calculated phenomenon can not be expected (15). Some of these traditional assumptions may be avoided depending on the physical situation of the fluid flow problem as shown in the Appendix 3F.

For the turbulent boundary layer a revised version of the Blasius's profile has been employed (see 3.7.9). The Momentum Integral equation (46) is used in solving the turbulent boundary layer. For the Regions 1 and 2 the transition point has been found by the laminar boundary layer separation and for the Region 3 no laminar layer is anticipated. For the Region-3 the turbulent boundary layer is more compatible with a such a positive pressure gradient at the rear surface of the cylinder than the laminar layer and consequently separation sets in further down stream. As a result of

the shifting of the separation point, connected with the turbulent boundary layer, the wake diminishes and shows a reduction in the pressure drag.

3.7.1 Governing Equations for The Laminar Boundary Layer

As shown by many authors in the past, strict and complete prescriptive equations for the laminar boundary layer are considerably complicated (15,17,20,49), hence are difficult to be used in obtaining required solution.

Restricting the attention to the two-dimensional laminar flow Prandtl's boundary layer equations are derived from the Navier-Stokes equations (15);

$$u \cdot \frac{\partial u}{\partial x} + v \frac{\partial u}{\partial y} = -\frac{1}{\rho} \frac{dP}{dx} + \nu \frac{\partial^2 u}{\partial y^2}$$

$$= U \frac{dU}{dx} + \nu \frac{\partial^2 u}{\partial y^2}$$

Further, assuming the main flow, outside the boundary layer to be inviscid, and considering the limiting conditions of the free stream $y \to \infty$, $u \to 0$, the above equation reduces to;

$$\frac{1}{\rho}\frac{dP}{dx} = U\frac{dU}{dx}$$

3.7-1 $$u\frac{\partial u}{\partial x} + v\frac{\partial u}{\partial y} - U\frac{dU}{dx} = \nu\left(\frac{\partial^2 y}{\partial x^2}\right)$$

by integrating both sides of the equation 3.7-1 with respect to y from $y = 0$ *to* $y = \delta$;

3.7-2 $$\int_0^{\delta}\left(u\frac{\partial u}{\partial x} + v\frac{\partial u}{\partial y} - U\frac{dU}{dx}\right)dy = \nu\left(\frac{\partial u}{\partial y}\right)_{\delta} - \nu\left(\frac{\partial u}{\partial y}\right)_0$$

The continuity equation may be integrated to give;

$$v = -\int_0^{y}\left(\frac{\partial y}{\partial x}\right)dy$$

and therefore, the equation 3.7-1 becomes;

3.7-3 $$\int_0^{\delta}\left(u\frac{\partial u}{\partial x} - \frac{\partial u}{\partial y}\int_0^{y}\frac{\partial u}{\partial x}y - U\frac{\partial U}{\partial x}\right)dy = -\frac{\nu U}{\delta}R + \nu\left(\frac{\partial u}{\partial y}\right)_{\delta}$$

By integrating the second term of 3.7-3;

3.7-4 $$\int_0^{\delta}\left(\frac{\partial u}{\partial y}\int_0^{y}\frac{\partial u}{\partial x}\cdot dy\right) = u\int_0^{\delta}\frac{\partial u}{\partial x}dy - \int_0^{\delta}u\frac{\partial u}{\partial x}dy$$

and hence the integral equation 3.7-3 becomes,

3.7-5 $$\int_0^{\delta}\left(2u\frac{\partial u}{\partial x} - U\frac{\partial u}{\partial x} - U\frac{\partial U}{\partial x}\right)dy = -\frac{\nu U}{\delta}R + \nu\left(\frac{\partial u}{\partial y}\right)_{\delta}$$

3.7-6 $$\int_0^{\delta} \frac{\partial}{\partial x}[u(U-u)]dy + \frac{dU}{dx}\int_0^{\infty}(U-u)dy = \frac{\nu U}{\delta}R - \nu\left(\frac{\partial u}{\partial y}\right)_{\delta}$$

Now since,

3.7-7 $$\int_0^{\delta} u(U-u)dy = U^2\theta$$

and

3.7-8 $$\int_0^{\delta}(U-u)dy = U\delta^*$$

Finally the momentum integral equation becomes;

3.7-9 $$\frac{d}{dx}\left(U^2\theta\right) + \delta^* U\frac{dU}{dx} = \frac{\nu U}{\delta}R - \nu\left(\frac{\partial u}{\partial y}\right)_{\delta}$$

at point M (Fig 3.16)

3.7-10 $$\left(\frac{\partial u}{\partial y}\right)_{y=\delta} \neq 0$$

Therefore,

3.7-11 $$\int_0^{\delta} u\frac{\partial u}{\partial x} + v\frac{\partial u}{\partial y} - U\frac{\partial U}{\partial x} = \frac{\nu U}{\delta}R - \nu\left(\frac{\partial u}{\partial y}\right)_{\delta}$$

and the boundary conditions are;

3.7-12 $y = 0 \qquad u = 0$

$$y = \delta \qquad u = \frac{\partial \phi}{\partial n} \qquad \left(\frac{\partial u}{\partial y}\right)_{\delta} = \frac{U}{\delta} \cdot R$$

3.7.2 Basic Assumptions Made for The Laminar Flow

In deriving the momentum integral equation for the laminar boundary layer it is assumed that the flow into the boundary layer is due to the shear stress τ on the surface. It is also assumed that the velocity profiles along the surfaces at different locations are similar, and hence may represent by the equation 3.7-13 in terms of the non-dimensional η,

3.7-13 $$f(\eta) = \frac{u}{u_{\infty}}$$

Where, $f(\eta)$ is only a function of η and does not contain any additional free parameters. At the wall $f(\eta)$ $limit \to 0$ and for η $limit \to \infty$, it tends to 1. It is also assumed that the influence of the wall-jet on η is negligible. Therefore the proposed 4th degree polynomial curve is fitted to the main flow at the edge of the boundary layer. In using the approximate method, the edge of the boundary layer is taken to be at a finite distance from the surface δ.

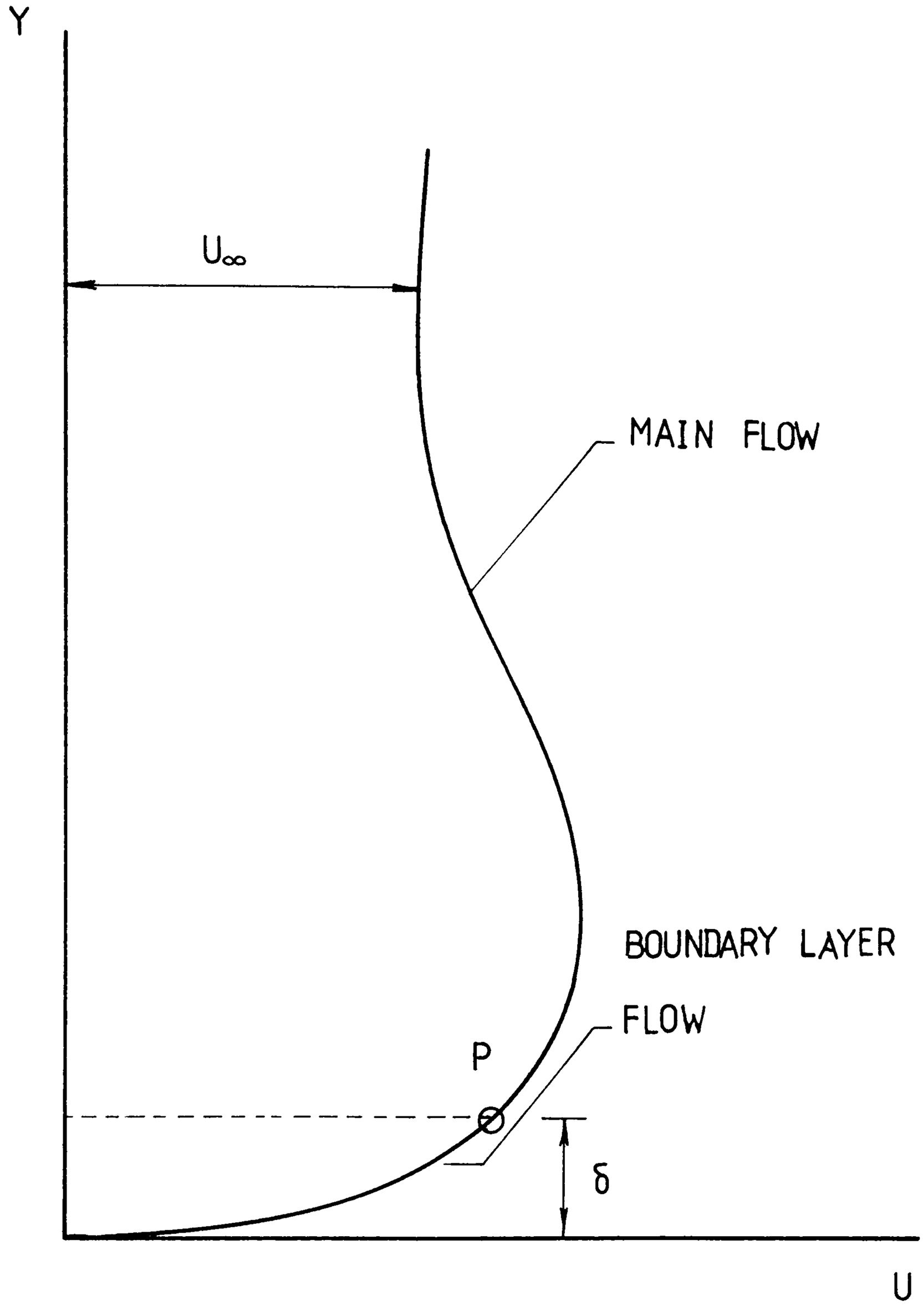

Fig 3.16 Boundary Layer Flow and
The Main Flow

3.7.3 Boundary Layer Flow in the Presence of Pressure Gradient

Momentum Integral equation (3.7-2) was extended by Pohlhausen to cover the case of two-dimensional laminar flow with pressure gradient (15). Pohlhausen's method is modified to estimate the influence of neglecting the shear-stress at the edge of the boundary layer which arises due to the modification of velocity profile in the presence of a wall-jet. A coordinate system is chosen in which "x" denotes the distance measured along the surface and "y" denotes the normal distance from the surface.

The velocity profile within the boundary layer is assumed to be a fourth-degree polynomial in η;

3.7-14 $$\frac{u}{U} = f(\eta) = A_0 + A_1\eta + A_2\eta^2 + A_3\eta^3 + A_4\eta^4$$

Where; $$\eta \left(\equiv \frac{y}{\delta} \right)$$

$\delta \equiv$ boundary layer thickness

$U \equiv$ velocity at the edge of the boundary layer obtained from the "Main Flow"

The various terms appearing in the alternative form of the Momentum Integral equation 3.7-9 are now derived based on the assumed form of the above velocity profile.

The momentum thickness θ, using the above equation for the velocity profile and equation 3.7-7, may now be expressed in the form;

3.7-15 $$\frac{\theta}{\delta} = \int_0^{\delta} f(\eta)[1 - f(\eta)]d\eta$$

and similarly from equations 3.7-8 and 3.7-14, the displacement thickness δ^* may be written as;

3.7-16 $$\frac{\delta^*}{\delta} = \int_0^{\delta} [1 - f(\eta)]d\eta$$

Further the slopes of the velocity profile at the wall and at the edge of the boundary layer may be expressed in terms of the function $f(\eta)$;

3.7-17 $$\left(\frac{\partial u}{\partial y}\right)_0 = \frac{U}{\delta}\frac{d}{d\eta} f(\eta)_{\eta=0}$$

3.7-18 $$\left(\frac{\partial u}{\partial y}\right)_{\delta} = \frac{U}{\delta}\frac{d}{d\eta} f(\eta)_{\eta=1}$$

The coefficients of the polynomial defining u/U, equation 3.7-14 will vary with (dp/dx). These are evaluated using the following boundary conditions for the velocity profile;

at $y = \delta$

3.7-19 $$(u)_\delta = U$$

$$\left(\frac{\partial u}{\partial y}\right)_\delta = \frac{U}{\delta} \cdot R$$

$$\left(\frac{\partial^2 u}{\partial y^2}\right)_\delta = 0$$

at $y = 0$

3.7-20 $$u = 0 \qquad \left(\frac{\partial^2 u}{\partial y^2}\right)_0 = -\frac{U}{\nu} \cdot \frac{dU}{dx}$$

It is assumed that, at the edge of the boundary layer, velocity profile is represented by a smooth curve without any extremum. (Fig 3.16)

Using the equation (3.7-9) and the Bernoulli's energy equation applied to the main flow out side the boundary

layer, the boundary conditions given by the equation 3.7-20 are obtained.

From the above boundary conditions, coefficients of the equation 3.7-14 are determined in terms of a non-dimensional shape factor Λ.
(See Appendix 3D)

3.7-21 $$\Lambda = \frac{\delta^2}{\nu} \cdot \frac{dU}{dx}$$

The coefficients are given by;

$$A_0 = 0 \qquad A_1 = \left(2 + \frac{\Lambda}{6} - R\right)$$

$$A_2 = -\frac{\Lambda}{2} \quad ; \quad A_3 = 2R + \frac{\Lambda}{2} - 2$$

$$A_4 = \left(1 - \frac{\Lambda}{6}\right) - R$$

Substituting the coefficients, the 4th degree polynomial velocity profile becomes;

$$\left(\frac{u}{U}\right) = f(\eta) = F(\eta) + \Lambda G(\eta) + R H(\eta)$$

Where,

$$F(\eta) = 2\eta - 2\eta^3 + \eta^4$$

$$G(\eta) = \frac{1}{6}\left(\eta - 3\eta^2 + 3\eta^3 - \eta^4\right)$$

$$H(\eta) = -\eta(1-\eta)\left(1 + \eta + \eta^2\right)$$

(See Appendix 3D)

Therefore substituting for $f(\eta)$, the terms of the Momentum Integral equation 3.7-9 given by equations 3.7-15 and 3.7-16 may be found as;

3.7-22 $$\left(\frac{\theta}{\delta}\right) = Q + J$$

(See Appendix 3D)

3.7-23 $$\left(\frac{\delta^*}{\delta}\right) = \left(\frac{3}{10} - \frac{\Lambda}{120}\right) - \frac{R}{5}$$

Where;

3.7-24 $$Q = \left(\frac{37}{315} - \frac{\Lambda}{945} - \frac{\Lambda^2}{9072}\right)$$

3.7-25 $$J = \frac{R}{7560}(29\Lambda - 372R + 744)$$

(see Appendix 3D)

and similarly from the equation 3.7-17;

3.7-26 $$\frac{\delta}{U}\left(\frac{\partial u}{\partial y}\right)_{y=0} = 2 + \frac{\Lambda}{6} - R$$

In the above equation R stands for;

3.7-27 $$R = \frac{\delta}{U} \cdot \left(\frac{\partial u}{\partial y}\right)_{y=\delta}$$

The shape factor Λ is still an unknown quantity since it contains the unknown boundary layer thickness δ.

The Momentum Integral equation (3.7-9) may be alternatively written in the following form, ready for the substitution of the various forms developed in terms of the assumed velocity profile;

3.7-28 $$U^2\frac{d\theta}{dx} + (2\theta + \delta^*)U\frac{dU}{dx} = \nu\left(\frac{\partial u}{\partial y}\right)_0 - \nu\left(\frac{\partial u}{\partial y}\right)_\delta$$

The above equation 3.7-28 may be considered as an ordinary differential equation for the shape factor Λ,

with x as the independent variable, the integration of which provides Λ as a function of **x.** Hence the boundary layer thickness δ may be obtained as a function of **x** through the equation 3.7-21 relating the shape factor Λ and boundary layer thickness δ. This ordinary differential equation will be expressed in an alternative form which has a mathematical advantage in the integration procedure as follows;

Multiplying the equation (3.7-28) by $(\theta/U\nu)$ we get;

3.7-29 $$\frac{U\theta}{\nu}\cdot\frac{d\theta}{dx}+\left(2+\frac{\delta^*}{\theta}\right)\frac{\theta^2}{\nu}\cdot\frac{dU}{dx}=\frac{\theta}{U}\left(\frac{\partial u}{\partial y}\right)_0-\frac{\theta}{U}\left(\frac{\partial u}{\partial y}\right)_\delta$$

Introducing the new variable;

3.7-30 $$K=Z\frac{dU}{dx}$$

Where

3.7-31 $$Z=\frac{\theta^2}{\nu}$$

Using the definition of Λ (see equation 3.7-21 and 3.7-22), K is expressed as;

3.7-32 $$K = \left(\frac{\theta^2}{\delta^2}\right)\Lambda \quad = \quad \Lambda(Q+J)^2$$

Using the equations 3.7-22, 3.7-23 and 3.7-26;

3.7-33 $$f_1 \equiv \frac{\delta^*}{\theta} = \frac{\delta^*/\delta}{\theta/\delta} = \left(\frac{3}{10} - \frac{\Lambda}{120} - \frac{R}{5}\right)/(Q+J)$$

$$\frac{\theta}{U}\left(\frac{\partial u}{\partial y}\right)_0 = \frac{\delta}{U}\left(\frac{\partial u}{\partial y}\right)_0\left(\frac{\theta}{\delta}\right) = \left(2 + \frac{\Lambda}{6} - R\right)(Q+J)$$

On differentiation of the equation 3.7-31;

$$\frac{dZ}{dx} = \frac{2\theta}{\nu}\frac{d\theta}{dx}$$

Now substituting the various terms into the Momentum Integral equation 3.7-29 becomes;

3.7-34 $$\frac{U}{2}\frac{dZ}{dx} = (Q+J)\left(2 - 2R + \frac{\Lambda}{6}\right) - \left(2 + f_1\right)K$$

Where,

K , f_1 , Q and J

are given by the equations 3.7-30, 3.7-33, 3.7-24 and 3.7-25.

The Momentum Integral equation (3.7-28) has thus been transformed into an ordinary differential equation (3.7-34) in which dU/dx does not appear explicitly. The Right Hand Side of the equation 3.7-34 contains terms which are all functions of the shape factor Λ. However the Λ and Z are related through equation 3.7-30. Here U and dU/dx are available as functions of x from the "Main Flow" solution. The determination of the Λ around the octagonal cylinder is therefore done by;

a) The integration of the equation 3.7-34 from the stagnation point S_2 to the point 1 (Fig 3.5) and from the point S_2 to the down stream separation point S utilising the "stagnation point initial conditions" considered in the next section.

and

b) The integration of the equation 3.7-34 from point 7 to the down stream separation point S utilising the "leading edge initial conditions" given in the next section (see 3.7.4).

3.7.4 Initial Conditions for The Integration of Momentum Integral Equation

For the integration procedure the initial values of Λ and the $(d\Lambda/dx)$ at $x=0$ are required.

For the **Region-1** and **Region-2** (see 3.7) at the starting point (S_2) of the integration (at the stagnation point) the shape factor (Λ_0) can be obtained using the argument which will be given in the section 3.7.5. The relevant equation for the Λ_0 is;

$$2-\frac{116\Lambda_0}{315}+\frac{79\Lambda_0^2}{7560}+\frac{\Lambda_0^3}{4536}-2R_0\left[1+\frac{\Lambda_0(29\Lambda_0-372R_0-12)}{7560}\right]=0$$

Where,

$$R_0\equiv\frac{1}{\sqrt{Re}}\cdot\sqrt{\frac{\Lambda_0}{dV/dx_0}}\cdot\frac{(dS/dx)_0}{(dV/dx)_0}$$

(The details are given in the Appendix 3F)

Based on the similar argument as above, at the stagnation point the value of $(d\Lambda/dx)_0$ is given by the expression;

$$\left(\frac{d\Lambda}{dx}\right)_0\left(L_0+\beta B_0-2E_0\right)=-4\sqrt{\nu\xi_0}$$

$$\cdot\left[1+\frac{\Lambda_0\left(29\Lambda_0-744R_0-12\right)}{7560}\right]\left[\alpha-\frac{\beta}{2}\frac{\left(d^2U/dx^2\right)_0}{\left(dU/dx\right)_0}\right]$$

$$+\quad\frac{\left(d^2U/dx^2\right)_0}{\left(dU/dx\right)_0}\cdot\Lambda_0\left[\left(Q_0+J'_0R_0\right)+\beta B_0\right]$$

Where;

$$\alpha=\frac{\left(d^2S/dx^2\right)_0-\beta\left(d^2U/dx^2\right)_0}{\left(dU/dx\right)_0}$$

$$\beta=\frac{\left(dS/dx\right)_0}{\left(dU/dx\right)_0}$$

$$B_0=\frac{\sqrt{\nu\xi_0}}{7560}\left(29\Lambda_0-744+744\right)\equiv\sqrt{\nu\xi_0}\,J_0$$

$$\frac{0.5\left(d^2S/dx^2\right)_0-\beta\left(d^2U/dx^2\right)_0}{\left(dU/dx\right)_0}$$

$$D_0 = -\frac{116}{315} + \frac{158\Lambda_0}{7560} + \frac{3\Lambda_0^2}{4536} - \frac{2R_0(58\Lambda_0 - 372R_0 - 12)}{7560}$$

$$E_0 = D_0 - \frac{\beta\sqrt{\nu\xi_0}}{\Lambda_0}\left[1 + \frac{\Lambda_0(29\Lambda_0 - 744R_0 - 12)}{7560}\right]$$

$$L_0 = \frac{37 - \Lambda_0}{315} - \frac{5\Lambda_0^2}{9072} + R_0\left[\frac{62 - 31R + (29/4)\cdot\Lambda_0}{630}\right]$$

$$\xi_0 = \frac{\Lambda_0}{(dU/dx)_0}$$

$$J'_0 = \frac{29\Lambda_0 - 372R_0 + 744}{7560}$$

$$S = \left(\frac{\partial u}{\partial y}\right)_{y=\delta}$$

$$Q_0 = Q \qquad for \qquad \Lambda = \Lambda_0$$

For the **leading edge** (at point 6, Fig 3.5) the initial conditions (see Appendix 3G) are;

$x \to 0$ $\qquad$ $\delta \to 0$

$U \to 0$ $\qquad$ $\Lambda \to 0\left(\equiv \frac{\delta^2}{\nu}\cdot\frac{dU}{dx}\right)$

and also

$$\lim_{x \to 0} \frac{dU}{dx} \to \neq 0$$

$$\lim_{x \to 0} S \to \neq 0$$

$$\lim_{x \to 0} \frac{dS}{dx} \to \neq 0$$

As seen from the equation 3.7-36, for the integration procedure in the Regions 1 and 2 it is necessary to determine the value of the second derivative (d^2U/dx^2) at the initial point S_2. This is obtained by a numerical differentiation procedure using the values of the derivative dU/dx available at the nodal points. Owing to the restriction imposed by the computer timing the number of segments in defining the boundary of the two-dimensional flow in using the NAG D03EAF solution (see 3.6.5) is restricted. This, results in inconsistent values of the dU/dx at some points due to numerical integration error. This causes instability in the integration process of the boundary layer around the vertices of the octagon. To overcome this, the computed slip velocity variation was smoothened around the vertices of the octagon by a curve fitting procedure. However the values computed with these

modifications give only an insignificant difference between the solutions using the appropriate values of **R** and for which **R=0** . In view of this and the inherent inaccuracies involved in the assumptions and numerical integration procedure **R=0** is used in the further work. This considerably simplifies the computing effort in the integration.

Although $R=0$ was used in the present work, $R\neq 0$ is a useful modification to the Momentum Integral equation when applied for a tangential wall-jet imposed on a free stream, and leads to the evaluation of the shear-stress at the edge of the laminar boundary layer. It was found that this procedure can successfully be utilized for the case of Circular cylinder, Flat plate or an aerofoil cross-section in a free-stream in the presence of a tangential jet.

3.7.5 Method of Solution for the Laminar Boundary Layer

The equation 3.7-34 using $R=0$, as discussed in the previous section reduces to;

3.7-37 $$\frac{U}{2}\frac{dZ}{dx}+(2+f_1)K=Q\left(2+\frac{\Lambda}{6}\right)$$

Where;

$$Q=\left(\frac{37}{315}-\frac{\Lambda}{945}-\frac{\Lambda^2}{9072}\right)$$

3.7-30 $$K=Z\frac{dU}{dx}$$

Where

3.7-31 $$Z=\frac{\theta^2}{\nu}$$

$$f_1\equiv\frac{\delta^*}{\theta}=\frac{\delta^*/\delta}{\theta/\delta}=\left(\frac{3}{10}-\frac{\Lambda}{120}\right)/(Q)$$

The equation (3.7-37), can also be expressed as;

3.7-38 $$\frac{dZ}{dx}=\frac{4Q}{U}\left[1-\Lambda\ \left(Q-\frac{16-\Lambda}{240}\right)\right]$$

(Equation 3.7-38 is derived in the Appendix 3E)

Where Z may now be expressed using the equation 3.7-30 as;

3.7-39 $$Z = \frac{K}{(dU/dx)}$$

Also for $R = 0$ from equation 3.7-32,

3.7-40 $$K = \Lambda Q^2$$

Right Hand Side of the equation 3.7-38 the shape factor Λ may be in principle be replaced by K through the implicit relationship of equation 3.7-40. Further K it self may be considered to be a function of Z and x from the equation 3.7-39. Hence the equation 3.7-38 represent a first-order non-linear differential equation for Z in terms of x. This equation is integrated by the Runge-kutta method of numerical integration and the values of Z and the shape factor Λ are obtained as a function of x. The relationship between Z and K (equation 3.7-38) and the implicit relationship between K and Λ, (equation 3.7-40) are also determined (47). For the three Regions on the counter C2; (Fig 3.5)

Region-1 Numerical integration starts at $x = 0$ from the stagnation point S_{2L}. The initial values at $x = 0$, for $\Lambda = \Lambda_0$ and $(d\Lambda/dx)$ are computed from equation 3.7-36, where $R_0 = 0$ and the integral procedure is

continued until the x attains a value corresponding to the point at which $\Lambda = -12$. Within this Region

Λ *remains* ≥ -12

Region-2 Similarly the numerical integration is from the stagnation point S_{2L} upto the down stream separation point S, where Λ *remains* ≥ -12.

(Fig 3.17)

Region-3 Numerical integration is started from point 7 upto to the down stream separation point S where, the initial value of $at \quad x = 0, \Lambda_0 = 0$ and remains $\Lambda \leq +14$

The influence of the assumed shape of the velocity profile in determining the boundary layer flow using these equations has been established (15). The use of the 4 th degree polynomial is physically feasible only for $-12 \leq \Lambda \leq +12$. Where $\Lambda > +12$, the velocity profile has a maximum within the boundary layer as shown in the Fig 3.17. For the $\Lambda = -12$ the solution predicts a laminar boundary layer separation point and for $\Lambda < -12$, a reversed flow with in the boundary layer is implied.

For the **stagnation point** initial conditions

$x = 0 \quad U = 0 \quad dU/dx$ *is finite* and $dU/dX \neq 0$. The value of the $dZ/dx \quad at \quad x = 0$ would become infinite at the point S_2, unless the right hand side of the equation 3.7-38 is

equal to 0 there simultaneously. This condition is utilized in the Appendix 3E to evaluate the Λ_0 and K_0. The values obtained are;

$$K_0 = 0.0770$$

or $$\Lambda_0 = 7.052$$

Hence , $\Lambda = \Lambda_0 = 7.052$ is taken as the shape factor at the stagnation point. However, the differentiation coefficient dZ/dx attains an indefinite form of 0/0, by stipulating right hand side of the equation 3.7-38 at x=0. The appropriate mathematical limit of this 0/0 form is evaluated (details are given in the Appendix 3E) to be;

$$\left(\frac{dZ}{dx}\right)_{x=0} = -0.0652\left[\frac{d^2U/dx^2}{(dU/dx)^2}\right]_{x=0}$$

A FORTRAN computer programme STTUR1 is developed and the subroutine "STGIC2" of this considers individual Regions 1, 2 and 3 and selects the appropriate slip velocity from the Stage-1 of the programme discussed in the section 3.6.3 from the main flow. From these values the derivative dU/dx was obtained at every location of x. (For the flow chart and the programme see Appendix 5B) The value of dU/dx is generally

expected to be > 0 for the first two Regions where smooth surfaces are encountered. However the slip velocities around the vertices of the octagon experience an oscillatory nature as discussed in the section 3.6.4. In the numerical integration this results in a negative value of dU/dx. Occurrence of this behaviour around the octagonal shape considered can be dealt by making the dU/dx to be a positive value at those points, where these negative values are predicted.

However for the prevailing conditions considered in this investigation, if the uninterrupted laminar boundary layer reaches the first point where the octagonal side changes, the flow loses its two-dimensionality and change over to a turbulent boundary layer (15). Hence though the approximate method employed is capable of determining the laminar boundary layer right around the octagonal cylinder, it has been used only upto the first separation point or otherwise only upto the first point on the next side of the octagon where the flow changes its direction.

Values of slipstream velocities determined by the D03EAF routine represents, velocities at 80 equally divided segments on octagon sides of the inner contour C2. Boundary layer development has been determined by

the Fourth-order Runge-Kutta integration. The integration step Δh was taken as 0.001. The Fourth-order Runge-Kutta integration has a truncation error of order h^5. The velocity, and the dU/dx were interpolated/extrapolated to determine the values at each step of the integration, as these values were available only at nodal points.

3.7.6 Evaluation of Λ for Given K

In the numerical integration of the equation 3.7-34 the values of Λ are to be obtained for specified values of K. The relationship between the Λ and K is given by;

3.7-40 $$K = \Lambda Q^2$$

Where;

$$Q \equiv \frac{37}{315} - \frac{\Lambda}{945} - \frac{\Lambda^2}{9072}$$

Hence $d\Lambda/dK$ and $d^2\Lambda/dK^2$ are readily available by differentiating polynomial expansion of Λ for K. From the Taylor's Expansion series (51);

$$K = K_P + \frac{dK}{d\Lambda}\left(\Lambda - \Lambda_P\right) + \frac{1}{2}\cdot\frac{d^2K}{d\Lambda^2}\left(\Lambda - \Lambda_P\right)^2 + \cdots$$

Where suffix P denotes the value of Λ and the corresponding values of K at a previous location.

by approximating to the first order terms;

$$K = K_P + \left(\frac{dK}{d\Lambda}\right)\left(\Lambda_1 - \Lambda_P\right)$$

Therefore the first approximation for the Λ is given by;

$$\Lambda_1 = \frac{\Delta K}{(dK/d\Lambda)} + \Lambda_P$$

Substituting for $\left(\Lambda - \Lambda_P\right)^2$,

in the Taylor's expansion, the term $\left(\Lambda_1 - \Lambda_P\right)^2$

$$\Delta K \equiv \frac{dK}{d\Lambda} \cdot \left(\Lambda - \Lambda_P\right) + 0.5\left(\frac{d^2K}{\left(d\Lambda^2\right)} \cdot \frac{(\Delta K)^2}{(dK/d\Lambda)^2}\right.$$

Here in solving of Λ the interpolated value is given by;

3.7-41 $$\Lambda = \frac{\Delta K}{dK/d\Lambda} - 0.5\frac{\left(d^2K/d\Lambda^2\right)(\Delta K)^2}{(dK/d\Lambda)^3} + \Lambda_P$$

Where $\Delta K = \left(K - K_P\right)$

Fig 3.18 shows the relationship between K and Λ and K reaches its first maximum of 0.0948 at $\Lambda = 12$. Although numerically shape factor Λ can reach higher values than 12 they do not represent any possible velocity profile defined by the Fourth-degree Polynomial.

Determination of the Λ for the regions 1 and 2 is started with $x = 0$ $U = 0$ and $\Lambda = 7.052$. Equation 3.7-41 was used to evaluate the shape factor Λ corresponding to the values of K, obtained at each step of numerical integration procedure. However in using this equation where the values of K are closer to 0.0948 the value of Λ was incorrectly determined. This is due to the $K-\Lambda$ relationship given by the equation 3.7-40 (Fig 3.18) having an extremum. at $\Lambda = +12, K = 0.0948$. Therefore as the K reaches its maximum value (K Max = 0.0948), for the determination of Λ "bi-Section" method (50) has been used. Details of the procedure is given in the flow chart of STTUR1 (see Appendix 5B).

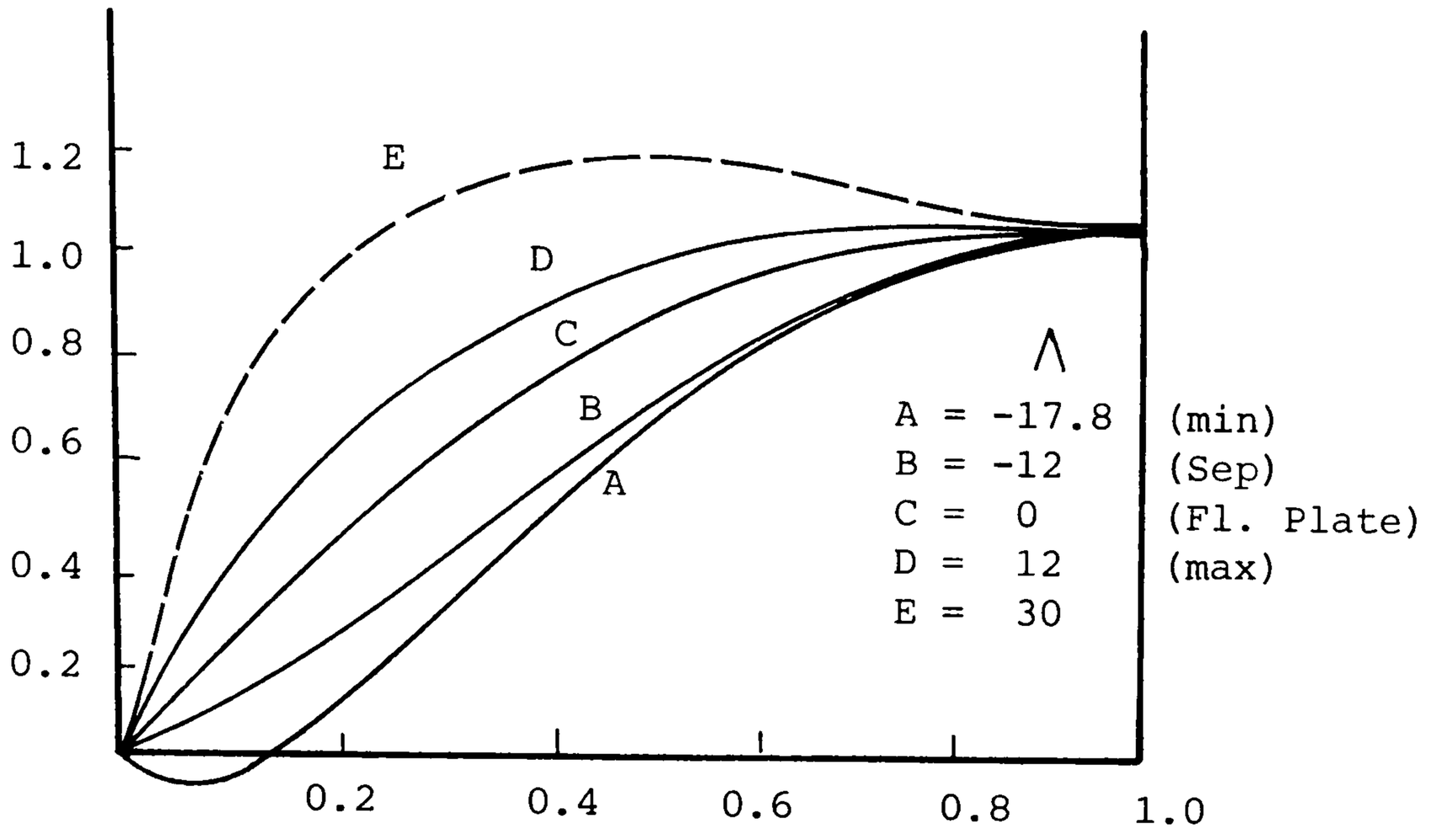

Fig 3.17 Shapes of the Velocity Profiles for the Method of Pohlhausen

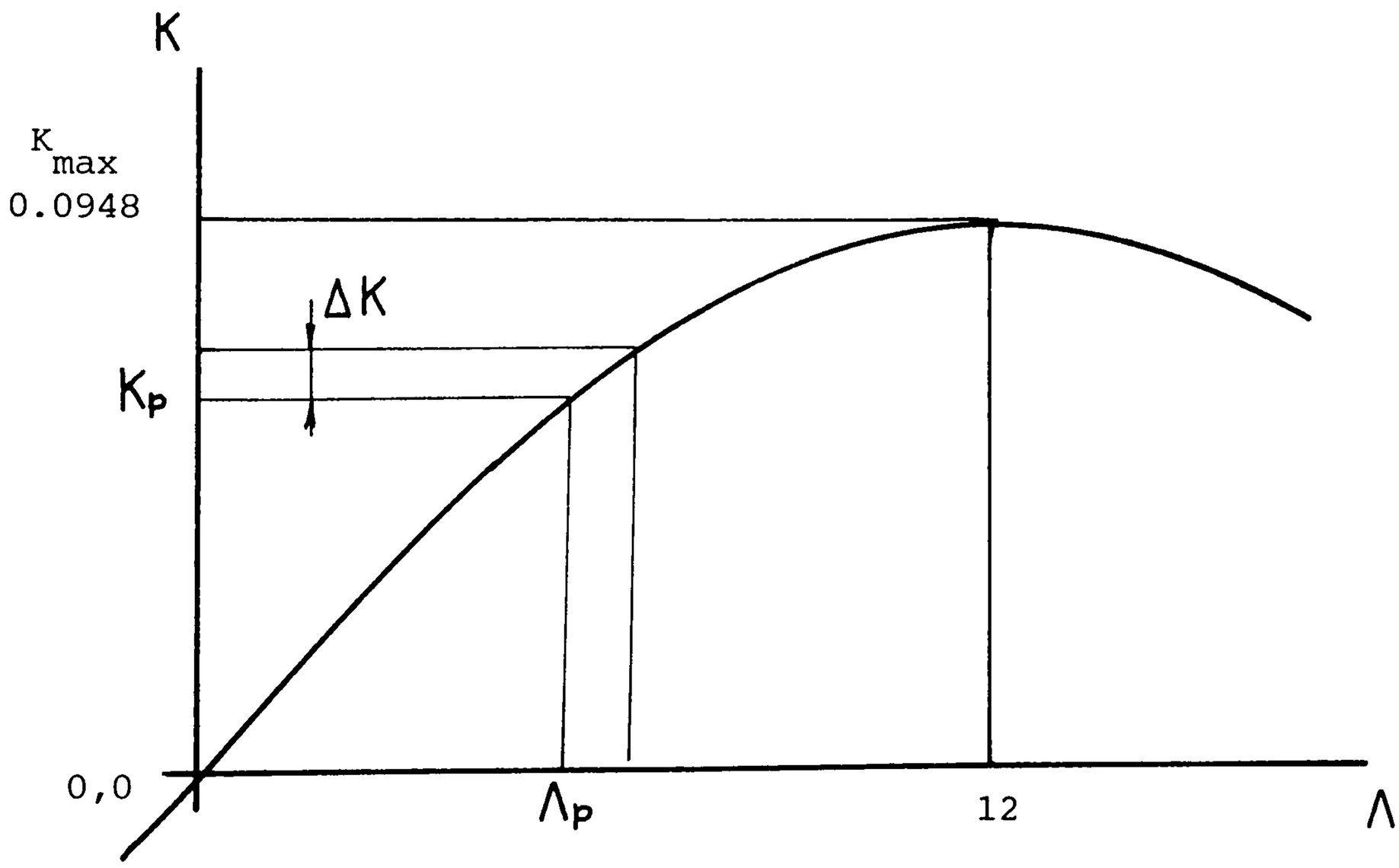

Fig 3.18 Shape Factor Vs K and the Method of Calculation of Λ

3.8.1 Turbulent Boundary Layer

In the regions 1 and 2 of the boundary layer (Fig 3.5) the boundary layer is initially laminar at the stagnation point S_2. In both the cases the boundary layer becomes turbulent along the octagonal surface as the first of the vertices is approached due to the change of direction. Boundary layer may also become turbulent preceding the approach of the first vertex of the octagon. The transition point decided in the STTUR1 FORTRAN programme (see Appendix 5B) is based on the shear-stress becoming zero and this is taken as the initial point for the turbulent boundary layer growth in the case of Region-1 and Region-2. The thickness of the laminar boundary layer at this transition point is taken as the initial value for the turbulent boundary layer thickness. For the Region-3, discussed in the section 3.7, the turbulent boundary layer is considered to begin from the point where the jet leaves the nozzle. Blasius's equation for the wall shear-stress for the turbulent flow is adopted in a modified form in the formulation of the Momentum Integral equation for the turbulent boundary layer. The modification results in solutions which are compatible with the physical conditions as shown in the section 3.8.3.

3.8.2 Momentum Integral Equation for The Determination of The Turbulent Boundary Layer

The turbulent boundary layer thickness around the octagonal cylinder is evaluated using the Momentum integral equation which may be expressed in the form;

3.8-1 $$\frac{d}{dX}\int_0^{\Delta}(V-v)v\,dY-\frac{dV}{dX}\int_0^{\Delta}v\,dY \;=\; 2\cdot\tau_{\omega n-d}-V\Delta^{*}\cdot\frac{dV}{dX}$$

(See Appendix 3H)

In the present development the laminar sub-layer of the turbulent boundary layer next to the wall surface is included, as was originally considered by Prandtl (52). Further inside the turbulent boundary layer the velocity profile is assumed to be given by the equation proposed by Prandtl for the case of a flat plate;

3.8-2 $$\frac{u}{U}=\left(\frac{y}{\delta}\right)^{1/7}$$

The above equation on differentiation gives the velocity gradient with respect to transverse direction, viz.,

3.8-3 $$\frac{du}{dy} = \frac{1}{7} \cdot \frac{U}{(\delta y^6)^{1/7}}$$

This shows that at the wall $(y = 0)$ the value of du/dy tends to infinity and predicts an infinite value for the shear-stress at the wall, this is a physically impossible condition (15,52). In reality the fluid turbulence always dies down in the neighbourhood of the wall. This anomaly arises owing to the assumption that the velocity profile is given by the equation (3.8-2) is applicable to the entire boundary layer thickness. However as mentioned earlier, the existence of the laminar sub-layer invalidates the use of the above profile near the wall and in fact the velocity variation should be expressed by different type of the function of the distance y, within the sub-layer. At the border between both the layers, the assumed velocity profiles are continuous but may have a discontinuity in slopes at the point of transition as shown in the Fig 3.19. However the use of equation (3.8-4) to evaluate the definite integral over the entire boundary layer thickness, appears on the Left Hand Side of the Momentum Integral equation (3.8-1) is justified as the corrections required in using the laminar sub-layer profile is quite small.

The non-dimensional wall shear-stress term appears on the Right Hand Side of the Momentum Integral equation (3.8-1) is initially assumed to be given by Blasius's equation;

3.8-4
$$\tau_{\substack{\omega \\ n-d}} = 0.0456 V^2 \left(\frac{\nu}{V W \Delta l} \right)^{0.25}$$

(The detailed formulation of the above equation is given in the Appendix 3H) In order to achieve algebraic simplicity a non-dimensional variable β is defined as follows;

3.8-5
$$\beta = \Delta^{5/4}$$

Utilising the velocity profile (3.8-13), substituting from equation 3.8-4 for the non-dimensional shear-stress and using the variable β the Momentum Integral equation 3.8-1 can be expressed as (see Appendix 3H);

3.8-6
$$\frac{d\beta}{dX} = \left[\left(-\frac{115}{28} \right) \left(\frac{dV}{dX} \right) \beta + \frac{90(0.0228) V^{3/4}}{Re^{1/4}} \right] / \ V$$

By integrating the above equation, with respect to X the value of β, and hence the non-dimensional boundary layer thickness δ is determined. At the edge of the

boundary layer the values of non-dimensional slip velocities V are obtained from the main flow solution (see 3.6.4)

3.8.3 Preliminary Investigation of The Effect of The dV/dX on The Turbulent Boundary Layer Growth

The equation 3.8-6 may be expressed as;

3.8-7 $$\frac{d\beta}{dX} = -\beta F(X) + G(X)$$

Where;

$$F(X) = \frac{115}{28} \cdot \frac{1}{V} \cdot \frac{dV}{dX}$$

$$G(X) = \alpha \cdot V^{-1/4}$$

$$\alpha \equiv \frac{90 \times 0.0228}{7 \times Re^{1/4}}$$

The linear differential equation 3.8-7 may be integrated using the integration factor the $\exp(F(X)dX)$, hence β is given by;

3.8-8 $$\beta \cdot \exp \int_0^X F(X)dX = \int_0^X G(X)\exp \int_0^X F(X)dX + \ Const$$

As shown in the Appendix 3J for the case where dV/dX is a constant, i.e.,

$$\frac{dV}{dX} = S$$

We get,

$$\exp \int_0^X F(X)dX = \left(\frac{V}{V_0}\right)^{115/28}$$

Where , V_0 is the value of V at $X = 0$, and 3.8-8 reduces to;

3.8-9 $$\beta\left(\frac{V}{V_0}\right)^{115/28} = \frac{7\alpha}{34SV_0^{115/28}} \cdot V^{34/7} + \ constant$$

Using the boundary conditions at

$$at \quad X = 0 \quad , \quad \beta = \beta_0$$

The Constant becomes;

3.8-10 $$Const = \beta_0 - \frac{7\alpha}{34 S V_0^{115/28}} \cdot \left(V_0\right)^{34/7}$$

(Details are are given in the Appendix 3J)

Therefore, by substituting the value of the constant into the equation 3.8-9,

3.8-11 $$\beta = \frac{7\alpha}{34 S} \cdot V^{-115/28}\left(V^{34/7} - V_0^{34/7}\right) + \frac{\beta_0}{\left(V/V_0\right)^{115/28}}$$

Where,

$$V = V_0 + \frac{dV}{dX} X$$

and $\beta_0 = 0$

Where, $S = 0$, β given by the above equation, attains a 0/0 form. The evaluation of the approximate limit using the L'Hospitals rule is given in the Appendix 3J.

3.8-12 $$\beta = \frac{7\alpha}{34 S} V_0^{21/28}\left[\frac{Z^{34/7} - 1}{Z^{115/28}}\right]$$

Where, $$Z = \left(\frac{V}{V_0}\right)$$

and

$$\psi(Z) \equiv \frac{Z^{34/7} - 1}{Z^{115/28}} > 0$$

$$For \quad all \quad Z > 0$$

For a typical value of $Re = 50000$

$$\alpha = \frac{90}{7} \cdot \frac{0.0228}{50000^{0.25}}$$

For a $dV/dX = Const$ value (non-zero) the ψ and Z are calculated. A typical set of results of the boundary layer growth $\delta n - d$ Vs the non-dimensional distance X is shown in the Fig 3.21. Here three possible cases are examined.

(i) For a boundary layer growth from a initial zero thickness $(\beta_0 = 0)$, for both the cases of $S > 0$ or $S < 0$ boundary layer thickness δ increases without an extremum. and hence the surface shear-stress. Therefore the possibility of the turbulent boundary layer separation is eliminated from the procedure.

(ii) For a boundary layer growth from a non-zero initial thickness, for sufficiently large positive values of the S, the boundary layer thickness decreases

to a minimum value and thus the surface shear stress. However as the X increases the boundary layer thickness starts to grow further without the turbulent separation.

(iii) For a boundary layer growth from a non-zero initial thickness, for adverse pressure gradients, boundary layer thickness increases without a limit. (Identical to the case (i)).

Therefore use of the Blasius equation along with the Momentum Integral Equation cannot identify the turbulent separation points and therefore for most of the cases boundary layer thickness grow to meaningless large values and thus the surface shear stress. This is mainly due to the approximation of the velocity profile at the laminar sub-layer is also represented by the same 1/7 th power law velocity profile as for the turbulent boundary layer. To be compatible with the physical situation (page 629, Ref 15), within the laminar sub-layer velocity is represented by a parabolic profile (see 3.8.4).

3.8.4 Evaluation of The Non-Dimensional Surface Shear stress Based on The Parabolic Velocity Profile Within The Laminar Sub-Layer

Velocity profile inside the laminar sub-layer is usually approximated by a linear variation (52). In the present work the turbulent boundary layer excluding the laminar sub-layer is represented by Prandtl's *1/7 power law* (3.8-2), and within the laminar sub-layer, the profile is approximated by a parabolic function given by (Fig 3.20);

3.8-13 $$\frac{U}{U_l} = A_0 + A_1\eta + A_2\eta^2$$

Where $$\eta = \left(\frac{y}{\delta l}\right) = \left(\frac{y}{\delta}\right)\left(\frac{\delta}{\delta l}\right)$$

Here the two velocity profiles are matched at the edge of the laminar sub-layer giving;

3.8-14 $$\frac{U_l}{U} = \left(\frac{\delta_l}{\delta}\right)^{1/7}$$

And using the boundary conditions as given in the Appendix 3I, constants of the equation 3.8-13 becomes,

$$A_0 = 0 \qquad A_1 = \left(1 + \frac{U}{U_l} \cdot \frac{\delta_l^2 \cdot (dU/dX)}{\nu} \right)$$

$$A_2 = -\frac{1}{2\nu} \cdot \delta_l^2 \cdot \frac{U}{U_l} \cdot \frac{dU}{dX}$$

For laminar sub-layer shear-stress at the wall is given by the Newtonian Viscosity equation (53)

3.8-15 $$\tau_\omega = \mu \frac{U_l}{\delta_l}(A_1) = \mu U \left(\frac{\delta_l}{\delta} \right)^{1/7} \left(\frac{1}{\delta_l} \right) \cdot A_1$$

Also from Blasius's equation;

3.8-16 $$\tau_\omega = 0.0228 \cdot \frac{\rho U^2}{(\rho U \delta / \mu)^{0.25}}$$

By assuming that the relationship between the δ and δ_l prevails, for (dP/dX) values closer to zero. The relationship between δ_l and δ can be obtained by equations 3.8-15 and 3.8-16;

3.8-17 $$\frac{\delta_l}{\delta} = \left(\frac{1}{0.0228} \right)^{7/6} \cdot \left(\frac{\nu}{U\delta} \right)^{7/8}$$

The values of δ_{n-d} and $\tau_{\underset{n-d}{\omega}}$ are given by the equation I-12 as;

3.8-18 $$\tau_{\substack{\omega \\ n-d}} = \frac{2}{Re} \cdot \frac{V_l}{\delta_{\substack{l \\ n-d}}} + V \frac{dV}{dX} \cdot \delta_{\substack{l \\ n-d}}$$

(Derivation is given in the Appendix 3I)

and from the equation I-13 of the Appendix 3I, the non-dimensional boundary layer thickness can be expressed as;

3.8-19 $$\delta_{\substack{l \\ n-d}} = \frac{1}{(0.0228)^{7/6} \cdot (Re)^{7/8}} \cdot \left(\frac{\delta_{n-d}^{1/8}}{V^{7/8}} \right)$$

By substituting the values given in the equations I-12, I-14, I-15 of the Appendix 3I to the Momentum Integral equation (3.8-1);

3.8-20 $$\frac{d\delta_{n-d}}{dX}\left(\frac{7}{72}V^2\right) + \delta_{n-d}\left(\frac{7}{36}V\frac{dV}{dX} - \frac{7}{8}\cdot V\frac{dV}{dX} + V\frac{dV}{dX}\right) = 0.5\tau_{\substack{\omega \\ n-d}}$$

Where;

$$0.5\tau_{\substack{\omega \\ n-d}} = \frac{0.0228}{Re^{0.25}}\left(\frac{V^7}{\delta_{n-d}}\right)^{1/4} + \frac{1}{2}\frac{dV}{dX}\left[\frac{\delta_{n-d}^{1/8}\cdot V^{1/8}}{(0.0228)^{7/6}\cdot Re^{7/8}}\right]$$

(Details are given in the Appendix 3I)

3.8.5 Typical Behaviour of Turbulent Boundary Layer Growth

The ordinary differential equation 3.8-20 for turbulent boundary layer thickness $\delta_{n\text{-}d}$ may be numerically integrated for given variation of V with respect to X. Using a similar method to the one discussed in the section 3.8.3, the turbulent boundary layer thickness, surface shear stress and the separation points have been computed (see 3.8.6) for a linear velocity profile given by;

$$V = V_0 + S \cdot X$$

using a typical set of initial data given in the Table T-4.

Results of the computation for the above case are given in the Fig 3.22 to Fig 3.24. Based on these investigations, use of the parabolic velocity profile inside the laminar sub layer leads to the following conclusions;

For adverse pressure gradient, growth of the turbulent boundary layer without an initial boundary layer thickness results in a turbulent boundary layer separation. As the magnitude of the adverse pressure

gradient increases, the boundary layer separation point move towards the leading edge. If the boundary layer growth is started with an initial boundary layer thickness, turbulent boundary layer separation point move towards the trailing edge (Fig 3.23).

For zero pressure gradient the turbulent boundary layer has a steady growth and as the initial boundary layer thickness increases the rate of the boundary layer growth increases (Fig 3.24).

For a positive pressure gradient with an initial boundary layer thickness the growth of the boundary layer reaches a minimum value and then continues to grow with a reduced rate. If the boundary layer growth is started without an initial thickness, the growth does not exhibit a minimum value. As the pressure gradient increases the rate of growth of the boundary layer thickness decreases with the distance (Fig 3.22).

However for positive and zero pressure gradients the turbulent boundary layer does not separate from the surface.

Table T-4

δ_o	S	H Ineg. Step	Re	V_0	Remarks
0.0	-0.65	0.01	50000	2.0	Adverse
0.05	-0.65	0.01	50000	2.0	Pressure
0.05	-0.35	0.01	50000	2.0	Gradient
0.0	-0.35	0.01	50000	2.0	
0.0	0.0	0.01	50000	2.0	Zero Pr.
0.05	0.0	0.01	50000	2.0	Gradient
0.05	0.35	0.01	50000	2.0	Fav.
0.0	0.35	0.01	50000	2.0	Pressure
0.0	0.65	0.01	50000	2.0	Gradient

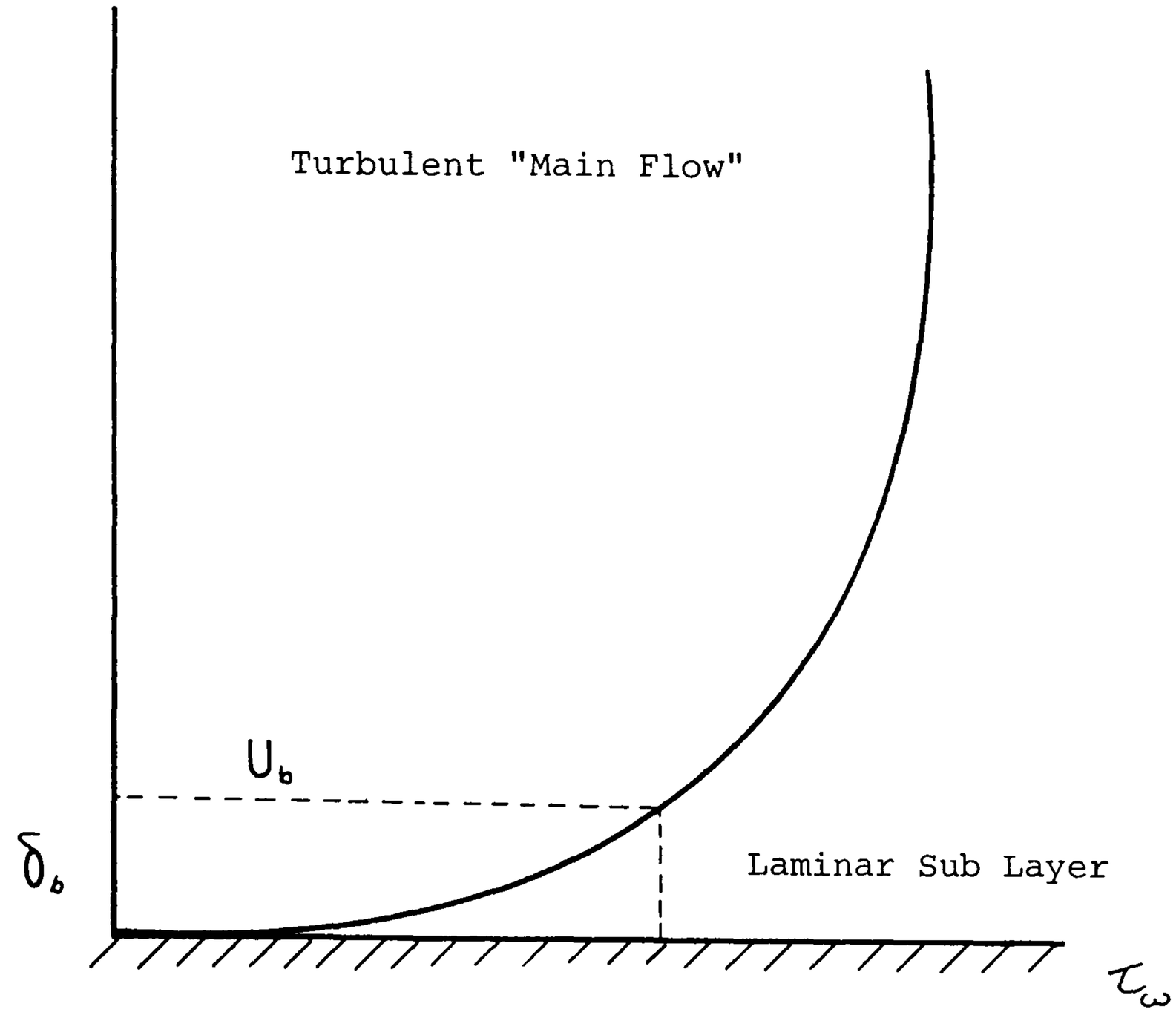

Fig 3.19 Prandtl's Turbulent Velocity Profile
and the Laminar Sub-layer

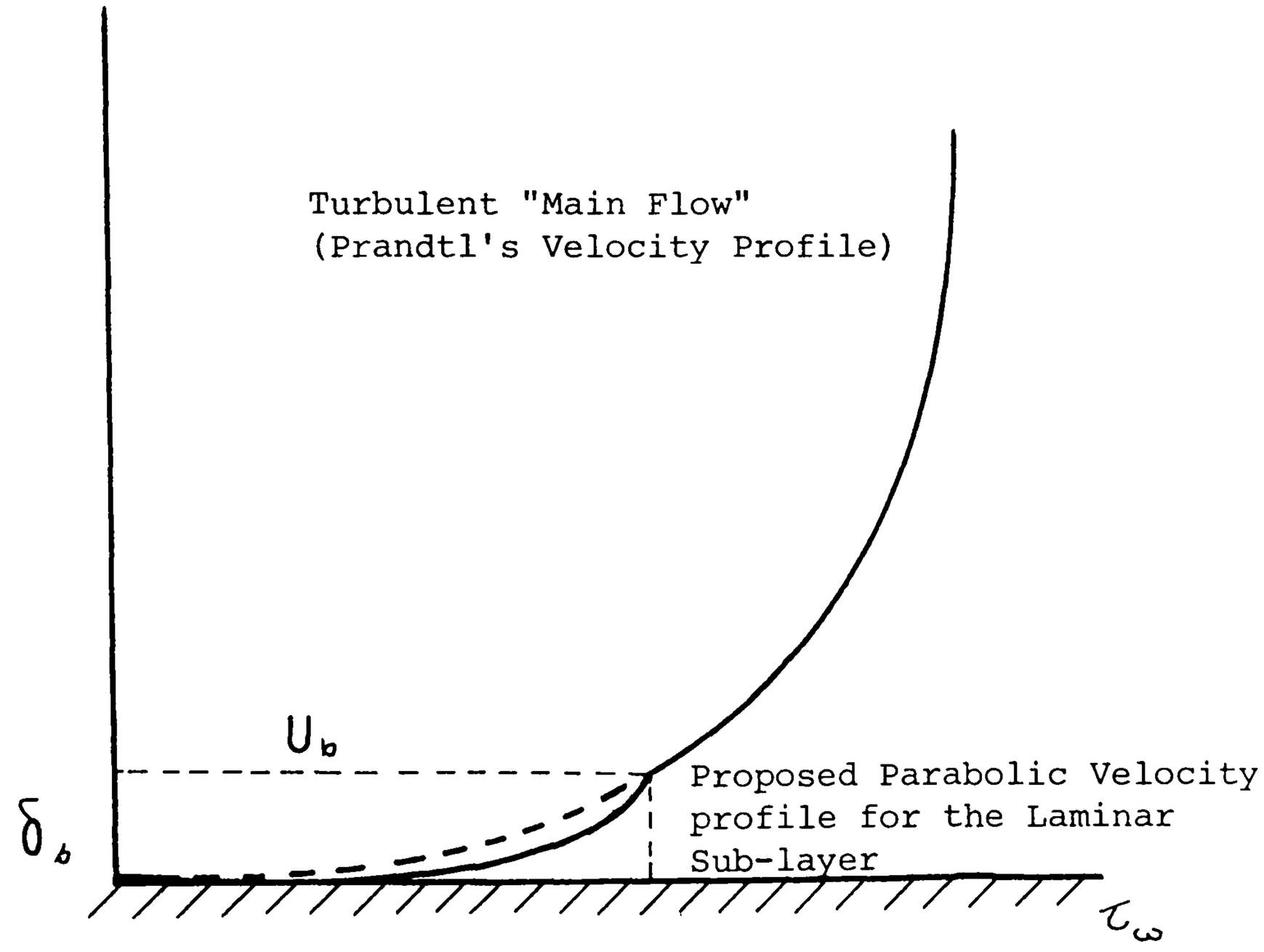

Fig 3.20 Proposed Laminar Sub-layer Profile

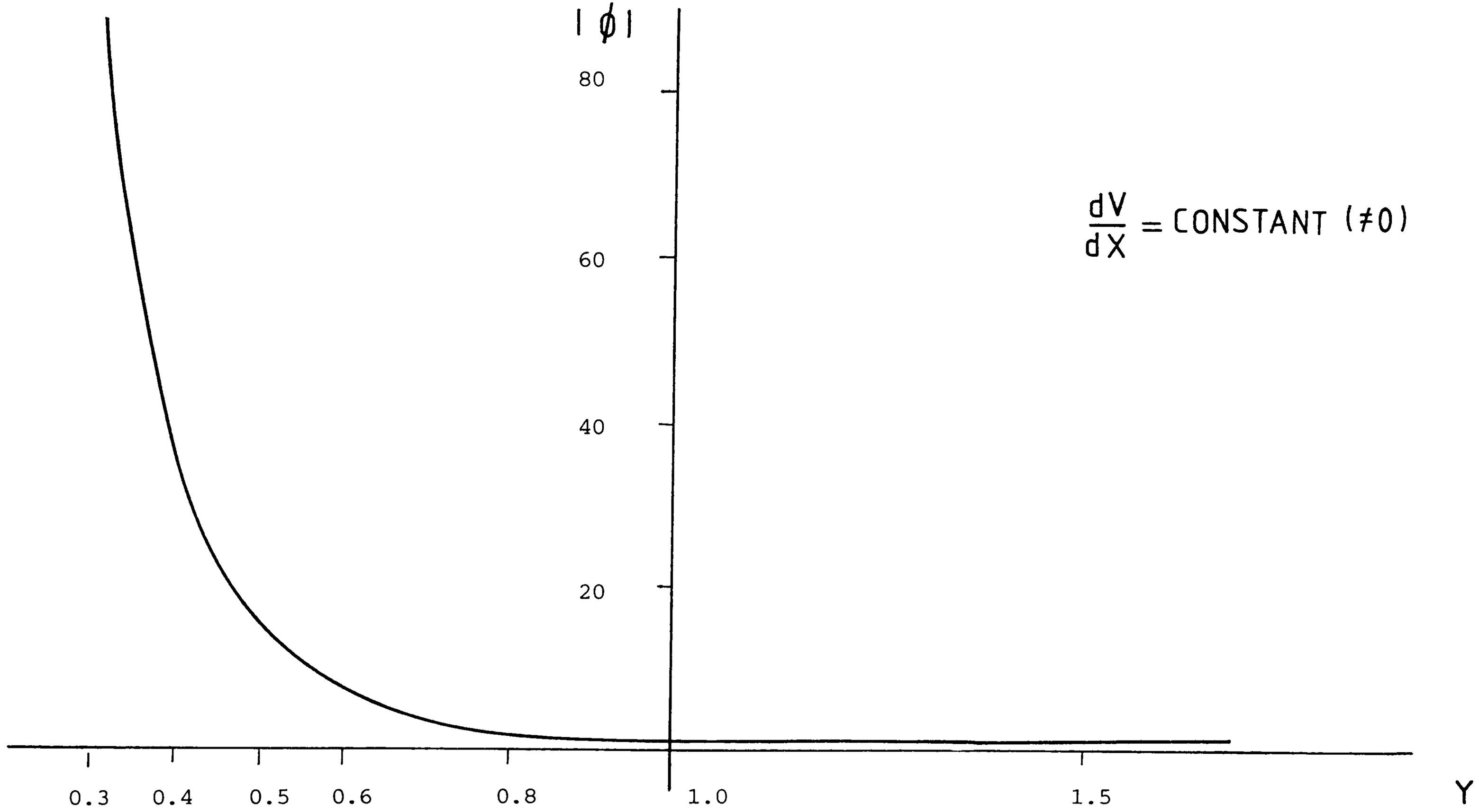

Fig 3.21 Prediction of the Boundary Layer Growth
With out the Laminar Sub-layer (Parabolic)

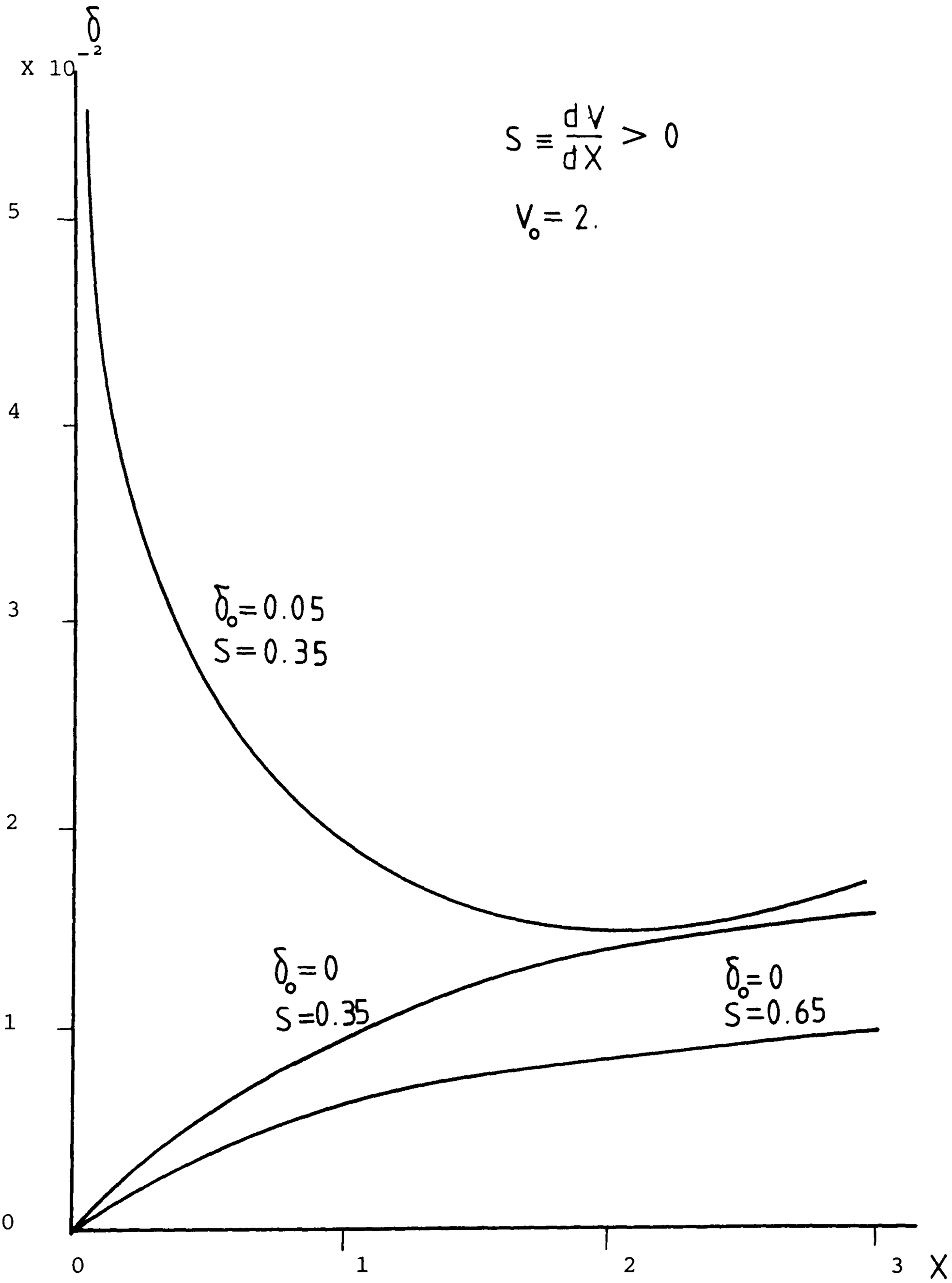

Fig 3.22 Turbulent Boundary Layer Growth Using the Parabolic Laminar Sub-layer dV/dX > 0

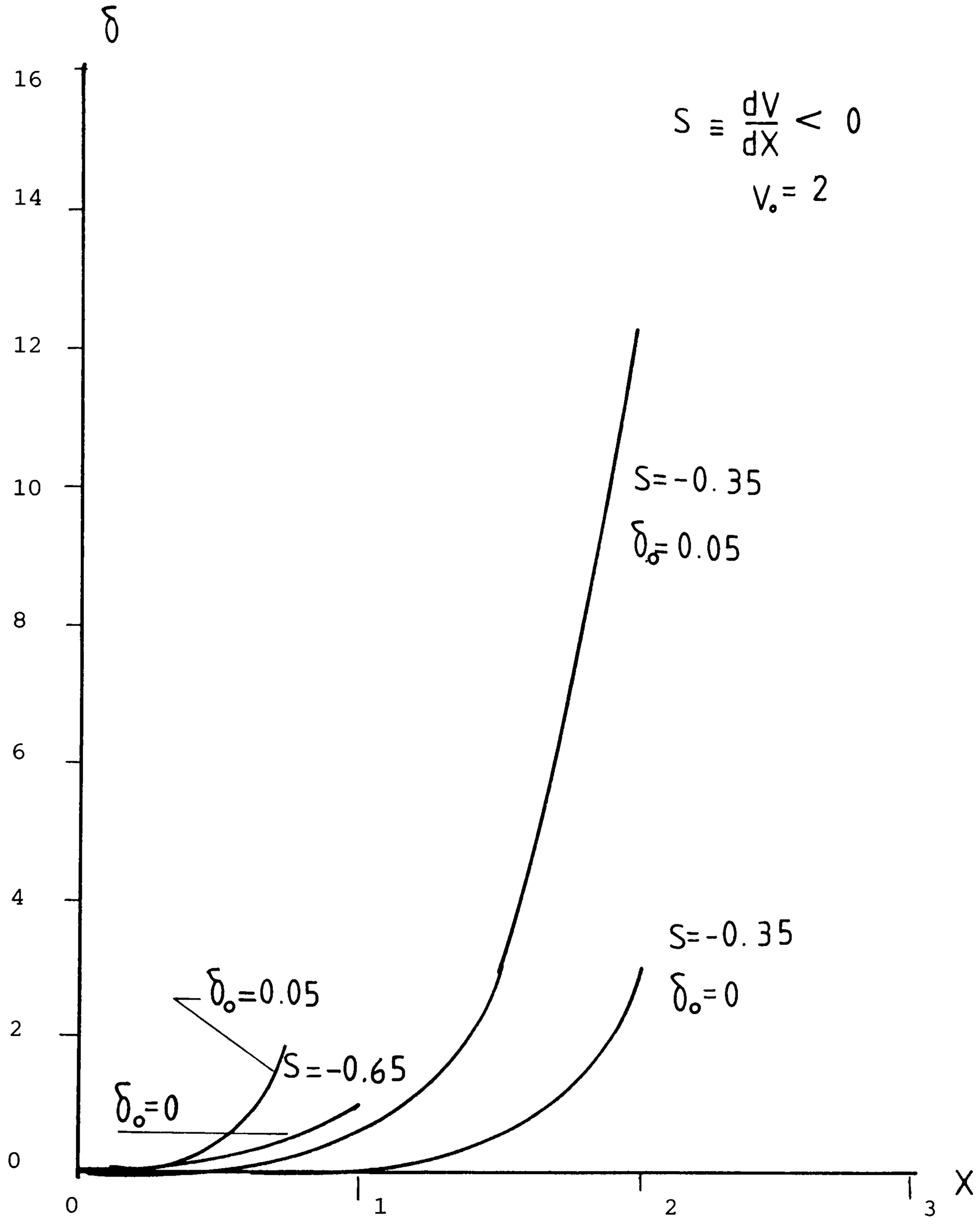

Fig 3.23 Turbulent Boundary Layer Growth Using the Parabolic Laminar Sub-layer dV/dX < 0

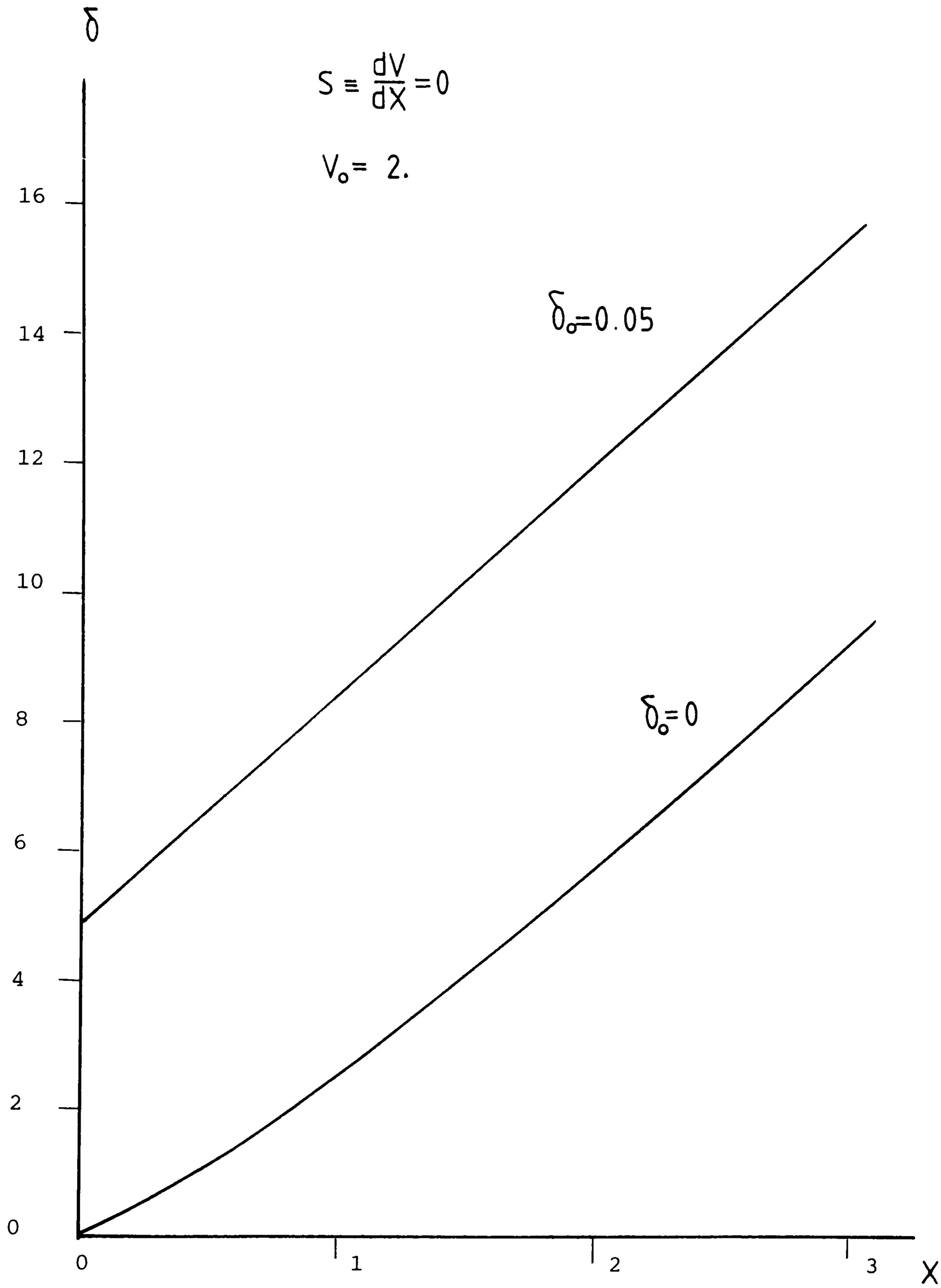

Fig 3.24 Turbulent Boundary Layer Growth Using the Parabolic Laminar Sub-layer dV/dX = 0

3.8.6 Computation of The Surface Shear Stress for The Laminar and The Turbulent Boundary Layer

The FORTRAN programme STTUR1 was developed to determine the surface shear stress on the octagonal cylinder. For the computational procedure the surface around the octagonal cylinder is divided into three regions as given in the section 3.7.5. The computation of the boundary layer thickness, the separation points and the surface shear stress on the octagonal surface is started from the Region-1. The Reynolds number of the flow, the slip stream velocities, the coordinates of the nodal points (see 3.6.2) and the coordinates of the vortices of the octagonal cylinder are supplied as the main input data to the computer programme. By calculating the shape factor Λ, the surface shear stress due to the laminar boundary layer is determined (see 3.7.6). As the laminar flow changes to a turbulent flow, the boundary layer thickness and the surface shear stress are determined as discussed in the section 3.8.4 and 3.8.5. At the transition point the laminar boundary layer thickness is taken as the initial value of the turbulent boundary layer thickness. If the laminar boundary layer separation does not take place before the first vertex of the octagon, then this location is taken as the starting point of the turbulent boundary layer. This is done by

comparing the coordinates of the vertices of the octagonal cross-section with the coordinates of the transition point where the laminar boundary layer separation occurs. The location of the turbulent boundary layer separation where it occurs is also determined. For the computation of the boundary layer for the Region-2 a similar procedure is used. For the Region-3, determination of the boundary layer thickness and the surface shear stress is started with the turbulent flow conditions. The accuracy of the solution is increased, by taking 1/10 of a length of a distance between nodal points as the integration step. The slip velocities at these points are interpolated accordingly by using the subroutine INTRO2 of the STTUR1. Computed surface shear stresses around the octagonal cylinder are used to correct the lift and the drag coefficients determined from the pressure distribution around the octagonal cylinder in the presence of the tangential wall-jet. The Flow Chart and the FORTRAN computer Programme STTUR1, developed for the laminar and turbulent boundary layer determination are given in the Appendix 5B.

3.8.7 Lift and The Drag Coefficients

The static pressure distribution and the surface shear stress around the octagonal cylinder are used to calculate the Lift and the Drag coefficients in the presence of a wall-jet resulting the boundary layer modification. In addition, at the jet entrance AB (Fig 3.25) the effect of the jet momentum on the lift and the drag coefficients are considered. For the present problem, boundary layer around the octagonal cylinder represents predominantly a turbulent flow condition for which there is a greater tendency for flow attachment to the octagonal surface resulting in flow separation to be delayed (15). The procedure used to evaluate the lift and the drag coefficients is as follows;

3.8-21
$$L_{y_n} = -H\int_B^A p'_x\left(\frac{dx_n}{dx}\right)dx + H\int_B^A p_\infty\left(\frac{dx_n}{dx}\right)dx + F_{j_{yn}}$$

3.8-22
$$L_{x_n} = -H\int_B^A p'_x\left(\frac{dy_n}{dx}\right)dx + H\int_B^A p_\infty\left(\frac{dy_n}{dx}\right)dx + F_{j_{xn}}$$

(In the above equations integral B to A is taken in the clock-wise direction)

Where in the above equations, $F_{j_{yn}}$ and $F_{j_{xn}}$ represents the forces due to the jet momentum, and can be given by the equations;

3.8-23

$$F_{\underset{xn}{j}} = H\int_{A}^{B} p_x\left(\frac{dy_n}{dx}\right)dx - \dot{M}_{\underset{xn}{J}}$$

3.8-24

$$F_{\underset{yn}{j}} = -H\int_{A}^{B} p_x\left(\frac{dx_n}{dx}\right)dx - \dot{M}_{\underset{yn}{J}}$$

Using the equations 3.8-23 and $p'_x = p_x - p_\infty$

we get;

3.8-25

$$F_{\underset{xn}{j}} = H\int_{A}^{B} p'_x\left(\frac{dy_n}{dx}\right)dx + H\,p_\infty\left(y_{NB} - y_{NA}\right) - \dot{M}_{\underset{xn}{J}}$$

3.8-26

$$F_{\underset{yn}{j}} = -H\int_{A}^{B} p'_x\left(\frac{dx_n}{dx}\right)dx - H\,p_\infty\left(x_{NB} - x_{NA}\right) - \dot{M}_{\underset{yn}{J}}$$

From the equations 3.8-21 and 3.8-26, the forces on the octagonal cylinder in the y direction can be given by;

3.8-27

$$L_{\underset{n}{y}} = -\int P_x\left(\frac{dx_n}{dx}\right)dx \cdot H - \dot{M}_{\underset{yn}{J}}$$

Similarly from equations 3.8-22 and 3.8-25 we get;

3.8-28

$$L_{\underset{n}{x}} = +\int P_x\left(\frac{dy_n}{dx}\right)dx \cdot H - \dot{M}_{\underset{xn}{J}}$$

In the equations 3.8-27 and 3.8-28 the cyclic integral term is formed by the respective integral terms of the equations 3.8-21, 3.8-26 and 3.8-22, 3.8-25.

Both the cyclic integrations are done in the clock-wise direction. From the Bernoulli's equation;

$$P_\infty + \frac{\rho W^2}{2} = P_x + \rho\left(U_x^2 + U_n^2\right)$$

and hence,

$$P_x = P_\infty + \frac{\rho\left(W^2 - U_x^2\right)}{2}$$

Where U_x denotes the tangential velocity at the surface,

$$\left(\equiv \frac{\partial \Phi}{\partial n}\right)$$

The above equations can be given in the non-dimensional form of;

3.8-29

$$L_{y_n}' = \frac{L_{y_n}}{\left(\rho W^2/2\right)\cdot 2RH} = -\int\left(\frac{l}{2R}\right)\left(P_x'\right)\left(\frac{dx_n}{dx}\right)dx$$

3.8-30

$$L'_{x_n} = \frac{L_{x_n}}{(\rho W^2/2)\cdot 2RH} = \int \left(\frac{l}{2R}\right)\left(P'_x\right)\left(\frac{dy_n}{dx}\right)dx$$

Let the surface shear stress τ has the sign of the tangential velocity $(\partial\Phi/\partial n)$. Since $\hat{n}$ is into the domain and the $(\hat{n}\times\hat{R})(\partial\Phi/\partial n)$ is the velocity vector tangential to the surface and is positive, where the shear stress τ is in the direction of the x $clock-wise$, and negative where τ is in the opposite direction to the x (Fig 3.25)

The Drag forces in the x and the y directions can be given by;

3.8-31

$$D_{x_n} = \int \tau\left[\, Sign \;\; of \;\; \left(\frac{\partial\Phi}{\partial n}\right)_{at\;\; x}\right]\frac{dx_n}{dx}dx\cdot H$$

3.8-32

$$D_{y_n} = \int \tau\left[\, Sign \;\; of \;\; \left(\frac{\partial\Phi}{\partial n}\right)_{at\;\; x}\right]\frac{dy_n}{dx}dx\cdot H$$

Where x is measured in the clock-wise direction. By defining the non-dimensional parameters;

3.8-33

$$D'_{x_n} = \frac{D_{x_n}}{(\rho W^2)/2\cdot 2RH}$$

3.8-34

$$D'_{y_n} = \frac{D_{y_n}}{(\rho W^2)/2 \cdot 2RH}$$

$$\tau' = \frac{\tau}{(\rho W^2/2)}$$

We get,

3.8-35

$$D'_{X_n} = \int \tau' \cdot \left[Sign \ \ of \ \left(\frac{\partial \Phi}{\partial n} \right) \right] \left(\frac{dX_n}{dX} \right) dX \left(\frac{l}{2R} \right)$$

3.8-36

$$D'_{Y_n} = \int \tau' \cdot \left[Sign \ \ of \ \left(\frac{\partial \Phi}{\partial n} \right) \right] \left(\frac{dY_n}{dX} \right) dX \left(\frac{l}{2R} \right)$$

Hence the Lift and the Drag Coefficients are given by;

3.8-37

$$C_L = \frac{\left(L_{Y_n} + D_{Y_n} \right)}{(\rho W^2 \cdot RH)} \equiv \left(L'_{Y_n} + D'_{Y_n} \right)$$

3.8-38

$$C_D = \frac{\left(L_{X_n} + D_{X_n} \right)}{(\rho W^2 \cdot RH)} \equiv \left(L'_{X_n} + D'_{X_n} \right)$$

Developed FORTRAN programme CLCDT to evaluate the lift and the drag coefficients is given in the Appendix 5C.

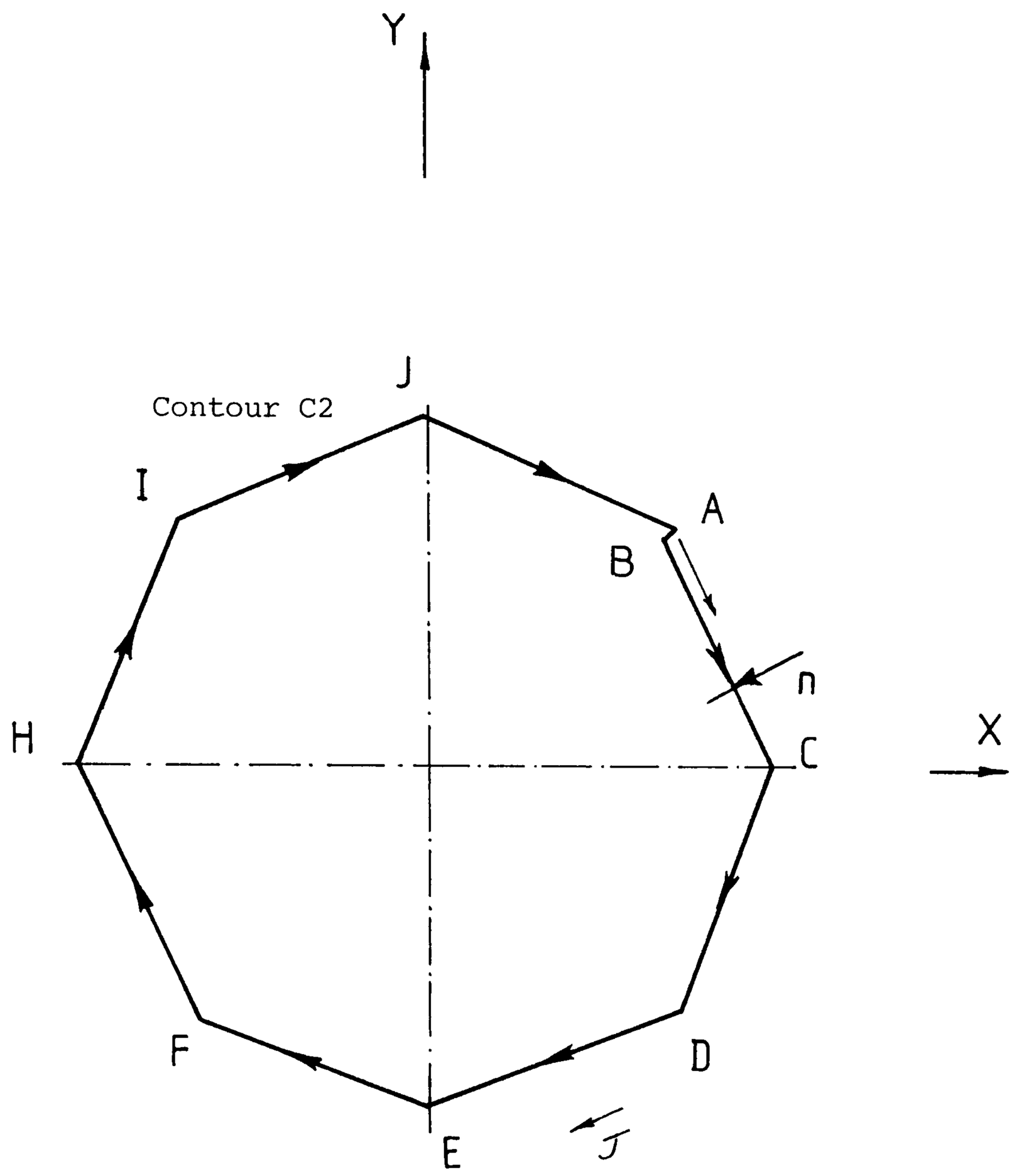

LIFT COEFFICIENT

$$C_L = L'_{Y_n} + D'_{Y_n}$$

DRAG COEFFICIENT

$$C_D = L'_{X_n} + D'_{X_n}$$

Fig 3.25 Lift and Drag Coefficients on the Contour C2 (Model-2)

CHAPTER 4

4 EXPERIMENTAL STUDIES - AERODYNAMIC LIFT DUE TO WALL-JET - ARRANGEMENT FOR WALL-JETS FOR ORBITING OCTAGONAL CYLINDERS

4.1 Aim and Programme of the Experimental Work

The experimental investigations, consisting of wind-tunnel studies, are carried-out under two main categories;

a) Study and understand the experimental techniques for introducing air for the wall-jet formation and observation of the flow field and determination of the lift and drag coefficients due to the tangential wall-jet.

b) Study the feasibility of the engineering application of the wall-jet principle by studying the orbiting octagonal cylinders and application of the switching over arrangement for wall-jets.

The theoretical calculations of the lift and drag coefficients and the power produced by the machine consisting of wall-jets made in the chapters 2 and 3 are based on a number of assumptions, i.e, the flow is

two-dimensional, irrotational. Therefore the results based on such an analysis require experimental verification. Furthermore the theoretical evaluation of circulation due to the tangential wall-jet on an octagonal cylinder requires extensive computation and hence an experimental determination is explored here. And also, all the theoretical predictions made on the proposed concept of the wind machine were based on the assumption, that the flow conditions pertaining to a static cylinder are applicable to the orbiting cylinder. The theoretical investigation also leaves a number of important practical issues associated with the wall-jet phenomenon unanswered. Such as 1) The optimum wall-jet location, 2) The number of wall jets required to achieve the aerodynamic lift, 3) The influence of the end plates on the aerodynamic lift, 4) The feasibility of the engineering application of the wall-jet principle for the proposed concept of a wind machine.

4.2.1 Details of Wind Tunnels and Compressed Air Supply Used in The Experimental Work

For the experimental studies two subsonic wind tunnels have been used.

(i) The Polytechnic wind tunnel measuring 1.5 x 1.0 m in cross section. In normal test conditions this wind tunnel can develop upto a velocity of 5 m/s. The wind tunnel was modified by reducing the cross-sectional area and by introducing an additional suction fan in series with the existing arrangement. After these modifications it was possible to achieve a steady maximum wind velocity of 12 m/s at its test section. Fig 4.7, shows the arrangement of the wind tunnel.

(ii) The central Electricity Research Laboratories of the Central Electricity Generating Board (Leatherhead) wind tunnel measuring 4.8 x 1.6 m and capable of providing upto 10 m/s wind velocity at its test section (Fig 4.8).

A central compressed air supply available in the laboratories was used to feed the tangential wall-jets. In both the cases compressed air line pressure was 500 kN/m^2. However during tests due to the pressure drop in the lines a supply pressure of 320 kN/m^2 was generally available for steady continuous operation.

4.2.2 Major Measuring and Recording Instruments Used in The Experimental Work

The following are the major instruments used in the experimental work reported here. The details of the instruments are given in the Appendix 4A. These instruments are listed with a serial number for the purpose of reference.

I.1. Transamerica Low pressure Transducer (BHL-4420) for pressure measurements

I.2. Phillips PR2011 Digital Data Logger System for recording and analysing the data

I.3. Modified Inclined Manometer for pressure measurements

I.4. Digital Micro Multimeter for voltage and resistant measurements

I.5. Hot-Wire Anemometer for the measurements of wind/jet air velocities

I.6. Digital Micro Manometer (MOC FC002) for pressure measurements

I.7. Stroboscope (Strobe 16K) for the rotational speed measurements

I.8. Micro Manometer (T 10750/1) for the pressure measurements

I.9. Gilkes Acribes Probe/Traverse Instrument

(GILKES- G.160) for the pressure measurements

I.10. IBM Personal Computer (AT) for recording and analysing the data from the digital data logger system

4.3.1 Exploratory Wind Tunnel Studies With the NACA 0018 Aerofoil

In order to establish the phenomenon of lift generation by the effect of the tangential wall-jet on symmetrical bodies, wind tunnel tests were carried-out on a NACA 0018 aerofoil in the Polytechnic wind tunnel. A specially made manifold with a slot and a jet flap was attached to the aerofoil to create the tangential wall-jet. To preserve the symmetry of the aerofoil a dummy flap was attached from the other side of the aerofoil to match the nozzle shape for the air jet introduction. Actual arrangement of the wall-jet is shown by the Fig 4.1.

Compressed air was supplied to the manifold from both the ends. A nearly uniform air velocity across the slot length was achieved by inserting a coil and a steel wool mesh into the manifold. The actual shape of the coil i.e., its diameter and pitch, and the location of the steel wool mesh were experimentally adjusted to obtain a uniform wall-jet velocity, measuring by the

(Inst. I.5) hot-wire anemometer. At both the ends of the manifold, two soft silicon tubes were connected through two ball-bearings which were housed inside a slot, machined to the exact diameter. This provided a nearly free rotating aerofoil about the axis of the manifold. Pressure tappings across the span of the aerofoil were connected to the micro manometer (Inst. I.8) through a distribution manifold.

During tests the modified aerofoil was placed in the wind tunnel with a zero angle of attack. In the absence of the jet air supply forces on the aerofoil were symmetrical and no lift was produced. However with the jet air supply forming a wall-jet on one surface of the aerofoil a low pressure region was created and thus the lift force (Fig 4.2) is generated. However when the air supply through the wall-jet was gradually increased the lift force reached to a maximum value and then to a lower value. Throughout the experiment by using a pulley, wire and dead weights the aerofoil was kept in the symmetrical position. This qualitative study showed clearly the principle of the aerodynamic lift generation due to the tangential wall-jet. These tests also established that for a given wind velocity and for different air jet momentum coefficients, a maximum lift force occurs for a particular momentum coefficient. It is to be noted

that all the experiments on the aerofoil were conducted with a zero angle of attack and hence the observed lift produced was entirely due to the modification of the boundary layer flow by the tangential wall-jet. These experiments were carried-out in the wind tunnel no 1 with jet air velocities upto 45 m/s.

4.3.2 Investigation of Lift and Drag for the Octagonal Cylinder in The Presence of Wall-jet

An octagonal cylinder having sides 42 mm and a height of 600 mm was used to experimentally determine the aerodynamic lift due to the tangential wall-jet. The model was fabricated with adjustable aluminium alloy sheets (Fig. 4.5). Jet air supply to one of the flat surfaces of the octagonal cylinder was achieved by a method similar to that given in the section 4.3.1. The manifold was made with a copper tube with a uniform slot across its span. To get a uniform jet velocity across its span a coil which has a varying diameter and pitch and a fine wire honey-comb were inserted into the copper tube. The coil has a maximum diameter at the middle of the manifold. The manifold was then installed inside the octagonal cylinder to form the tangential wall-jet. These inserts produce a nearly uniform velocity across the span. In their absence,

the air introduced from the ends of the manifold creates a maximum velocity at the centre due to impinging streams of air. The surface of the octagonal cylinder made of Aluminium alloy sheets were made to over-lap where air was introduced to maximize the tangential component of the jet to the surface of the cylinder. Arrangement of the tangential wall-jet is shown by the Fig 4.3.

On the octagonal side of the cylinder, where the boundary layer was modified by the in coming jet-air, 8 pressure tappings along its width were installed. Across the height of this side 16 of such rows were introduced (see 4.5). These pressure tappings were connected with 2 mm ID flexible silicon tubes to a manifold and then to the modified inclined manometer (Instrument I.1). All experimental data were recorded by the Data Logger System and the IBM (AT) Personal Computer.

Conditions for which the tests were carried-out on the octagonal cylinder are given in the Table 4-1. The tests no 1 to 48 cover jet angles of 125°,135°,145° for different wind velocities and jet momentum coeffi-cients. These jet angles are selected since the maximum aerodynamic lift is likely to occur at a jet angle of 135°, from the up-wind direction, as observed

in the previous studies (13) involving circular cylinders. This is confirmed for the case of an octagonal cylinder by conducting the tests 49 to 58. Results and the discussion on these experimental data are given in Chapter 5.

Table 4-1

Exp No	Wind Vel.	Jet Angle	Jet Momt.	Exp No	Wind Vel.	Jet Angle	Jet Momt.
1	4	125°	0.25	9	8	125°	0.25
2	4	125°	0.40	10	8	125°	0.40
3	4	125°	0.55	11	8	125°	0.55
4	4	125°	0.75	12	8	125°	0.75
5	6	125°	0.25	13	10	125°	0.25
6	6	125°	0.40	14	10	125°	0.40
7	6	125°	0.55	15	10	125°	0.55
8	6	125°	0.75	16	10	125°	0.75
Exp No	Wind Vel.	Jet Angle	Jet Momt.	Exp No	Wind Vel.	Jet Angle	Jet Momt.
17	4	135°	0.25	25	8	135°	0.25
18	4	135°	0.40	26	8	135°	0.40
19	4	135°	0.55	27	8	135°	0.55
20	4	135°	0.75	28	8	135°	0.75
21	6	135°	0.25	29	10	135°	0.25
22	6	135°	0.40	30	10	135°	0.40
23	6	135°	0.55	31	10	135°	0.55
24	6	135°	0.75	32	10	135°	0.75

Exp No	Wind Vel.	Jet Angle	Jet Momt.	Exp No	Wind Vel.	Jet Angle	Jet Momt.
33	4	145°	0.25	41	8	145°	0.25
34	4	145°	0.40	42	8	145°	0.40
35	4	145°	0.55	43	8	145°	0.55
36	4	145°	0.75	44	8	145°	0.75
37	6	145°	0.25	45	10	145°	0.25
38	6	145°	0.40	46	10	145°	0.40
39	6	145°	0.55	47	10	145°	0.55
40	6	145°	0.75	48	10	145°	0.75
Exp No	Wind Vel.	Jet Angle	Jet Momt.	Exp No	Wind Vel.	Jet Angle	Jet Momt.
49	8	0	0.55	54	8	135°	0.55
50	8	30°	0.55	55	8	180°	0.55
51	8	45°	0.55	56	8	225°	0.55
52	8	60°	0.55	57	8	270°	0.55
53	8	90°	0.55	58	8	315°	0.55

59	8	45°	0.0

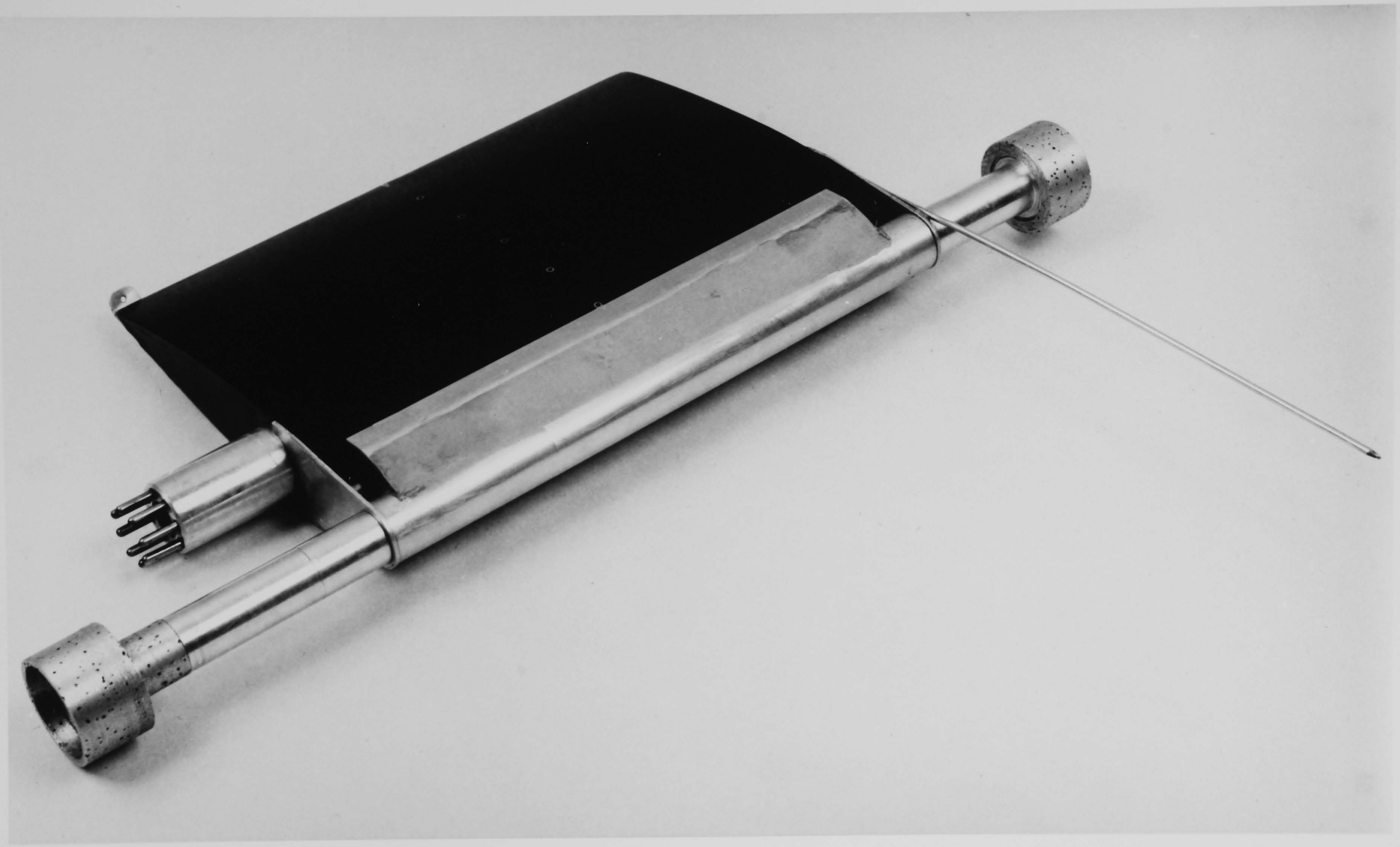

FIG 4.1 NACA 0018 Aerofoil With a Tangential Wall-jet

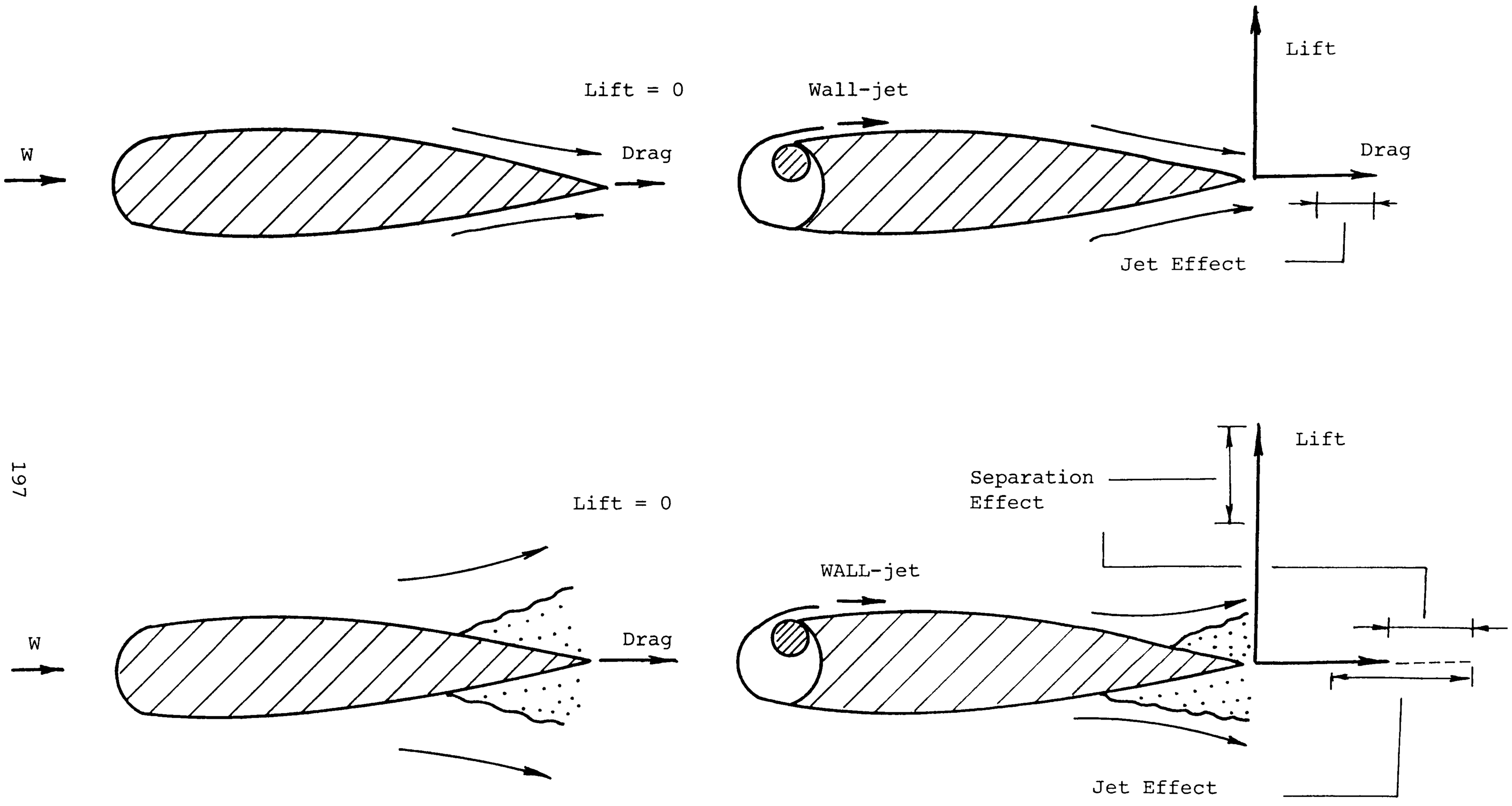

Fig 4.2 Aerodynamic Lift Due to the Tangential Wall-jet

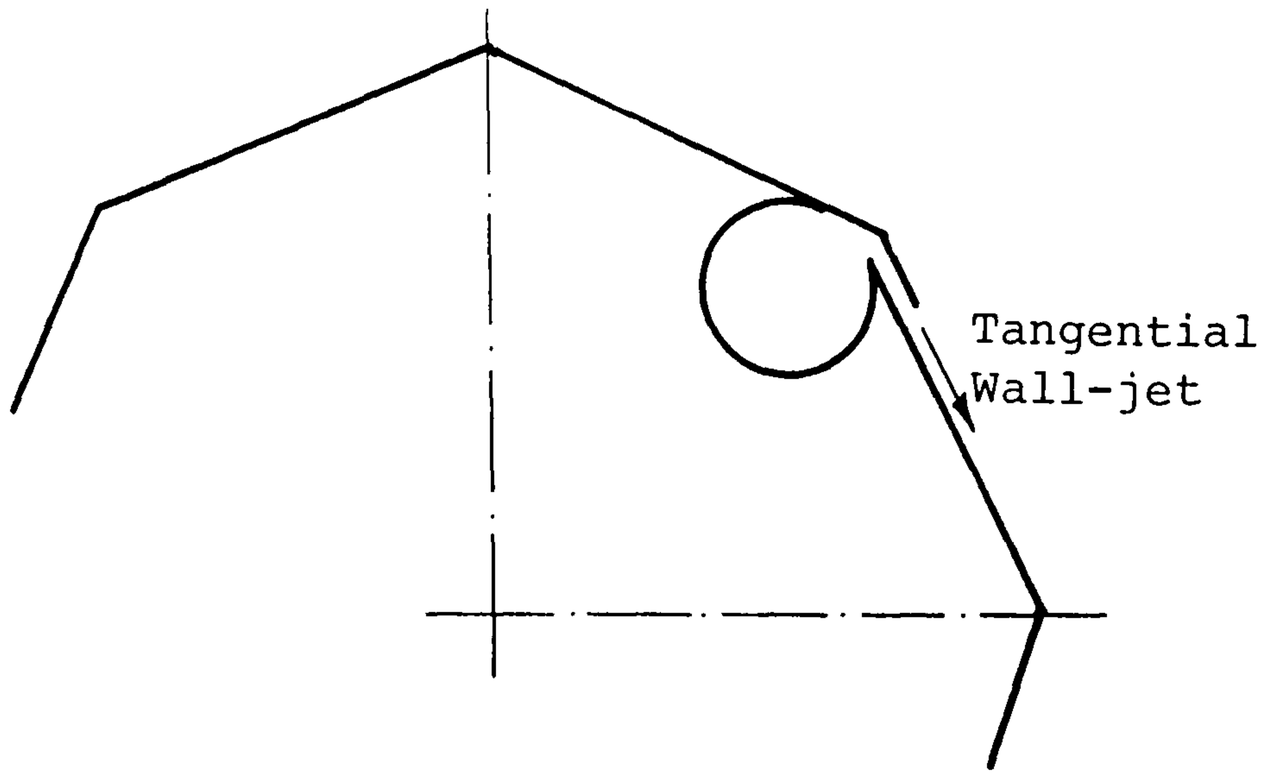

Fig 4.3 Arrangement of the Tangential Wall-jet

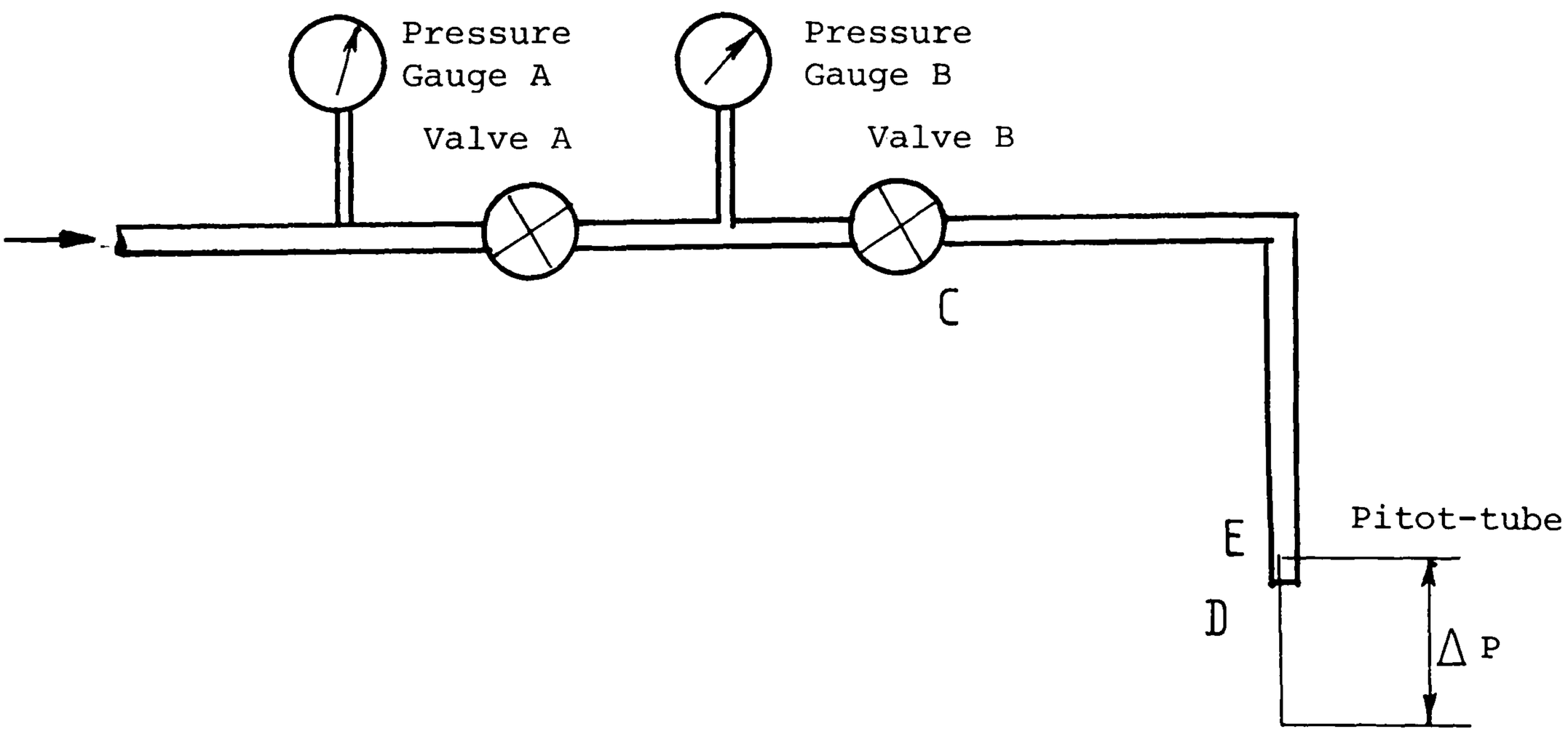

Fig 4.4 Calibration of the Pressure Gauges
for Velocity Measurements

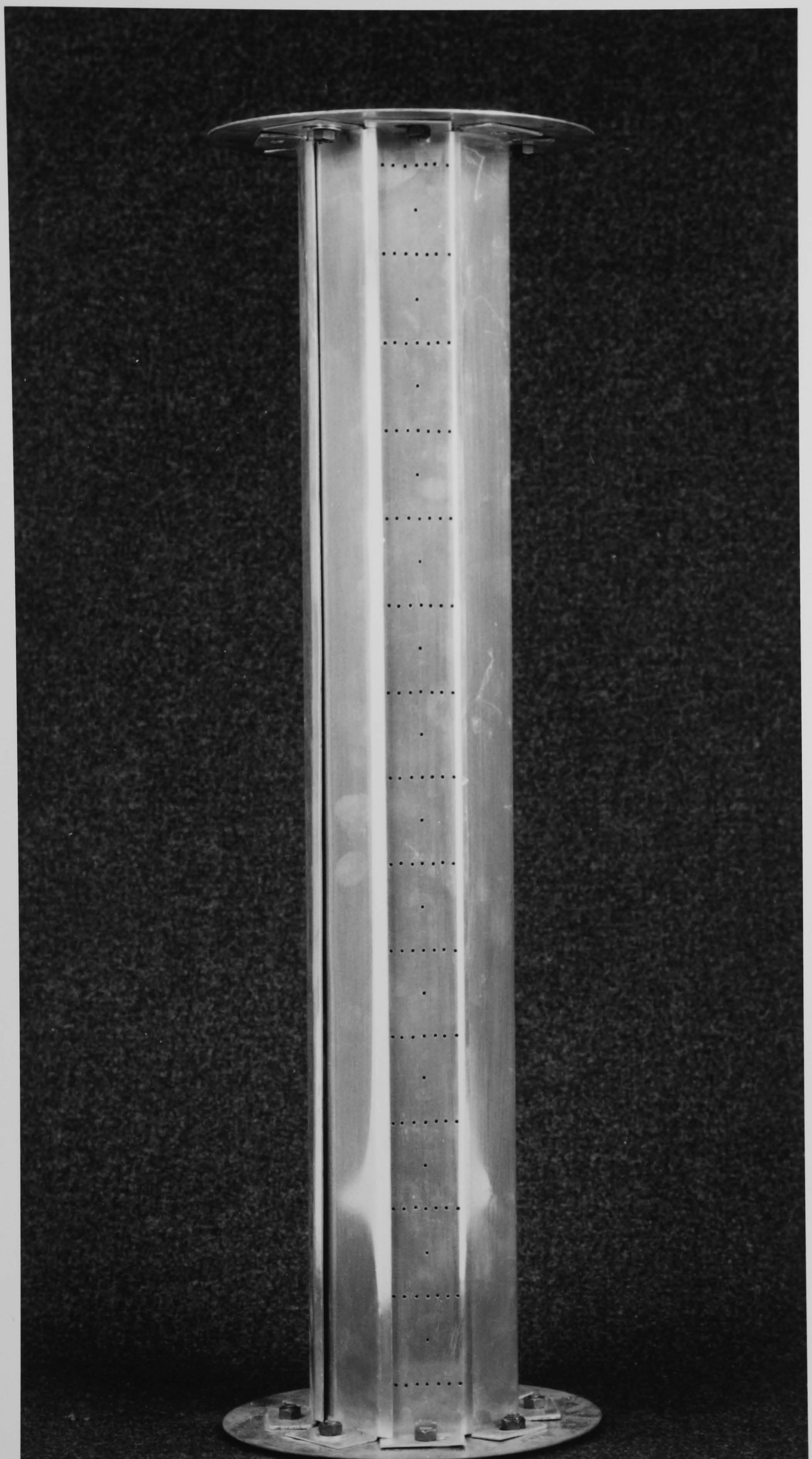

FIG 4.5 Octagonal Cylinder With Pressure Tappings

4.3.3 The Jet Momentum Coefficient and The Jet Mean Velocity

The mean velocities of air from the nozzles have been used to determine the jet momentum coefficient of the wall-jets. For the measurement of the wall-jet velocity, if any probes are to be installed at the jet exit, the flow pattern and the boundary layer development due to the tangential wall-jet may be disturbed. The mean jet velocity depends on the volume flow rate of air through the jet which in turn depends on the supply pressure to the manifold of the jet air supply. Hence it is possible to calibrate the mean velocity of jet in terms of the supply line pressure. Therefore the pressure gauges on the compressed air line have been calibrated to give the mean air velocity at the wall-jets. The arrangement of the instruments for the calibration process is shown in the Fig 4.4.

The gate valve **A** was used for the simulation of the tangential wall-jets in the Octagonal cylinder. A long circular pipe **CD** was equipped with a pitot-tube for the velocity measurements. First, valve **B** was set to give $260 kN/m^2$ with the valve **A** fully open. Valve **A** is gradually closed to give $(p - \Delta p)$, while without disturbing the valve **B**. At point **E** the flow was assumed to be fully developed and therefore the

velocities measured at this point have been used to calculate the flow rate of air. Fig 4.6 shows the relationship between the supply pressure to the nozzle manifold and the mean jet air velocity.

4.4.1 Feasibility of The Engineering Application of The Tangential Wall-jets Principle - Axial Rotary Valve

A model of the Vertical Axis Wind Turbine Generator (VAWTG) consisting of 3 octagonal cylinders capable of orbiting on a vertical axis was fabricated for wind tunnel studies to establish the feasibility of the application of the tangential wall-jets for a new concept of Vertical Axis Wind Turbine Generator and to test the arrangements for the switching of wall-jets for orbiting octagonal cylinders (Fig 4.8). The new concept of VAWTG requires, switching on and off of the wall-jets located on the octagonal cylinders as they orbit (see 2.4). This can be done by using Solenoid valves or pneumatic valves or mechanically operated valves/ports. In the present study an axial rotary valve arrangement which consists of ports located on the vertical axis of the VAWTG has been designed for the wind tunnel model. The compressed air for the wall-jets was supplied through the hollow shaft and ports arrangement described in the 4.4.3 (Fig 4.9).

4.4.2 Octagonal Cylinders for The Model

Octagonal cylinders measuring 42 mm in sides and 600 mm in height were made with light aluminium alloy sheets. The cylinders were fixed with end plates having a diameter ratio of 2 (see 2.7.2). In the present wind tunnel study only two sets of wall-jets per cylinder were provided (Fig 4.11). With such an arrangement it is not possible to experimentally investigate the optimization of the wall-jet application mentioned in the section 2.4. Each of the wall-jets was formed with the air issuing from nozzles specially fabricated by flattening ends of 18 short 8 mm ID copper tubes. This arrangement gave an uninterrupted jet air supply across the span of the cylinder. By connecting all the 18 nozzles to a manifold, and also supplying compressed air at a distance of, a third from either end of the manifold, a reasonably uniform jet air velocity was achieved. Manifolds with the nozzles were fixed to the inner side of the octagonal plates to form the tangential wall-jets. The surfaces of the octagonal cylinder corresponding to each side of the octagon were made to over-lap where the wall-jets were introduced to maximize the tangential component of the velocity of the jet to the surface of the cylinder (Fig 4.12).

4.4.3 Air Supply and the Switching-On and Off of Jets

Air supply to the cylinders was through the centre column of the machine through the rotary valve consisting of ports. On the centre hollow column (Fig 4.10) coaxial with the wind turbine generator and forming its main support three slots of height 8 mm and circumferential length covering a 180° angle were made. These slots were at different heights and are staggered circumferentially through an angle of 120° in between them (Fig 4.13). Six compressed air tappings were made to supply air to the six manifolds of the three octagonal cylinders. These tappings were located with each three in two axial rows which are diametrically opposite to one and another. The axial separation of the tappings is such that they are against three slots on the inner fixed column. As the octagonal cylinders orbit, only wall-jets concerned for the lift generation receive compressed air through the tappings of the outer column. With this distribution arrangement, octagonal cylinders with tangential wall-jets produce aerodynamic lift as described in the 2.4. to generate useful power. Therefore, in general, at any single point of the orbit two out of the three cylinders of this model of the wind machine produce useful aerodynamic lift.

4.4.4 Arrangement of The Bearings Between The Outer Shaft and The Inner Shaft

Octagonal cylinders were mounted on to the rotating outer shaft of the centre column. Therefore to carry the full mechanical load during operation, between the outer shaft and the inner shaft two taper roller bearings (SKF 30210, SKF 30211) were used. For the accurate manufacturing and assembling process these bearings were selected to be in two different diameters. The top and the bottom of outer shaft was made to house the two bearings and was covered with end caps, to protect and give a minimum friction during operation (Fig 4.10). Inner diameter of the outer shaft was made (52 - 0.001) mm and the outer diameter of the central column was made (52 + 0.001) mm. This small clearance between the cylinders was essential to keep the friction to minimum while keeping the air leakage between the shafts negligibly small.

4.4.5 Wind Tunnel Tests on The Model

Aim of the wind tunnel tests on the model were mainly, to establish the feasibility of the engineering application of the tangential wall-jet principle for a

wind energy conversion system and to test the switching over arrangement for the wall-jets for orbiting octagonal cylinders.

Tests on the feasibility of the application of the axial rotary valves for the switching over of air-jets were conducted with different wind velocities and jet momentum coefficients. The mean jet-air velocity was obtained from the inlet supply air pressure by the calibration method discussed in the section 4.4.3. The jet air velocity was also measured with a pitot-tube for a stationary cylinder for a range of inlet supply air pressures to confirm the above calibration. The relevant experimental data is presented in the Table 4-2.

The power generated by the model being quite small, a simple rope-drum brake was used as a dissipating means. The brake-drum was driven through a timer-belt and associated pulleys. The rotational speed ratio between the main axis and the break-drum was 1:1. Tests were conducted for various wind velocities, jet momentum coefficients and breaking torques. The jet momentum coefficient was varied by the supply of air to the wall-jet manifolds. The braking torque was varied by varying the tension in the rope brake. For each operation condition, the model was allowed to attain a

steady state and the rotational speed of the model and other operating parameters were recorded. The data obtained is given in the Table 4-2.

Table 4-2

W m/s		1	2	1	2	1	2	1	2
2 m/s	C_μ	1.52	1.42	2.13	1.99	2.54	2.38	3.20	2.93
	N rpm	28		32		37		42	
3 m/s	C_μ	0.68	0.63	0.94	0.88	1.13	1.05	1.42	1.30
	N rpm	30		35		41		46	
4 m/s	C_μ	0.38	0.35	0.53	0.49	0.63	0.59	0.80	0.74
	N rpm	38		43		41		46	
5 m/s	C_μ	0.24	0.23	0.34	0.32	0.41	0.38	0.51	0.46
	N rpm	22		27		44		41	
6 m/s	C_μ	0.17	0.16	0.24	0.22	0.28	0.26	0.35	0.32
	N rpm	18		22		28		36	

1 Jet-momentum (Through Air inlet pressure)

2 Jet-momentum (Through Mean Jet Air Velocity)

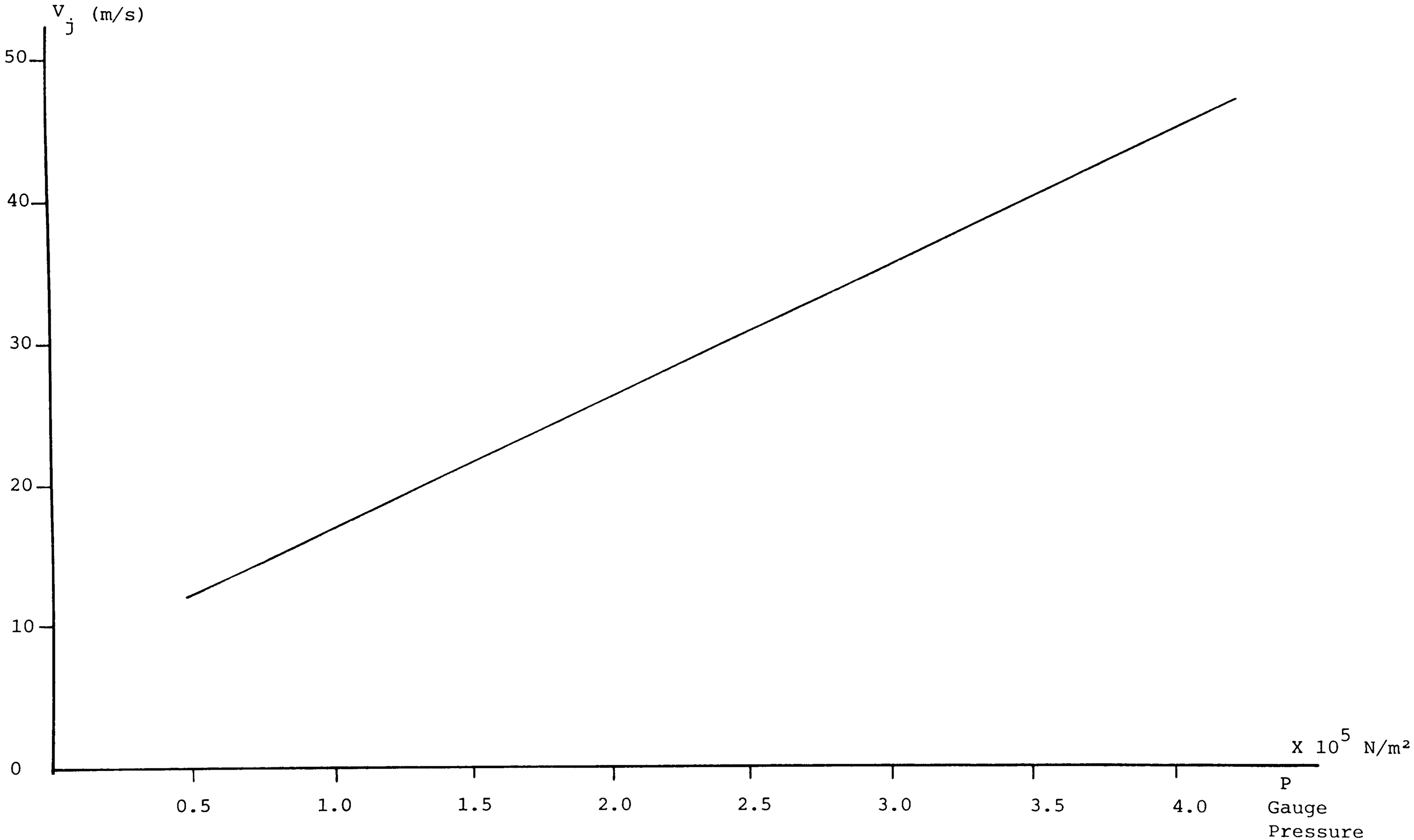

Fig 4.6 Gauge Pressure Vs Mean Jet Velocity

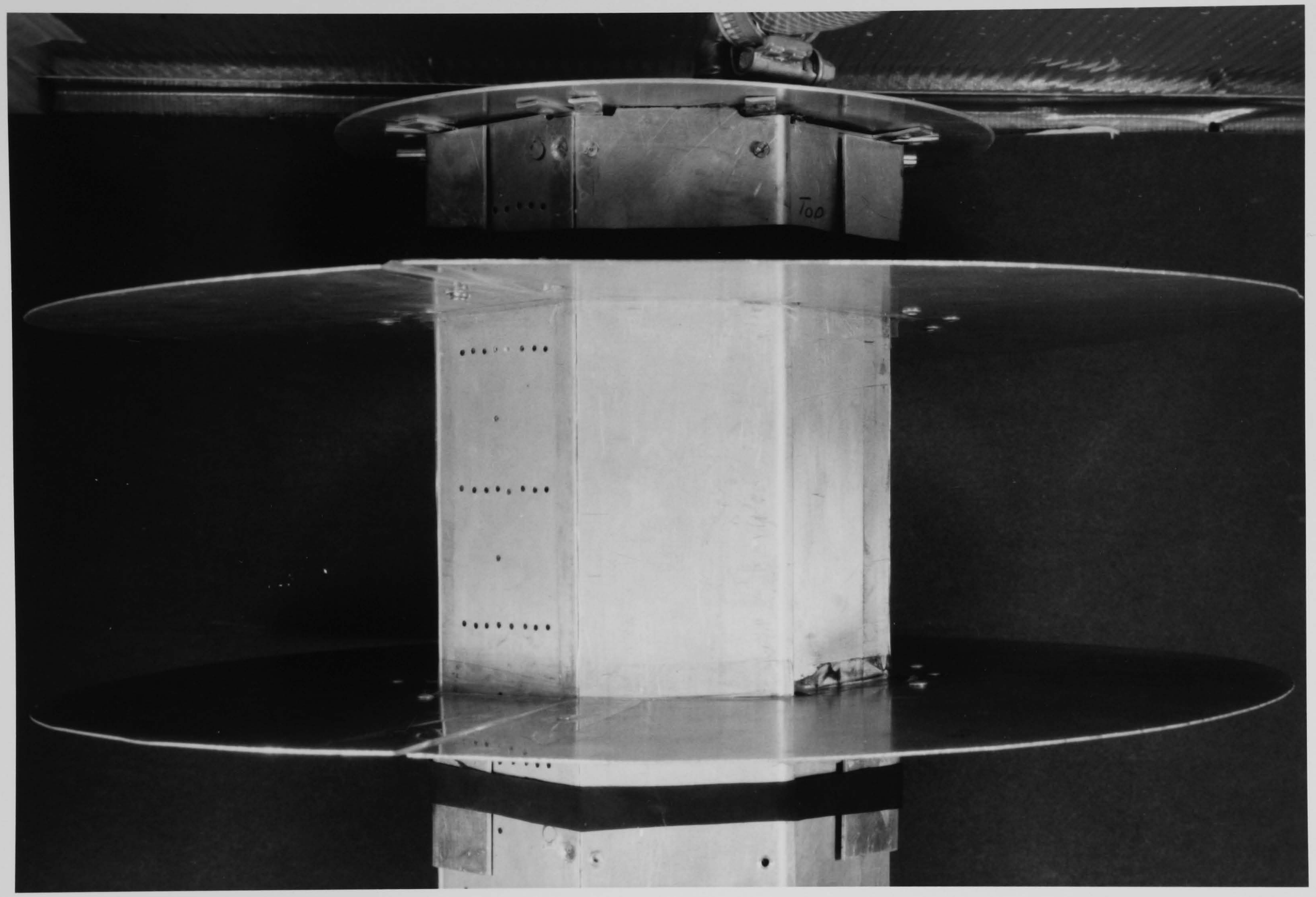

FIG 4.7 Tests on the Octagonal Cylinder with End Plates

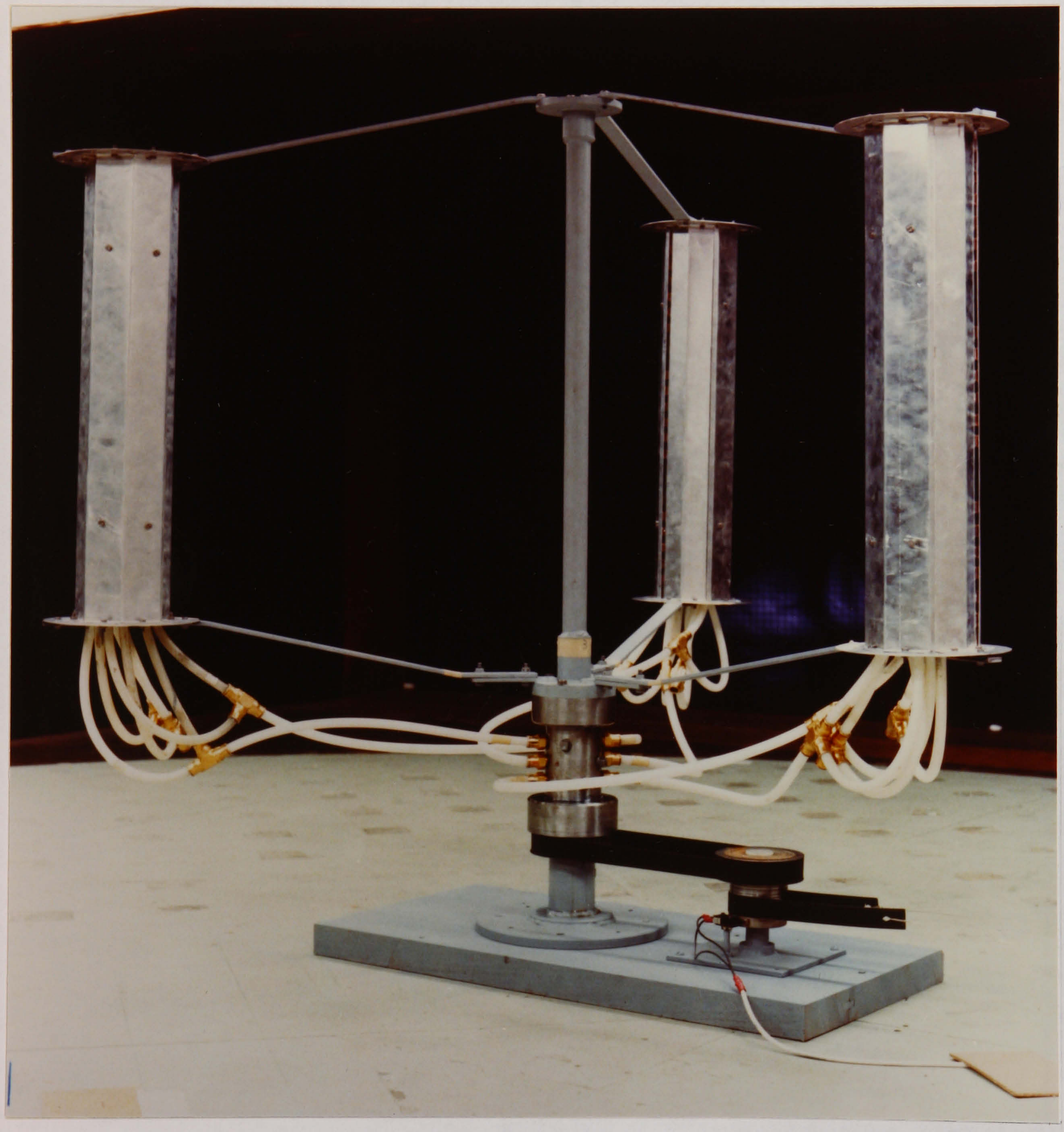

FIG 4.8 Wind Tunnel Model of the VAWTG

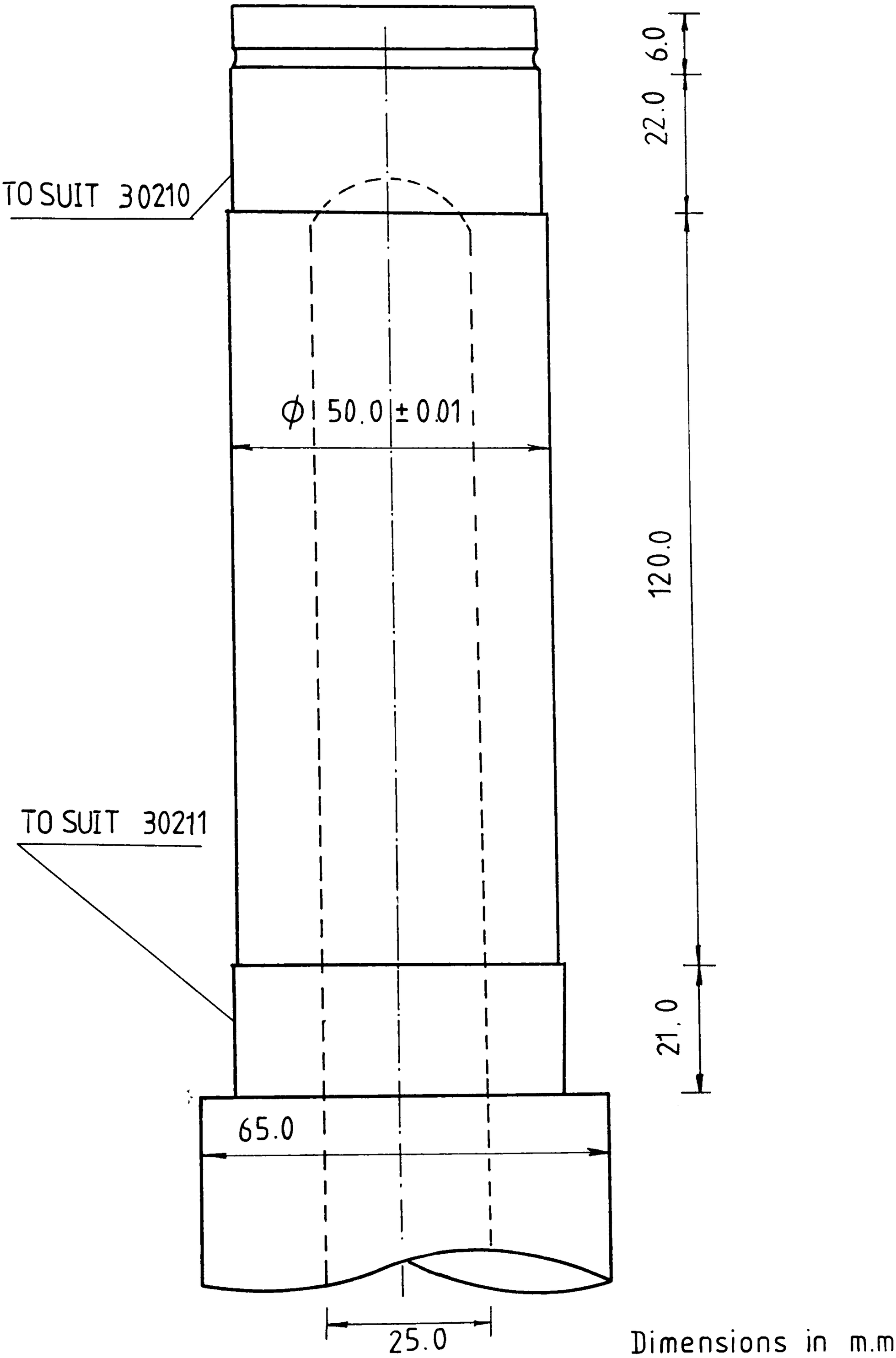

Fig 4.9 Centre Column of the Wind Machine

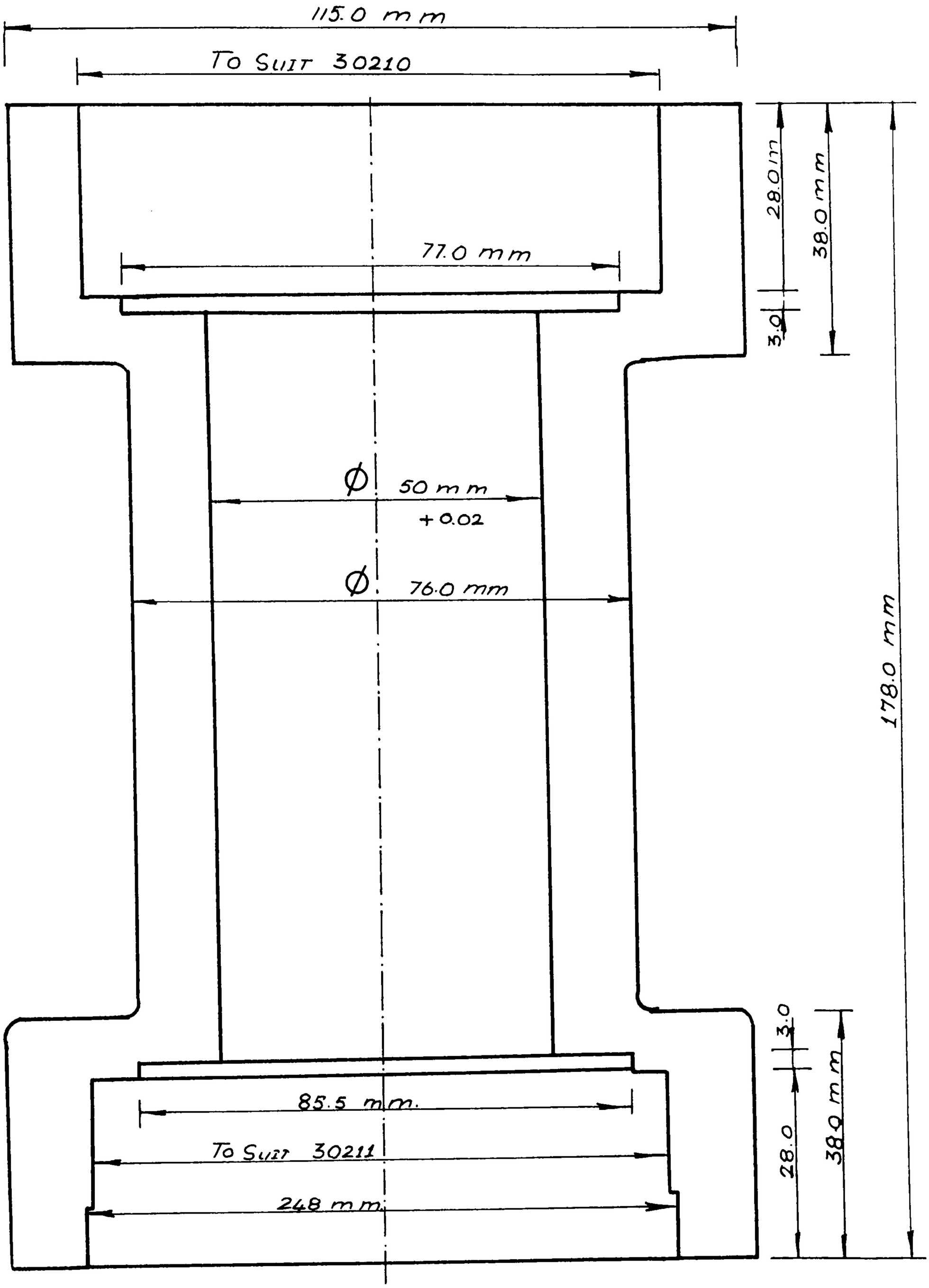

Fig 4.10 Outer Shaft (Cylinder) With End Caps

FIG 4.11 Tangential Wall-jets (Air - Nozzles)

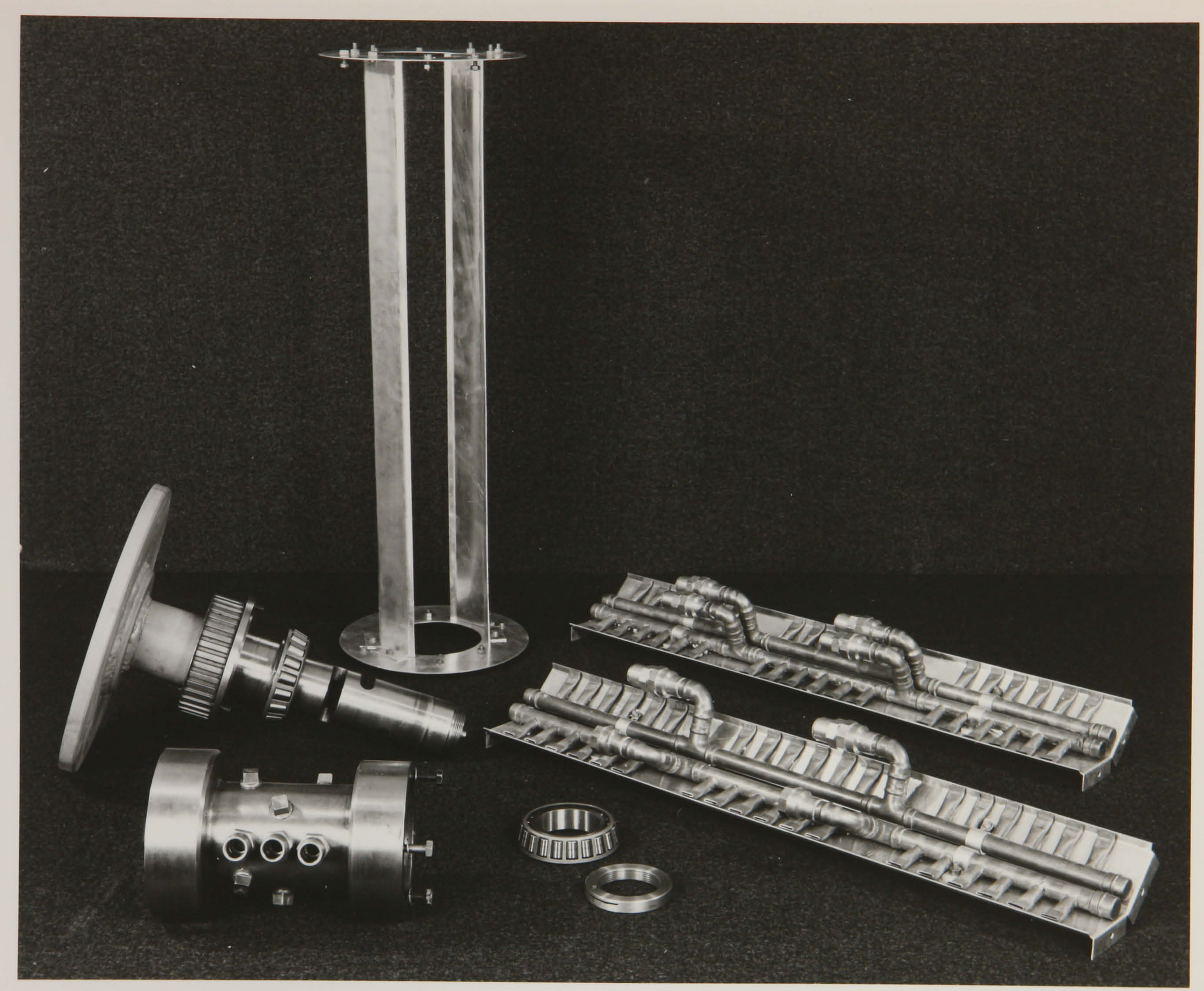

FIG 4.12 Air Distribution System

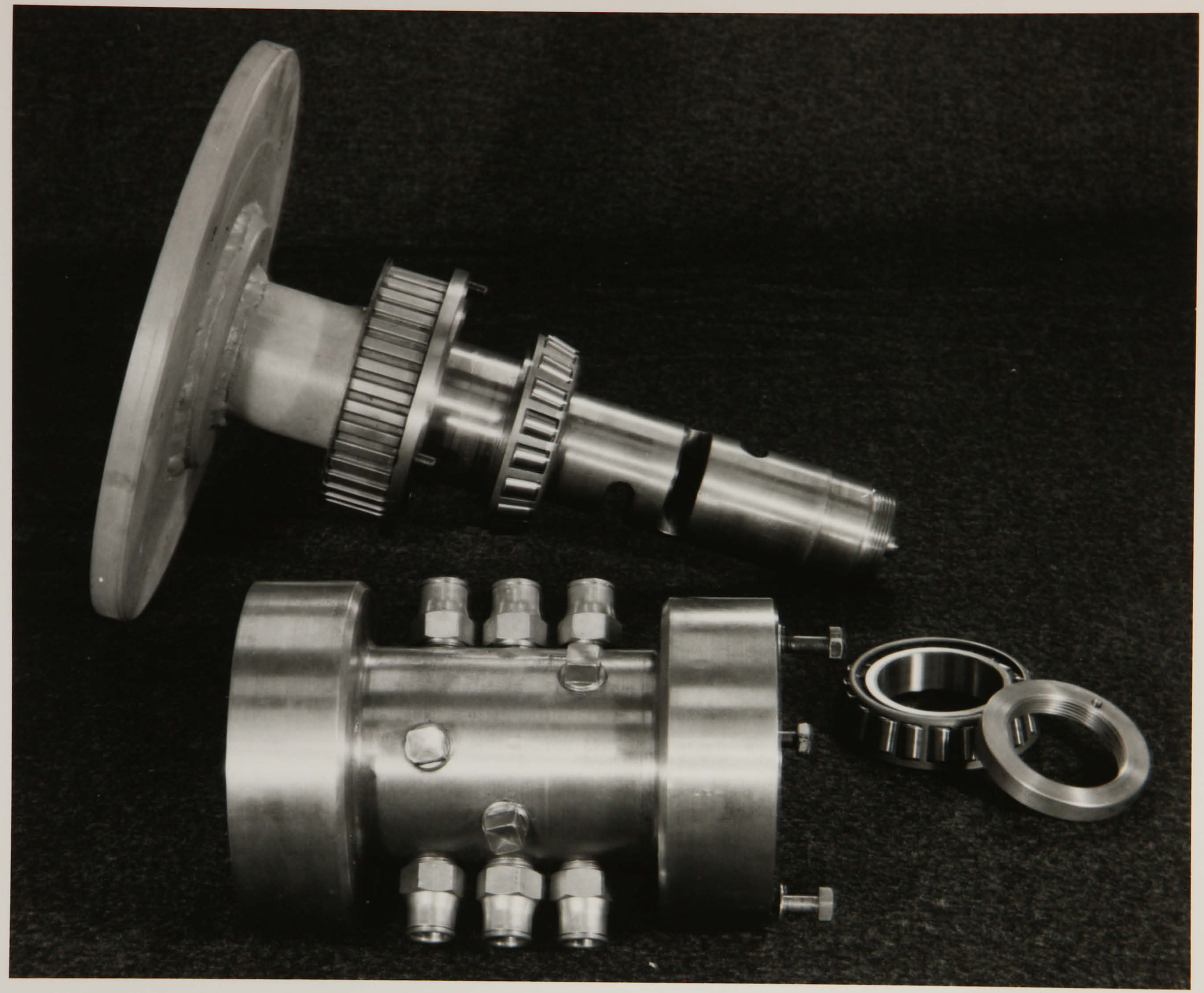

FIG 4.13 Centre Column and the Taper Roller Bearings

CHAPTER 5

CHAPTER 5 RESULTS AND CONCLUSIONS

5.1 Pressure Components of Lift and Drag Coefficients

The values of the pressure components of lift and the drag coefficients (3.8.7) which are based on the static pressure distribution around the octagonal cylinder subjected to the tangential wall-jet are experimentally obtained. The basic results of these investigations, the details of which are given in section 4.3.2 are presented in Fig 5.1 to 5.8. Fig 5.1 shows the lift and drag coefficients obtained for different locations of the jet position for which other conditions are kept constant as specified by the exp no 49 to exp no 58 of the Table 4-1 (page 194). This shows that for the octagonal cylinder the maximum aerodynamic lift coefficient occurs around a jet angle of 145° measured from the upwind direction.

Pressure components of the lift and drag coefficients are plotted against jet momentum coefficient for four values of Reynolds numbers, Re_o, (Appendix 3A), 2.8×10^4, 4.3×10^4, 5.8×10^4, 7.3×10^4, and for three jet angles 125°, 135°, 145°. These are shown as broken lines in Fig 5.2 to Fig 5.5. As the jet angle increases from 125° to 145° the magnitudes of the pressure component of the lift and drag coefficients increase. However for

the four Reynolds numbers tested here the "magnification factor" based on the pressure component lift coefficient decreases. "Magnification factor" is defined as the ratio of lift to jet momentum coefficient (38). For example, where the Reynolds number is constant and 5.8×10^4 the "magnification factor" increases from 14.9 for jet momentum coefficient of 0.75 to a value of 30.8 for a jet momentum coefficient of 0.25 (Fig 5.4).

For increasing values of Reynolds numbers for a given jet momentum coefficient the pressure components of the lift and the drag coefficients increase in magnitude. This type of variation may be explained from the fact that the measured values of the pressure components of the lift and the drag coefficients do not take into account the effect of the shear stress at the octagonal surface. It may be noted that for zero jet momentum coefficient the pressure component drag coefficients are essentially in the range of 0.45 to 0.95 over the range of Reynolds number of 2.8×10^4 to 5.8×10^4.

5.2 Lift and Drag Coefficients

The theoretical procedure for estimating the lift and the drag coefficients from the experimentally measured values of the pressure coefficients of the lift and the

drag coefficients is given in the sections 3.8.7. This theoretical procedure allows for the shear stress at the octagonal surface and the jet reaction effect. The values of the lift and the drag coefficients obtained by the procedure are shown in Fig 5.2 to 5.5. The values of the lift coefficients are always lower than the values of the corresponding pressure components. However the values of the drag coefficients are greater than the values of the corresponding pressure components. This is due to the effect of the surface shear forces on the drag forces on the octagonal cylinder. The general trends of the variation for the pressure components of the lift and the drag coefficients with respect to the jet momentum coefficient, jet angle, and the Reynolds number stated in the section 5.1 are essentially valid for the lift and drag coefficients. As the Reynolds number (Re_o) increases from 2.7×10^4 *to* 5.5×10^4 the effect of the surface shear stress decreases for a given value of C_μ or with increased values of C_μ for a given Re_o. However as the Reynolds number increases from 5.5×10^4 *to* 6.9×10^4 the effect of the surface shear stress on the drag coefficient increases.

For zero values of the jet momentum coefficients the drag coefficients are essentially in the range of 0.5 to 1.1. These results correspond to the values of the

drag coefficients for an octagonal cylinder for cross-flow within the above range of Reynolds numbers, neglecting the effect of the protruding lip for the jet formation (Fig 3.5) and the effect of the orientation of the octagonal cylinder. Maximum values of the lift coefficients ($C_L(\mathrm{Max})$ for the test range of Reynolds numbers (Re_d) 2.7×10^4, 4.3×10^4, 5.8×10^4, 7.3×10^4, shown in Fig 5.2 to 5.5, are located and these maximum values are re-plotted against C_μ for different jet angles and are shown in the Fig 5.6. As the jet momentum coefficient increases the maximum values of the lift coefficients increase. Fig 5.6 also shows the relationship of $C_L(\mathrm{Max})/C_D$ against the C_μ. Here C_D is the drag coefficient corresponding to the conditions for the occurrence of $C_L(\mathrm{Max})$. It may be observed that the lift to drag coefficient decreases with C_μ for all jet angles, θ within the range of $C_\mu = 0.25$ *to* 0.75. However this ratio should be zero for $C_\mu = 0$ indicating that a maximum value for the lift to drag ratio within the range of $C_\mu = 0$ *to* 0.25.

5.3 Effective Circulation Γ

Assuming the validity of the Joukowski's theorem for the case of an octagonal cylinder with a tangential wall-jet the relationship between the effective circulation and the non-dimensional jet velocity (V_j/W)

is calculated from the equations in section 3.6.8. Fig 5.7 shows the relationship between the effective circulation and the non-dimensional jet velocity. It may be noted that the circulation created by the tangential wall-jet is essentially independent of the Reynolds number within the range of Reynolds numbers 4.3×10^4, 5.8×10^4, 7.3×10^4. Flow field created by the tangential wall-jet is similar in nature to a flow field created by a axially rotating cylinder. Circulation due to a axially rotating cylinder (Magnus Effect) is calculated and shown by a coloured line in the Fig 5.7. Comparisons of the circulation created by the tangential wall-jet and the Magnus Effect has been made. Upto a non-dimensional peripheral velocity of 3.8, with an End plate to Diameter ratio of 2 the circulation created by the Magnus Effect is lower to the circulation created by a tangential wall-jet having a non-dimensional jet velocity of 3.8 for flow conditions with Reynolds numbers 4.3×10^4, 5.8×10^4, 7.3×10^4. Hence it is possible to achieve a higher lift force by using a single tangential wall-jet, than the Magnus Effect for corresponding values of non-dimensional jet velocity and non-dimensional peripheral velocity respectively.

5.4 Stream Lines for the Main Flow

Stream lines around the octagonal cylinder for different flow conditions are shown in Fig 5.9 to 5.13. The flow field around the octagonal cylinder is modified by the tangential wall-jet and as mentioned earlier the flow pattern created is similar in nature to that of the Magnus Effect. In the present work, in the mathematical Model-2 (Left Hand Contour) (3.2.2) the upstream stagnation point has been calculated for the Model-2 (Right Hand Contour) (3.2.2) and for different values of the jet momentum coefficient upstream stagnation point has been kept unchanged. This has caused the distortion of the stream lines at a point closer to the upstream stagnation point. It is possible to eliminate this distortion due to the strip on the upstream flow field and on the stream lines by relocating the upstream stagnation point for different flow conditions. This will require repetition of the computer runs with the FORTRAN programme PART4N (Appendix 5A) for all the different flow conditions i.e., jet momentum coefficients, and jet angles. However this was not carried out as the influence of the distortion has negligible effect on the calculation of the pressure distribution.

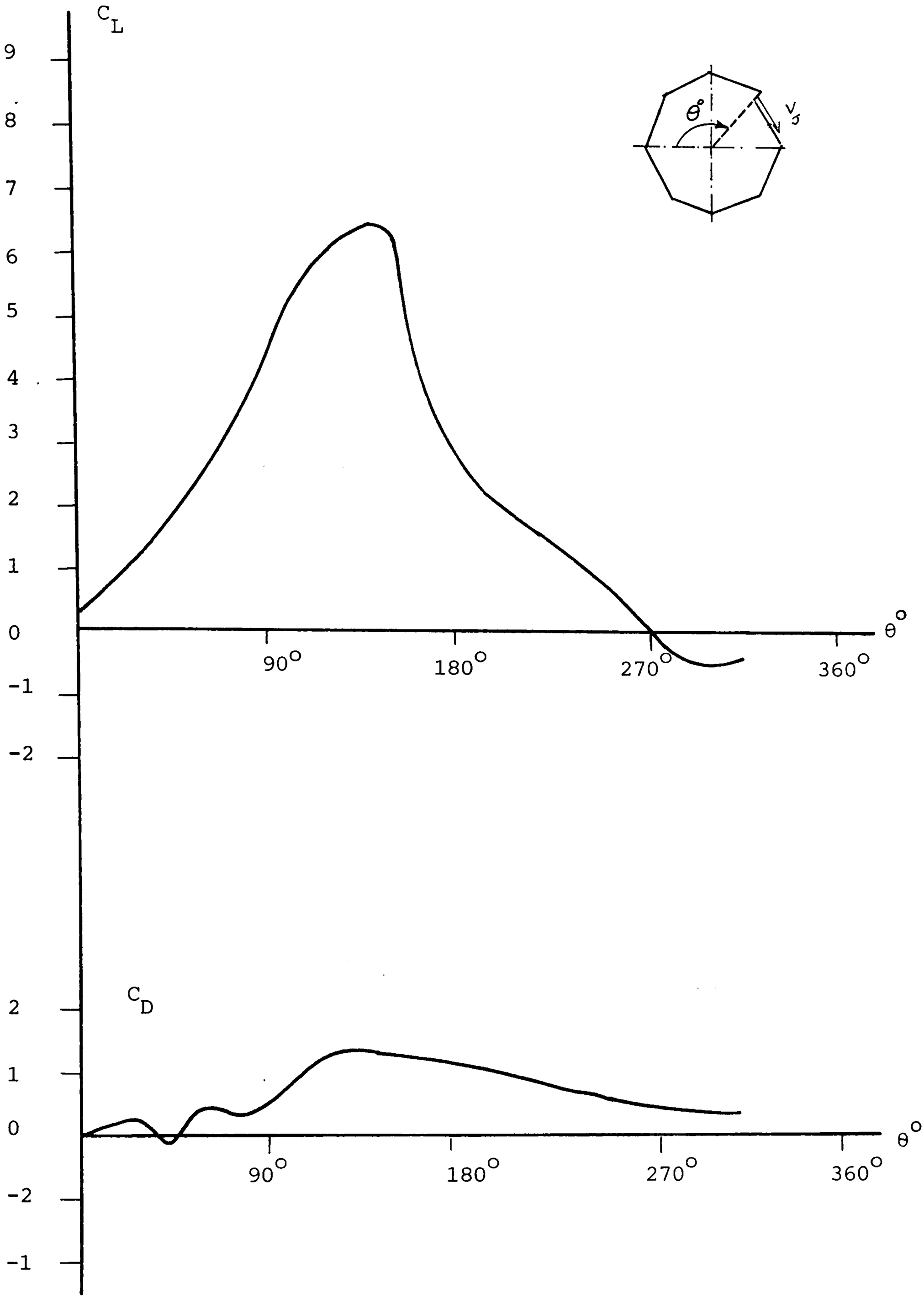

Fig 5.1 Effect of the Jet Angle on Lift and Drag Coefficients

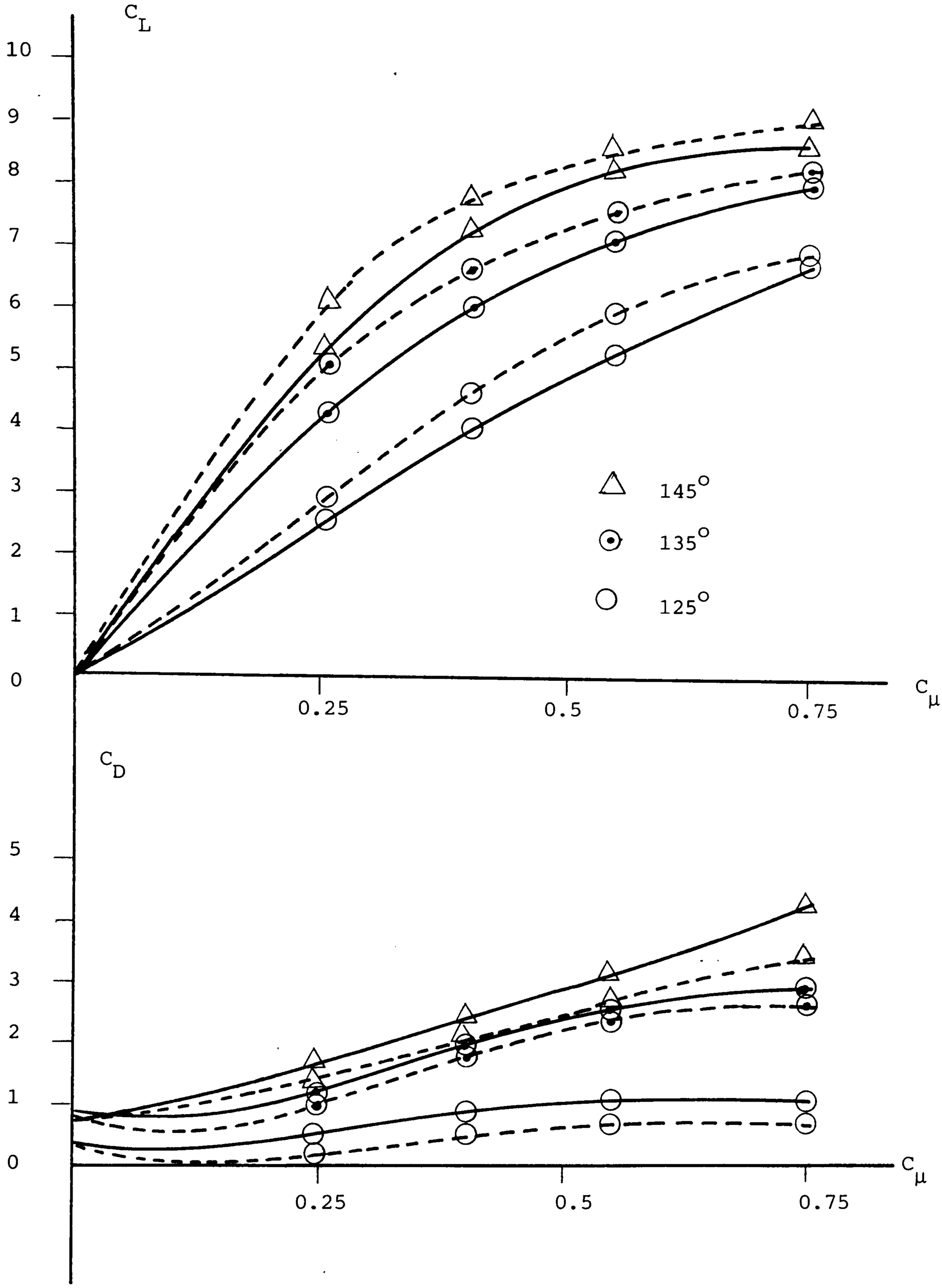

Fig 5.2 Lift and Drag Coefficients against Jet-momentum Coefficient (θ_j=125°, 135°, 145°)
$Re_o = 2.8 \times 10^4$

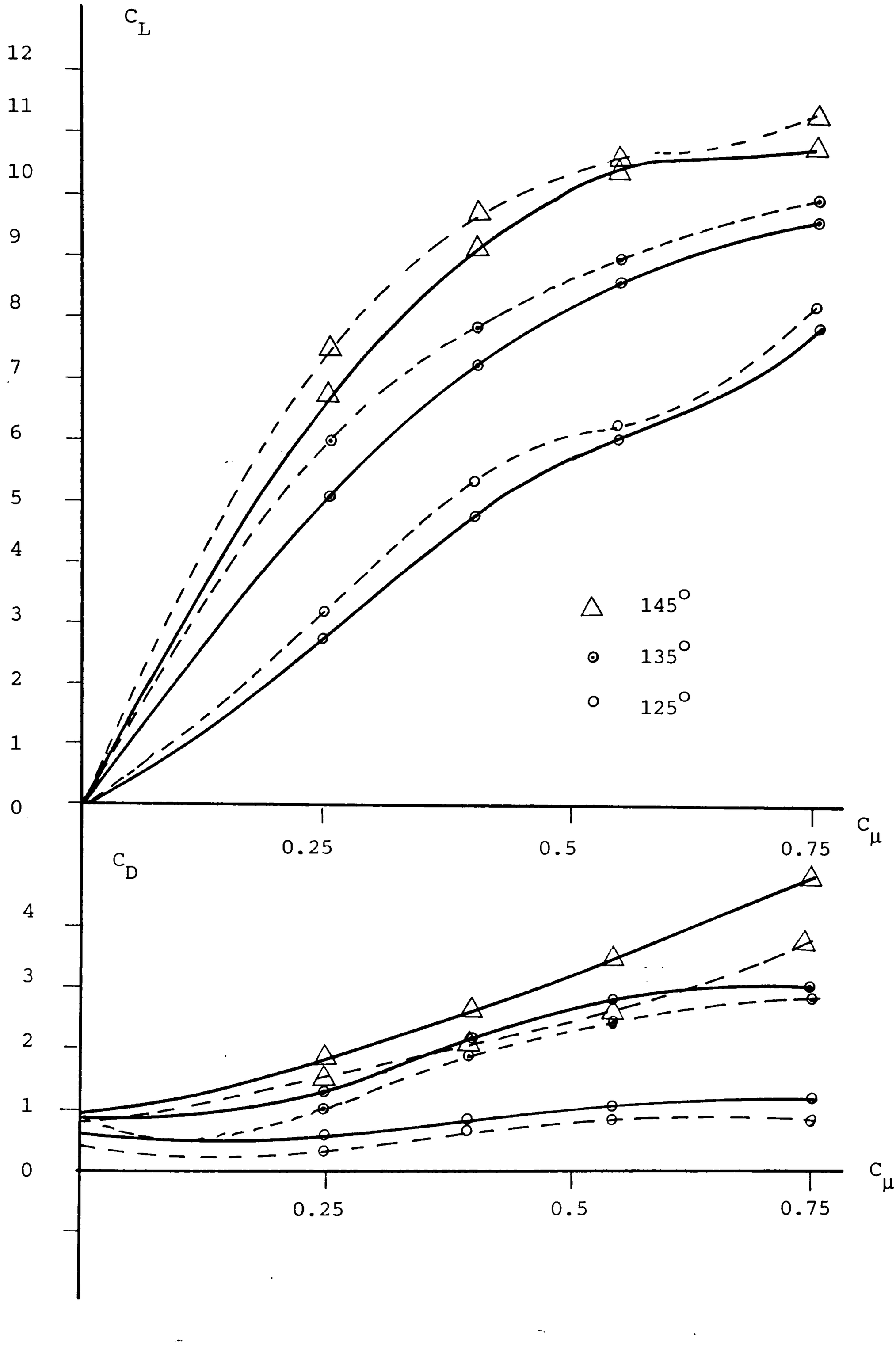

Fig 5.3 Lift and Drag Coefficients against Jet-momentum Coefficient (θ_j = 125°, 135°, 145°) $Re_o = 4.3 \times 10^4$

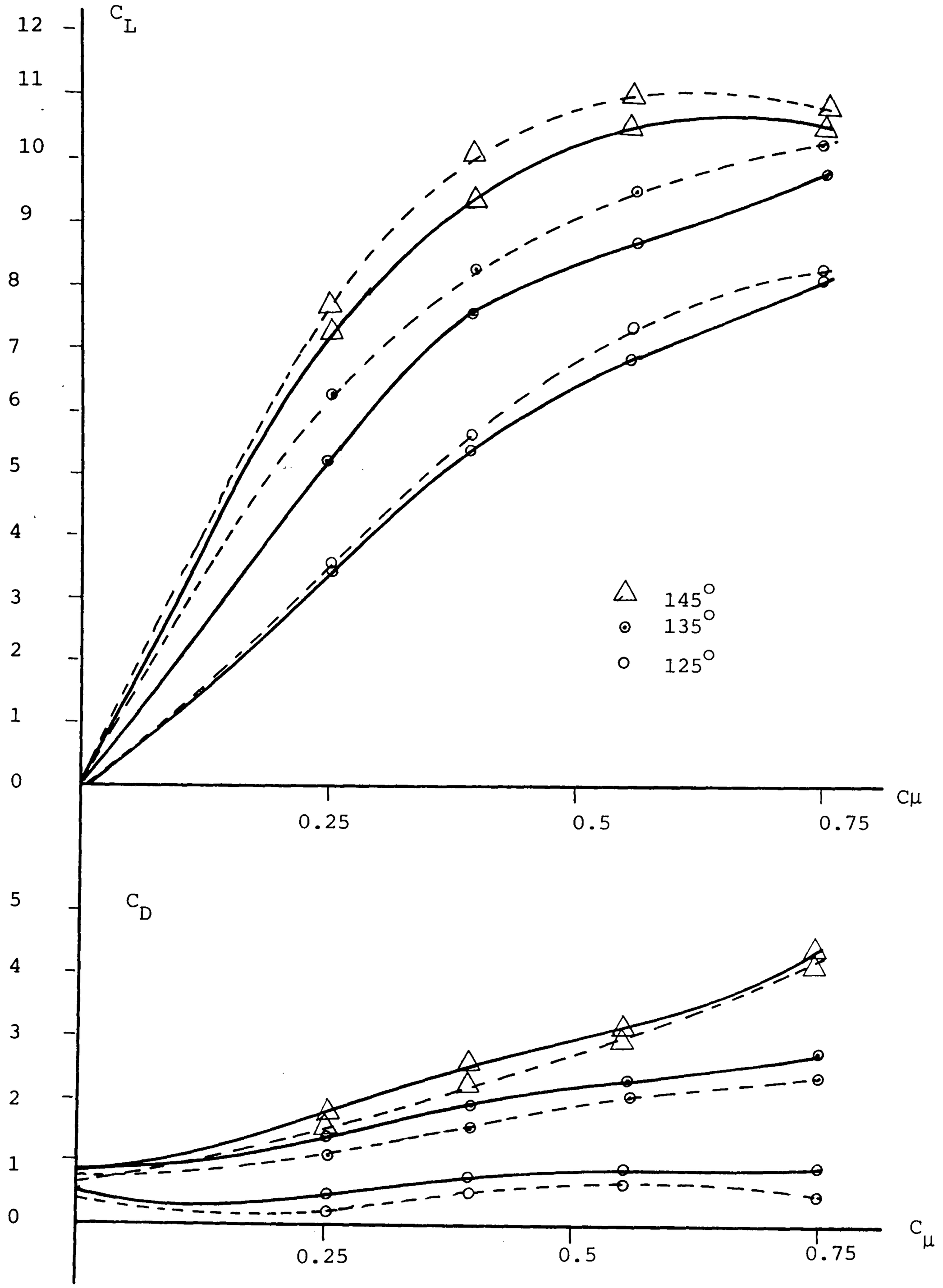

Fig 5.4 Lift and Drag Coefficients against jet-momentum Coefficient (θ_j = 125°, 135°, 145°) $Re_o = 5.8 \times 10^4$

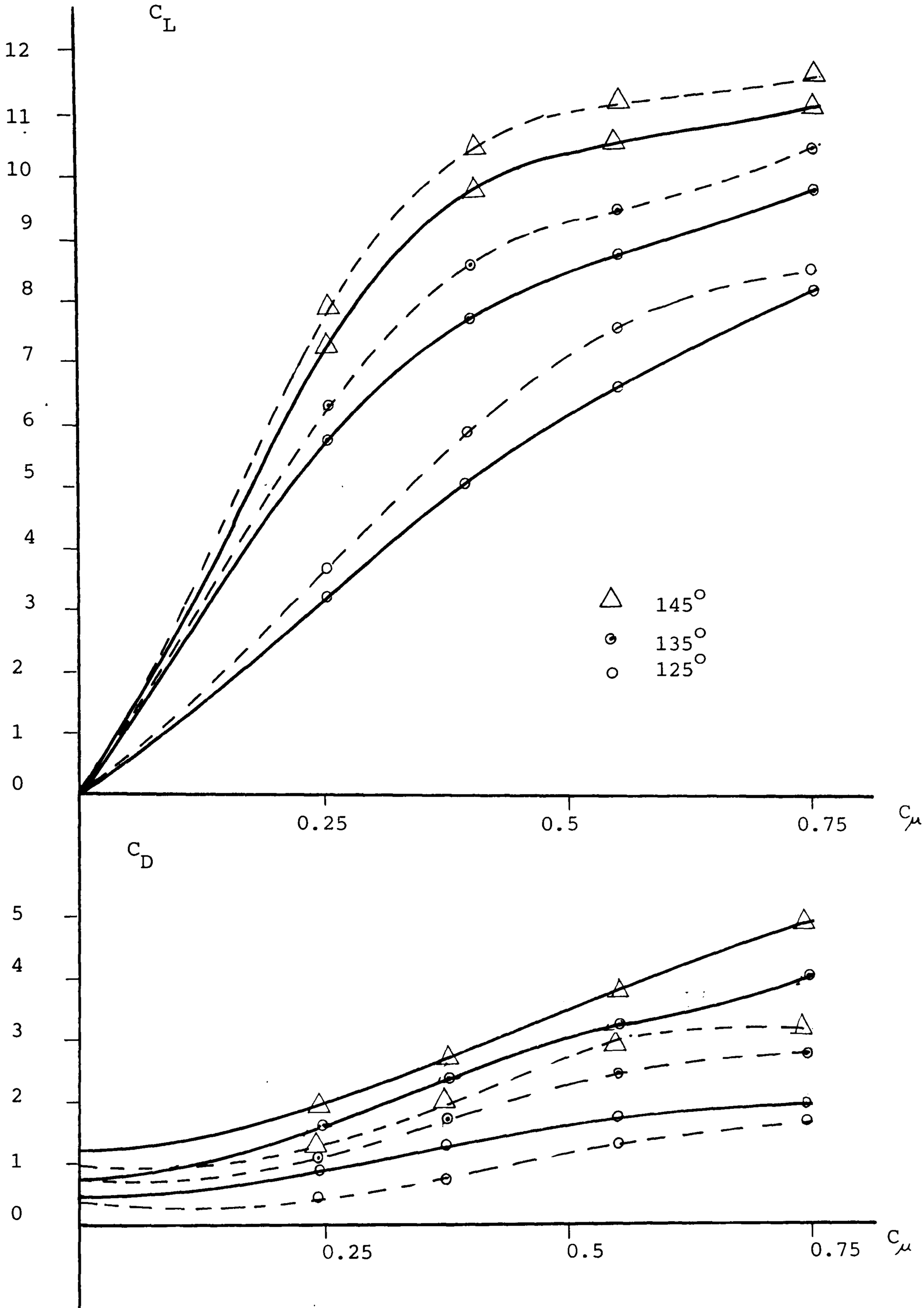

Fig 5.5 Lift and Drag Coefficients against Jet-momentum Coefficients (θ_j = 125°, 135°, 145°) $Re_o = 7.3 \times 10^4$

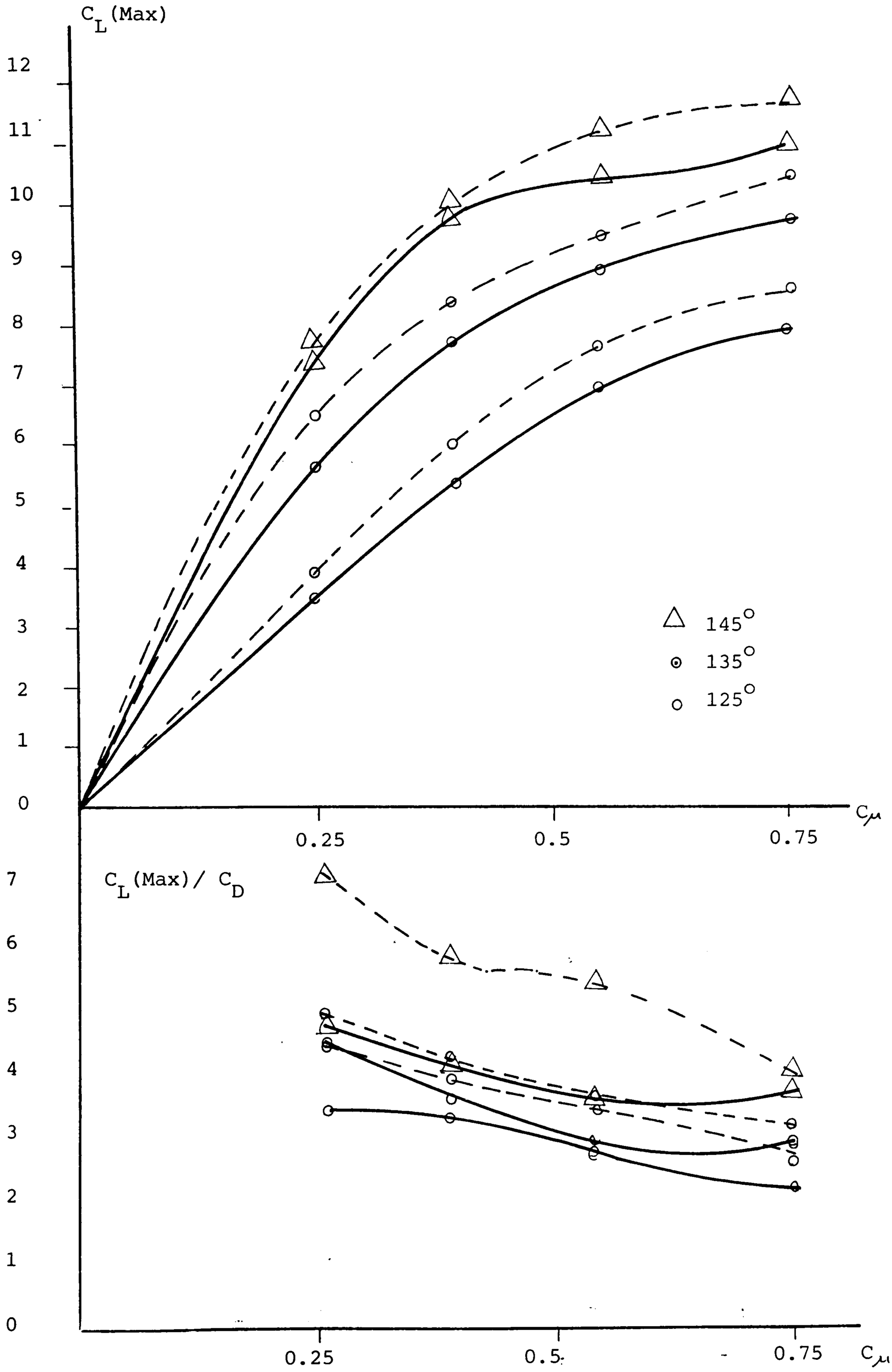

Fig 5.6 C_L(Max), C_L(Max)/ C_D against C
for θ_j = 125°, 135°, 145°

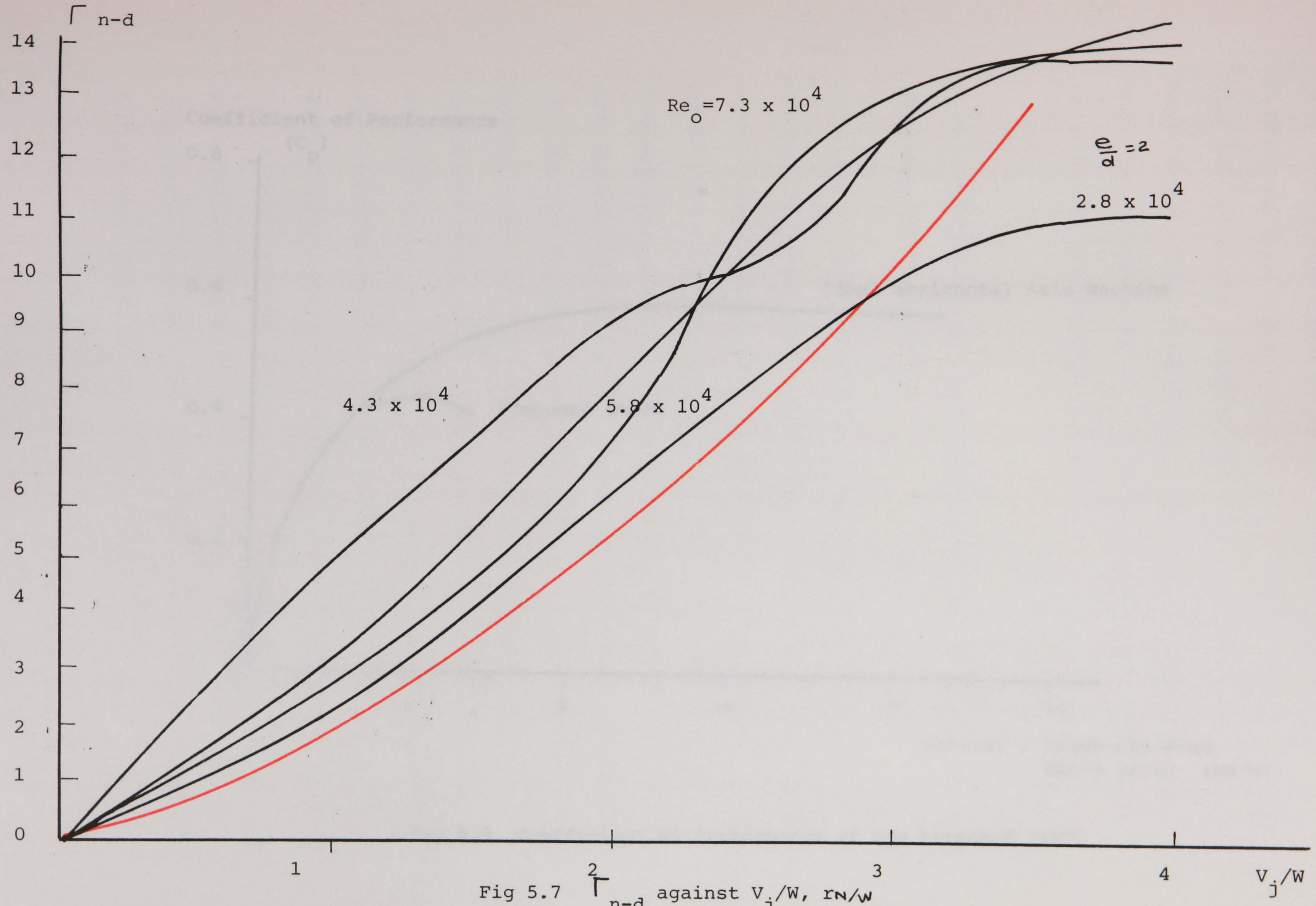

Fig 5.7 Γ_{n-d} against V_j/W, r_N/W

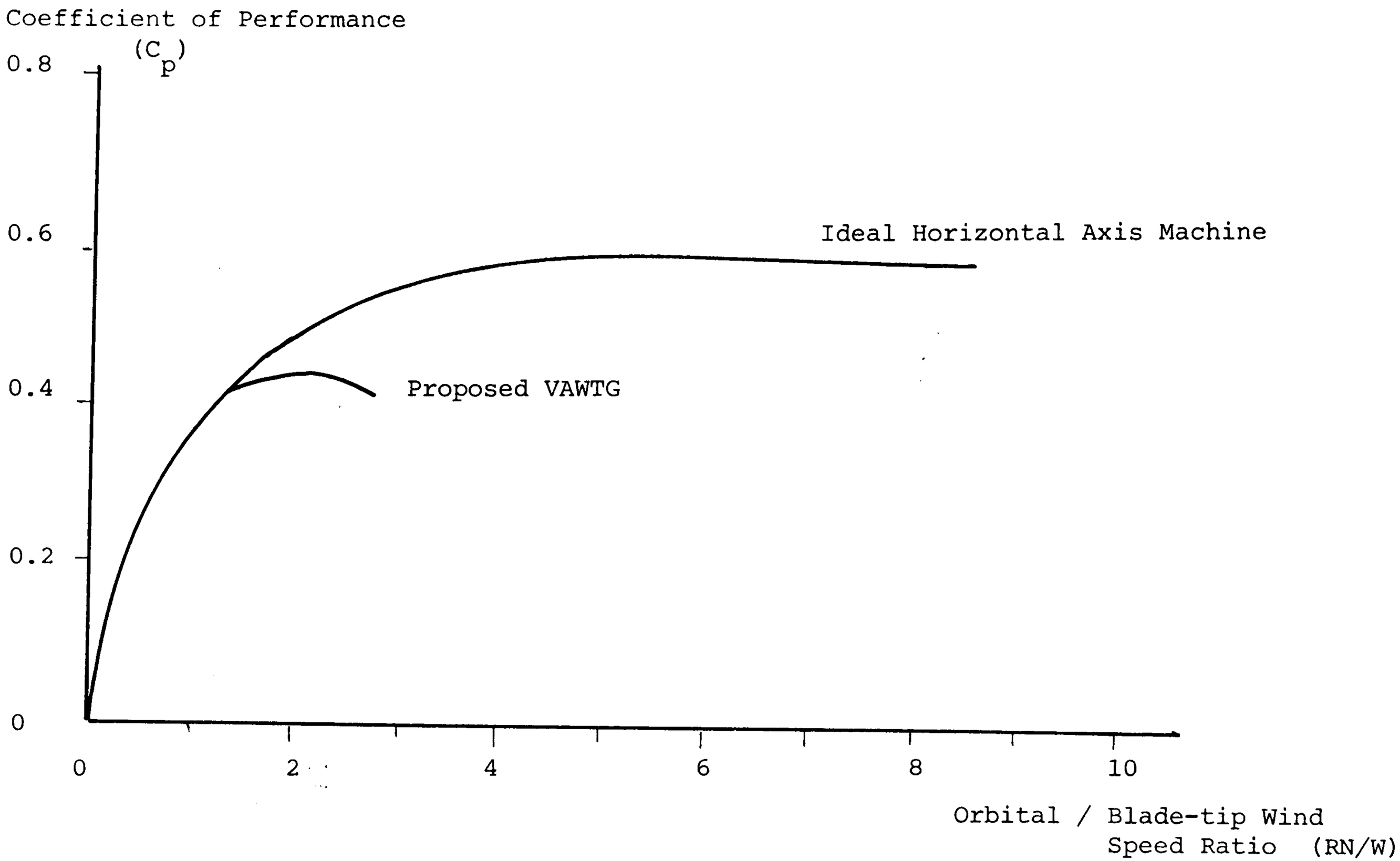

Fig 5.9 Coefficient of Performance of the Proposed VAWTG

Flow field represented by the stream lines for different flow conditions also indicate the effect of the jet momentum coefficient and the jet angle on the aerodynamic lift created by the tangential wall-jet. This is possible by a comparison with the flow field created by the Magnus Effect.

5.5 Coefficient of Performance of the Proposed Wind Turbine Generator

Results of the theoretical evaluation for different values of blade-tip / wind speed ratio for the optimum power coefficient of the proposed wind turbine generator concept is shown in Fig 5.8. The present evaluation is based on three octagonal cylinders with a jet height ratio of 0.1, which has a direct influence on the jet momentum coefficient, (C_μ). The power coefficient of the wind machine increases with an increase value of C_μ. However the magnitude of jet height ratio is limited by the practical arrangement for introducing the two-dimensional wall-jets. The drag coefficient also increases with a greater value of jet height ratio, due to the increased octagonal cylinder projected area. A value of 0.1 is thus a compromise between the requirement for achieving a high C_μ and the above detrimental effects.

5.6 Major Parameters for a Three Bladed 100 kW Machine

Following are the major parameters for a Vertical Axis Wind Turbine Generator with tangential wall-jets for a rated net power out put of 100 kW. Investigation and the equations given in the sections 2.3, 2.6.3 and 2.6.4 are been used. It is to be noted that non of the advantages or optimization given in the sections 2.4, 2.6.1 and 2.6.2 have been included in determining the following major parameters

1 Rated power of the Machine 158 kW

2 Net out put power of the machine 100 kW

3 Power required for the Jet 58 kW

4 Number of blades 3

5 Operational Wind Speed 10 m/s

6 Height of the octagonal cylinders 16.2 m

7 Radius of the Machine 18.9 m

8 Coefficient of performance 43 %

9 Solidity Ratio 0.28

10 Jet height 0.189 m

11 Volume rate of air required for tangential wall-jets of three octagonal cylinders for simultaneous operation 229.63 m^3/s

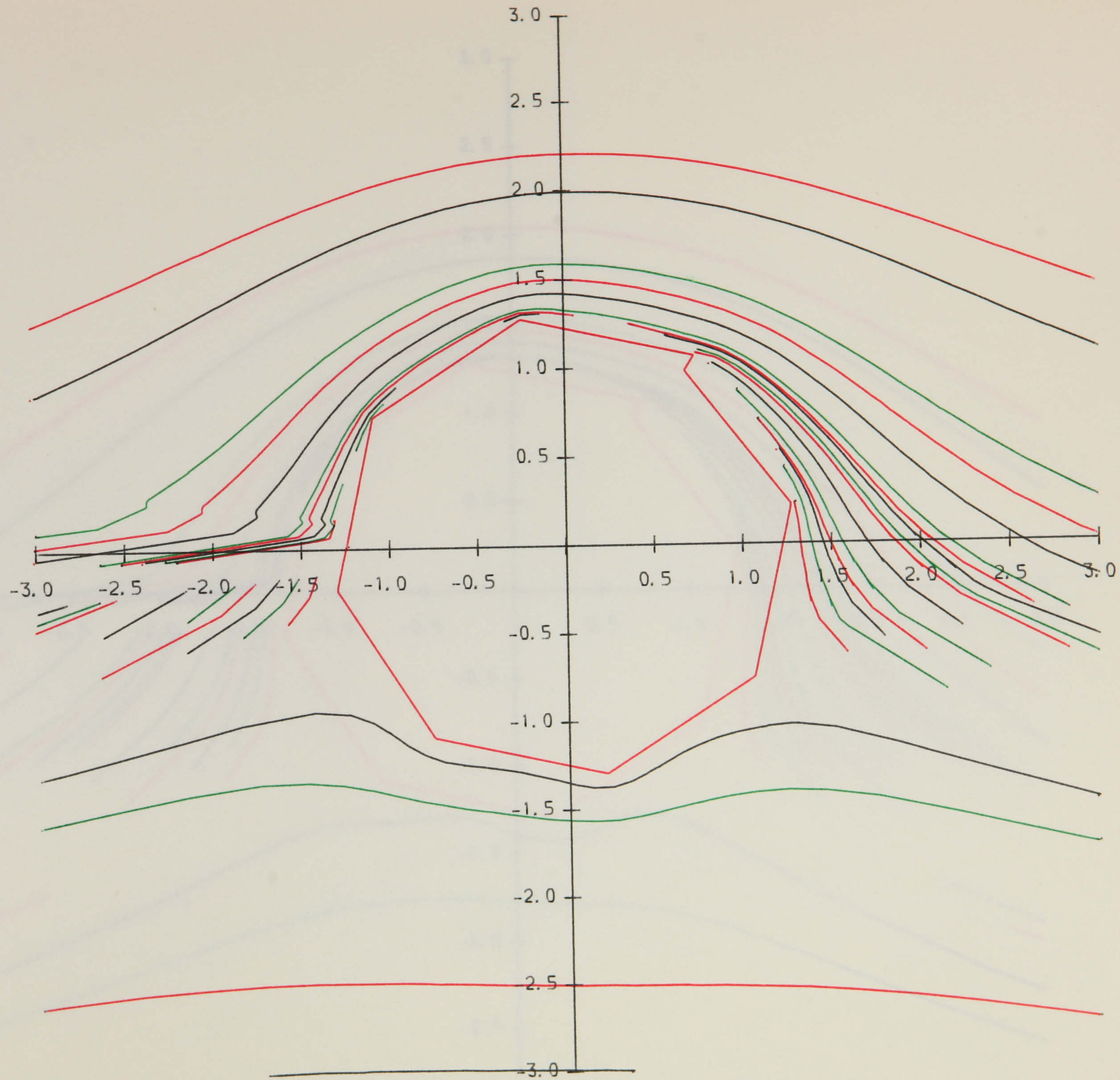

Fig 5.9 Stream Lines for $\theta=125^{\circ}$, $C_{\mu}=0,25$

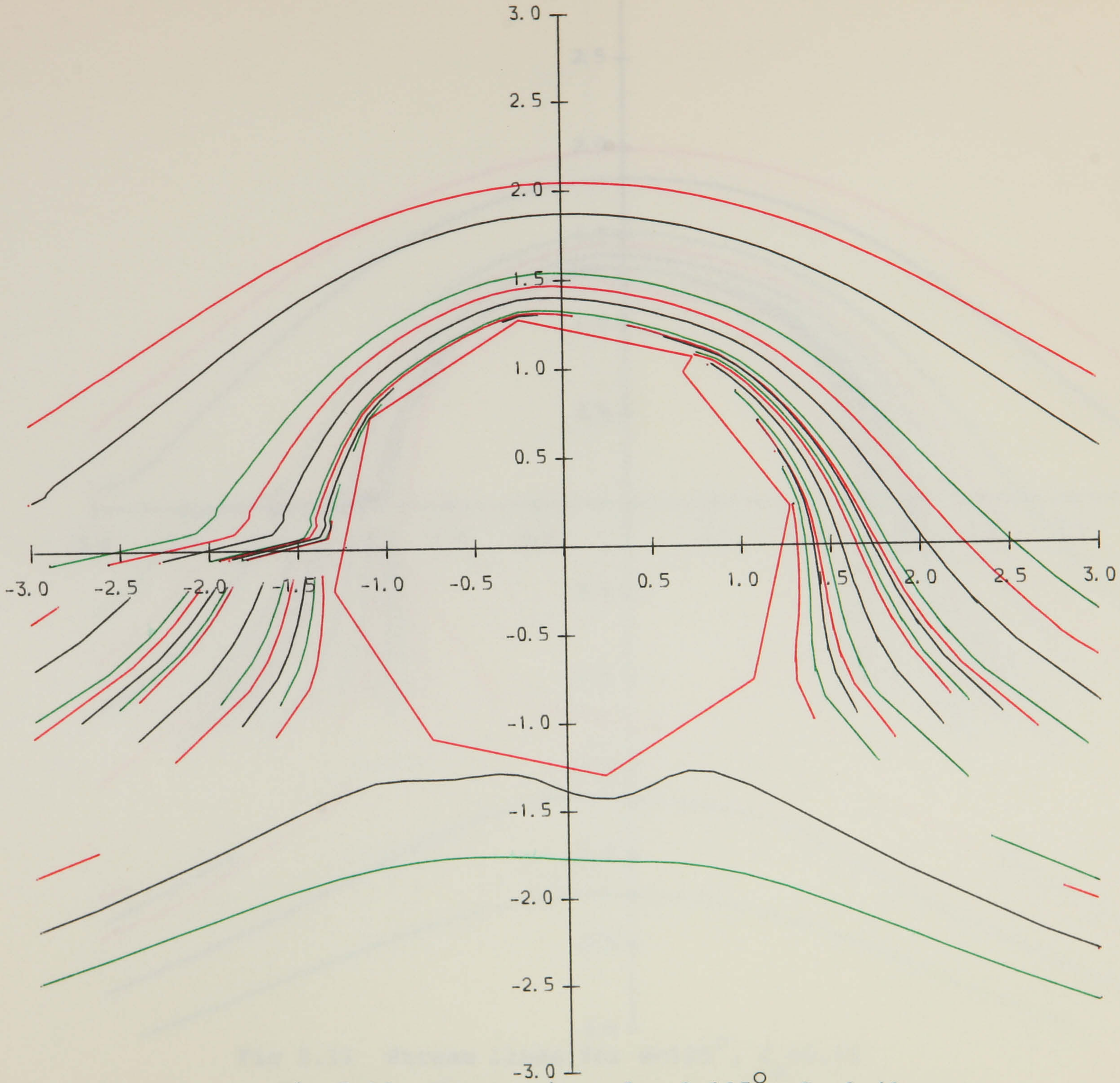

Fig 5.10 Stream Lines for $\theta=125^{\circ}$, $C_{\mu}=0.40$

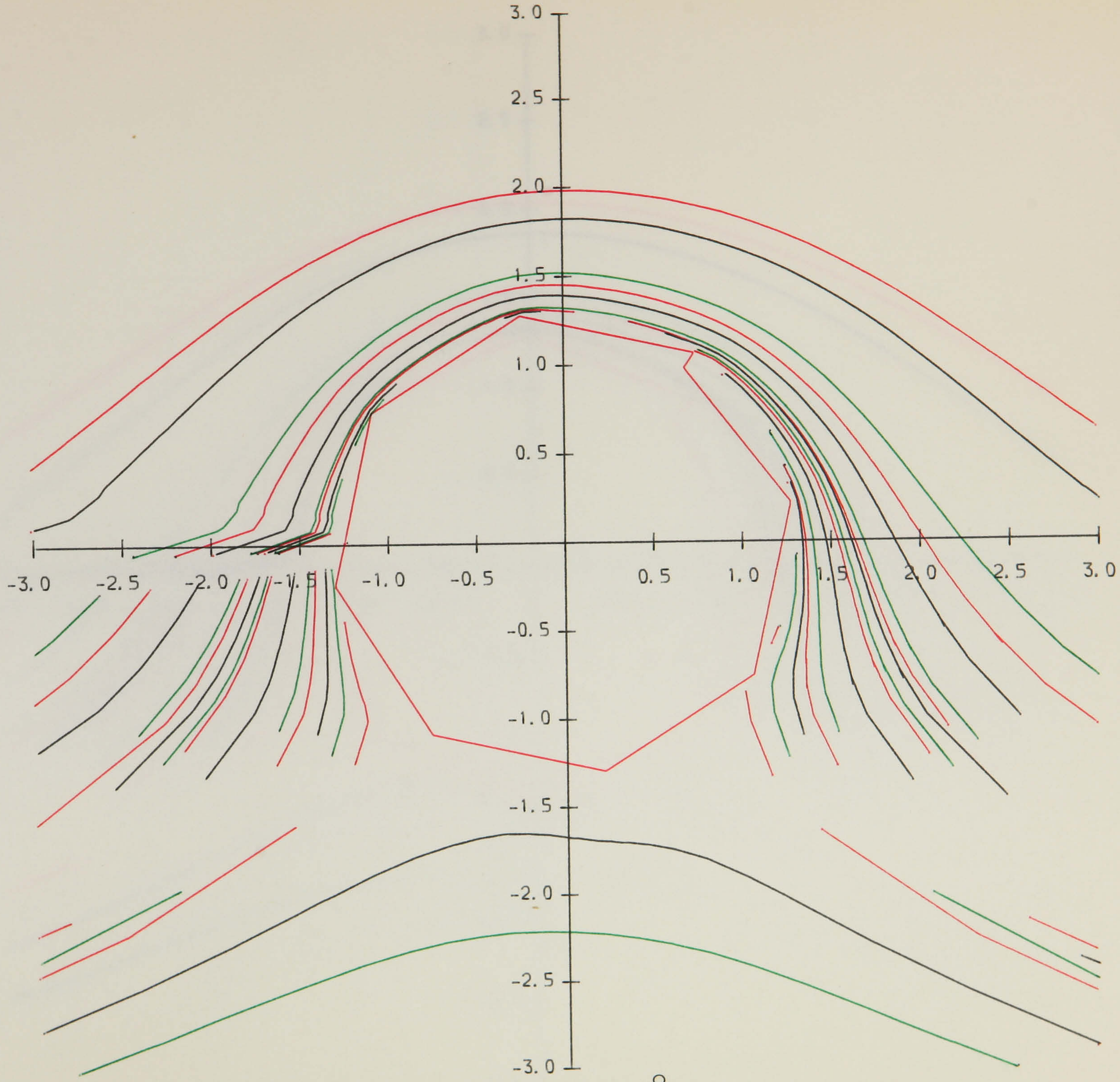

Fig 5.11 Stream Lines for θ=125°, C_μ=0.55

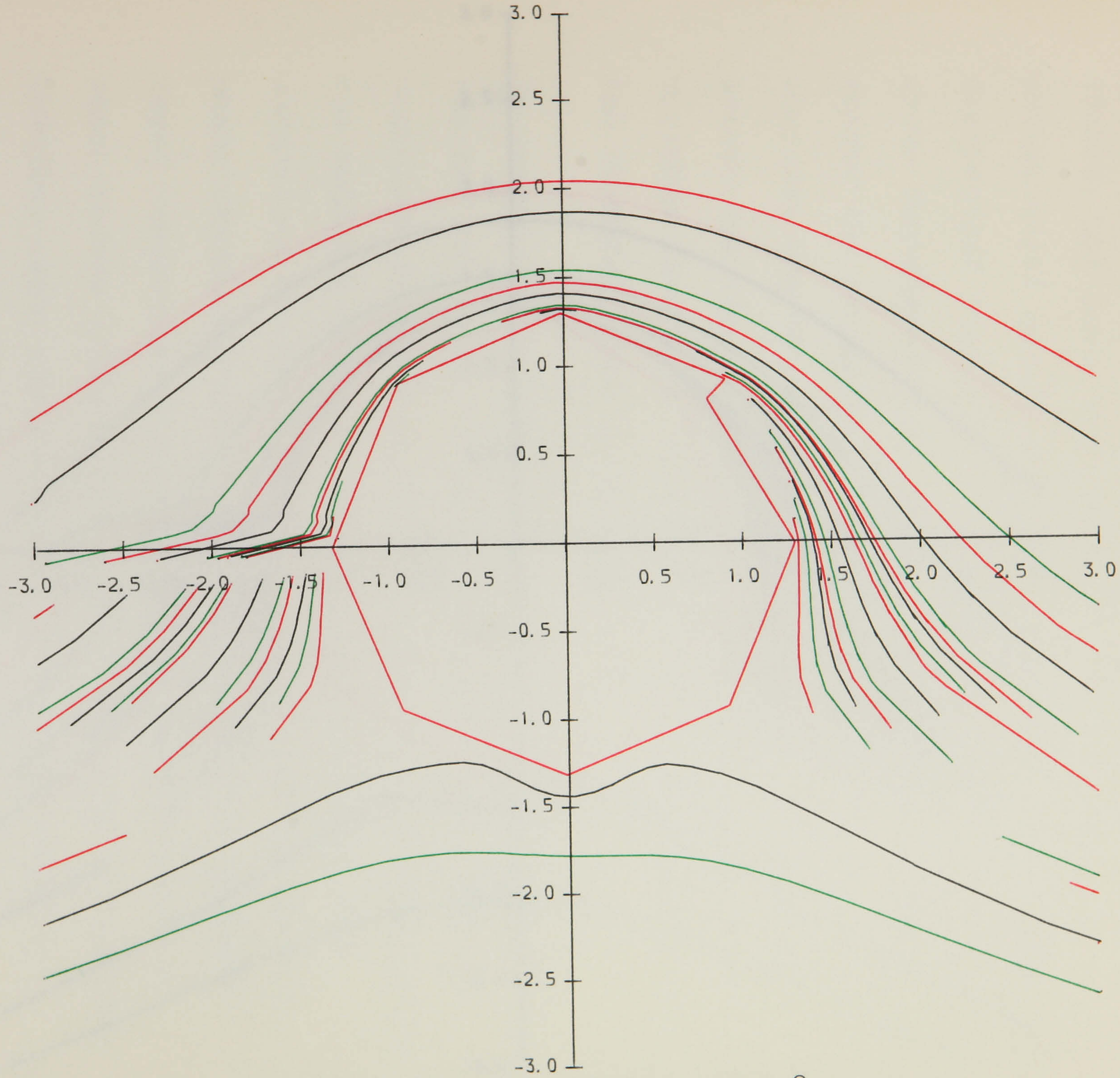

Fig 5.12 Stream Lines for $\theta=135^{\circ}$, $C_{\mu}=0.40$

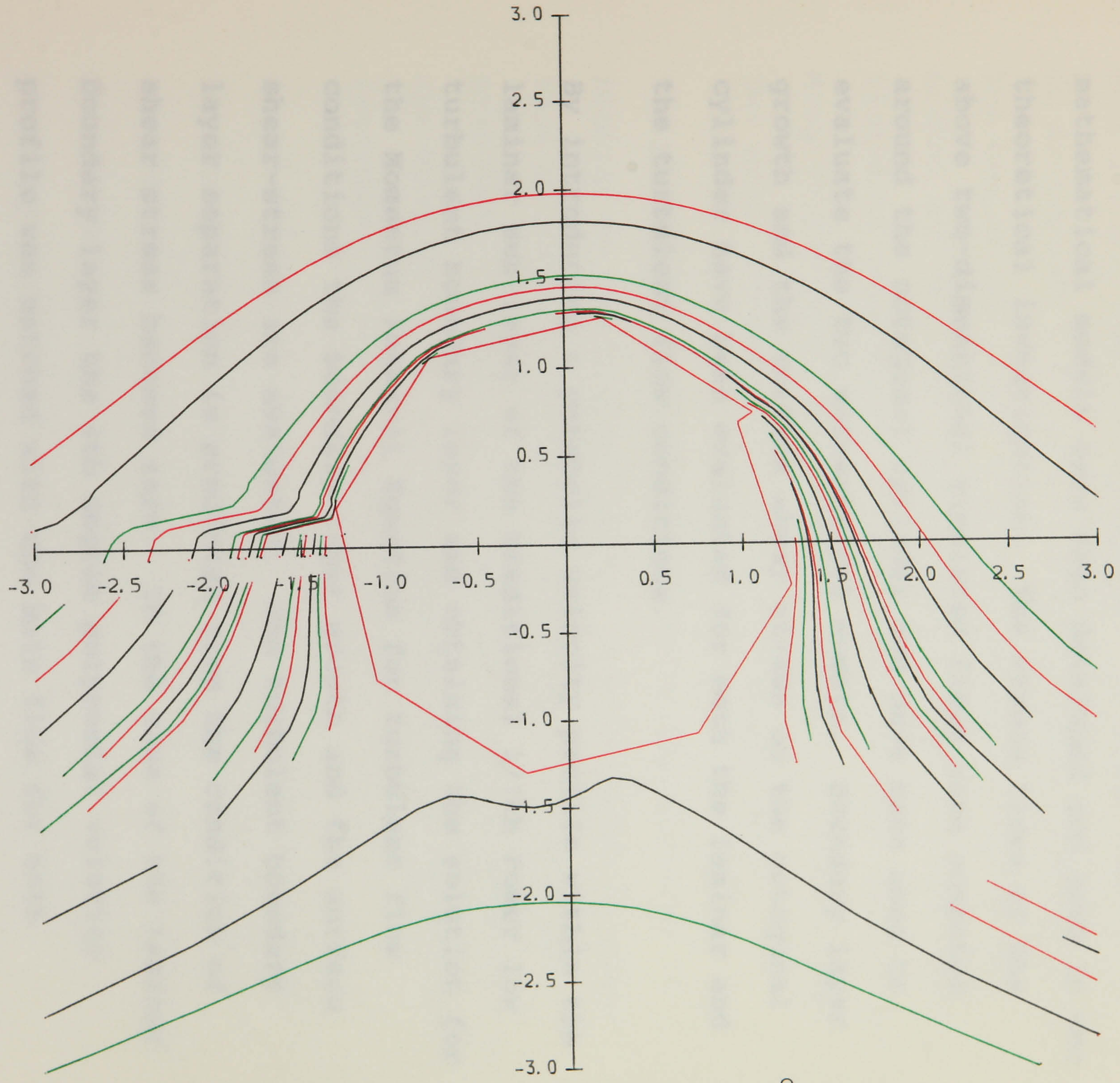

Fig 5.13 Stream Lines for $\theta=145^{\circ}$, $C_{\mu}=0.55$

5.7 Conclusions

The generation of aerodynamic lift due to the tangential wall-jet on an octagonal cylinder for the application to a Vertical Axis Wind Turbine Generator (VAWTG) has been investigated. Two fluid flow mathematical models have been developed and used in the theoretical investigation. The stream lines of the above two-dimensional simulated flows were computed around the octagonal cylinder and have been used to evaluate the two mathematical models. Boundary layer growth and the surface shear stress on the octagonal cylinder have been evaluated for both the laminar and the turbulent flow conditions.

By introducing a parabolic velocity profile within the laminar sub-layer of the traditional 1/7th Power law turbulent boundary layer and obtaining the solution for the Momentum Integral Equation for turbulent flow conditions the boundary layer growth and the surface shear-stress are evaluated. The turbulent boundary layer separation is predicted from the condition of shear stress becomes zero. In the case of the Laminar boundary layer the 4th degree polynomial velocity profile was matched with the main flow for both magnitude and gradient. This modification to the traditionally used procedure for obtaining the laminar boundary layer development is applied for the case of a

tangential wall-jet with a non-zero pressure gradient. The feasibility of this procedure for flow past bodies such as flat plates, smooth circular cylinders with tangential wall-jets have been tested. In the present investigation the laminar boundary layer occurs only over a small region. Therefore the above modification in evaluating the laminar boundary layer comparable to the use of the traditional Pohlhausen's approximate method and does not significantly influence the overall lift/drag calculation. Pressure components of lift and drag forces have been obtained which are allowing for the shear stresses and the jet reaction force.

The principle of lift generation by the wall-jet is similar to the Magnus effect. A preliminary examination of the application of the tangential wall-jet principle in place of the axially rotating cylinders in the Madaras Rotor Concept gives as much as much as 30 % increment in the net-power out put.

A new concept of VAWTG based on the aerodynamic lift due to the tangential wall-jet is proposed. Such a machine will have an optimum value of power coefficient for blade-tip /wind ratio of about 1.0. Optimum jet momentum coefficient and the corresponding power required for the formation of the tangential wall-jets have been established. Net power out-put by the machine has been evaluated.

Investigations showed that the power coefficient for certain operating and design conditions for this type of wind machine may exceed the traditional Betz limit. This is due to the pressure variation along the surface of the "stream tube" past the "Actuator Disc" representing the machine. Hence the limiting values of the performance coefficient depend on the shape of the stream tube considered. It is shown that in general the use of the Betz limit as the performance indicator for a VAWTG where the pressure recovery between the operating elements is possible may be misleading.

Experimental studies have been carried out on a stationary octagonal cylinder with a tangential wall-jet and the pressure components of the lift and the drag forces have been obtained. A single tangential wall-jet at an angle of about 145° from the up-wind direction can generate lift, adequate for the proposed wind turbine generator. A wind tunnel model of the proposed concept of the wind machine consisting of three octagonal cylinders mounted on a vertical axis was fabricated and tested for the feasibility of the application of the tangential wall-jet principle.

Theoretical and experimental studies have confirmed that it is feasible to use the principle of aerodynamic

lift due to the tangential wall-jet on an octagonal cylinder for a Medium / Large scale Vertical Axis Wind Turbine Generator.

Further work is required through prototype development and testing to compare the theoretical performance of the machine with the actual operational performance and to evaluate the practical difficulties in implementation of the tangential wall-jets.

REFERENCES

1. Chase Victor; "13 Wind Machines", Popular Science, vol 213, No 3 Sep 1978.

2. Beans E. W: Approximate aerodynamic Analysis for the Darrieus rotor wind turbine", Wind Energy Conversion 1986, Proceedings of the 8th BWEA conference, pp 243, MEP, 1986.

3. Cheeseman I. C; "Circulation control and its application to stopped rotor aircraft", AIAA Paper No 67-747, 10th Anglo-American Aeronautical Conference, Los Angeles, 1967.

4. Cheeseman I. C; "The application of circulation control by blowing to helicopter rotors", J. Aeronautical Society, 71, pp 451, 1967.

5. Musgrove P. J, Mays I. D; "Experience in the development of vertical axis wind turbines in the UK", IEE Energy Options Conference, Appendix 276, 1987.

6. Mays I. D, Musgrove P. J and others; "The evolution of the straight bladed vertical axis turbine", British Wind Energy Association 10th Annual Conference, CEGB, London 1988.

7. Yen J. T; "Summary of recent progress on Tornado-type wind energy system", Proceedings of the 3rd Biennial Conference and Workshop on wind energy conversion systems, Vol 2, JBF., Washington D C, Sep 1977.

8. Ayad S. S; "Numerical study of Tornado-type wind energy system", J. Energy, Vol 7 No2 pp 134, March-April 1983.

9. Minardi J. E, Lawson M. O; "Electrofluid (EFD) wind driven generator", University of Dayton Research Institute, Ohio, USA, 1978.

10. Minardi J. E, Lawson M. O; "Progress in Electrodynamic wind driven generator research", 3rd Biennial Conference and Workshop in wind energy conversion systems, Washington D C, Sep. 1977.

11. Lawson M, Von Ohian H; "Electrofluid dynamic energy conversion present status and research areas", Trans. of ASME 1971.

12. Whiteford D. F, Minandi J and others; "Analysis of the Madaras rotor power plant", An alternative method extracting large amount of power from the wind, Executive Summary, Dayton University Research Institute, Ohio, 1978.

13. Whiteford D. F, Minandi J and others; "Analysis of the Madaras rotor power plant", An alternative method of extracting large amount of power from the wind, Technical report, Dayton University Research Institute, Ohio, 1978.

14. Swanson W. M; "The Magnus effect -a summary of investigation upto date", Journal of Basic Engineering, pp 461, Sep 1961.

15. Schlichting H; "Boundary Layer Theory", 4th ed., McGraw-Hill, New York, 1960.

16. Bublitz P; "Periodic normal forces on a circular cylinder in a cross-flow and unsteady Magnus effect", Z Flugwiss Weltrassmrforst, Vol 7 part 4 pp 253-262, 1983.

17. Dunham J; "A theory of circulation control by slot blowing applied to a circular cylinder", J. Fluid Mechanics, Vol 33 pp 495-514, 1968.

18. Sigalla A; "Measurement of skin friction in a plane turbulent wall-jet", J. Royal Aeronautical Society, Vol 62 pp 873, 1958.

19. Fothmanne E; "Turbulent jet expansions", Translated NACA Technical memo 789, 1936.

20. Bradshaw P, Gee M. T; "Turbulent wall-jets with and without an external stream", Report and memoranda no 3252, June 1960.

21. Glauert M. B; "The wall-jet", J. Fluid Mechanics, Vol 1 pp 625, 1956.

22. Bakke P; "An experimental investigation of a wall-jet", J. Fluid Mechanics, Vol 2 pp 467, 1957.

23. Sigalla A;, "Experimental data on turbulent wall-jets", Aircraft Engineering, pp131, 1983.

24. Tetrevin N; "Laminar flow of a slightly viscous incompressible fluid that issues from a slit and passes over a flat plate , NASA Technical note 1644, 1944, 1948.

25. Carriere P, Eichelbrenner E A; "Theory of flow attachment by a tangential jet discharging against a strong adverse pressure gradient", Boundary layer and flow control London, pp 209-231, 1961.

26. Furuya Y, Yoshino F; "Aerodynamic forces acting on a circular cylinder with a tangential injection of air", B. JSME V 18, n123, Sep 1978.

27. Yoshino F, Waka R and others; "The effect of a side wall on aerodynamic characteristics of a circular cylinder with tangential blowing", B. JSME V 24, n129, June 1981.

28. Yoshino F, Waka R and others; "Aerodynamic characteristics at the mid span of a circular cylinder with tangential blowing", B. JSME V 26, n215, May 1983.

29. El-Shaarawi M. A, El-Refaie M. F and El-Bedeawi A; "Numerical solution of Laminar boundary layer flow about a rotating sphere in an axial stream", J. Fluid Eng, Vol 107, March 1985.

30. Bychkof N. M, Kovolenko V M; "Aerodynamic of a circular cylinder in a cross-flow", Fluid Mechanics-Soviet Research, Vol 12 No 1 pp 1-16, Jan 1983.

31. Bychkof N. M, Kovolenko V M; "Aerodynamic forces on a smooth rotating cylinder in a cross-flow", Fluid Mechanics-Soviet Research, Vol 12 No 1 pp 17-32, Jan 1983.

32. Bychkof N. M, Kovolenko V M; "Aerodynamic forces on a rough rotating cylinder in a cross-flow", Fluid Mechanics-Soviet Research, Vol 12 No 1 pp 47-57, Jan 1983.

33. Zubarev V. M; "Boundary layer on the moving surface of a cylinder", Fluid Mechanics Soviet Research, No 6 pp 38-42. Sep 1982.

34. Parkinson G. V, Jandali T; "A wake source model for bluff body potential flow" J. Fluid Mechanics, Vol 40 part 3 pp 577-594, 1970.

35. Gresho M, Steven S. T and others; "A modified finite element method for solving the time-dependent incompressible Navier-Stokes equations", Int. J. Numerical Methods in Fluids, Vol 4 pp 619-640, 1984.

36. Galerkin M; "Finite element method for solving the time-dependent incompressible Navier-Stokes equations", Int. J. Numerical Methods in Fluids, Vol 4, 1984.

37. Head N. R, Patel V. C; "Improved entrainment method for calculating turbulent boundary layer development", Reports and Memoranda N0 3643, 1968.

38. Rajarathnam N; "Turbulent Jets", Elsevier, 1976.

39. Eskinazki S, Kruka V; "Mixing of a turbulent wall-jet into a free stream", Proceedings of the ASCE 88, April 1962.

40. Kruka V, Eskinazi S; "The wall-jet in a moving stream", J. Fluid Mechanics, Vol 20 Part 4 pp 555-579, 1964.

41. Rao H. V, Perera G. E. L; "The Aerodynamics of wall-jet action on octagonal cylinders for application to a VAWTG", Wind energy conversion 1987, Proceedings of the 9th BWEA Conference, ed. Galt J, pp 225- 229 MEP, 1987.

42. Rao H. V, Perera G. E. L; "Application of tangential wall-jets for high lift generation", Wind energy conversion 1986, Proceedings of the 8th BWEA Conference, MEP, 1986.

43. NAG FORTRAN Mini Manual, Mark 10, NAGFLIB. 2022/1977, 1983.

44. Symm G. T, Pitfield R. A; "Solution of Laplace's equation in two-dimensions", NPL report NAC44, 1974.

45. Snedon I. N; "Elements of partial differential equations", Mc-Graw Hill, 1986.

46. Sokolnikof I. S, Redhrffer R. M; "Mathematics of physics and modern engineering", Mc-Graw Hill, 1984.

47. Grimson J; "Advanced Fluid dynamics and heat transfer", Mc-Graw Hill, 1971.

48. Rosenhead L; "Laminar boundary layers", Fluid motion memories, Clarendon Press, Oxford, 1963.

49. Streeter V. L; "Hand Book of Fluid Mechanics", 1St. ed., MacGraw-Hill, 1961.

50. McCormic J. M, Salvadori M. G; "Numerical methods in FORTRAN", Prentice -Hall, 1968.

51. Bender C. M, Orszag S. A; "Advanced mathematical methods for scientists and engineers", Mc-Graw Hill, 1978.

52. Eckert E. R, Drake R. M; "Heat and mass transfer", 2nd Ed., Mc-Graw Hill, 1974.

53. Massey B. S; "Mechanics of Fluids", 5th Ed., Van Nostrand Reinhold, 1986

54. Lipman N. H; "Wind energy for the eighties", BWEA, Peter Peregrinus, 1982.

55. Betz A; "Introduction to the theory of flow machines", (Translated by R G Randal) Pergomon Press, London 1965.

56. Bergy K. H; "The Lanchester Betz limit", J. Energy, Vol 31, no 6, 1979.

57. Rao H. V, Perera G. E. L; "Betz-type limit for vetical axis wind turbine generators", 10th British Wind Association Annual Conference, CEGB, London, 1988.

58. Loth J. L; "Wind power limitations associated with vortices", J. Energy, Vol 2 no 4, 1978.

59. Loth J. L, McCoy H; "Optimization of Darrieus turbines with an upwind and downwind momentum model", J. Energy, Vol 7 no 4, 1983.

60. Patel V. C, Celik; "Calculation of the mean flow past circular cylinder by viscous inviscid interaction", Trans. ASME, Vol 107 pp 218-223, June 1985.

APPENDICES

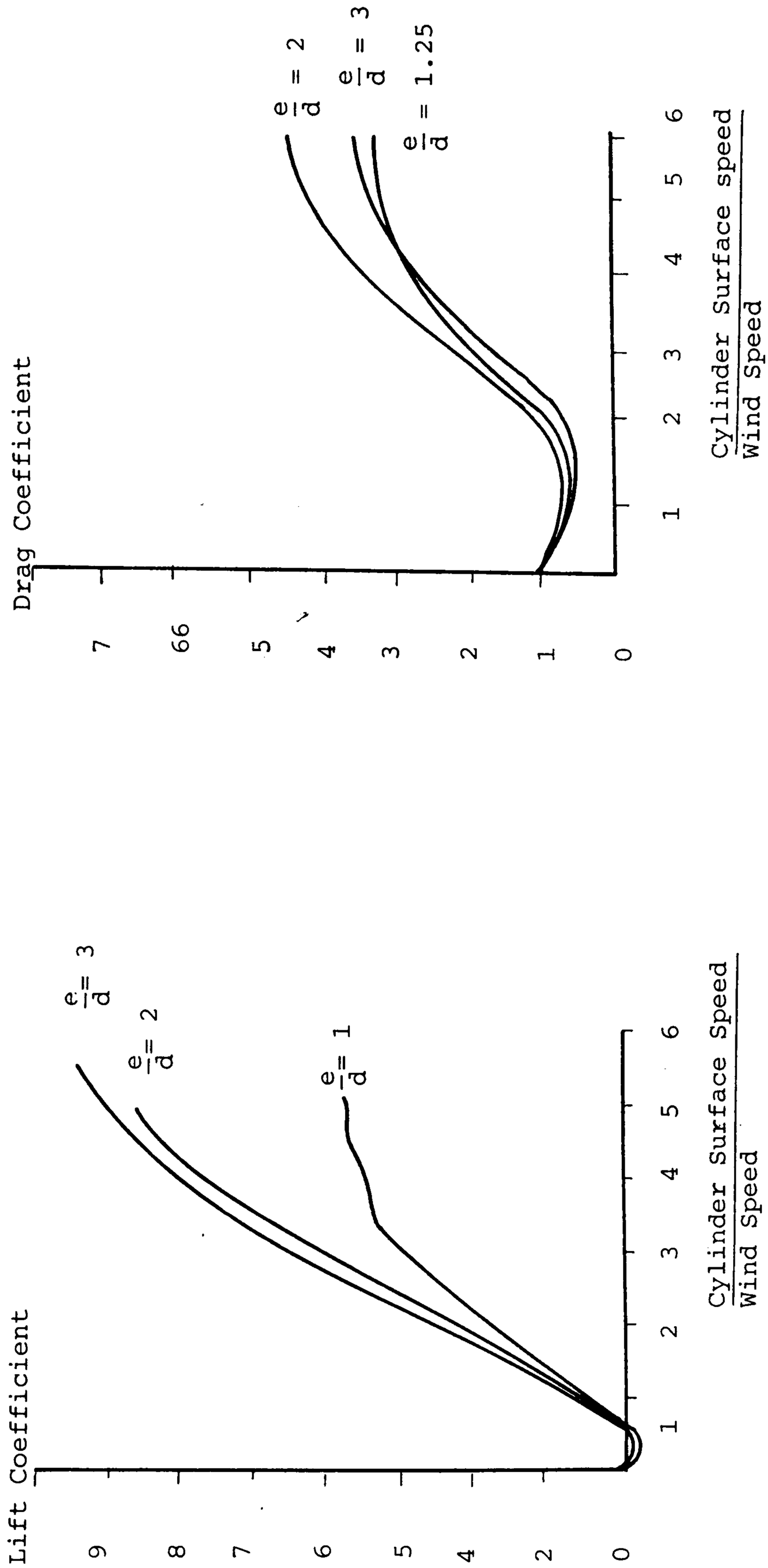

Fig 1A.1 Lift and the Drag Coefficients due to the Magnus Effect

Appendix 2A

Lift and Drag Forces Due to the Magnus Effect

Lift force due to the axial rotation of a cylinder can be expressed in the form of a vector as;

2A-1 $$\overline{L} = \left(-2\Pi r^2 H \rho\right)(\overline{\omega} \times \overline{U})$$

The drag force due to the axial rotation can be expressed in the form of a vector as;

2A-2 $$\overline{D} = \left(C_D \rho r H U_m\right)\overline{U}$$

Where;

$$\overline{U} = \overline{W} - \overline{V}$$

$$\overline{V} = (\Omega \times R)$$

(see Fig 2A.1)

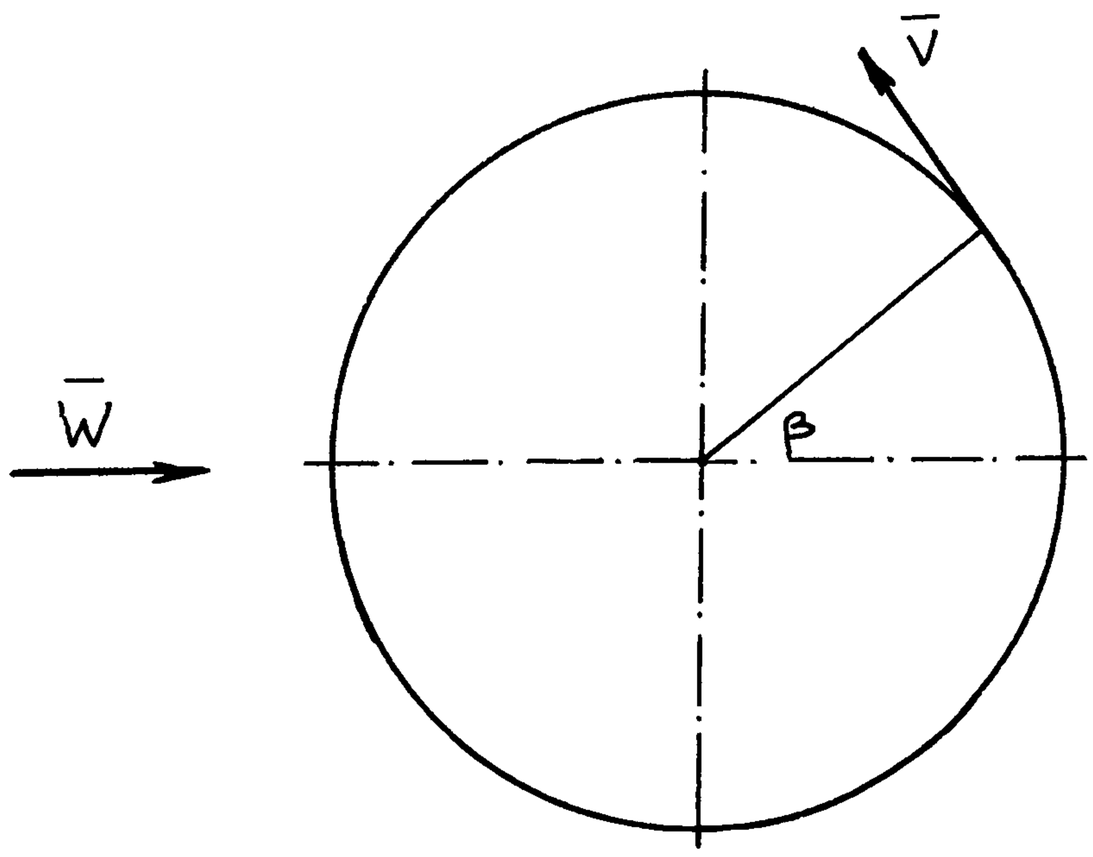

Fig 2A.1

Therefore by using the unit vectors $i, \hat{j}, \hat{k}$.,

$$\overline{R} = (R\cos\beta)\hat{i} + (R\sin\beta)\hat{j}$$

$$\overline{\Omega} = (\Omega_z)\hat{k}$$

$$\overline{\omega} = (\omega_z)\hat{k}$$

$$\overline{W} = W\hat{i}$$

Therefore;

$$\overline{V} = \begin{pmatrix} i & j & k \\ 0 & 0 & \Omega_z \\ k\cos\beta & R\sin\beta & 0 \end{pmatrix}$$

$$= \hat{i}[-R\Omega_z\sin\beta] + \hat{j}[R\Omega_z\cos\beta]$$

hence the components of the V in the non-dimensional form can be given by;

2A-3

$$V_x = -\Omega_z \cdot \sin\beta \cdot \left(\frac{R}{W}\right)$$

$$V_y = \Omega_z \cdot \cos\beta \cdot \left(\frac{R}{\Omega}\right)$$

equation 2A-1 can also be expressed as;

$$\overline{L} = -2\Pi r^2 \rho H \begin{pmatrix} i & j & k \\ 0 & 0 & \omega_z \\ U_x & U_y & \omega_z \end{pmatrix}$$

$$= -2\Pi r^2 \rho H\left[\hat{i}(-U_y\omega_z) + \hat{j}(U_x\omega x)\right]$$

Therefore the components of the non-dimensional lift force can also be written in the form;

2A-4

$$L_x = \frac{2\Pi r^2 \rho H \omega_z (U_y)}{(\rho W^2 r H)}$$

$$L_y = -\frac{2\Pi r^2 \rho H \omega_z U_x}{(\rho W^2 r H)}$$

The components of the relative velocity of the cylinder can be expressed as;

2A-5 $$U_x = W - V_x$$

$$U_y = -V_y$$

The two components of the non-dimensional drag force can expressed as;

2A-6 $$D_x = \frac{C_D \rho (r H) U_m U_x}{(\rho W^2 r H)}$$

$$D_y = \frac{C_D \rho (y H) U_m U_y}{(\rho W^2 r H)}$$

Therefor the the non-dimensional lift force given by the equation 2A-4 can also be expressed as;

2A-7 $$L_x = 2\Pi \left(\frac{r}{R}\right)\left(\frac{\omega_z}{\Omega_z}\right)\left(\frac{R\Omega_z}{W}\right)U_y$$

$$L_y = -2\Pi \left(\frac{r}{R}\right)\left(\frac{\omega_z}{\Omega_z}\right)\left(\frac{R\Omega_z}{W}\right)U_x$$

and similarly the components of the non-dimensional forces given by the equation 2A-6 can be expressed as;

2A-8 $$D_x = C_x U_m U_x$$

$$D_y = C_D U_m U_y$$

Therefore the components of the total force at any orbital point can be expressed as;

2A-9 $$F_x = D_x + L_x$$

$$F_y = D_y + L_y$$

and therefore the instananeous power due to the axial rotation is;

2A-10 $$P = \overline{F} \cdot \overline{V} = F_x V_x + F_y V_y$$

Appendix 2B

Lift and Drag Forces due to the Tangential Wall-jet and the Power Required to Form the Jet

The components of the lift force due to the wall-jet on an octagonal cylinder may be obtained from

2B-1 $$\bar{L} = -\rho C_r r^2 H U_m (\bar{C}\mu \times \bar{U})$$

Where, C_r is the ratio of the lift coefficient to the jet momentum coefficient, C_L/C_μ;

$$C_\mu = \frac{1}{2}\left(\frac{V_j}{U_m}\right)^2 \left(\frac{b}{r}\right)$$

Therefore the non-dimensional components of the lift are;

2B-2 $$L_x = \frac{\rho C_r r H U_m (\mu_z U_y)}{\rho W^2 (r H)}$$

2B-2 $$L_y = -\frac{\rho C_r r H U_m (\mu_z U_x)}{\rho W^2 (r H)}$$

And the components of the non-dimensional drag coefficient can be expressed by the equation 2A-6 of the Appendix 2A.

The Jet momentum coefficient $\mu_z = (\pm C_\mu)$

and from the jet location angle range (Fig 2.2B)

$$0 > \beta > \frac{\Pi}{2}$$

$$\frac{3\Pi}{2} > \beta > 2\Pi$$

The jet momentum coefficient C_μ is taken as the negative value, and the jet location angle range of,

$$\frac{\Pi}{2} > \beta > \frac{3\Pi}{2}$$

The jet momentum coefficient C_μ is taken as a positive value. (See Fig 2B.1)

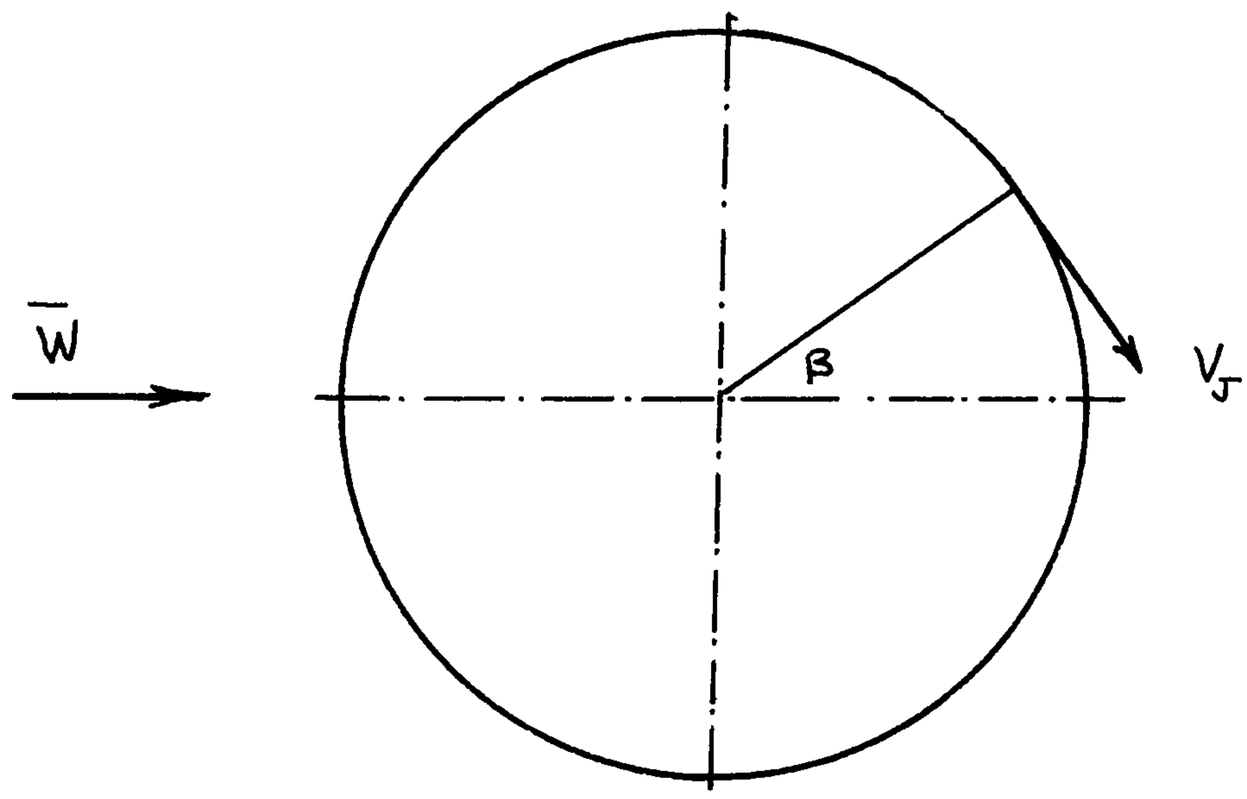

Fig 2B.1

Power required to form the tangential wall-jet P_N can be expressed as;

2B-3 $$P_N = \dot{m} C_p (T_0 - T_a)$$

and $$\frac{V_j^2}{2} = \eta_N (h_0 - h_1)$$

Where η_N is the efficiency of the nozzle.

$$(h_0 - h_1) = C_p (T_0 - T_1'$$

$$= C_p T_1' \left(\frac{T_0}{T_1'} - 1 \right)$$

By substituting the,

$$\frac{T_0}{T_1'} = \left(\frac{p^0}{p_1'} \right)^n = \left(\phi^n \right)$$

Where, $n = \dfrac{\nu - 1}{\nu}$

2B-4 $$\frac{V_j^2}{2} = \eta_N C_p T_1' \left(\phi^n - 1 \right)$$

and $$\eta_c = \frac{T_0' - T_a}{T_0 - T_a}$$

Therefore,

2B-5 $$T_0 - T_a = \frac{i}{\eta_c} \cdot T_a \left(\phi^n - 1 \right)$$

and

2B-6 $$T_1' = \frac{T_a}{\phi^n} \left[1 + \frac{1}{\eta_c} \left(\phi^n - 1 \right) \right]$$

$$\frac{V_j^2}{2} = \left(\eta_N C_p T_a \right) \left[\frac{1 + 1/\eta_c \left(\phi^n - 1 \right)}{\phi^n} \right] \left[\phi^n - 1 \right]$$

Therefore the power required to form the jet is;

2B-7 $$P_N = \frac{\dot{m} C_p T_a \left(\phi^n - 1 \right)}{\eta_c}$$

Appendix 3A

Non Dimensional Conversions Used in the Document

Following are the basic non-dimensional conversions used in the thesis.

1. Non-dimensional Distance = $\frac{Distance}{l}$

2. Non-dimensional Velocity = $\frac{Velocity}{W}$

3. Non-dimensional Force = $\frac{Force}{\rho W^2 (rH)}$

4. Non-dimensional Power = $\frac{Power}{\rho W^3 (rH)}$

5. Non-dimensional Circulation = $\frac{\Gamma}{W \cdot l}$

6. Non-dimensional Shear Stress = $\frac{Shear\ \ Stress}{\rho W^2/2}$

7. Reynolds Number $Re = \frac{\rho W l}{\mu}$

8. Reynolds Number $Re_o = \frac{\rho W (2r)}{\mu}$

Appendix 3B

Determination of the boundary conditions at the Jet-entrance

In prescribing the boundary conditions of the contour C2, in 3.4.1 the stream function at the point A of the jet has been taken to be zero ($\phi_A = 0$). The velocity profile at the jet entrance is prescribed by the 1/7th Power Law (Fig 3B.1)

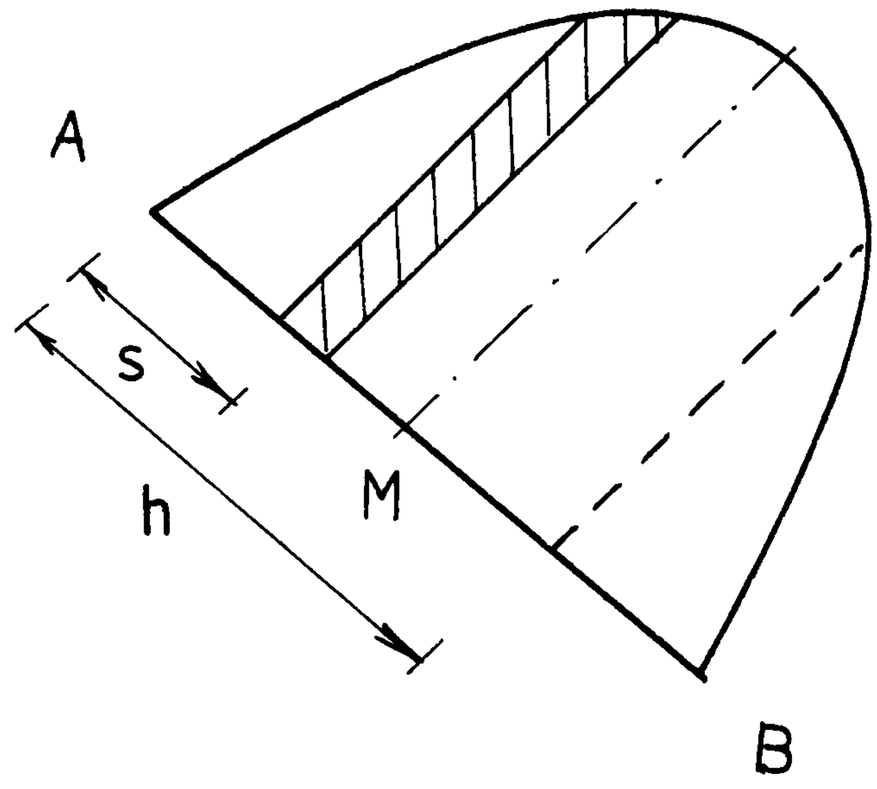

Fig 3B.1 Jet Velocity Profile

$$\Phi_A = 0$$

$$\frac{q}{q_{max}} = \left(\frac{s}{h/2}\right)^{1/7}$$

3B-1

$$q = q_{max}\left(\frac{2s}{h}\right)^{1/7}$$

Where,

3B-2

$$q_{mean} = \frac{2}{h}\int_0^{h/2} q\,ds$$

and hence,

$$q_{mean} = \frac{7}{8}q_{max}$$

The jet momentum Coefficient C_μ

$$C_\mu = \frac{Jet\,Momentum}{Wind(air)\,Momentum}$$

Therefore,

3B-3

$$C_\mu = \frac{\rho q_{mean}(hX1)q_{mean}}{\rho W(2rX1)W}$$

$$C_\mu = \frac{q_{mean}^2}{W^2}\cdot\frac{h}{2r}$$

From 3B-2,

$$C_\mu = \left(\frac{7}{8}q_{max}\right)^2\cdot\frac{h}{W^2 2r}$$

$$\frac{q_{max}}{W} = \frac{8}{7}\sqrt{\frac{C_\mu}{(h/2r)}}$$

Therefore

$$q_{\substack{max\\n-d}} = \frac{8}{7}\sqrt{\frac{C_\mu}{(h/l)\sin(\pi/8)}}$$

For the octagonal cross-section, $\frac{h}{2r} = \frac{h}{l}\sin\frac{\pi}{8}$

From 3B-1,

$$q_{n-d} = \left(\frac{2s}{h/l}\right)^{m} \cdot q_{\substack{\max \\ n-d}}$$

Where; $$m = \frac{1}{7}$$

On the jet AB upto the mid-point M the stream function can be expressed in the form of;

$$\Phi_{p1} = -\left(\frac{2}{h/l}\right)^{m} \cdot q_{\substack{\max \\ n-d}} \cdot \frac{1}{m1} \cdot S^{m1}$$

(Fig 3B.1)

Where; $m1 = m + 1$

and from the mid-point M to the point B the stream function can be expressed in the form of;

$$\Phi_{p2} = -2K1K2\left(\frac{h}{2l}\right)^{m1} + K1K2S^{m1}$$

Where; $$K1 = q_{\substack{\max \\ n-d}}$$

$$K2 = \left(\frac{2}{h/l}\right)^{m} \cdot \frac{1}{m1}$$

(Fig 3B.1)

Hence, at point M the stream function becomes;

$$\Phi_{M} = -K1K2 \cdot \left(\frac{h}{2l}\right)^{m1}$$

and at point B stream function becomes;

$$\Phi_{B} = -K1K2 \cdot \left(\frac{h}{2l}\right)^{m1}$$

or, $\Phi_B = 2\Phi_M$

Now with respect to the boundary conditions at A, B boundary conditions on the remaining sides of the contours C1 and C2 are determined. (3.4.1 , 3.5.1)

Appendix 3C

Slip stream velocities at the contour C2

Considering a uniform stream of velocity U parallel with the x axis, (Fig 3C.1) for the stream function on the contour C2 ϕ is;

(for y=constant)

$$\phi = U\,y$$

or, $$\phi = U\,r\,\mathrm{Sin}\,\theta$$

By differentiating gives

$$u = \frac{\partial \phi}{\partial y} = U$$

$$v = -\frac{\partial \phi}{\partial x} = 0$$

For a uniform stream velocity V parallel with the y axis (Fig 3C-2) (for x=constant)

$$\phi = -V\,x \quad or \quad \phi = V\,r\,\mathrm{Cos}\,\theta$$

By differentiating the above equation we get;

$$u = \frac{\partial \phi}{\partial y} = 0$$

$$v = -\frac{\partial \phi}{\partial x} = V$$

Therefore a uniform stream having velocity components U and V in the directions of x and y,

$$\phi = U\,y - V\,x$$

or $$\phi = U\,r\,\mathrm{Sin}\,\theta - V\,r\,\mathrm{Cos}\,\theta$$

Therefore the slip velocity on the contour C2 is given by;

$$\frac{\partial \phi}{\partial n} = -U\,\mathrm{Sin}\,\theta + V\,\cos\theta$$

Appendix 3D

Momentum integral equation with $\left(\frac{\partial U}{\partial y}\right)_{\delta} = \frac{UR}{\delta}$

The momentum integral equation is written in the form;

D-1 $$U^2 \frac{d\theta}{dX} + \left(2\theta + \delta^*\right) U \frac{dU}{dX} = \frac{\tau_0}{\rho} - \nu \left(\frac{\partial u}{\partial y}\right)_{\delta}$$

For a non-zero pressure gradient, the velocity profile may be expressed as a fourth degree polynomial equation;

$$\frac{u}{U} = A_0 + A_1 \eta + A_2 \eta^2 + A_3 \eta^3 + A_4 \eta^4$$

Where ; $\eta = \frac{y}{\delta}$

By using the boundary conditions;

D-2

At $y = \delta$ $(U)_{\delta} = U$

$\eta = 1$, $\left(\frac{\partial u}{\partial y}\right)_{\delta} = \frac{U}{\delta} R$

D-3

$$\left(\frac{\partial^2 u}{\partial y^2}\right)_{\delta} = 0$$

At $y = 0$ $u = 0$, $\eta = 1$

$$\left(\frac{\partial^2 u}{\partial y^2}\right)_0 = -\frac{U}{\nu}\cdot\left(\frac{dU}{dX}\right)$$

using the boundary conditions given by the equations D-2 and D-3 with the fourth degree polynomial;

$$A_0 = 0, \qquad A_1 = 2 + \frac{\Lambda}{6} - R$$

$$A_2 = -\frac{\Lambda}{2}, \qquad A_3 = -2 + 2R + \frac{\Lambda}{2}$$

$$A_4 = 1 - \frac{\Lambda}{6} - R$$

Where; $$\Lambda = \frac{\delta^2}{\nu}\frac{dU}{dX}$$

Hence the velocity profile can be expressed;

$$\frac{u}{U} = \left(2 + \frac{\Lambda}{6} - R\right)\eta - \frac{\Lambda}{2}\eta^2 - \left(2 - 2R - \frac{\Lambda}{2}\right)\eta^3 + \left(1 - \frac{\Lambda}{6} - R\right)\eta^4$$

OR , $$\frac{u}{U} = F(\eta) + \Lambda G(\eta) + RH(\eta)$$

D-4

Where; $$F(\eta) = 2\eta - 2\eta^3 + \eta^4$$

$$G(\eta) = \frac{1}{6}\left(\eta - 3\eta^2 + 3\eta^3 - \eta^4\right)$$

$$H(\eta) = -\eta(1-\eta)\left(1 + \eta - \eta^2\right)$$

The displacement thickness;

$$\left(\frac{\delta^*}{\delta}\right) = \int_0^1 \left(1 - \frac{u}{U}\right) d\eta$$

$$= \int_0^1 [\,1 - F(\eta) - \Lambda G(\eta) - R H(\eta)\,] d\eta$$

$$\left(\frac{\delta^*}{\delta}\right) = \int_0^1 \left(1 - \frac{u}{U}\right) d\eta$$

$$= \int_0^1 [\,1 - F(\eta) - \Lambda G(\eta) - R H(\eta)\,] d\eta$$

D-5 $$\frac{\delta^*}{\delta} = \left(\frac{3}{10} - \frac{\Lambda}{120}\right) - \frac{R}{5}$$

and the momentum thickness; $$\left(\frac{\theta}{\delta}\right) = \int_0^1 \frac{u}{U}\left(1 - \frac{u}{U}\right) d\eta$$

D-6

$$\int_0^1 [F(\eta) + \Lambda G(\eta) + R H(\eta)][\,1 - F(\eta) - \Lambda G(\eta) - R H(\eta)\,] d\eta$$

$$= Q - R \int_0^1 H(\eta)[F(\eta) + \Lambda G(\eta) - 1 + F(\eta) + \Lambda G(\eta) + R H(\eta)] d\eta$$

Where; $$Q = \left(\frac{37}{315} - \frac{\Lambda}{945} - \frac{\Lambda^2}{9072}\right)$$

from equations D-4 and D-6;

$$\frac{\theta}{\delta} = Q + J$$

Where; $$J = \frac{R}{7560}(29\Lambda - 372R + 744)$$

Therefore;

$$\frac{\delta^*}{\theta} = \frac{\delta^*/\delta}{\theta/\delta} = \frac{\left(\frac{3}{10} - \frac{\Lambda}{120} - \frac{R}{5}\right)}{Q + J} \equiv f_1$$

$$\frac{\tau_0\theta}{\mu U} = \frac{\tau_0\delta}{\mu U}\cdot\frac{\theta}{\delta} = \left(2 + \frac{\Lambda}{6} - R\right)(Q + J) \equiv f_2$$

by defining,

D-7
$$K = \frac{\theta^2}{\nu}\cdot\frac{dU}{dX}$$

D-8
$$Z = \frac{\theta^2}{\nu}$$

D-9
$$K = Z\cdot\frac{dU}{dX}$$

Therefore;
$$K = \left(\frac{\theta}{\delta}\right)^2\Lambda = \Lambda(Q + J)^2$$

The momentum integral equation becomes;

$$\frac{U}{2}\cdot\frac{dZ}{dX} + \left(2 + f_1\right)K = f_2 - R(Q + J)$$

if $R = 0$ from equations D-6, D-7, D-8, D-9

$$K = 4Q\left[1 - \Lambda\left(Q - \frac{16 - \Lambda}{240}\right)\right]$$

If S is the distance measured along the surface in the down stream direction of the boundary layer flow, the momentum integral equation becomes;

D-10
$$\frac{d}{ds}\left(\frac{\Lambda Q^2}{dv/ds}\right) = \frac{4Q}{V}\left[1 - \Lambda\left(Q - \frac{16 - \Lambda}{240}\right)\right]$$

Appendix 3E

Initial Values of Z and dZ/dX at the Stagnation Point

For the numerical integration procedure given in the section 3.7.5 for the Region 1 and Region 2 the initial conditions of Z and dZ/dX are determined. With the approximation $R = R(x) = 0$ the initial values are calculated in this section (The initial conditions for $R = R(x) \neq 0$ are determined in the Appendix 3F).

From the equation 3.7-38;

$$\frac{dZ}{dX} = \frac{F(K)}{U}$$

and, $K = Q^2 \Lambda$

$$K = Z \frac{dU}{dX}$$

definitions are used to calculate the initial values of,

$$Z\left(\equiv Z_0\right) \quad and \quad \frac{dZ}{dX}\left(\equiv \frac{dX}{dX_0}\right)$$

using the non-dimensionalisation;

$$X \equiv \left(\frac{x}{l}\right) \qquad V \equiv \left(\frac{U}{w}\right)$$

Therefore, $K = Z \cdot \frac{w}{l} \cdot \frac{dV}{dX}$

E-1
$$Z^* \equiv \frac{Z W}{l} \equiv \frac{\theta^2 W}{\nu l} \equiv Re\left(\frac{\theta}{l}\right)^2$$

OR
$$Z^* \equiv Re\left(\frac{\theta}{\delta}\right)^2 \cdot \left(\frac{\delta}{l}\right)^2$$

$$= Re \cdot Q^2 \cdot \frac{\nu \Lambda}{(dU/dX)} \cdot \frac{1}{l^2}$$

$$= Re \cdot Q^2 \cdot \frac{\nu l}{W} \cdot \frac{\Lambda}{(dV/dX)} \cdot \frac{1}{l^2}$$

$$Z^* = \frac{Q^2 \Lambda}{(dV/dX)} = \frac{K}{(dV/dX)}$$

E-2
$$\frac{dZ^*}{dX} = \frac{F(K)}{V}$$

E-3
$$Z^* = \frac{K}{(dV/dX)}$$

and
$$K = Q^2 \cdot \Lambda$$

Where,
$$Q = \frac{37}{315} - \frac{\Lambda}{945} - \frac{\Lambda^2}{9072}$$

$$F(K) = 2f_2 - 2K(2 + f_1)$$

Therefore,

E-4
$$F(K) = 2Q\left[2 - \frac{2\Lambda}{15} - \Lambda\left(2Q - \frac{\Lambda}{120}\right)\right]$$

From E-2 and E-4,

$$\frac{dZ^*}{dX} = \frac{2Q\left[2 - \frac{2}{15}\Lambda - \Lambda\left(2Q - \frac{\Lambda}{120}\right)\right]}{V}$$

$$= \frac{4Q}{V}\left[1 - \Lambda\left(Q - \frac{\Lambda - 16}{240}\right)\right]$$

Initial conditions for the stagnation point S;

$$Z_0^* = \frac{K_0}{(dV/dX)_0} = \frac{0.0770}{(dV/dX)_0}$$

If $X \to 0, \qquad V \to 0$

$$\frac{F(K)}{V} \to \left(\frac{0}{0}\right)$$

Therefore by taking the limiting values,

$$\lim_{X \to 0} \frac{F(K)}{V} = \frac{\frac{d}{dX}[F(X)]}{dV/dX} = \frac{dK/dX}{dV/dX} \cdot \left[\frac{dF(K)}{dK}\right]$$

$$Z^* = \frac{K}{dV/dX}$$

$$\frac{dZ^*}{dX} = \frac{\frac{dV}{dX} \cdot \frac{dK}{dX} - K \cdot \frac{d^2V}{dX^2}}{(dV/dX)^2}$$

$$\frac{dF(K)}{dK} = \frac{\frac{d}{d\Lambda}\left[2Q\left[2 - \frac{2\Lambda}{15} - \Lambda\left(2Q - \frac{\Lambda}{120}\right)\right]\right]}{\frac{d}{d\Lambda}(Q^2\Lambda)}$$

$$= \frac{2Q\left[-\frac{2}{15} - 2\Lambda\frac{dQ}{d\Lambda} - 2Q + \frac{\Lambda}{60}\right] - 2\frac{dQ}{d\Lambda}\left[2 - \frac{2\Lambda}{15} - \Lambda\left(2Q - \frac{\Lambda}{120}\right)\right]}{\left(Q^2 + 2\Lambda Q\frac{dQ}{d\Lambda}\right)}$$

Hence, for $K \to K_0, \qquad X \to 0$

$$Q_0 = \frac{37}{315} - \frac{\Lambda_0}{945} - \frac{\Lambda_0^2}{9072} = 0.1045$$

$$\Lambda_0 = 7.052$$

$$\left(\frac{dQ}{d\Lambda}\right)_0 = -\frac{1}{945} - \Lambda_0 4536 = 2.612 \times 10^{-3}$$

$$\left[\frac{dF(K)}{dK}\right]_{\lim \to 0} = -5.556$$

Therefore; $$\left(\frac{dZ^*}{dX}\right)_0\left(1+\frac{1}{5.556}\right) = -K_0\frac{\left(d^2V/dX^2\right)}{(dV/dX)^2}$$

$$\left(\frac{dZ^*}{dX}\right)_0 = 0.0652\ \frac{\left(d^2V/dX^2\right)}{(dV/dX)_0^2}$$

Appendix 3F

Initial Conditions for Stagnation point for $R \neq 0$

From the boundary conditions specified by the equation B-2 in the Appendix 3B;

F-1 $$R = \frac{\delta}{U}\left(\frac{\partial U}{\partial y}\right)_{\delta}$$

employing $$\Lambda = \frac{\delta^2}{\nu} \cdot \frac{dU}{dx}$$

and $$\xi \equiv \frac{\Lambda}{dU/dx}$$

$$S = \left(\frac{\partial U}{\partial y}\right)_{\delta}$$

F-2 $$\delta = \sqrt{\frac{\nu \Lambda}{dU/dx}} = \sqrt{\nu} \cdot \sqrt{\xi}$$

$$R = \frac{\sqrt{\nu}}{U} \cdot \sqrt{\xi} \cdot S$$

Therefore;

$$\frac{dR}{dx} = \sqrt{\nu}\left(\frac{S}{U}\frac{1}{2\sqrt{\xi}}\frac{d\xi}{dx} + \frac{\sqrt{\xi}}{U}\frac{dS}{dx} - \frac{S\sqrt{\xi}}{U^2}\frac{dU}{dx}\right)$$

F-3 $$\frac{dR}{dx} = \frac{\sqrt{\nu\xi}}{U}\left[\frac{S}{2\xi}\left(\frac{d\Lambda/dx}{dU/dx} - \frac{\xi}{dU/dx} \cdot \frac{d^2U}{dx^2}\right)\right.$$

$$\left. + \frac{dS}{dx} - \left(\frac{s}{U}\right)\frac{dU}{dx}\right]$$

from the equation 3.7-39, $$Z = \frac{K}{(dU/dx)}$$

F-4 $$\frac{dZ}{dx} = \frac{(dU/dx)(dK/dx) - K \cdot \left(d^2U/dx^2\right)}{(dU/dx)^2}$$

But,

F-5 $$\frac{dK}{dx} = \frac{d\Lambda}{dx}(Q+J)^2 + 2\Lambda(Q+J)\left(\frac{dQ}{dx} + \frac{dJ}{dx}\right)$$

from the equation B-6, F-3 and F-4 ;

F-6 $$\frac{U}{2}\left[\frac{(dK/dx)}{(dU/dx)} - K\ \frac{d^2U/dx^2}{(dU/dx)^2}\right] = -\left(2+f_1\right)\Lambda(Q+J)^2$$

$$+\ (Q+J)\left(2-2R+\frac{\Lambda}{6}\right)$$

When, $(Q+J) \neq 0$

The differential equation F-6 for Λ may be expressed as;

F-7 $$L\frac{d\Lambda}{dx} = 2T'\frac{dU/dx}{U} + \Lambda(Q+J'R)\cdot\frac{d^2U/dx^2}{dU/dx}$$

$$-\ \frac{2\Lambda}{7560}\left(\frac{dR}{dx}\right)(29\Lambda - 744R + 744)$$

Where,

F-8 $$L \equiv (Q+JR) + 2\Lambda\left(\frac{dQ}{d\Lambda} + \frac{29R}{7560}\right)$$

$$Q \equiv \left(\frac{37}{315} - \frac{\Lambda}{945} - \frac{\Lambda^2}{9072}\right)$$

$$J' \equiv \frac{29\Lambda - 372R + 744}{7560}$$

F-9

$$T' \equiv T - 2R - 2\Lambda R\left(2J' - \frac{1}{5}\right)$$

$$T \equiv 2 - \frac{116\Lambda}{315} + \frac{79\Lambda^2}{7560} + \frac{\Lambda^3}{4536}$$

Hence;

$$L = \frac{37 - \Lambda}{315} - \frac{5\Lambda^2}{9072} + R\left(\frac{62 - 31R + 29\Lambda}{630}\right)$$

$$T' = \left(2 - \frac{116\Lambda}{315} + \frac{79\Lambda^2}{7560} + \frac{\Lambda^3}{4536}\right) - 2R\left[1 + \frac{\Lambda(29\Lambda - 372R - 12)}{3780}\right]$$

from equations F-3 and F-7,

$$\frac{d\Lambda}{dx}\left[L + \frac{2\Lambda}{7560}(29\Lambda - 744R + 744)\sqrt{\nu\xi}\cdot\frac{S}{2U\xi(dU/dx)}\right] = 2T'\frac{dU/dx}{U}$$

$$+\Lambda(Q + J'R)\frac{(d^2U/dx^2)}{(dU/dx)} - \frac{2\Lambda}{7560}(29\Lambda - 744R + 744)\left(\frac{\sqrt{\nu\xi}}{U}\right)$$

F-10

$$\left[-\frac{S(d^2U/dx^2)}{2(dU/dx)} + \frac{ds}{dx} - S\left(\frac{dU/dx}{U}\right)\right]$$

For $x \rightarrow 0$

$U \rightarrow 0$

$\frac{dU}{dx} \rightarrow (\neq 0)$

$\Lambda \rightarrow (\neq 0) \rightarrow (\Lambda_0)$

Left Hand Side of the differential equation F-10,

$$R \rightarrow R_0 = \sqrt{\nu}\sqrt{\frac{\Lambda_0}{(dU/dx)_0}} \cdot \lim_{x\to 0}\left(\frac{S}{U}\right)$$

Assuming that $S \rightarrow 0$ at $x \rightarrow 0$

The case where $S \rightarrow \neq 0$ $(\equiv S_0)$ is later considered. Where in that case $\left(\frac{d\Lambda}{dx}\right)_0 \rightarrow \infty$

$$\underset{x\to 0}{limit}\left(\frac{S}{U}\right) = \frac{(dS/dx)_0}{(dU/dx)_0} \equiv \beta$$

$$R_0 = \sqrt{\nu}\sqrt{\frac{\Lambda_0}{(dU/dx)_0}} \cdot \frac{(dS/dx)_0}{(dU/dx)_0}$$

Assuming that the S/U is a finite limit,

$$L \rightarrow \frac{37-\Lambda_0}{315} - \frac{5\Lambda_0^2}{9072} + R_0\left(\frac{62-31R+(29/4)\cdot\Lambda_0}{630}\right) \equiv L_0$$

$$T' \rightarrow T_0 - 2R_0\left(1+\frac{29\Lambda_0(\Lambda_0-372R_0-12)}{3780}\right) \equiv T'_0$$

When, $T_0 \rightarrow T$ for $\Lambda = \Lambda_0$

Therefore the differential equation F-10 reduces to,

$$\left(\frac{d\Lambda}{dx}\right)_0\left(L_0+\frac{\beta\sqrt{\nu\xi_0}}{7560}(29\Lambda_0-744R_0+744)\right) = \frac{2T_0(dU/dx)_0}{U}$$

$$\left(-\frac{2\Lambda_0}{7560}\sqrt{\nu\xi}\cdot\left(\frac{dS}{dx}\right)_0(29\Lambda_0-744R_0+744)\right.$$

$$+\left.\frac{\sqrt{\nu\xi_0}}{7560}\cdot 2\xi_0\left(\frac{dU}{dx}\right)_0^2 B(29\Lambda_0-744R_0+744)\right) / U$$

$$+\frac{(d^2U/dx^2)_0}{(dU/dx)_0}\Lambda_0\left((Q_0+J'_0R_0)+\frac{\sqrt{\nu\xi_0}}{7560}\beta(29\Lambda_0-744R_0+744)\right)$$

For a finite value of $(d\Lambda/dx)_0$ the numerator of the RHS of the equation F-12 should be equal to zero.

Hence;

$$T'_0\left(\frac{dU}{dx}\right)_0 - \frac{\sqrt{\nu\xi_0}}{7560}\Lambda_0(29\Lambda_0 - 744R + 744)\left(\frac{dS}{dx}\right)_0$$

$$\left[1 - \frac{(dU/dx)_0}{(dU/dx)_0}\cdot\frac{(dU/dx)_0}{(dU/dx)_0}\right] = 0$$

Thus, $$T'_0\left(\frac{dU}{dx}\right)_0 = 0$$

$$T'_0 = 0$$

For $X \rightarrow 0$ the differential equation has the form,

$$\left(\frac{d\Lambda}{dx}\right)_0(L_0 + \beta B_0) = \frac{2T'_0(dU/dx)_0}{U}$$

$$+\frac{(d^2U/dx^2)_0}{(dU/dx)_0}\cdot\Lambda_0[(Q_0 + J'_0R_0) + \beta B_0]$$

Where, $$B_0 = \frac{\sqrt{\nu\xi}}{7560}(29\Lambda_0 - 744R_0 + 744)$$

Using the L'Hospitals rule,

$$\left(\frac{d\Lambda}{dx}\right)_0(L_0 + \beta B_0) = 2\frac{d}{dx}(T') + \frac{(d^2U/dx^2)_0}{(dU/dx)_0}\cdot\Lambda_0(Q_0 + J'_0R_0 + \beta B_0)$$

But,

$$\frac{dT'}{dx} = \left(\frac{d\Lambda}{dx}\right)_0\left(-\frac{116}{315} + \frac{158\Lambda_0}{7560} + \frac{3\Lambda_0^2}{4536}\right) - 2\left(\frac{dR}{dx}\right)\left[1 + \frac{\Lambda_0(29\Lambda_0 - 372R_0 - 12)}{3780}\right]$$

$$- 2R\left[\left(\frac{d\Lambda}{dx}\right)_0\left(\frac{29\Lambda_0 - 362R_0 - 12}{3780}\right)\right]\frac{\Lambda_0}{3780}\left[29\left(\frac{d\Lambda}{dx}\right)_0 - 372\frac{dR}{dx}\right]$$

Thus the last two terms of the equation F-2 for,

$$\left(\frac{dR}{dx}\right) \quad have \quad a \quad \left(\frac{0}{0}\right) \quad form$$

If,

$$\alpha = \frac{(dS/dx) - (S/U)(dU/dx)_0}{U}$$

$$\alpha = \left[U\left(\frac{d^2S}{dx^2}\right) - \frac{S}{U} \cdot \frac{d^2U}{dx^2} \cdot \frac{dU}{dx}\left(\frac{dS}{dx} - \frac{S}{U}\frac{dU}{dx}\right)\right] / [U(dU/dx)]$$

$$\alpha = \left[\frac{d^2S}{dx^2} - \beta\left(\frac{d^2U}{dx^2}\right) - \frac{dU}{dx} \cdot (\alpha)\right] / [(dU/dx)]$$

$$\alpha = 0.5 \left[\frac{d^2S}{dx^2} - \beta\frac{d^2U}{dx^2}\right] / [(dU/dx)]$$

From equation F-15,

$$\frac{dT'}{dx} = \left(\frac{d\Lambda}{dx}\right)_0 \left[-\frac{116}{315} + \frac{158\Lambda_0}{7560} + \frac{3\Lambda_0^2}{4536} - 2R_0\left(\frac{58\Lambda_0 - 372R_0 - 12}{3780}\right)\right]$$

$$- \quad 2\frac{dR}{dx}\left[-\frac{372}{3780}\Lambda_0 R_0 + 1 + \frac{\Lambda_0(29\Lambda_0 - 372R_0 - 12)}{3780}\right]$$

also can be expressed in the form of;

$$\left(\frac{dT'}{dx}\right)_0 = \frac{d\Lambda}{dx_0}(D_0) - 2\frac{dR}{dx}\left[1 + \frac{\Lambda_0(29\Lambda_0 - 744R_0 - 12)}{3780}\right]$$

Where, $$D_0 = -\frac{116}{315} + \frac{158\Lambda_0}{7560} + \frac{3\Lambda_0}{4536} - 2R_0\frac{(58\Lambda_0 - 372R_0 - 12)}{3780}$$

But on substitution for α in the equation for (dR/dx)

$$\left(\frac{dR}{dx}\right)_0 = \sqrt{\nu\xi_0}\left[\frac{\beta}{2\xi_0}\left(\frac{(d\Lambda/dx)_0}{(dU/dx)_0} - \xi_0\frac{(d^2U/dx^2)_0}{(dU/dx)_0}\right) + \alpha\right]$$

Substituting for $\left(\frac{dR}{dx}\right)_0$

$$\left(\frac{dT'}{dx}\right)_0 = \left(\frac{d\Lambda}{dx}\right)_0 E_0 - 2\left[1 + \frac{\Lambda_0(29\Lambda_0 - 744R_0 - 12)}{3780}\right] \cdot$$

$$\left(\sqrt{\nu\xi_0}\right) \cdot \left[\alpha - \frac{\beta}{2}\frac{\left(\frac{d^2U}{dx^2}\right)_0}{\left(\frac{dU}{dx}\right)_0}\right]$$

Where;

$$E_0 = D_0 - \frac{\beta\sqrt{\nu\xi_0}}{\Lambda_0}\left[1 + \frac{\Lambda_0(29\Lambda_0 - 744R_0 - 12)}{3780}\right]$$

Hence substituting for $(dT'/dx)_0$ into equation for

$(d\Lambda/dx)_0$

$$\left(\frac{d\Lambda}{dx}\right)_0 (L_0 + \beta B_0 - 2E_0) = -4\sqrt{\nu\xi_0}\left[1 + \frac{\Lambda_0(29\Lambda_0 - 744R_0 - 12)}{3780}\right]$$

$$\left[\alpha - \frac{\beta}{2}\frac{\left(\frac{d^2U}{dx^2}\right)_0}{\left(\frac{dU}{dx}\right)_0}\right] + \frac{(d^2U/dx^2)_0}{(dU/dx)_0} \cdot \Lambda_0(Q_0 + J'_0 R_0 + \beta B_0)$$

Appendix 3G

Initial Conditions for the Leading Edge

Integration of the boundary layer for the Region-3 has been stared with the initial conditions;

$$x \to 0 \qquad \delta \to 0$$

$$and \qquad U \to \neq 0$$

Therefore $$\Lambda \to 0 \quad \left(\equiv \frac{\delta^2}{\nu} \cdot \frac{dU}{dx} \right)$$

and $$\lim_{x \to 0} \quad \frac{dU}{dx} \to \neq 0$$

$$\lim_{x \to 0} \quad S \to \neq 0$$

$$\lim_{x \to 0} \quad \frac{dS}{dx} \to \neq 0$$

from F-2

$$R \to \left(\equiv \frac{\sqrt{\nu}}{U} \cdot \sqrt{\frac{\Lambda}{(dU/dx)}} S \right) \quad \to 0$$

from F-8;

$$L = (Q + JR) + 2\Lambda \left(\frac{dQ}{d\Lambda} + \frac{29R}{7560} \right)$$

Where; $$Q = \left(\frac{37}{315} - \frac{\Lambda}{945} - \frac{\Lambda^2}{9072} \right)$$

Therefore; $$\lim_{x \to 0} \qquad L \to \frac{37}{315}$$

From F-9

$$T' = T - 2R - 2\Lambda R\left(2J' - \frac{1}{5}\right)$$

Where,

$$T = 2 - \frac{116\Lambda}{315} + \frac{79\Lambda^2}{7560} + \frac{\Lambda^3}{4536}$$

Hence; $T' \lim_{x \to 0} \to 2$

Therefore;

$$\left(\frac{d\Lambda}{dx}\right)_{x\to 0}\left[\frac{37}{315}\right] = \frac{(dU/dx)}{U} \times 4$$

$$\left(\frac{d\Lambda}{dx}\right)_{x\to 0} = \frac{315 \times 4}{37} \cdot \frac{(dU/dx)}{U}$$

$$\left(\frac{d\Lambda}{dx}\right)_{x\to 0} = \frac{1260}{37} \cdot \frac{(dU/dx)}{U}$$

It may be noted that

$$\frac{d\Lambda}{dx} \quad and \quad \frac{dU}{dx}$$

should always take the same sign.

Appendix 3H

Momentum Integral Equation for the Turbulent Boundary Layer

In the presence of a laminar sub-layer. Momentum Integral Equation can be expressed in the form;

H-1
$$\frac{1}{l}\frac{d}{dX}W^2(l)\int_0^{\delta}(V-v)v\,dY - \frac{lw^2}{l}\cdot\frac{dV}{dX}\int_0^{\delta}v\,dY$$

$$=\frac{\tau_{\omega}}{\rho}+\frac{l\delta_{n-d}}{\rho}$$

Also from the Bernoulli's equation, for the flow outside the boundary layer;

H-2
$$\frac{dP}{dX}+\rho\cdot U\cdot\frac{dU}{dX}=0$$

For $\rho = Constant$

The equation H-1 becomes;

H-3
$$\frac{1}{l}\frac{d}{dX}W^2(l)\int_0^{\delta}(V-v)v\,dy - \frac{lW^2}{l}\cdot\frac{dV}{dX}\int_0^{\delta}v\,dY$$

$$=\frac{\tau_W}{\rho}+\frac{l}{\rho}\cdot\delta_{n-d}\left(-\rho V\frac{dV}{dX}\right)\frac{W^2}{l}$$

The shear-stress at the wall can be expressed by the Blasius semi-emperical equation;

H-4
$$\tau_{\omega_{n-d}}=0.0456\times V^2\left[\frac{\nu}{VW\cdot\delta_n\cdot l}\right]^{1/4}$$

Which also can be expressed in the form of;

H-5
$$\tau_{\omega_{n-d}} = 0.0456 \cdot \frac{V^2}{(V \cdot \delta_{n-d})^{1/4}} \cdot \left(\frac{1}{Re}\right)^{1/4}$$

By using the substitution

H-6 $$\delta_{n-d} = \beta^{0.8}$$

Equation H-5 becomes;

H-7
$$\tau_{\omega_{n-d}} = \frac{0.0456}{(Re)^{1/4}} \cdot \frac{V^{7/4}}{\beta^{0.2}}$$

and thus the equation H-3 can be expressed in the form;

H-8
$$\frac{d}{dX}\int_0^{\delta}(V-v)v\,dY - \frac{dV}{dX}\int_0^{\delta} v\,dY$$

$$= \left[\frac{0.0228}{(Re)^{1/4}}\right] \cdot \left(\frac{V^7}{\delta_{n-d}}\right)^{1/4} - \delta_{n-d}\frac{V^{dV}}{dX}$$

OR

$$L \cdot H \cdot S \cdot = \frac{d}{dx}(I_1) - I_2 \cdot \left(\frac{dV}{dX}\right)$$

$$R \cdot H \cdot S \cdot = \left[\frac{0.0228}{(Re)^{1/4}}\right] \cdot \left(\frac{V^7}{\Delta}\right)^{1/4} - \Delta V\frac{dV}{dX}$$

The velocity profile inside the turbulent boundary layer can be expressed by the Prandtl's 1/7 th Power equation, Where;

H-9
$$\frac{u}{U} = \left(\frac{y}{\delta}\right)^{1/7}$$

Therefore;
$$I_1 = \int_0^{\delta}(V-v)v\,dY$$

$$= \int_0^{\delta} V^2 \left[1 - \left(\frac{Y}{\delta_{n-d}} \right)^{1/7} \right] \left[\frac{Y}{\delta_{n-d}} \right]^{1/7} \cdot dY$$

$$= V^2 \int_0^{\delta_{n-d}} \left[\left(\frac{Y}{\delta_{n-d}} \right)^{1/7} - \left(\frac{y}{\delta_{n-d}} \right)^{2/7} \right] dY$$

$$I_1 \equiv V^2 \Delta \cdot \frac{7}{72}$$

$$I_2 = \int_0^{\delta} v \, dY$$

$$= V \int_0^{\delta} \left(\frac{Y}{\delta_{n-d}} \right)^{1/7} \cdot dY$$

$$= \frac{V}{\left(\delta_{n-d} \right)^{1/7}} \cdot \frac{y^{8/7}}{(8/7)}$$

$$I_2 = V \cdot \delta_{n-d} \cdot \frac{7}{8}$$

Therefore the equation H-8 becomes;

$$\frac{d\delta_{n-d}}{dX} \left(\frac{7}{72} V^2 \right) + \delta_{n-d} \left(\frac{7}{36} V \frac{dV}{dX} - \frac{7}{8} V \frac{dV}{dX} + V \frac{dV}{dX} \right)$$

$$- \frac{0.0228}{(Re)^{0.25}} \cdot \left(\frac{V^7}{\delta_{n-d}} \right)^{1/4}$$

OR

$$\frac{d\delta_{n-d}}{dX} \left[\frac{7}{72} \left(V^2 \right) \right] + \frac{23}{72} \left(V \cdot \frac{dV}{dX} \right) \delta_{n-d} - \frac{0.0228}{Re^{1/4}} \cdot \left(\frac{V^7}{\delta_{n-d}} \right)^{1/4} = 0$$

OR

H-10 $$\Delta^{1/4} \frac{d\delta_{n-d}}{dX} \cdot \frac{7}{72} V^2 + \frac{23}{72} V \frac{dV}{dX} \delta_{n-d}^{5/4}$$

$$- \frac{0.0228}{(Re)^{1/4}} \cdot V^{7/4} = 0$$

Here ; $\lim_{X \to 0} \frac{d\delta_{n-d}}{dX} \to \infty$

$\lim_{\delta_{n-d} \to 0}$ *and*

$$\delta_{n-d}^{0.25} \cdot \frac{d\delta_{n-d}}{dX} \to \quad Finite \quad limit$$

$$If \quad \beta = \delta_{n-d}^{5/4}$$

H-11 $$\frac{d\beta}{dX} = \frac{5}{4} \cdot \delta_{n-d}^{0.25} \cdot \frac{d\delta_{n-d}}{dx}$$

and thus the equation H-9 becomes;

H-12 $$\frac{d\beta}{dX} \cdot \frac{28}{360} V^2 + \frac{23}{72}\left(V \frac{dV}{dX}\right)\beta$$

$$- \frac{0.0228}{Re^{1/4}} \cdot V^{7/4}$$

In the equation H-11;

For $X \to 0$ $\beta \to 0$ *but*

$$at \quad \lim_{X \to 0} \frac{d\beta}{dX} \to \quad finite \quad value$$

Therefore from the equation H-11;

$$\frac{d\beta}{dX} = \left(-\frac{115}{28} \cdot \frac{dV}{dX}\beta + \frac{90}{7} \cdot \frac{0.0228V^{3/4}}{Re^{1/4}} \right) / V$$

Where $\beta = 0$ $X = 0$ $V \neq 0$

Appendix 3I

Parabolic Velocity Profile for the Laminar Sub Layer

In the Laminar sub layer velocity profile is prescribed by;

I-1 $$\frac{u}{U_l} = A_0 + A_1\eta + A_2\eta^2$$

Where;

$$\eta = \frac{y}{\delta_l} = \left(\frac{y}{\delta}\right)\cdot\left(\frac{\delta}{\delta_l}\right)$$

and the turbulent layer is prescribed by;

I-2 $$\frac{u}{U} = \left(\frac{y}{\delta}\right)^{1/7}$$

Therefore; $$\frac{U_l}{U} = \left(\frac{\delta_l}{\delta}\right)^{1/7}$$

$$\delta_{n-d} = \left(\frac{\delta}{l}\right)$$

$$\underset{n-d}{\delta_l} = \left(\frac{\delta_l}{\delta}\right)$$

Applying the boundary conditions for the equation I-1;

I-3 $$\left(\frac{d^2y}{dy^2}\right)_{y=0} = \frac{U}{\rho\nu}\cdot\frac{dp}{dx} = -\frac{U}{\nu}\cdot\frac{dU}{dx}$$

I-4 Where; $y = \delta_l, \quad u = U_l$

I-5 $u = 0, \quad \eta = 0$

therefore, A_0

and $$\frac{u}{U_l} = A_1\eta + A_2\eta^2$$

I-6 $$\frac{du}{dy} = \frac{U_l}{\delta_l}\left(A_1 + 2A_2\eta\right)$$

$$\frac{d^2u}{dy^2} = \left(\frac{U_l}{\delta_l^2}\right)(2A_2)$$

Therefore For the Laminar sub-layer shear stress at the wall

I-7 $$\tau_\omega = \mu\left(\frac{U_l}{dy}\right)_{y=0}$$

I-8 $$\tau_\omega = \mu\left(\frac{U_l}{\delta_l}\cdot A_1\right)$$

From the conditions given in the equation I-3;

$$\left(\frac{U_l}{\delta_l^2}\right)\cdot 2A_2 = -\frac{U}{\nu}\cdot\frac{dU}{dx}$$

I-9 Therefore, $$A_2 = -\frac{1}{\nu}\cdot\delta_l^2\cdot\frac{U}{U_l}\cdot\frac{dU}{dx}$$

From the conditions described by the I-4;

$$u = U_l \quad for \quad A_1 + A_2 = 1$$

and $$A_1 = \left[1 + \frac{U}{U_l}\cdot\frac{\delta_l^2(dU/dx)}{\nu}\right]$$

From equation I-6;

I-10 $$\left(\frac{du}{dy}\right)_{\eta=0} = \left(\frac{U_l}{\delta_l}\right)\left(1 + \frac{U}{U_l}\cdot\frac{\delta_l^2}{2\nu}\cdot\frac{dU}{dx}\right)$$

$$U_l = U \cdot \left(\frac{\delta_l}{\delta} \right)^{1/7}$$

Therefore,

$$\frac{U_l}{\delta_l} = U \left(\frac{\delta_l}{\delta} \right)^{1/7} \cdot \left(\frac{1}{\delta_l} \right)$$

$$\frac{U}{U_l} = \left(\frac{\delta}{\delta_l} \right)^{1/7}$$

From Blasius's equation for the case where,

$$(dP/dX) = 0 \quad \vee \quad (dU/dX) = 0$$

$$\mu \left(\frac{du}{dy} \right)_{y=0} = 0.0228 \frac{\rho U^2}{(\rho U \delta / \mu)^{1/4}}$$

$$= \quad \mu \left(\frac{U_l}{\delta_l} \right) = \mu U \cdot \left(\frac{\delta_l}{\delta} \right)^{1/7} \cdot \frac{1}{\delta_l}$$

Assume that the same relationship between the δ $\wedge$ *the* δ_l prevails for the (dp/dx) values closer to zero and hence;

$$(\delta_l)^{6/7} = \delta^{6/7} \cdot \frac{1}{0.0228} \cdot \left(\frac{\nu}{U \delta} \right)^{3/4}$$

OR $$\left(\frac{\delta_l}{\delta} \right) = \left(\frac{1}{0.0228} \right)^{7/6} \cdot \left(\frac{\nu}{U \delta} \right)^{7/8}$$

and therefore,

$$\tau_{\substack{\omega \\ n-d}} = \frac{2\tau_\omega}{\rho W^2} = \frac{\mu (du/dy)_{y=0}}{\rho (W^2/2)}$$

From the equation I-10;

$$\tau_{\substack{\omega \\ n-d}} = \frac{2\nu}{W^2} \cdot \frac{U_l}{\delta_l}\left(1 + \frac{U}{U_l} \cdot \frac{\delta_l^2}{2\nu} \cdot \frac{dU}{dx}\right)$$

$$= \left(\frac{2\nu}{W l}\right) \cdot \frac{V_l}{\delta_{\substack{l \\ n-d}}} + \left(V \delta_{\substack{l \\ n-d}} \cdot \frac{dV}{dX}\right)$$

But

I-12 $$\tau_{\substack{\omega \\ n-d}} = \frac{2}{Re} \cdot \frac{V_l}{\delta_{\substack{l \\ n-d}}} + V \frac{dV}{dX} \cdot \delta_{\substack{l \\ n-d}}$$

and from the equation I-11;

I-13 $$\frac{\delta_{\substack{l \\ n-d}}}{\delta_{n-d}} = \left(\frac{1}{0.0228}\right)^{7/6} \cdot \left(\frac{\nu}{V \delta_{n-d} W l}\right)^{7/8}$$

Therefore;

$$\delta_{\substack{l \\ n-d}} = \frac{1}{(0.0228)^{7/6}} \cdot \frac{1}{(Re)^{7/8}} \cdot \left(\frac{\delta_{n-d}^{1/8}}{V^{7/8}}\right)$$

$$\frac{V_l}{\delta_{\substack{l \\ n-d}}} = \left[\frac{1}{(0.0228)^{1/6}} \cdot \frac{1}{(Re)^{1/8}} \cdot \frac{1}{\left(V \delta_{n-d}\right)^{1/8}}\right]^7 \cdot V$$

$$/\left(\frac{1}{(0.0228)^{7/6}} \cdot \frac{1}{(Re)^{7/8}} \cdot \left(\frac{\delta_{n-d}}{V^7}\right)^{1/8}\right)$$

Therefore;

$$\frac{V_l}{\delta_l} = \left(\frac{V^7}{\delta_{n-d}}\right)^{1/4} \cdot (0.0228)(Re)^{3/4}$$

By substituting the value of I-14, I-13 and I-12 in I-8 the momentum integral equation becomes;

$$\frac{d\delta_{n-d}}{dx}\left(\frac{7}{72}\cdot V^2\right)+\delta_{n-d}\left(\frac{7}{36}\cdot V\frac{dV}{dx}\right.$$

$$\left.-\frac{7}{8}\cdot V\frac{dV}{dX}+V\frac{dV}{dX}\right)=\frac{1}{2}\cdot\tau_{\substack{\omega\\ n-d}}$$

Where;

$$\frac{1}{2}\cdot\tau_{\substack{\omega\\ n-d}}=\frac{0.0228}{(Re)^{1/4}}\left(\frac{V^7}{\delta_{n-d}}\right)^{1/4}+$$

$$+\frac{1}{2}\frac{dV}{dX}\cdot\frac{\delta_{n-d}^{1/8}\cdot V^{1/8}}{(0.0228)^{7/6}\cdot(Re)^{7/8}}$$

Appendix 3J

Turbulent Boundary Layer Thickness and the dV/dX

By finding a numerical solution to the equation H-13 the turbulent boundary layer growth is evaluated;

$$\frac{d\beta}{dx} = \left(\frac{-115}{28}\cdot\frac{1}{V}\cdot\frac{dV}{dX}\right)\cdot\beta + \left(\frac{90\times 0.0228}{7\times Re^{0.25}}\right)V^{-0.25}$$

Therefore, $$\frac{d\beta}{dx} = -\beta\cdot F(X) + G(X)$$

Where $$F(X) = \frac{115}{28}\cdot\frac{1}{V}\cdot\frac{dV}{dX}$$

$$G(X) = \alpha\cdot V^{-0.25}$$

$$\alpha = \frac{90\times 0.0228}{7\times Re^{0.25}}$$

Hence; $$\frac{d\beta}{dX} + \beta F(X) = G(X)$$

Therefore;

$$\beta \exp\int F(X)dX = \int G(x)\exp\int F(X)dX + Const$$

also,

$$\int F(X)dX = \frac{115}{28}\int\frac{1}{V}\frac{dV}{dX}\cdot dX$$

$$= \frac{115}{28}\cdot\ln V = \frac{115}{28}\ln\left(\frac{V}{V_0}\right)$$

For $X = X_0 \quad , V = V_0 , \wedge \quad let \quad V_0 \neq 0$

Then,

$$\exp \int_0^X F(X) dX = \left(\frac{V}{V_0} \right)^{115/28} .$$

Also let $\frac{dV}{dX} = S \equiv K_m$

and hence, $$\int G(X) \left(\frac{V}{V_0} \right)^{115/28} \cdot dX$$

$$= \frac{\alpha}{S V_0^{115/28}} \int \frac{V^{115/28} \cdot dV}{V^{1/4}}$$

$$= \frac{\alpha}{S V_0^{115/28}} \cdot \frac{7}{34} \cdot V^{34/7}$$

Therefore,

$$\beta \cdot \left(\frac{V}{V_0} \right)^{115/28} = \frac{7\alpha}{34 S V_0^{115/28}} \cdot V^{34/7} + Const$$

If, $\beta = 0 \qquad at \qquad X = 0$

Then $$Const = - \frac{7\alpha}{34 S V_0^{115/28}} \cdot V_0^{34/7}$$

Therefore ;

$$\beta \left(\frac{V}{V_0} \right)^{115/28} = \frac{7\alpha}{34 S V_0^{115/28}} \left(V^{34/7} - V_0^{34/7} \right)$$

and also $$\beta = \frac{7\alpha}{34 S} \cdot V^{-115/28} \left(V^{34/7} - V^{34/7} - V_0^{34/7} \right)$$

For $S > 0 \qquad V > V_0$

For $S = 0$

Therefore using the L'Hospital's rule ;

$$\beta = \frac{7\alpha V_0^{34/7}}{34 S V_0^{115/28}} \cdot \left(\frac{V}{V_0}\right)^{-115/28}\left[\left(\frac{V}{V_0}\right)^{34/7} - 1\right]$$

$$\beta = \frac{7\alpha V_0^{21/28}}{34 S} \cdot \frac{(V/V_0)^{34/7} - 1}{(V/V_0)^{115/28}}$$

Therfore

$$\beta = \frac{7\alpha}{34 S} V_0^{21/28}\left(\frac{y^{34/7} - 1}{y^{115/28}}\right)$$

$$\beta = 4 \times 10^{-3} \cdot V_0^{21/28}[\Phi]$$

Where, $$y = \left(\frac{V}{V_0}\right)$$

$$\Phi = \frac{y^{34/7} - 1}{y^{115/28}}$$

Therefore, $\Phi = y^{21/28} - y^{-115/28}$

$$\frac{d\Phi}{dy} = \frac{21}{28} \cdot y \cdot + \frac{115}{28} y$$

$$= \frac{1}{28}\left(21 y^{-1/4} + 115 y^{-143/28}\right)$$

$$\wedge \frac{d\Phi}{dy} > 0 \quad for \quad \forall \quad y > 0$$

Typical set of values for Φ as a function of **y** is given the Table T-J1.

Table T-J1

Y	$\phi(Y)$	Y	$-\phi(Y)$
1.0	0	0.95	0.27
1.2	0.67	0.90	0.61
1.4	1.04	0.80	1.65
1.6	1.27	0.70	3.56
1.8	1.47	0.60	7.47
2.0	1.62	0.50	16.6
4.0	2.8	0.40	42.59
8.0	4.76	0.20	742.3
10.0	8.0	0.10	12798

Appendix 3K

A solution for the Flow Around a Circular Cylinder Using the Nag DO3EAF Routine

Table T-K1

X	Y	Slip Vel.
-0.1000E+02	0.1000E+01	0.1096E+02
-0.1000E+02	0.2000E+01	0.1195E+02
-0.1000E+02	0.3000E+01	0.1295E+02
-0.1000E+02	0.4000E+01	0.1397E+02
-0.1000E+02	0.5000E+01	0.1500E+02
-0.1000E+02	0.6000E+01	0.1604E+02
-0.1000E+01	0.1000E+01	0.1053E+02
-0.1000E+01	0.2000E+01	0.1163E+02
-0.1000E+01	0.3000E+01	0.1275E+02
-0.1000E+01	0.4000E+01	0.1382E+02
-0.1000E+01	0.5000E+01	0.1488E+02
0.0000E+00	0.1000E+01	0.1001E+02
0.0000E+00	0.1100E+01	0.1020E+02
0.0000E+00	0.1200E+01	0.1038E+02
0.0000E+00	0.1300E+01	0.1055E+02
0.0000E+00	0.1400E+01	0.1071E+02
0.0000E+00	0.1500E+01	0.1086E+02
0.0000E+00	0.1600E+01	0.1100E+02
0.0000E+00	0.1700E+01	0.1114E+02
0.0000E+00	0.1800E+01	0.1127E+02
0.0000E+00	0.1900E+01	0.1140E+02
0.0000E+00	0.2000E+01	0.1153E+02
0.0000E+00	0.2200E+01	0.1178E+02
0.0000E+00	0.2400E+01	0.1202E+02
0.0000E+00	0.2600E+01	0.1226E+02
0.0000E+00	0.2800E+01	0.1249E+02

0.0000E+00	0.3000E+01	0.1271E+02
0.0000E+00	0.3500E+01	0.1327E+02
0.0000E+00	0.4000E+01	0.1381E+02
0.1000E+01	0.0000E+00	0.1000E+02
0.1000E+01	0.1000E+01	0.1053E+02
0.1000E+01	0.2000E+01	0.1163E+02
0.1000E+01	0.3000E+01	0.1275E+02
0.1000E+01	0.4000E+01	0.1382E+02
0.1000E+01	0.5000E+01	0.1488E+02
0.7071E+00	-0.7071E+00	0.1004E+02
-0.7071E+00	-0.7071E+00	0.9958E+02
-0.7071E+00	0.7071E+00	0.9958E+02

Appendix 3L

Set of Typical Values of Slip Velocities Around the Contour C2

Table T-L1

Side	Slip Velocity	Side	Slip Velocity
AB	0.000000E+00	DE	-0.251919E+02
	0.000000E+00		-0.185590E+02
	0.000000E+00		-0.119261E+02
	0.000000E+00		-0.173760E+02
	0.000000E+00		-0.192101E+02
	0.000000E+00		-0.199946E+02
BC	-0.115644E+03		-0.158086E+02
	-0.753181E+02		-0.166300E+02
	-0.340921E+02		-0.169059E+02
	-0.159202E+02		-0.171181E+02
	-0.829200E+01	EF	-0.865634E+02
	-0.530377E+01		-0.865572E+02
	-0.338044E+02		-0.865511E+02
	-0.517450E+02		-0.856502E+02
	-0.574094E+02		-0.865007E+02
	-0.630737E+02		-0.845152E+02
CD	-0.238803E+02		-0.819519E+02
	-0.202634E+02		-0.816981E+02
	-0.166466E+02		-0.820292E+02
	-0.146739E+02		-0.923602E+02
	-0.156750E+02		
	-0.128799E+02		
	-0.104761E+02		
	-0.104110E+02		
	-0.116186E+02		
	-0.128263E+02		

See Fig 3.25

FH	-0.583437E+02	IJ	0.285344E+01
	-0.477506E+02		-0.271284E+01
	-0.371575E+02		-0.827913E+01
	-0.268633E+02		-0.227060E+02
	-0.184475E+02		-0.257419E+02
	-0.870399E+01		-0.399195E+02
	0.110540E+01		-0.526711E+02
	0.299809E+01		-0.716744E+02
	0.357436E+01		-0.924683E+02
	0.415603E+01		-0.113262E+03
HI	0.415603E+02	JA	-0.655732E+02
	0.490882E+02		-0.641151E+02
	0.554637E+02		-0.627287E+02
	0.587969E+02		-0.612934E+02
	0.606138E+02		-0.598556E+02
	0.619919E+02		-0.584259E+02
	0.608528E+02		-0.569861E+02
	0.579001E+02		-0.555497E+02
	0.540625E+02		-0.541275E+02
	0.502250E+02		-0.527053E+02

Appendix 4A

Major Measuring and Recording Instruments used for the Wind Tunnel Tests

1. Pressure Transducer Transamerica BHL-4420

A miniature semiconductor strain gauge transducer is used. Pressure transducer gives a high level out put directly proportional to the applied pressure.

Following are the specifications of the Transducer;

Pressure range 0 - 50 kN/m^2

With input supply of 11 to 15 Volts dc and 60 mA Maximum

Output Span of 0 - 5 Volts ± 1%

Alternative out put 0 - 35 mV

accuracy; The combined non-linearity, and non-repeatability value less than 0.35% Span

2. Digital Data Logger System

Philips PR2011 series data acquisitional and monitoring system was used. This computer controlled intelligent data logger system is capable of measuring, monitoring and recording upto 256 physical quantities. In the present experimental work this was used only for low

static pressure measuring and recording purposes. The instrument can acknowledge upto 480 measurements per second. The alarm levels on channels were used as a special monitoring and cut off system, for excessive static pressures over loading the other instruments. The data logger system was connected to a IBM AT Personal computer through a IEC interface to provide and to receive signals to and from the data logger system.

3. Inclined Manometer

A sensitive inclined manometer was modified for accurate pressure readings. A travelling microscope and a potential meter have been used to obtain a accurate a differential pressure reading of upto accuracy of 0.001 mm of Water. The resistance of the potential meter was used as a indicator for the conversion of the pressure readings of the inclined manometer.

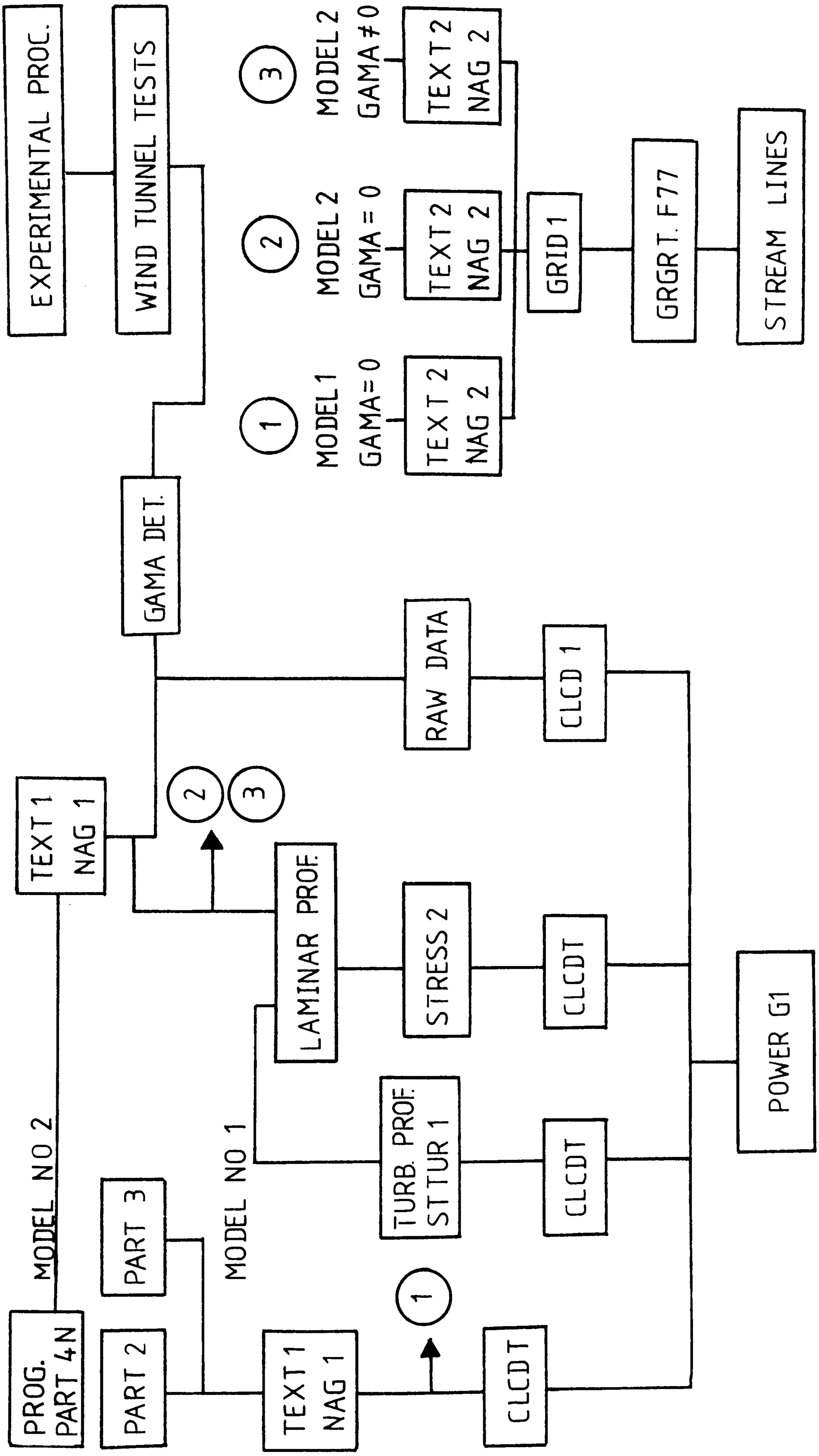

FLOW CHART OF COMPUTER PROGRAMS

```
      PROGRAM PART4N
      REAL M, M1,K1,K2
      INTEGER SG(21),SG11(11)
      LOGICAL REDO,RSC
      COMMON X,Y,PHI,PHID,XS,YS,NEST,SG,N1P1,N,PHIB
      COMMON RSC,PI,NST
      DIMENSION IO(9),IVECS(20)
      EQUIVALENCE (IOA,IO(1)),(IOB,IO(2)),(IOC,IO(3))
     *(IOD,IO(4)),(IOE,IO(5)),(IOF,IO(6)),(IOH,IO(7))
     *(IOI,IO(8)),(IOJ,IO(9))
      DIMENSION DELNMS(25)
      DIMENSION SRS(26)
      DIMENSION XS(21), YS(21), NEST(21)
      DIMENSION PHI(116), X(233), Y(233), PHID(116)
      COMMON XM(80),YM(80)
C     N=SEGMENTS REFER TO NAG NOTATION
C     SG(1) TO SG(21) SEGMENTS FOR EACH SIDE
C     N1P1=(2N+1) COORD POINTS ON CONTOUR REF TO NAG NOTAT.
C     NODAL POINTS ARE MID -POINT OF SEGMENTS= N IN NUMBER
962   FORMAT (1X ,2E13.6)
903   FORMAT (1X ,I10)
800   FORMAT('    THETAD       SHOL          CMU'/1H ,3E13.6)
555   FORMAT(I10)
850   FORMAT(1H ,I10/(1H ,2E13.6))
951   FORMAT(1X ,3E13.6)
861   FORMAT(1H ,2E13.6)
961   FORMAT(14X ,E13.6)
869   FORMAT(1H ,5I3)
      F(S)=-K1*K2*(S**M1)
      G(S)=-2*K1*K2*((SHOL/2.)**M1)+K1*K2*(S**M1)
      FYCK(X1,X2,Y1,Y2,XZ)=Y1+(Y2-Y1)*(XZ-X1)/(X2-X1)
910   FORMAT(1X,2L1,2I2)
      DATA DELNMS/0.01,0.02,0.03,0.04,0.05,0.06,0.07,0.08,
     *0.09,0.1,0.11,0.12,0.13,0.14,0.16,0.18,0.20,0.22,
     *0.24,0.26,0.28,0.30,0.32,0.34,0.36/
      NU=15
      OPEN(UNIT=NU,FILE='PIN15')
      OPEN(UNIT=10,FILE='PIN10')
      OPEN(UNIT=9,FILE='PIN9')
      READ(7,910)REDO,RSC,ICOUNT,KST
      PI=3.141593
      R1=1./(2.*SIN(PI/8.))
      DB=2.*PI/80.
      SRS(1)=R1
      DO 500 I=2,26
500   SRS(I)=SRS(I-1)+DELNMS(I-1)
      IF(REDO) GO TO 3334
      IF(RSC)GO TO 3331
      READ(10,962)(X(J),Y(J),J=1,233)
      READ(9,962)(XS(I),YS(I),I=1,21)
      READ(15,903)IFRP
      READ(15,961)PHID
      DATA SG11/1,1,1,4,4,8,4,4,1,1,1/
```

```
C       DELNM,DELNMS ARE INCREMENTS FOR LACATING M-POINTS
3331    READ(7,951) THETAD, SHOL, CMU
        WRITE (8,800)THETAD,SHOL,CMU
        GO TO 3339
3334    READ(7,951)THETAD,SHOL,CMU
        READ(9,962)(XS(I),YS(I),I=1,21)
        IF(KST.NE.0) READ(21,995)(IVECS(I),I=1,KST)
995     FORMAT(1X,5I5)
        GO TO 3333
3339    THETA=THETAD*PI/180.
        M=1./7.
        M1=M+1.
        K1=8./7.*SQRT(CMU/(SHOL*SIN(PI/8.)))
        R1R2=0.5*R1*SQRT(2.)
        CT=COS(THETA)
        ST=SIN(THETA)
        K2=((2./SHOL)**M)/M1
        IF(RSC) GO TO 525
        CALL UPSTGN
        IN=2.*NST
        XS(1)=X(IN)
        YS(1)=Y(IN)
        IN1=IN-1
        XS(11)=X(IN)+0.01*(X(IN1)-X(IN))
        YS(11)=Y(IN)+0.01*(Y(IN1)-Y(IN))
        CALL BETA(XS(1),YS(1),BET1)
        TTEMP=THETA
        DO 540 I=1,5
        TTEMP=TTEMP+PI*0.25
        IF(BET1.GE.TTEMP) GO TO 540
        ISN=I+1
        GO TO 530
540     CONTINUE
530     CONTINUE
        GO TO 535
525     ISN=8
C       SUPPLY THE KPN KNS, NUM.OF FULL SIDES OF OCT. P-N &S-N
C       KPN &KNS ARE FOR DOWNST.STG.POINT AT 67.5 +OR-10 DEG.
        KPN=6
        KNS=1
        GO TO 575
535     CONTINUE
C       NST IS AVAILABLE AT THIS STAGE
C       ALSO IFRP IS READ IN
        KNS=((NST-10+IFRP)/10)+2
        KPN=7-KNS
        IFR=NST+IFRP-10*(KNS-1)
575     IOA=ISN
        IOB=ISN+1
        J=IOB
        DO 413 I=1,KNS
        J=J+1
        IP2=I+2
```

```
413     IO(IP2)=J
        J=IP2
        DO 414 I=1,KPN
        J=J+1
414     IO(J)=(I+1)
        IOP=1
        IOS=11
C       COORDINATES OF A
        XS(IOA)=R1*CT
        YS(IOA)=R1*ST
C       CORDINATES OF B
        XS(IOB)=(R1-SHOL)*CT
        YS(IOB)=(R1-SHOL)*ST
C       COORDINATES OF C
        XS(IOC)=R1R2*(ST+CT)
        YS(IOC)=R1R2*(ST-CT)
C       CORDINATES OF D
        XS(IOD)=YS(IOA)
        YS(IOD)=-XS(IOA)
C       COORDINATES OF E
        XS(IOE)=YS(IOC)
        YS(IOE)=-XS(IOC)
C       COORDINATES OF F
        XS(IOF)=-XS(IOA)
        YS(IOF)=-YS(IOA)
C       COORDINATES OF H
        XS(IOH)=-XS(IOC)
        YS(IOH)=-YS(IOC)
C       COORDINATES OF I
        XS(IOI)=-XS(IOD)
        YS(IOI)=-YS(IOD)
C       COORDINATES OF J
        XS(IOJ)=-XS(IOE)
        YS(IOJ)=-YS(IOE)
        IF(RSC) GO TO 444
        GO TO 445
C       INITIAL RUN TO DECIDE UPSTREAM STG POINT
444     TCD=(YS(IOC)-YS(IOD))/(XS(IOC)-XS(IOD))
        T=-TAN(PI/8.)
        XINT=(TCD*XS(IOC)-YS(IOC))/(TCD-T)
        FR=10.*(XINT-XS(IOD))/(XS(IOC)-XS(IOD))
        IFR=FR
        IF(IFR.EQ.10)IFR=9
        FR=0.1*FLOAT(IFR)
        XS(1)=XS(IOC)+FR*(XS(IOD)-XS(IOC))
        YS(1)=YS(IOC)+FR*(YS(IOD)-YS(IOC))
        FR=FR-0.01
        XS(11)=XS(IOC)+FR*(XS(IOD)-XS(IOC))
        YS(11)=YS(IOC)+FR*(YS(IOD)-YS(IOC))
C       IFR IS ALREADY AVAILABLE FOR RIGHT CONTOUR
C       SG(1) TO SG(10) DEPENDS ON STGN POINT POSITION
445     CONTINUE
        SG(1)=10-IFR
```

```
      SG(10)=IFR
C     FROM POINT P TO NOZZLE
      DO 411 I=1,KPN
411   SG(I+1)=10
      SG(ISN)=6
      J=ISN
C     FROM NOZZLE TO POINT S
      DO 412 I=1,KNS
      J=J+1
412   SG(J)=10
C     SG(11) TO SG(21) ARE SET USING DATA FROM SG(11)
      DO 480 I=1,11
480   SG(I+10)=SG11(I)
      IF(REDO) GO TO 3333
      N=0
C     CALCULATE NO OF SEGMENTS =NODAL POINTS
      DO 1 I=1,10
1     N=N+SG(I)
C     CALCULATE M P FOR DO3EAF
      N1P1=2*N+1
      NE=0
C     EVALUATE THE COORD. OF ALL THE POINTS USE DO L-10
      DO 10 I=1,10
      NB=NE+1
      NBP1=NB+1
      NIS=SG(I)
      NE=2*NIS+NB-1
      NEST(I)=NE
C     NE DENOTES END POINT -1.
      X(NB)=XS(I)
      Y(NB)=YS(I)
C     DELX,DELY =0.5*DISTANCE BETWEEN NODAL POINTS
      IP1=I+1
      DELX=0.5*(XS(IP1)-XS(I))/FLOAT(NIS)
      DELY=0.5*(YS(IP1)-YS(I))/FLOAT(NIS)
      DO 11 J=NBP1,NE
      X(J)=X(J-1)+ DELX
11    Y(J)=Y(J-1)+ DELY
10    CONTINUE
C     PHID VALUES SET=0 FOR DIRECHLETE INTERIOR PROBLEM
      DO 100 J=1,116
100   PHID(J)=0.
C     PROG. FOR FINDING PHI VALUES FOR NODAL POINTS
C     NBD= THE POINT CORRRESPONDS MID POINT OF NOZZLE SEG
      NBD=1+SG(ISN)+NEST(ISN-1)
      J=0
      DO 25 I=2,N1P1,2
      J=J+1
      IF(I.GT.NEST(ISN-1)) GO TO 65
      PHI(J)=0.
      GO TO 25
65    IF(I.GT.NBD) GO TO 66
      S=SQRT((XS(ISN)-X(I))**2+(YS(ISN)-Y(I))**2)
```

```
      PHI(J)=F(S)
      GO TO 25
66    IF(I.GT.NEST(ISN)) GO TO 68
      S=SQRT((XS(ISN+1)-X(I))**2+(YS(ISN+1)-Y(I))**2)
      PHI(J)=G(S)
      IF(I.NE.NEST(ISN)) GO TO 25
      PHIB=-2.*K1*K2*((SHOL/2.)**M1)
      GO TO 25
68    PHI(J)=PHIB
25    CONTINUE
      GO TO 3335
3333  CONTINUE
      CALL BETA(XS(1),YS(1),BL)
      CALL BETA(XS(14),YS(14),BH)
      BL=BL-DB
      BH=BH+DB
C     EXPECT BH GT. BL NORMALLY
C     IF BH LT. BH INTER CHANGE
      IF(BH.GT.BL) GO TO 4499
      B=BH
      BH=BL
      BL=B
4499  CONTINUE
      WRITE(20,2657)(SRS(J),J=1,26),BH,DB
2657  FORMAT(1H ,2E13.6)
      I=0
      B=BH
443   IF(B.GT.BL) GO TO 441
      GO TO 442
441   B=B-DB
      I=I+1
      GO TO 443
442   IMAX=81-I
C     I=1 TO MAX CLEAN RADIALS
      B=BH
      SR=SRS(ICOUNT)
      DO 450 I=1,80
      XT=SR*COS(B)
      YT=SR*SIN(B)
      IF(I.LE.IMAX) GO TO 550
      IF(XT.LT.-2.5)GO TO 557
      YCK=YS(1)+FYCK(XS(1),XS(21),YS(1),YS(21),XT)
      IF(YT.GT.YCK)GO TO 550
      YCK=YS(11)+FYCK(XS(11),XS(12),YS(11),YS(12),XT)
      IF(YT.LT.YCK) GO TO 550
C     A  BORDER POINT IS FOUND TO BE REJECTE
      GO TO 580
557   YCK=YS(21)+FYCK(XS(21),XS(20),YS(21),YS(20),XT)
      IF(YT.GT.YCK) GO TO 550
      YCK=YS(12)+FYCK(XS(12),XS(13),YS(12),YS(13),XT)
      IF(YT.LT.YCK)GO TO 550
C     A BORDER POINT IS FOUND TO BE REJECTED
580   KST=KST+1
```

```
      IVECS(KST)=(ICOUNT-1)*80+I
550   XM(I)=XT
      YM(I)=YT
      B=B+DB
450   CONTINUE
      GO TO 3336
3335  CALL SUBP3N
      WRITE (13,888)IFR
C     WRITE (13,851)PHID
888   FORMAT(1H ,I10)
      WRITE (16,861)(XS(I),YS(I),I=1,21)
      WRITE (8,861)(X(J),Y(J),J=1,N1P1)
      WRITE (12,861)(X(J),Y(J),J=1,N1P1)
      WRITE (12,861)(PHI(J),PHID(J),J=1,N)
      WRITE(17,861)(X(J),Y(J),J=1,N1P1)
      WRITE(19,861)(X(JT),Y(JT),JT=2,172,2)
      WRITE(19,861)(XS(I),YS(I),I=1,21)
      WRITE(19,869)(IO(IJ),IJ=1,9)
      IF(RSC) GO TO 3338
      REDO=.TRUE.
3338  RSC=.FALSE.
      GO TO 3400
3336   WRITE(4,861)(XM(I),YM(I),I=1,80)
      IF(KST.EQ.0) GO TO 3745
      WRITE(18,895)(IVECS(I),I=1,KST)
3745  CONTINUE
895   FORMAT(1H ,5I5)
      ICOUNT=ICOUNT+1
      IF(ICOUNT.EQ.27) GO TO 81
3400  WRITE(14,860)REDO,RSC,ICOUNT,KST
863   FORMAT(1H ,3E13.6)
      WRITE(14,863)THETAD,SHOL,CMU
81    STOP
860   FORMAT(1H ,2L1,2I2)
      END
      SUBROUTINE SUBP3N
      LOGICAL RSC,REDO
      INTEGER SG(21),SG11(11)
      COMMON X,Y,PHI,PHID,XS,YS,NEST,SG,N1P1,N,PHIB
      COMMON RSC,PI,NST
      DIMENSION DELNMS(25)
      DIMENSION SRS(26)
      DIMENSION XS(21),YS(21),NEST(21)
      DIMENSION PHI(116),X(233),Y(233),PHID(116)
      COMMON XM(80),YM(80)
      DATA D/10./
C     ASSUME LEFT CONTOUR
      XS(17)=D
      YS(17)=D
      XS(15)=-D
      YS(15)=-D
      XS(16)=D
      YS(16)=-D
```

```
      XS(18)=-D
      YS(18)=D
      IF(.NOT.RSC) GO TO 460
      DO 461 I=15,18
      XS(I)=-XS(I)
461   YS(I)=-YS(I)
      IF(RSC) GO TO 465
C     COORDINATE OF Q=19,COORD R=14
460   XS(14)=-D
      XS(19)=-D
      YS(19)=-10.+20.*(10.+PHIB)/(20.+PHIB)
      YS(14)=YS(19)-0.01
C     CALCULATA COORDS. OF P1,P2,S1,S2/21,20,12,13
      XS(20)=-9.
      YS(20)=YS(19)
      XS(21)=-2.5
      YS(21)=YS(1)*(-2.5)/XS(1)
      XS(12)=XS(21)
      XS(13)=XS(20)
      YS(12)=YS(21)-0.01
      YS(13)=YS(20)-0.01
      GO TO 4651
465   CONTINUE
C     RIGHT CONTOUR POINTS TO BE FOUND
      XS(14)=D
      XS(19)=D
      YS(19)=-10.+20.*D/(20.-PHIB)
      YS(14)=YS(19)+0.01
C     COORDINATES OF 21,20,12,13
      YS(20)=YS(19)
      XS(20)=9.0
      XS(21)=2.5
      YS(21)=YS(1)*(2.5)/XS(1)
      XS(12)=XS(21)
      XS(13)=XS(20)
      YS(12)=YS(21)+0.01
      YS(13)=YS(20)+0.01
4651  N=116
C     CALCULATE NO OF SEG.=NOD POINTS
      N1P1=2*N+1
C     SETS PHID VALUES =0 FOR INT. DIRCH. PROBLEM
      DO 100 J=87,116
100   PHID(J)=0.
C     CALCULATE THE COORDINATES OF ALL POINTS DO L-10
      NE=NEST(10)
      DO 10 I=11,21
      NB=NE+1
      NBP1=NB+1
C     NO OF INTERVALES IN THE SECTION(I)
      NIS=SG(I)
      NE=2.*NIS+NB-1.
      NEST(I)=NE
C     NE DENOTES THE END POINT -1.
```

```
      X(NB)=XS(I)
      Y(NB)=YS(I)
      IP1=I+1
      IF(IP1.EQ.22) IP1=1
      DELX=0.5*(XS(IP1)-XS(I))/FLOAT(NIS)
      DELY=0.5*(YS(IP1)-YS(I))/FLOAT(NIS)
      DO 11 J=NBP1,NE
      X(J)=X(J-1)+DELX
11    Y(J)=Y(J-1)+DELY
10    CONTINUE
C     CONTOUR IS COMPLETED BY REPEATING START POINT
      X(N1P1)=X(1)
      Y(N1P1)=Y(1)
C     FINDING PHI VALUES FOR NODAL POINTS
      J=86
      NNOD11=NEST(10)+2
      DO 25 I=NNOD11,N1P1,2
      J=J+1
C     SECTION K-R HAS A CONST STREAM FUNTION
      IF(I.GT.NEST(13)) GO TO 35
      PHI(J)=PHIB
      GO TO 25
35    PHI15=-D
      IF(RSC)PHI15=D
      IF(I.GT.NEST(14)) GO TO 37
      PHI(J)=(Y(I)-YS(14))*(PHI15-PHIB)/(YS(15)
     *-YS(14))+PHIB
      GO TO 25
37    IF(I.GT.NEST(15)) GO TO 39
      PHI15=-D
      IF(RSC)PHI15=D
      PHI(J)=PHI15
      GO TO 25
39    IF(I.GT.NEST(16)) GO TO 41
      PHI(J)=Y(I)
      GO TO 25
41    IF(I.GT.NEST(17)) GO TO 43
      PHI17=D
      IF(RSC)PHI17=-D
      PHI(J)=PHI17
      GO TO 25
43    IF(I.GT.NEST(18)) GO TO 45
      PHI(J)=-PHI15*(1-(Y(I)-YS(18))/(YS(19)-YS(18)))
      GO TO 25
45    PHI(J)=0.
25    CONTINUE
      RETURN
      END
      SUBROUTINE UPSTGN
      LOGICAL REDO,RSC
      INTEGER SG(21),SG11(11)
      COMMON X,Y,PHI,PHID,XS,YS,NEST,SG,N1P1,N,PHIB
      COMMON RSC,PI,NST
```

```
      DIMENSION DELNMS(25)
      DIMENSION SRS(26)
      DIMENSION XS(21),YS(21),NEST(21)
      DIMENSION PHI(116),X(233),Y(233),PHID(116)
      COMMON XM(80),YM(80)
C     READ PHID VALUES FROM TEXT1 OUT-PUT AFTER FIRST RUN
C     WITH  RSC=TRUE AND REDO=FALSE
C     DECIDE THE UPSTREAM STG.POINT
      IS=14
10    IS=IS+1
      IF(PHID(IS).GE.0.)GO TO 10
      DO 20 I=IS,86
      IS=IS+1
      IF(PHID(IS)*PHID(IS-1).GT.0.) GO TO 20
      NST=IS
      GO TO 25
20    CONTINUE
      WRITE(13,800)
800   FORMAT('CHECK NO UPSTREAM STGN POINT  FOUND')
25    RETURN
      END
      SUBROUTINE  BETA(XD,YD,B)
      LOGICAL REDO,RSC
      INTEGER SG(21),SG11(11)
      COMMON X,Y,PHI,PHID,XS,YS,NEST,SG,N1P1,N,PHIB
      COMMON RSC,PI,NST
      DIMENSION DELNMS(25)
      DIMENSION SRS(26)
      DIMENSION XS(21),YS(21),NEST(21)
      DIMENSION PHI(116),X(233),Y(233),PHID(116)
      COMMON XM(80),YM(80)
      IF(ABS(XD).LT.1.E-08) GO TO 10
      BBASE=ATAN(ABS(YD/XD))
      GO TO 11
10    BBASE=0.5*PI
11    IF(XD.LT.0.) GO TO15
      IF(YD.LT.0.) GO TO 20
C     FIRST QUART.
      B=BBASE
      GO TO 25
20    B=2.*PI-BBASE
      GOTO 25
15    IF(YD.LT.0.)GO TO 30
      B=PI-BBASE
      GO TO 25
30    B=PI+BBASE
25    RETURN
      END
```

MAIN FLOW CHART OF THE
FORTRAN PROGRAM SITUR1

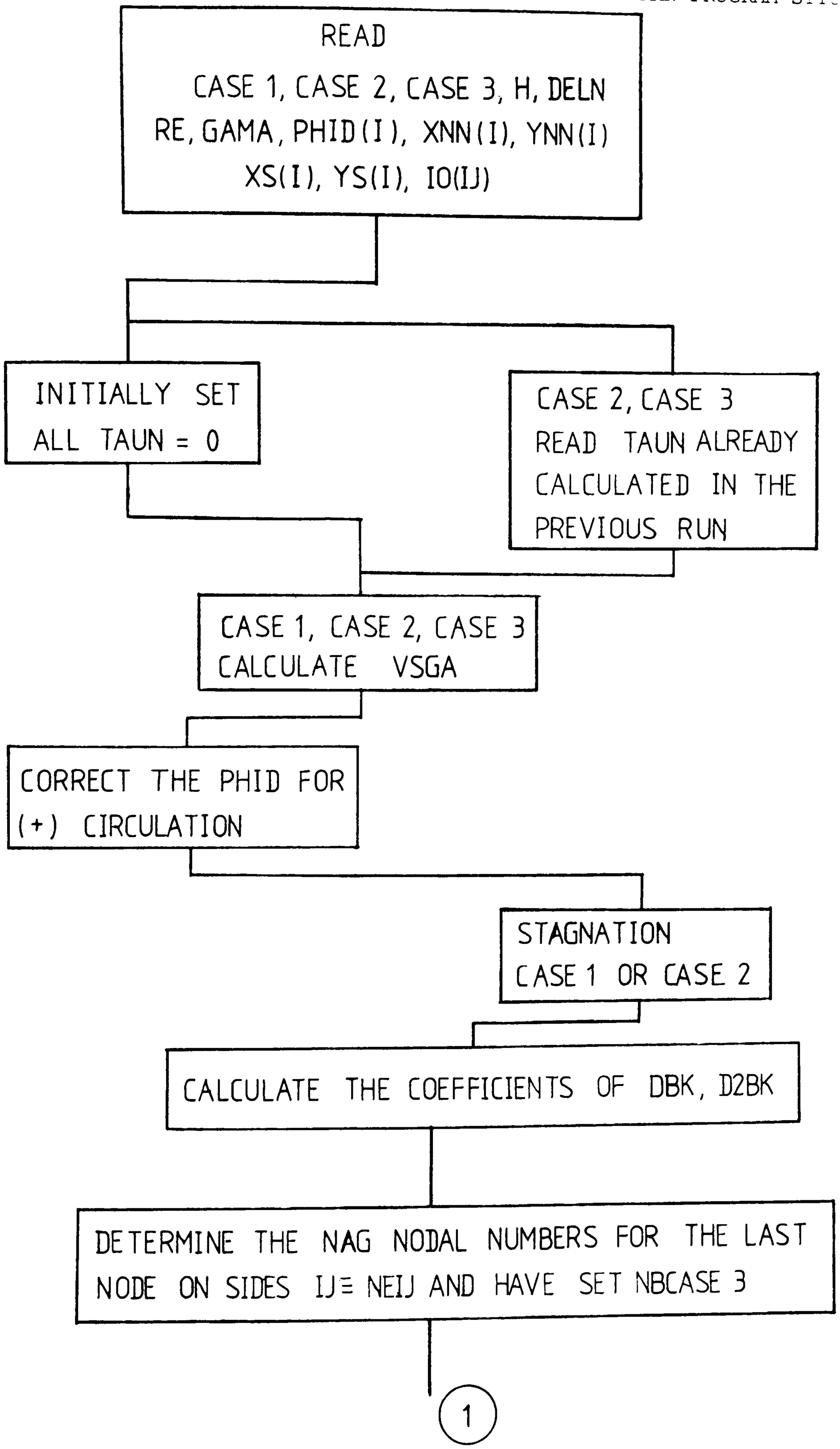

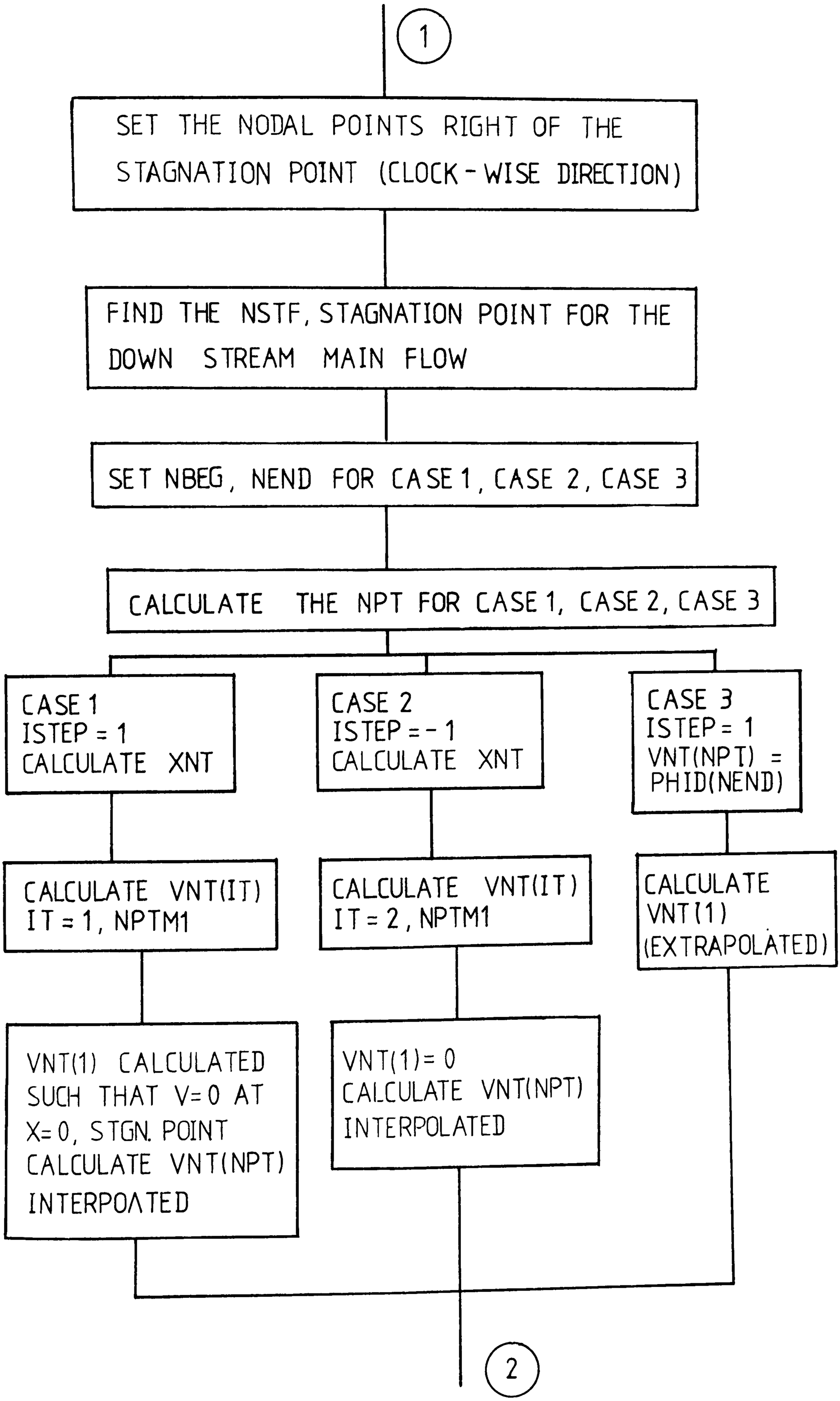
1
SET THE NODAL POINTS RIGHT OF THE STAGNATION POINT (CLOCK-WISE DIRECTION)
FIND THE NSTF, STAGNATION POINT FOR THE DOWN STREAM MAIN FLOW
SET NBEG, NEND FOR CASE 1, CASE 2, CASE 3
CALCULATE THE NPT FOR CASE 1, CASE 2, CASE 3
CASE 1
ISTEP = 1
CALCULATE XNT
CASE 2
ISTEP = -1
CALCULATE XNT
CASE 3
ISTEP = 1
VNT(NPT) = PHID(NEND)
CALCULATE VNT(IT)
IT = 1, NPTM1
CALCULATE VNT(IT)
IT = 2, NPTM1
CALCULATE VNT(1)
(EXTRAPOLATED)
VNT(1) CALCULATED SUCH THAT V=0 AT X=0, STGN. POINT
CALCULATE VNT(NPT)
INTERPOLATED
VNT(1)= 0
CALCULATE VNT(NPT)
INTERPOLATED
2

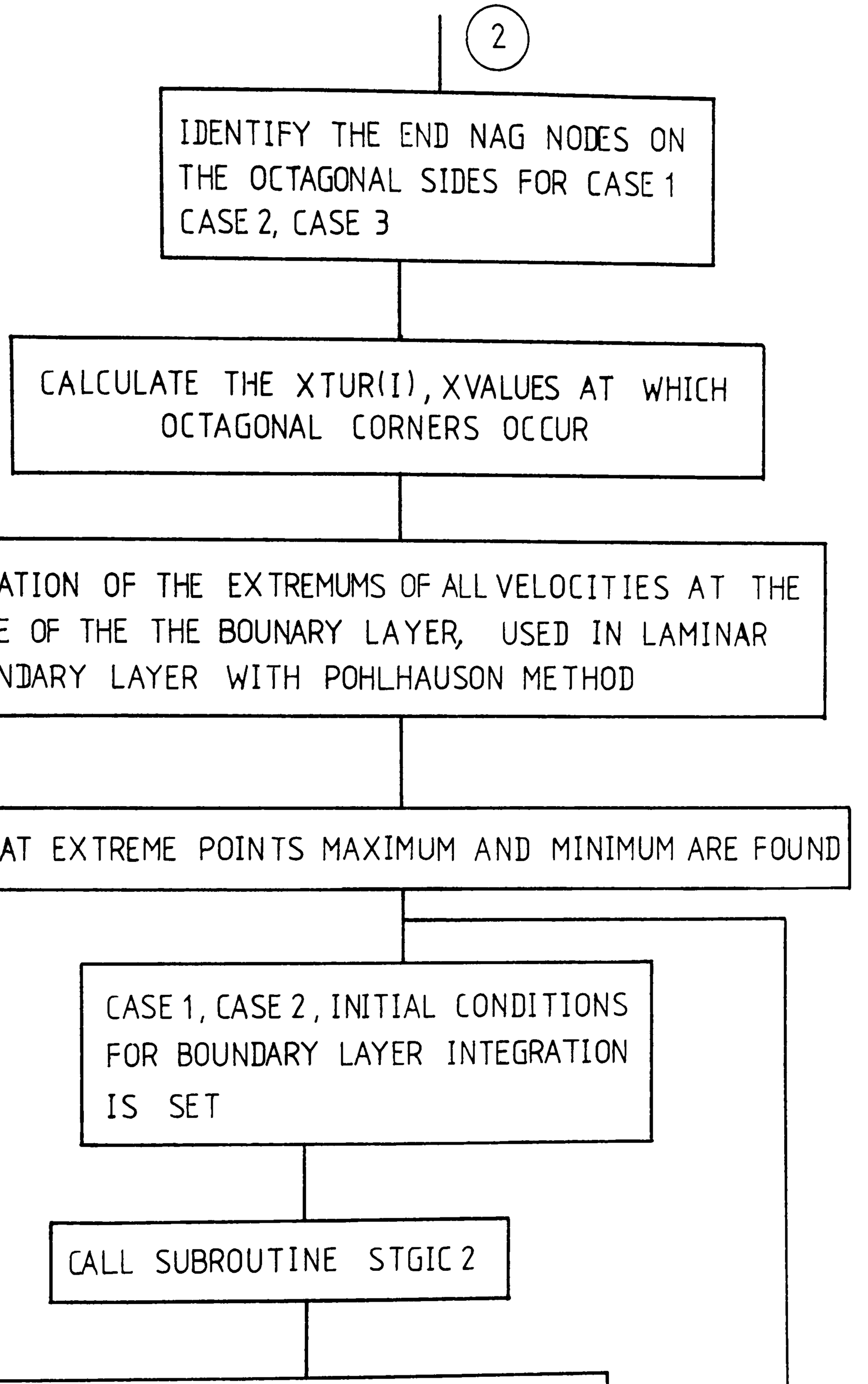
2
IDENTIFY THE END NAG NODES ON THE OCTAGONAL SIDES FOR CASE 1 CASE 2, CASE 3
CALCULATE THE XTUR(I), XVALUES AT WHICH OCTAGONAL CORNERS OCCUR
LOCATION OF THE EXTREMUMS OF ALL VELOCITIES AT THE EDGE OF THE THE BOUNARY LAYER, USED IN LAMINAR BOUNDARY LAYER WITH POHLHAUSON METHOD
AT EXTREME POINTS MAXIMUM AND MINIMUM ARE FOUND
CASE 1, CASE 2, INITIAL CONDITIONS FOR BOUNDARY LAYER INTEGRATION IS SET
CALL SUBROUTINE STGIC 2
INITIAL CONDITIONS FOR THE POHLHAUSON METHOD OF STAGNATION CONDITION IS SET Λ = 7.052
3
4

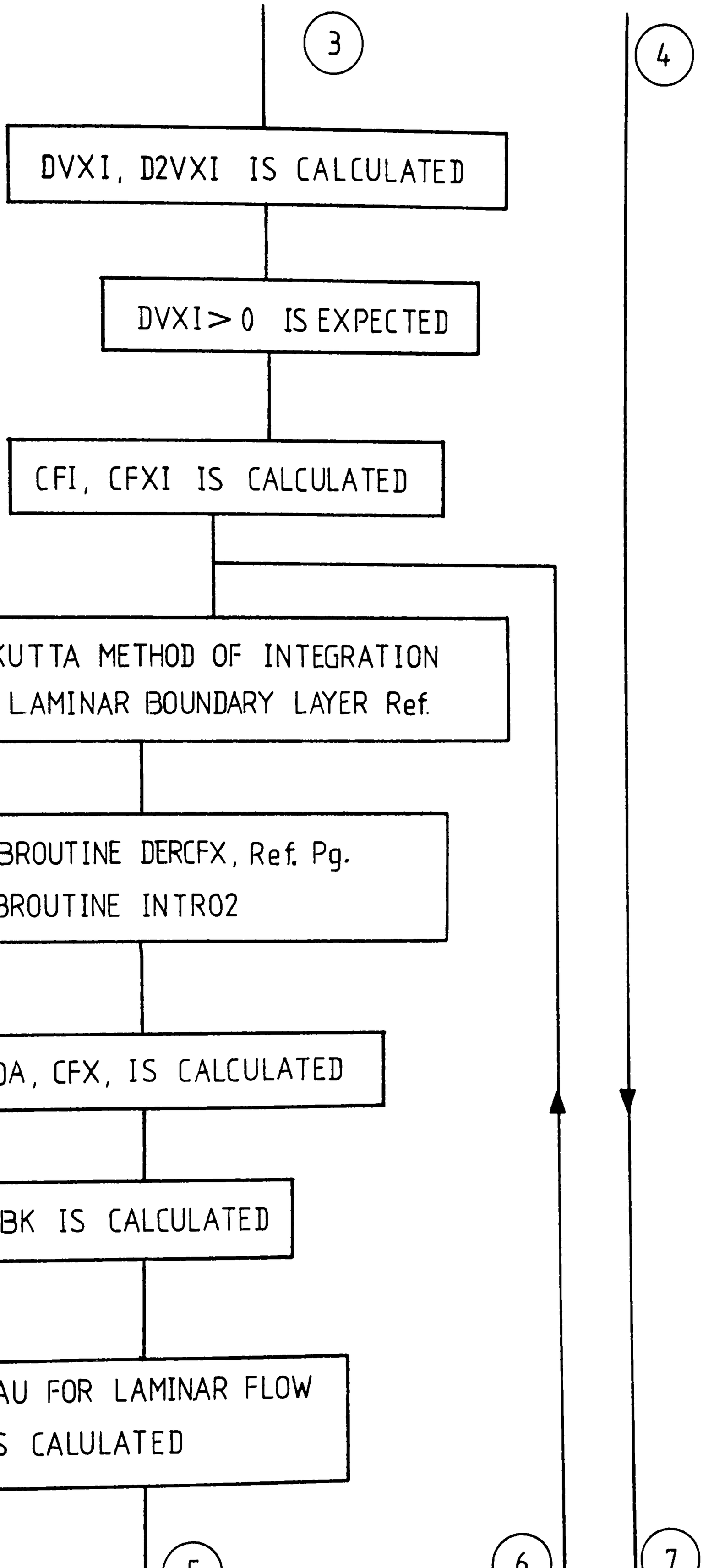
3
4
DVXI, D2VXI IS CALCULATED
DVXI > 0 IS EXPECTED
CFI, CFXI IS CALCULATED
RUNGE KUTTA METHOD OF INTEGRATION
FOR THE LAMINAR BOUNDARY LAYER Ref.
CALL SUBROUTINE DERCFX, Ref. Pg.
CALL SUBROUTINE INTRO2
LAMDA, CFX, IS CALCULATED
BK IS CALCULATED
TAU FOR LAMINAR FLOW
IS CALULATED
5
6
7

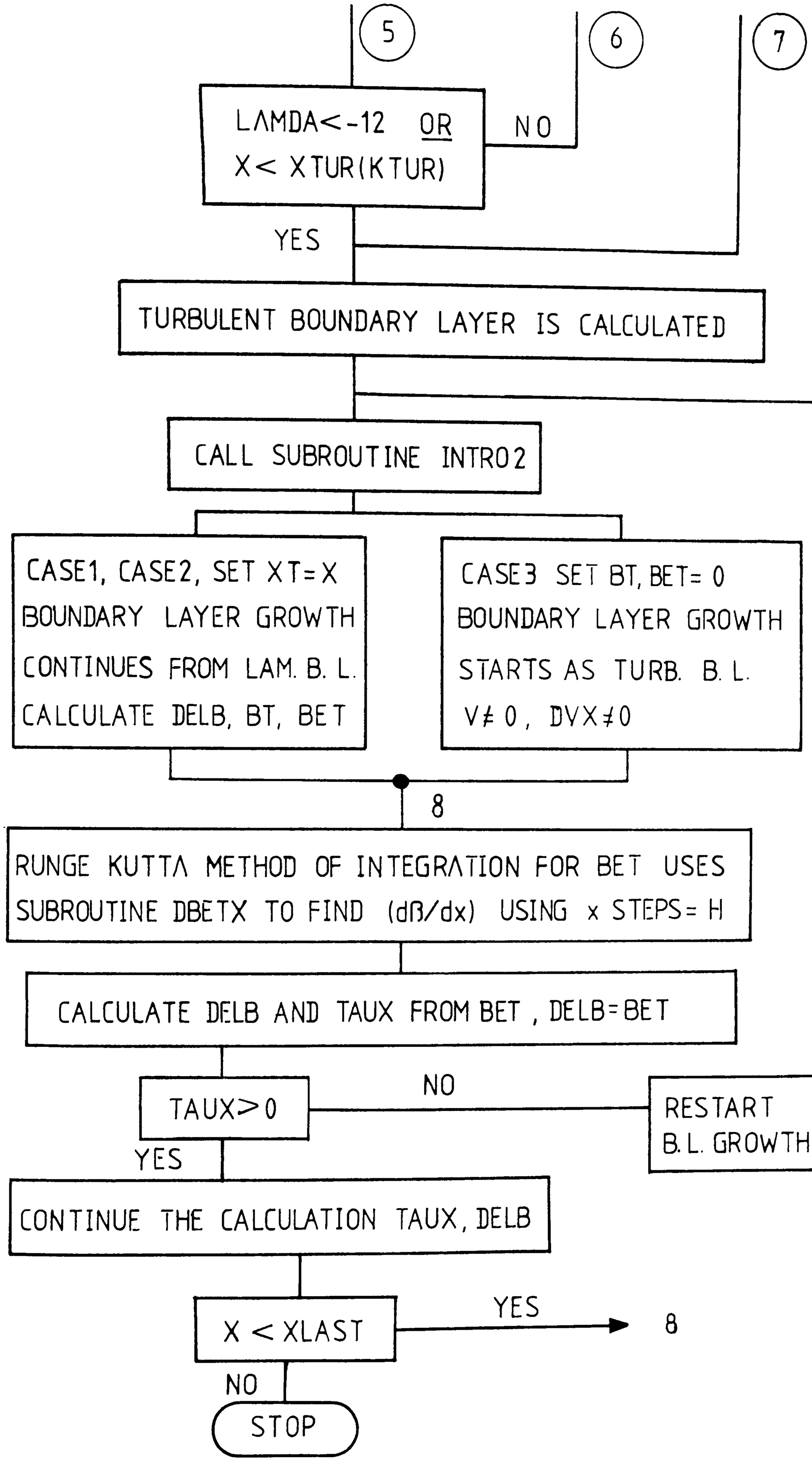
5
6
7
LAMDA<-12 OR
X< XTUR(KTUR)
NO
YES
TURBULENT BOUNDARY LAYER IS CALCULATED
CALL SUBROUTINE INTRO2
CASE1, CASE2, SET XT=X
BOUNDARY LAYER GROWTH
CONTINUES FROM LAM. B. L.
CALCULATE DELB, BT, BET
CASE3 SET BT, BET= 0
BOUNDARY LAYER GROWTH
STARTS AS TURB. B. L.
V≠ 0, DVX≠0
8
RUNGE KUTTA METHOD OF INTEGRATION FOR BET USES
SUBROUTINE DBETX TO FIND (dβ/dx) USING x STEPS= H
CALCULATE DELB AND TAUX FROM BET , DELB=BET
TAUX>0
NO
RESTART
B. L. GROWTH
YES
CONTINUE THE CALCULATION TAUX, DELB
X < XLAST
YES
8
NO
STOP

FK(LDA1) = LDA1(SA - LDA1 (SB + SC * LDA1)) * * 2

CALL INRO 2
INTERPOLATION OF LDA AT XT

BK IS CALCULATED

IF BK > 0,0949

YES

WRITE THE
DIAG. REPORT

STOP

NO

DBKP, DB2KP IS CALCULAED

LDA IS CALCULATED
TAYLOR SERIES IS USED

IF LDA> +12

YES

NO

DVX * LDA > 0

7

YES

NO

Q=SA-LDA*(SB+LDA*SC)

CFX IS CALCULATED

RETURN

SET X = XEXT(KK)

RESTART THE INTEGRATION
SET XT = X , LDA = 0, BK = 0
BKP = 0, D'BKP = SA0, D2BKP = SB0

RETURN

CALL INTRO2

SET IQ=2, DVX = 0, KK = KK + 1

1

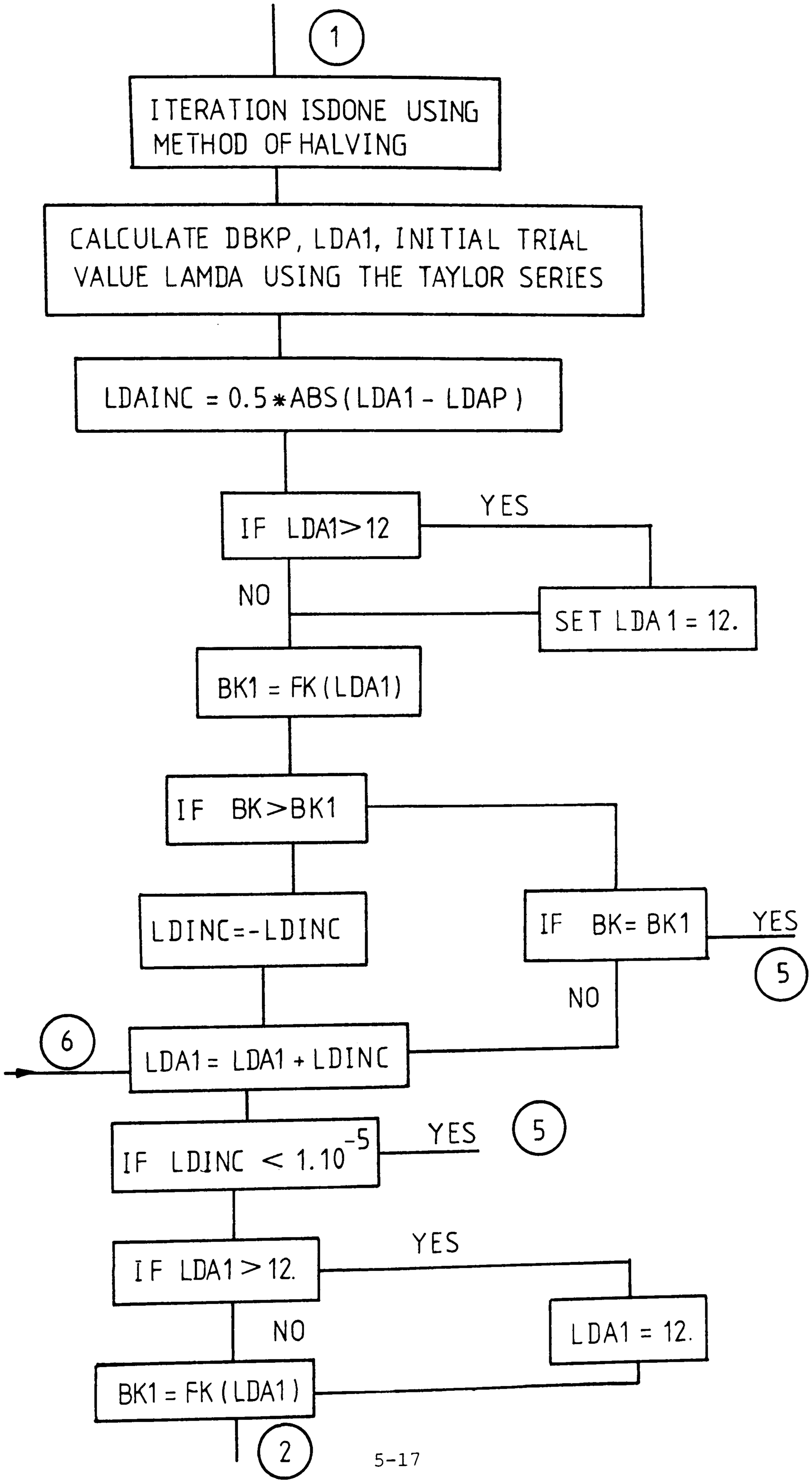
1
ITERATION ISDONE USING METHOD OF HALVING
CALCULATE DBKP, LDA1, INITIAL TRIAL VALUE LAMDA USING THE TAYLOR SERIES
LDAINC = 0.5*ABS(LDA1 - LDAP)
IF LDA1>12
YES
NO
SET LDA 1 = 12.
BK1 = FK(LDA1)
IF BK>BK1
LDINC=-LDINC
IF BK= BK1
YES
5
NO
6
LDA1 = LDA1 + LDINC
IF LDINC < 1.10^-5
YES
5
IF LDA1 > 12.
YES
NO
LDA1 = 12.
BK1 = FK(LDA1)
2

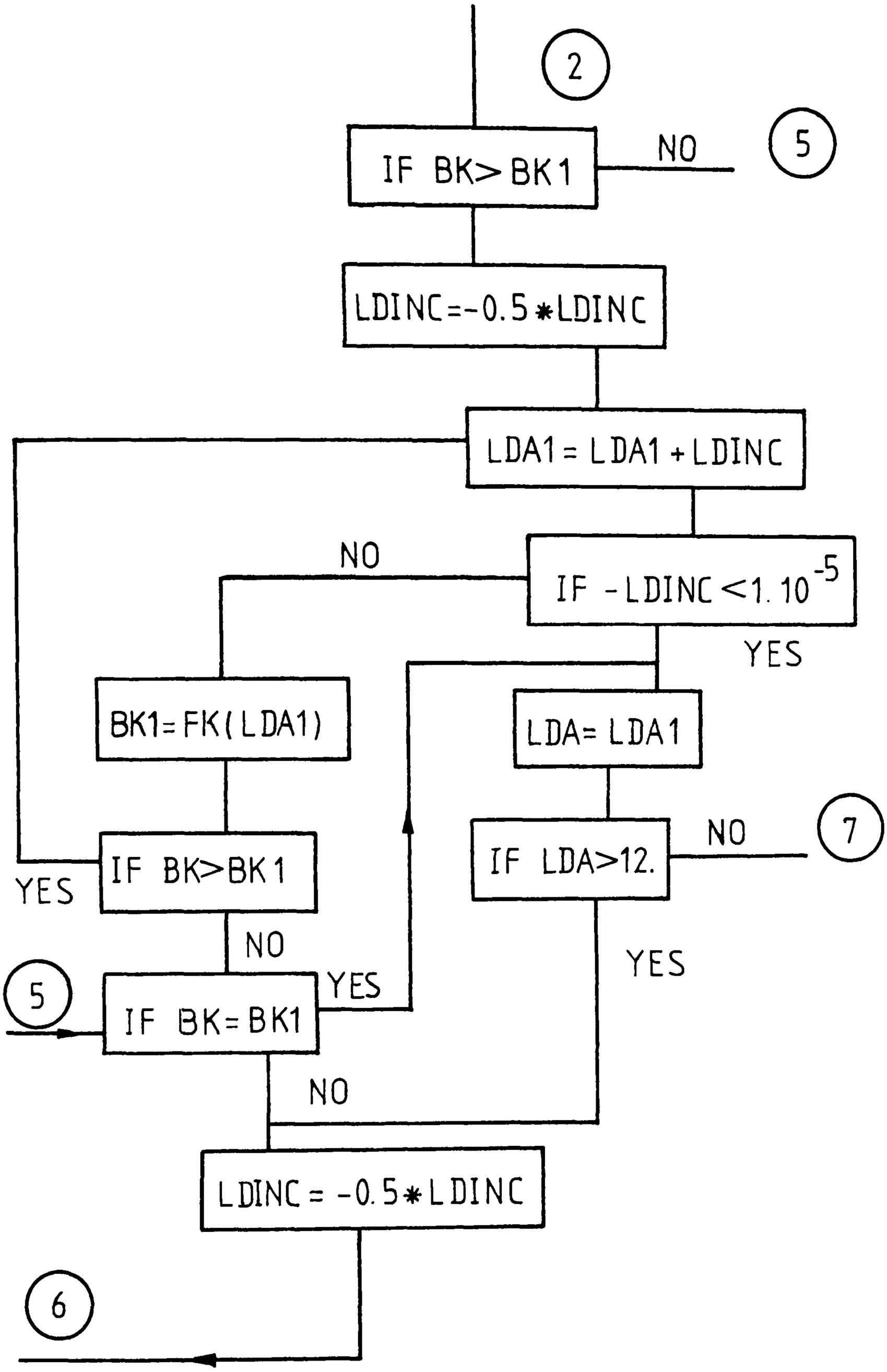
2
IF BK> BK1
NO
5
LDINC=-0.5*LDINC
LDA1 = LDA1 + LDINC
NO
IF -LDINC <1. 10 -5
YES
BK1= FK(LDA1)
LDA= LDA1
YES
IF BK>BK1
IF LDA>12.
NO
7
YES
NO
5
IF BK= BK1
YES
NO
LDINC = -0.5*LDINC
6

```
      PROGRAM STTUR1
      LOGICAL STAGTN,CASE1,CASE2,CASE3,LNODE,LSTEPA,EXWRIT
      DIMENSION XNN(86),YNN(86),XS(21),YS(21)
      DIMENSION IO(9)
      COMMON/A/ XNT(42),VNT(42),PHID(92),TAUN(92),XEXT(10)
      COMMON/B/ X,XT,LDA,YT,LDAX,V,DVX,D2VX,NPT,NPTM1,XCHK
      COMMON/C/ H,HO2,DELN,DELNO2,RDN2,RDNS,R6,R1,R2,R8,R9
      COMMON/D/ SA0,SA1,SA2,SA3,SB0,SB1,SB2,SC1,SD0,SD1,SD2
      COMMON/E/ SE0,SE1,SF0,CF,CFI,CFX,CFXI,SD,TD,LDAI,DVXI
      COMMON/F/ SQ0,SA4,SA,SB,SC,R240,DBKP,D2BKP,Q,D2VXI,KK
      COMMON/G/ VSCA,RE,IC,ZT,BKP,SB3,LDAP,IQ
      REAL LDA,LDAI,LDAX,LDAP
      F(VNTP)=(VNTPM-VNTPP)/(VNTPM+VNTPP-2.*VNTP)*DELNO2
  801 FORMAT(1H ,5I3)
  802 FORMAT (1H ,E13.6)
  815 FORMAT (1H ,2E13.6)
  810 FORMAT (1H ,7E13.6)
  820 FORMAT (E13.6)
  830 FORMAT(' LAST POINT IN CASE3 INK'/1H ,I3)
  840 FORMAT(' LAST POINT IN CASE4 INL'/1H ,I3)
 8000 FORMAT(' TURB. PROF.  X  BET TAU V DELB'/1H ,5E13.6)
  850 FORMAT('XEXT VALUES'/1H ,6E13.6)
  875 FORMAT(1H ,3E13.6)
  975 FORMAT(1X, 2E13.6)
  900 FORMAT (1X, E13.6)
  901 FORMAT (4L2)
  902 FORMAT (1X, 4E13.6)
  969 FORMAT(1X ,5I3)
C     DELN=DIST. BETWEEN NODAL POINTS
C     H IS THE INCREMENT FOR THE INTEGRATION
C     RE IS THE RENOLDS NUMBER
C     XLAST=POINT AT THE END OFTWO SECT.BC-CD OR IH-HG
      READ(3,901) EXWRIT
      READ (3,901) CASE1,CASE2,CASE3
      READ (3,902) H,DELN,RE,GAMA
      READ (3,900) (PHID(I),I=1,86)
      READ(8,975)(XNN(I),YNN(I),I=1,86)
      READ(8,975)(XS(I),YS(I),I=1,21)
      READ(8,969)(IO(IJ),IJ=1,9)
      WRITE(7,875)(XNN(I),YNN(I),PHID(I),I=1,86)
      PI=3.141592
      CONSG1=(SIN(PI/8.))/PI
      VSGA=GAMA*CONSG1
C     CORRECT THE PHID FOR (+)VE CIRCULATION
      DO 350 I=1,86
  350 PHID(I)=PHID(I)+VSGA
      STAGTN=CASE1.OR.CASE2
      DELNO2=DELN*0.5
      RDN2=0.5/DELN
      RDNS=RDN2/DELN
      HO2=H*0.5
      R6=1./6.
      R8=1./SQRT(RE)
```

```
      R9=2.*R8
      R240=1./240.
      RE1=1./(RE)**0.25
      TAUC=RE1*0.0456
      SAT1=-115./28.
      SATB1=2.052/7.
      SBRE=SATB1*RE1
C     COEFFICIENTS OF Q
      SA=37./315.
      SB=1./945.
      SC=1./9072.
C     COEF. OF DBK & D2BK(1ST & 2ND DEF. OF BK WRT LDA)
      SA0=SA**2
      SA1=-4.*SA*SB
      SA2=3.*(SB**2-2.*SA*SC)
      SA3=8.*SB*SC
      SA4=5.*SC**2
      SB0=SA1
      SB1=2.*SA2
      SB2=3.*SA3
      SB3=4.*SA4
C     CHANGING TO THE NEW NUMBERING FOR LEFT CONTOUR
      IOI=IO(8)
      XNI=XS(IOI)
      YNI=YS(IOI)
      IOJ=IO(9)
      XNJ=XS(IOJ)
      YNJ=YS(IOJ)
      IF(XNI.EQ.XNJ) GO TO 10
      DO 15 I=1,86
      IF(XNN(I).LT.XNJ) GO TO 15
      NEIJ=I-1
      GO TO 20
15    CONTINUE
10    DO 16 I=1,86
      IF(YNN(I).LT.YNJ) GO TO 16
      NEIJ=I-1
      GO TO 20
16    CONTINUE
20    CONTINUE
      NECAS1=NEIJ+10
      WRITE(4,969) NECAS1
      NBCAS3=NECAS1+7
C     SET NODAL POINT RIGHT OF STAG POINT(CLOCKWISE-D.)
      NSTB=NECAS1+30
65    NSTB1=NSTB
      IF(NSTB.GT.86) NSTB1=NSTB-86
      IF(PHID(NSTB1).LT.0.) GO TO 60
      NSTB1=NSTB1+5
      GO TO 65
60    NSTB=NSTB1
      NSTE=NSTB+43
      DO 61 I=NSTB,NSTE
```

```
      IN=I
      IF(I.GT.86) IN=I-86
      IF(PHID(IN).LE.0.) GO TO 61
      GO TO 62
61    CONTINUE
62    NST=IN
C     FINDING THE NST, NAG NODE OF STAGN. UPSTREAM
C     NSTF NAG NODE FOR THE STAGN POINT UPSTREAM
      NSTB=NBCAS3
      DO 66 I=NSTB,86
      IF(PHID(I).GE.0.) GO TO 66
      GO TO 67
66    CONTINUE
67    NSTF=I
C     SET NBEG & NEND FOR THE APPROPRIATE CASE
C     ALSO SET VNT(1)  FOR CASES 1 & 2
C     NOTE VNT(1) IS EXTRAPOLATED FOR CASES 3
      IF(.NOT.CASE1) GO TO 23
      NBEG=NST-1
      NEND=NECAS1
C     LSTPA IS SET TRUE FOR SMOOTH INCR. OF NAG NODE COUNT
C     (IF NO STEP CHANGE FROM 1 TO 86) & VICE VERSA
      LSTEPA=NBEG.LT.NEND
      GO TO 30
C     CASE 2
23    IF(.NOT.CASE2) GO TO 24
      NBEG=NST
      NEND=NSTF+5
C     LSTPA FOR CASE2 SIMILAR TO CASE 1
      LSTEPA=NBEG.GT.NEND
      GO TO 30
C     CASE 3 IS NOW LEFT
24    NBEG=NBCAS3
      NEND=NSTF-1
30    CONTINUE
C     NPT ETC. ARE CALCULATED
C     NUMBER OF NAG NODES FOR POLHAUSEN B LAYER INTEGR.
      IF(CASE1.OR.CASE3) NPT=NEND-NBEG+1
      IF(CASE2) NPT=NBEG-NEND+1
      IF(CASE3) GO TO 4260
      IF(LSTEPA) GO TO 4230
C     NPT IS MODIFIED TO ACC FOR STEP IN NAG NODE AT 1&86
      NPT=NPT+86
4230  CONTINUE
      IF(IN.EQ.1.OR.IN.EQ.86)LSTEPA=.FALSE.
C     LSTEPA MADE FALSE TO GET "IN" FOR XNODE CALCULATION
C     SEE SECTION GO TO 300 -..... 300 CONTINUE
4260  CONTINUE
      NPTM1=NPT-1
      NPTM2=NPT-2
      NPTM3=NPT-3
      IF(.NOT.CASE3) GO TO 40
      VNT(NPT)=PHID(NEND)
```

```
C       XNT VECTOR
40      SUM=-(DELN+DELNO2)
        DO 26 IT=1,NPT
        SUM=SUM+DELN
26      XNT(IT)=SUM
        IF(CASE2) GO TO 27
C       NOW CASE 1 IS CONSIDERED
C       ISTEP DEPENDS ON THE FLOW DIRECTION
C       SET VALUES OF VNT(IT) IT=2,NPTM1
        ISTEP=1
        NBEG1=NBEG-1
        DO 31 IT=2,NPTM1
        I=NBEG1+IT
        IN=I
        IF(I.GT.86)IN=I-86
31      VNT(IT)=PHID(IN)
        GO TO 155
C       ONLY CASES 2  LEFT
27      NBEG1=NBEG+1
C       "IN" CALCULATION ISTEP=-1 FOR CASE 2
        ISTEP=-1
        DO 32 IT=2,NPTM1
        I=NBEG1-IT
        IF(I.LE.0) I=I+86
32      VNT(IT)=-PHID(I)
155     IF(CASE3) GO TO 42
C       VNT(1) FOR CASES 1&2 FROM PARABOLA THRU VNT(2)&(3)
C       THIS IS TO FORCE V=0. AT X=0. FOR CASES 1&2
        VNT(1)=-2.*VNT(2)+VNT(3)/3.
C       FOR CASE 1&2 INTERPOLATION
        VNT(NPT)=3.*(VNT(NPTM1)-VNT(NPTM2))+VNT(NPTM3)
        GO TO 156
C       ONLY CASES 3 LEFT
42      VNT(1)=3.*(VNT(2)-VNT(3))+VNT(4)
C       TEMP COND FOR THE WRITING OF STAGNATION POINTS
156     CONTINUE
        WRITE(9,801)NPT,NST
        WRITE(9,802)(VNT(IT),IT=1,NPT)
        WRITE (4,815)(VNT(IT),IT=1,NPT)
326     WRITE (4,860) NPT
860     FORMAT(' NPT',I10)
        WRITE(4,815) (XNT(I),VNT(I),I=1,NPT)
320     KK=0
        IF(VNT(2)-VNT(1))201,202,203
C       INITIAL EXTREME LOCATED
202     KK=KK+1
        VNTP=VNT(2)
        VNTPM=VNT(1)
        VNTPP=VNT(3)
        XEXT(KK)=F(VNTP)+XNT(I-1)
C       DECIDE WHETHER MAX OR MIN TO BE FOUNDED
        IF(VNT(2).LT.VNT(3)) GO TO 203
C       MIN TO BE FOUND
```

```
201     IP=1
        GO TO 209
C       MAX TO BE FOUND
203     IP=2
209     VNTP=VNT(2)
        DO 205 I=3,NPT
        GO TO (206,207),IP
206     IF(VNT(I).LT.VNTP) GO TO 205
        IP=2
        GO TO 208
207     IF(VNT(I).GT.VNTP) GO TO 205
        IP=1
208     KK=KK+1
        VNTPM=VNT(I-2)
        VNTPP=VNT(I)
        XEXT(KK)=F(VNTP)+XNT(I-1)
205     VNTP=VNT(I)
C       SET VALUE OF XLAST FOR ALL CASES
        XLAST=XNT(NPT)-DELNO2
        IF(KK.GT.0) GO TO 210
        KK=1
        XEXT(1)=XLAST
        XEXT(2)=XLAST
210     WRITE(4,850)(XEXT(I),I=1,KK)
C       INITIALISATION FOR B.LAYER INTEGRATION
        IN=NBEG
        IT=2
        XNODE=XNT(2)
        LNODE=.FALSE.
        X=0.
        KK=1
        IQ=1
        XCHK=XEXT(KK)
C       INITIAL COND FOR STAGN CASES 1 & 2 (1 OR 2 TRUE)
        IF(STAGTN) GO TO 72
C       INITIAL CONDITIONS FOR LEADING EDGE CASES 3
C       NOTE VN EQUAL TO ZERO AT X=0.
        XT=X
        CALL INTRO2
        BT=0.
        DELB=0.
        BET=0.
        GO TO 775
C       SG-SA INTEG. IS START. WITH STAGNATION POINT CONDT.
72      CALL STGIC2
        XT=X
        V=0.
        CFX=CFXI
        LDA=LDAI
        DVX=DVXI
        CF=CFI
        ZT=CF
        GO TO 1
```

```
5       IC=1
        CALL DERCFX
        GO TO (1,425),IQ
425     IQ=1
        GO TO 5
1       CONTINUE
        BK=CF*DVX
        BKP=BK
        LDAP=LDA
C       WRITING ONLY AT NODAL POINTS
        IF(X.LT.XNODE) GO TO 300
        IT=IT+1
        IN=IN+ISTEP
        IF(CASE3) GO TO 4250
        IF(LSTEPA) GO TO 4250
        IF(IN.LE.0) IN=IN+86
        IF(IN.GT.86) IN=IN-86
4250    CONTINUE
        XNODE=XNT(IT)
        LNODE=.TRUE.
300     CONTINUE
C       CASE 3 IS TURBULENT B L
        IF(CASE3) GO TO 770
        IF(CASE1) GO TO 51
C       TAU CALCULATION SUSPENDED UPTO X=XNT(2)=DEL/2
        IF(IT.EQ.2) GO TO 101
C       TAU IS NON-DIM ; TAU(DIMEN)/(RHO*W**2*0.5)
        TAU=R9*V*(2.+R6*LDA)*SQRT(DVX/LDA)
        IF(TAU.GT.0) GO TO 55
        XLAST=XT
        WRITE (4,820) XLAST
        WRITE (4,830) IN
        GO TO 225
C       IN CASE3 IN=INK, IN CASE2 IN=INL
55      IF(LNODE) GO TO 54
        GO TO 101
51      IF(LNODE) GO TO 52
        GO TO 101
52      TAU=R9*V*(2.+R6*LDA)*SQRT(DVX/LDA)
C       TAU(IN) TO BE USED WITH LIFT/DRAG PROG.
54      TAUN(IN)=TAU
        LNODE=.FALSE.
626     FORMAT('X LDA TAU V BL.THICKNESS'/1H ,5E13.6)
        DELB=SQRT(LDA/DVX)
        WRITE(4,626) X,LDA,TAU,V,DELB
101     D1=H*CFX
        XT=X+HO2
        ZT=CF+0.5*D1
        IC=2
        CALL DERCFX
        GO TO (426,427),IQ
427     IQ=1
        GO TO 5
```

```
426     D2=H*CFX
        ZT=CF+0.5*D2
        IC=3
        CALL DERCFX
        GO TO (428,429),IQ
429     IQ=1
        GO TO 5
428     D3=H*CFX
        XT=X+H
        ZT=CF+D3
        IC=4
        CALL DERCFX
        GO TO (430,431),IQ
431     IQ=1
        GO TO 5
430     D4=H*CFX
        ZT=CF+(D1+2.*(D2+D3)+D4)*R6
        X=XT
        CF=ZT
3334    IF(X.GT.XLAST) GO TO 225
        GO TO 5
C       TURBULENT BOUNDARY LAYER INTEGRATION
770     CONTINUE
        DBX=(SAT1*BT*DVX+SBRE*V**0.75)/V
775     IC=1
        GO TO 776
771     CONTINUE
        IF(CASE3) GO TO 117
        IF(LDA.LE.-12.) GO TO 7720
117     IF(X.EQ.0.) GO TO 7720
C       WRITE AT NODAL POINTS FIND INK INL THE SEP. POINTS
        IF(X.LT.XNODE) GO TO 7300
        IT=IT+1
        IN=IN+ISTEP
        IF(CASE3)  GO TO 7250
        IF(LSTEPA) GO TO 7250
        IF(IN.LE.0) IN=IN+86
        IF(IN.GT.86) IN=IN-86
7250    CONTINUE
        XNODE=XNT(IT)
        LNODE=.TRUE.
7300    CONTINUE
        IF(CASE1) GO TO 751
        TAU=TAUC*V**1.75/BET**0.2
        IF(TAU.GT.0.) GO TO 755
        XLAST=XT
        WRITE(4,820) XLAST
        WRITE(4,830) IN
        GO TO 225
C       IN WRITTING ABOVE IS INK FOR CASE3 & INL FOR CASE2
755     IF(LNODE) GO TO 754
        GO TO 7101
751     IF(LNODE) GO TO 752
```

```
      GO TO 7101
752   TAU=TAUC*V**1.75/BET**0.2
C     TAUN(IN) TO BE USED IN THE LIFT PROG.
754   TAUN(IN)=TAU
      LNODE=.FALSE.
      DELB=BET**0.8
      WRITE(4,8000)X,BET,TAU,V,DELB
7720  CONTINUE
7101  D1=H*DBX
      BT=BET+0.5*D1
      XT=X+HO2
      IC=2
      GO TO 776
772   D2=H*DBX
      BT=BET+0.5*D2
      IC=3
      GO TO 776
773   D3=H*DBX
      BT=BET+D3
      XT=X+H
      IC=4
      GO TO 776
774   D4=DBX*H
      BT=BET+(D1+2.*(D2+D3)+D4)*R6
      BET=BT
      X=XT
      IF(X.GT.XLAST) GO TO 225
      GO TO 775
776   GO TO (472,471,472,471) IC
471   CALL INTRO2
472   CONTINUE
      GO TO (771,772,773,774) IC
225   STOP
      END
      SUBROUTINE STGIC2
      REAL LDA,LDAX,LDAI,LDAP
      COMMON/A/ XNT(42),VNT(42),PHID(92),TAUN(92),XEXT(10)
      COMMON/B/ X,XT,LDA,YT,LDAX,V,DVX,D2VX,NPT,NPTM1,XCHK
      COMMON/C/ H,HO2,DELN,DELNO2,RDN2,RDNS,R6,R1,R2,R8,R9
      COMMON/D/ SA0,SA1,SA2,SA3,SB0,SB1,SB2,SC1,SD0,SD1,SD2
      COMMON/E/ SE0,SE1,SF0,CF,CFI,CFX,CFXI,SD,TD,LDAI,DVXI
      COMMON/F/ SQ0,SA4,SA,SB,SC,R240,DBKP,D2BKP,Q,D2VXI,KK
      COMMON/G/ VSGA,RE,IC,ZT,BKP,SB3,LDAP,IQ
      EQUIVALENCE(SQD3,SA3),(SZ2,SF0),(SZD2,SD2)
801   FORMAT (18H DV/DX IS NAGETIVE)
C     NUM. OF NODAL POINTS ON EACH SIDE=10
      D2VXI=(VNT(1)+VNT(3)-2.*VNT(2))/DELN**2
C     NOTE DVXI SHOULD BE POSSITIVE
      DVXI=(VNT(2)-VNT(1))/DELN
      IF(DVXI.GT.0.) GO TO 50
C     DIAGNOSTIC REPORT TO GIVE ATT. TO DVXI(-)
      WRITE(4,801)
      DVXI=0.1
```

```
50      CONTINUE
C       POHLHAUSENS METHOD FOR STAG. CONDITION
        LDAI=7.052
        Q=SA-LDAI*(SB+SC*LDAI)
        CFI=(LDAI*Q**2)/DVXI
        CFXI=-0.0652*(D2VXI/DVXI**2)
        RETURN
        END
C       SUBROUTINE FOR INTERPOLATION
        SUBROUTINE INTRO2
        COMMON/A/ XNT(42),VNT(42),PHID(92),TAUN(92),XEXT(10)
        COMMON/B/ X,XT,LDA,YT,LDAX,V,DVX,D2VX,NPT,NPTM1,XCHK
        COMMON/C/ H,HO2,DELN,DELNO2,RDN2,RDNS,R6,R1,R2,R8,R9
        COMMON/D/ SA0,SA1,SA2,SA3,SB0,SB1,SB2,SC1,SD0,SD1,SD2
        COMMON/E/ SE0,SE1,SF0,CF,CFI,CFX,CFXI,SD,TD,LDAI,DVXI
        COMMON/F/ SQ0,SA4,SA,SB,SC,R240,DBKP,D2BKP,Q,D2VXI,KK
        COMMON/G/ VSGA,RE,IC,ZT,BKP,SB3,LDAP,IQ
        REAL  LDA,LDAX,LDAI,LDAP
C       LOCATE THE NEAREST NODAL POINT
        M2=NPT
        DO 89 I=2,NPTM1
        IF(XNT(I).LE.XT) GO TO 89
        M2=I
        GO TO 90
89      CONTINUE
90      IF((XNT(M2)-XT).GT.DELNO2) M2=M2-1
        DELINT=XT-XNT(M2)
C       3-P METHOD WITH LOCATED (.) NEAR TO MIDDLE OF 3-P
        M1=M2-1
        M3=M2+1
        VN1=VNT(M1)
        VN2=VNT(M2)
        VN3=VNT(M3)
        SAX=(VN3-VN1)*RDN2
        SBX=(VN1+VN3-2.*VN2)*RDNS
        V=VN2+DELINT*(SAX+DELINT*SBX)
        DVX=SAX+DELINT*2.*SBX
        RETURN
        END
C       SUBROUTINE FOR THE CALCULATION OF LAMDA ,CR
        SUBROUTINE DERCFX
        COMMON/A/ XNT(42),VNT(42),PHID(92),TAUN(92),XEXT(10)
        COMMON/B/ X,XT,LDA,YT,LDAX,V,DVX,D2VX,NPT,NPTM1,XCHK
        COMMON/C/ H,HO2,DELN,DELNO2,RDN2,RDNS,R6,R1,R2,R8,R9
        COMMON/D/ SA0,SA1,SA2,SA3,SB0,SB1,SB2,SC1,SD0,SD1,SD2
        COMMON/E/ SE0,SE1,SF0,CF,CFI,CFX,CFXI,SD,TD,LDAI,DVXI
        COMMON/F/ SQ0,SA4,SA,SB,SC,R240,DBKP,D2BKP,Q,D2VXI,KK
        COMMON/G/ VSGA,RE,IC,ZT,BKP,SB3,LDAP,IQ
        REAL LDA,LDAP,LDAI,LDAX
C       USES XT FROM COMMON TO EVALUATE V, DVX AT XT
C       INTERPOLATION FOR LDA AT XT FOR GIVEN ZT
        GO TO (2,1,2,1),IC
1       CALL INTRO2
```

```
2       CONTINUE
        BK=ZT*DVX
        DELK=BK-BKP
        GO TO (31,30,31,31),IC
30      DBKP=SA0+LDAP*(SA1+LDAP*(SA2+LDAP*(SA3+LDAP*SA4)))
        D2BKP=SB0+LDAP*(SB1+LDAP*(SB2+LDAP*SB3))
31      TR1=DELK/DBKP
        TR2=D2BKP/DBKP
        LDA=LDAP+TR1*(1.-0.5*TR1*TR2)
        IF(LDA.LT.-17.75) STOP
        IF(LDA.GT.12.) STOP
        IF(LDA*DVX.GE.0) GO TO 36
C       NOTE LDA & DVX HAVE ALWAYS SAME ALGEBRIC SIGN
C       HENCE AT EXTREMUM DVX CHANGES SIGN MAKING LDA & DVX
C       NEG. / TO REDIRECT B.L INTEG. BEYOND EXTREMUM
        X=XEXT(KK)
        XT=X
        LDA=0.
        BK=0.
        LDAP=0.
        BKP=0.
        DBKP=SA0
        D2BKP=SB0
C       USE INTRO2 FOR GETTING V NOTE DVX=0 SINCE X=XEXT
        CALL INTRO2
        DVX=0.
C       INTEGRATION ABONDONED AND IQ=2 SET FOR RESTARTING
        IQ=2
        KK=KK+1
        XCHK=XEXT(KK)
        RETURN
860     FORMAT(' DIAG LDA CF DVX CFX XCHK '/1H ,5E13.6)
C       EVALUATION OF DZX AT XT AND ZT
36      Q=SA-LDA*(SB+LDA*SC)
        CFX=4.*Q*(1.-LDA*(Q-(LDA-16.)*R240))/V
        RETURN
        END
```

```
      PROGRAM CLCDT
      DIMENSION NB(10),NE(10),XNN(86),YNN(86),PHIDM(86)
      DIMENSION DXNDXC(10),DYNDXC(10),YLX(86),YDX(86)
      DIMENSION YLY(86),NEVAL(8),YVAL(86,4),TAUN(86)
      DIMENSION SUMS(4),Z2(4),Z4(4),Z1S(86),YDY(86)
      COMMON/A/ SLX,SLY,SDX,SDY
      COMMON YLX,YLY,YDX,YDY
      EQUIVALENCE (YLX,YVAL)
      EQUIVALENCE (SLX,SUMS)
      READ(3,900) DELN,DELNJ
      READ(3,900) CMU,SHOL
      READ (7,920) (XNN(I),YNN(I),PHIDM(I),I=1,86)
C     READ NAG COORD AND VELOCITY AT B.L. EDGE AFTER
C     ACC FOR CIRCULATION PHIDM VALUES FROM PROG STTUR1
C     NOTE GAMA (+) VE FOR CLOCK WISE DIRECTION
C     NEVAL VALUES FROM THE PROG. STTUR1
      READ(7,929)(NEVAL(I),I=1,8)
C     READING TAUN FROM STTUR1 PROG AFTER RUN CASES123
      READ(7,931)(TAUN(I),I=1,86)
929   FORMAT(1X, 8I3)
931   FORMAT(1X, E13.6)
900   FORMAT (2E13.6)
920   FORMAT (1X ,3E13.6)
930   FORMAT (E13.6)
800   FORMAT ('       CL             CD      '/1H ,2E13.6)
810   FORMAT(1H , 4E13.6)
      PI=3.141593
      SL2R=SIN(PI/8.)
      SM=1./7.
      VMAX=(8./7.)*SQRT(CMU/(SHOL*SIN(PI/8.)))
C     NEVAL(1) TO NEVAL(8) GIVE NAG NODES AT ENDS OF SIDES
C     JA, IJ, HI, (FG), DE, BC, IN ORDER
      NB(1)=1
      NE(10)=86
      DO 299 IN=1,86
      DO 299 IV=1,8
      IF(IN.NE.NEVAL(IV)) GO TO 299
      IVS=IV
      NE(1)=IN
      GO TO 399
299   CONTINUE
399   IV=IVS
      DO 499 IS=2,10
      NB(IS)=NCOR86(NE(IS-1)+1)
C     IV=1 CORRESPONDS TO SIDE JA HENCE LOCATE NOZZLE
      IF(IV.EQ.1) GO TO 599
      NE(IS)=NCOR86(NB(IS)+9)
      GO TO 499
599   NE(IS)=NCOR86(NB(IS)+5)
      IV=8
C     ISS IS SIDE NUMBER FOR SIDE BC OF OCTAGON
      ISS=IS+1
      GO TO 799
```

```
499     IV=IV-1
799     IVLST=IVS
        DO 899 IS=ISS,10
        NB(IS)=NCOR86(NE(IS-1)+1)
        IF(IV.EQ.IVLST) GO TO 999
        IV=IV-1
        IF(IS.EQ.10) GO TO 899
        NE(IS)=NCOR86(NB(IS)+9)
899     CONTINUE
999     CONTINUE
C       SLOPES DXN/DX AND DYN/DX FOR SEGMENTS
C       NOTE SEGMENT NO INCREMENTS CLOCK-WISE DIRECTION
        KSP=1
        DO 2 I=1,10
        JB=NB(I)
        JE=NE(I)
C       CHECK FOR ONE NODE ONLY FOR SIDES 1 & 10
        IF(I.EQ.1) GOTO 171
        IF(I.EQ.10) GO TO 173
171     IF(JB.NE.JE) GO TO 174
        KSP=2
        GO TO 2
173     IF(JB.NE.JE) GO TO 174
        KSP=3
        GO TO 2
174     DELX=(XNN(JE)-XNN(JB))
        DELY=(YNN(JE)-YNN(JB))
        DXC=SQRT(DELX**2+DELY**2)
        DXNDXC(I)=DELX/DXC
        DYNDXC(I)=DELY/DXC
2       CONTINUE
C       DETERMINE THE SLOPE 1&10 FOR SINGLE NODE CASE
        IF(KSP.EQ.1) GO TO 176
        IF(KSP.NE.2) GO TO 175
        DXNDXC(1)=DXNDXC(10)
        DYNDXC(1)=DYNDXC(10)
175     DXNDXC(10)=DXNDXC(1)
        DYNDXC(10)=DYNDXC(1)
176     CONTINUE
        WRITE(4,803) DXNDXC,DYNDXC
803     FORMAT(' DXNDXC, DYNDXC'/1H ,5E11.3)
C       MODIFIED PHID FOR JET TO ACC FOR NORMAL VEL COMP.
        KBEG=NEVAL(1)+1
        KEND=KBEG+5
        XABN=XNN(KEND)-XNN(KBEG)
        DXAB=XABN/5.
        XAB=ABS(XABN+DXAB)
        XNM=(XNN(KBEG+2)+XNN(KBEG+3))*0.5
        DO 60 I=KBEG,KEND
        T=ABS(XNN(I)-XNM)
        SX=XAB*0.5-T
        ARG=2.*SX/XAB
        V=ARG**SM*VMAX
```

```
      PHIDM(I)=SQRT(PHIDM(I)**2+V**2)
60    CONTINUE
C     CALCULATION OF NON-DIM. PRES. BY BERNOULLI EQ.
      DO 100 I=1,86
100   Z1S(I)=1.-PHIDM(I)**2
      WRITE(4,802) Z1S
802   FORMAT(1H ,7E10.2)
801   FORMAT(1H ,6E10.2/1H ,8(5E10.2))
      DO 10 IS=1,10
      CDXN=DXNDXC(IS)
      CDYN=DYNDXC(IS)
      JB=NB(IS)
      JE=NE(IS)
      DO 1000 IN=JB,JE
      Z1=Z1S(IN)
      ALSN=TAUN(IN)
      IF(PHIDM(IN).LT.0.)ALSN=-ALSN
      YDX(IN)=ALSN*CDXN
      YDY(IN)=ALSN*CDYN
      YLX(IN)=Z1*CDYN
1000  YLY(IN)=Z1*CDXN
10    CONTINUE
      JFOUR=4
C     CHECK SECTION STARTS HERE
      JFOUR=1
      XT=0.
      DO 37 IS=1,10
      JB=NB(IS)
      JE=NE(IS)
      DO 38 IN=JB,JE
      IF(IS.EQ.(ISS-1)) GO TO 40
      XT=XT+DELN
      GO TO 38
40    XT=XT+DELNJ
      YLX(IN)=XT**3
38    CONTINUE
37    CONTINUE
3700  CONTINUE
      DO 91 IS=1,10
      JB=NB(IS)
      JE=NE(IS)
C     FOR SIDES HAVING 2 OR 1 NODES TRAP. RULE FO INTG.
      IF((JE-JB).LE.1) GO TO 92
      JL1=JB
      JL2=JB+1
      JL3=JB+2
      JR1=JE
      JR2=JE-1
      JR3=JE-2
C     END AREAS FROM PARABOLIC FIT EQUATION
C     NOTE MULTIPLICATION WITH "H" IS REQUIRED
      DO 51 J=1,JFOUR
      SUMS(J)=34.*(YVAL(JL1,J)+YVAL(JR1,J)-14.*(YVAL
     *(JL2,J)+YVAL(JR2,J))+4.*(YVAL(JL3,J)+YVAL(JR3,J)))
```

```
51      CONTINUE
        NSTRIP=(JE-JB)
        NO2=NSTRIP/2
        IF(2*NO2.EQ.NSTRIP) GO TO 95
C       NSTRIP IS ODD NOW
C       USE 3/8 SIMPSONS RULE FOR FIRST THREE STRIPS
        J0=JB
        J1=JB+1
        J2=JB+2
        J3=JB+3
        DO 52 J=1,JFOUR
        SUMS(J)=SUMS(J)+0.375*(YVAL(J0,J)+3.*(YVAL(J1,J)
       *+YVAL(J2,J))+YVAL(J3,J))
52      CONTINUE
        NSTRIP=NSTRIP-3
        JB=J3
95      IF(NSTRIP.EQ.0) GO TO 14
C       1/3 SIMPSONS RULE FOR EVEN STR. NODES JB TO JE
C       JB IS MOD IF 3/8 RULE IS ALREADY USED FOR ODD STRIPS
        J4ST=JB+1
        J4EN=JE-1
        DO 53 J=1,JFOUR
        Z4(J)=0.
        DO 25 IN=J4ST,J4EN
25      Z4(J)=Z4(J)+YVAL(IN,J)
53      CONTINUE
        IF(J4ST.EQ.J4EN) GO TO 15
C       THERE ARE TWO STRIPES ONLY
C       NOW THERE ARE FOUR OR MORE STRIPES
        J2ST=JB+2
        J2EN=JE-2
        DO 54 J=1,JFOUR
        Z2(J)=0.
        DO 26 IN=J2ST,J2EN
26      Z2(J)=Z2(J)+YVAL(IN,J)
        SUMS(J)=SUMS(J)+2.*Z2(J)
54      CONTINUE
15      CONTINUE
        DO 55 J=1,JFOUR
        SUMS(J)=SUMS(J)+4.*Z4(J)
55      CONTINUE
14      CONTINUE
        DO 56 J=1,JFOUR
        IF(IS.EQ.(ISS-1)) GO TO 30
        SUMS(J)=SUMS(J)*DELN
        GO TO 91
30      SUMS(J)=SUMS(J)*DELNJ
56      CONTINUE
92      CONTINUE
        DO 58 J=1,JFOUR
        IF(IS.EQ.1) SUMS(J)=0.
        DO 58 IN=JB,JE
        SUMS(J)=SUMS(J)+DELN*YVAL(IN,J)
```

```
58      CONTINUE
91      CONTINUE
C       NOTE ISS IS NO FOR BC
C       DELNJ IS REARRANGED FOR JET, IS=ISS-1
C       DELET THE NEXT WRITE CHECK
        WRITE(8,810)SUMS(1)
        SLX=SLX*SL2R
        SLY=-SLY*SL2R
        SDX=SDX*SL2R
        SDY=SDY*SL2R
        CL=SLY+SDY
        CD=SLX+SDX
        WRITE (4,800) CL,CD
5000    STOP
        END
        FUNCTION NCOR86(NT)
        IF(NT.GT.86) NT=NT-86
        NCOR86=NT
        RETURN
        END
```

```
      PROGRAM POWERG1
      LOGICAL ROT,END
      DIMENSION  PDOMF(13),PDGF(13)
      DIMENSION FST(13),PIDST(13),PBDST(13),PMUDST(13)
      DIMENSION LXST(13),LYST(13),DXST(13),DYST(13)
      DIMENSION PDST(13),PDOMST(13),BETST(13)
      DIMENSION PDF(13),CMUS(13),SCL(13),CDS(13),UMS(13)
900   FORMAT(5E15.0)
800   FORMAT('    RR        VM        THETC       RSBOM     '
     */1H ,4E13.6)
801   FORMAT(' E*          PERCENT JET POWER '/1H ,2E15.8)
810   FORMAT('    BETA(DEG)      CMU            CL          CD
     *   NON DIM REL VEL' )
802   FORMAT(1H ,5E15.6)
815   FORMAT('    BETA(DEG)     CL          CD        NON  DIM
     *REL VEL')
803   FORMAT(1H ,4E15.6)
816   FORMAT('     F      P*(I)       P*(B)      P*(MU)   ')
805   FORMAT(1H ,4E15.6)
891   FORMAT('   BETA(DEG)      PD         PDOM' )
890   FORMAT(1H  ,3E15.6)
820   FORMAT ('     LXST      LYST      DXST      DYST     ')
821   FORMAT (1H ,4E13.6)
804   FORMAT('    RR   VM  THETAC  SBSR  VJM'/1H ,5E13.6)
901   FORMAT(2L1)
      REAL LX,LY,MUZ,MAD
      READ(1,901) ROT
      NS=0
      NST=1
      PI=3.141592
      IF(ROT) GOTO75
      READ(1,900) RR,VM,THETC,SBSR,VJM
150   NS=0
      NST=1
      VJM=VJM+0.25
      WRITE(6,804) RR,VM,THETC,SBSR,VJM
      CON2=0.5*SBSR*VJM**2
      CON5=0.5*VJM**3*SBSR
      GOTO76
75    READ(1,900)RR,VM,THETC,RSBOM
      WRITE(6,800) RR,VM,THETC,RSBOM
      CON1=2.*PI*RR*RSBOM*VM
      VMRR=VM*RR
76    CONTINUE
      PIO6=30.
      BETAA=(180.-THETC)/2.
      BETAB=BETAA+THETC
      BETAC=BETAA+180.
      BETAD=BETAC+THETC
      BETAINC=3.0
      K=1
      SUM=0.
      SUMG=0.
```

```
      SUMJ=0.
      BETA=0.
      DO 200 N=1,121
      IF(BETA.GT.BETAA)GO TO 10
      AR=-1.
      GO TO 50
10    IF(BETA.GT.BETAB)GO TO 20
      AR=2.*(BETA-BETAA)/THETC-1.
      GO TO 50
20    IF(BETA.GT.BETAC)GO TO 30
      AR=1.
      GO TO 50
30    IF(BETA.GT.BETAD)GO TO 40
      AR=1.-2.*(BETA-BETAC)/THETC
      GO TO 50
40    AR=-1.
50    BETAR=BETA*PI/180.
      IF(AR.GE.0.) GO TO 130
      ABAR=-AR
      SIGN=-1.
      GO TO 131
130   ABAR=AR
      SIGN=1.
131   CONTINUE
      VX=-VM*SIN(BETAR)
      VY=VM*COS(BETAR)
      UX=1.-VX
      UY=-VY
      UM=SQRT(UX**2+UY**2)
      IF(.NOT.ROT)GO TO 60
      OMR=RSBOM*ABAR
      MAD=VM*RR*OMR/UM
      IF(MAD.GT.0.8) GO TO 51
      CL=0.
      GO TO 53
51    IF(MAD.GT.4.) GO TO 52
      CL=4.2*MAD-3.77
      GO TO 53
52    CL=13.
53    CONTINUE
      IF(MAD.GT.2.5) GO TO 54
      CD=0.8
      GO TO 57
54    IF(MAD.GT.4.75) GO TO 55
      CD=1.64*MAD-3.31
      GO TO 57
55    CD=4.5
57    CONTINUE
      LX=CL*UY*SIGN
      LY=-CL*UX*SIGN
      DX=CD*UY*SIGN
      DY=-CD*UX*SIGN
      IF(RSBOM.NE.0) GO TO 70
```

```
      PDOM=0
      GO TO 70
60    CMU=CON2*(AR/UM)**2
      CL=20.*CMU
      IF(CL.GT.8.) CL=8.
      CD=(16.*CMU+9.7)/13.3
      IF(CMU.NE.0.) GOTO66
      LX=0.
      LY=0.
      GOTO67
66    CLS=CL/CMU
      MUZ=-CMU
      IF(BETA.LE.90.)GO TO 65
      IF(BETA.GT.270.)GO TO 65
67    MUZ=CMU
65    CON3=UM*CLS*MUZ
      LX=CON3*UY
      LY=-CON3*UX
      PDOM=CON5*ABAR**3
70    CONTINUE
      DX=CD*UM*UX
      DY=CD*UM*UY
      FX=LX+DX
      FY=LY+DY
      IF(.NOT.ROT) GO TO 78
      F=SQRT(FX**2+FY**2)
      CON4=RR*VM
      PID=5.*(RSBOM*CON4)**3/RSBOM
      PBD=0.8*CON4*OMR*(0.02856*F+0.0225)
      PMUD=0.00737*(CON4*OMR)**2.8
      PDOM=PID+PBD+PMUD
      CONTINUE
78    PD=FX*VX+FY*VY-PDOM
C     PDG=GROSS POWER PRODUCED
      PDG=FX*VX+FY*VY
      IF(N.LT.NST)GO TO 80
      NST=NST+10
      NS=NS+1
      BETST(NS)=BETA
      UMS(NS)=UM
      IF(.NOT.ROT)CMUS(NS)=CMU
      CDS(NS)=CD
      SCL(NS)=CL
      PDST(NS)=PD
      PDOMST(NS)=PDOM
      LXST(NS)=LX
      LYST(NS)=LY
      DXST(NS)=DX
      DYST(NS)=DY
      GO TO 80
      PIDST(NS)=PID
      PBDST(NS)=PBD
      PMUDST(NS)=PMUD
```

```
80      PDF(K)=PD
        PDGF(K)=PDG
        PDOMF(K)=PDOM
        K=K+1
        IF(K.LE.3)GO TO 200
        K=2
        SUMJ=SUMJ+(PDOMF(1)+4.*PDOMF(2)+PDOMF(3))
        PDOMF(1)=PDOMF(3)
        SUMG=SUMG+(PDGF(1)+4.*PDGF(2)+PDGF(3))
        PDGF(1)=PDGF(3)
        SUM=SUM+(PDF(1)+4.*PDF(2)+PDF(3))
        PDF(1)=PDF(3)
200     BETA=BETA+BETAINC
        E=SUM/360.
        EG=SUMG/360.
C       PERCENT JET POWER
        E1=SUMJ/(3.6*EG)
        WRITE(6,801) E,E1
        IF(ROT)GO TO 300
        WRITE(6,810)
        WRITE(6,802)(BETST(I),CMUS(I),SCL(I),CDS(I)
       *,UMS(I), I=1,NS)
        GO TO 400
300     WRITE(6,815)
        WRITE(6,803)(BETST(I),SCL(I),CDS(I),UMS(I), I=1,NS)
        WRITE(6,816)
        WRITE(6,805)(PIDST(I),PBDST(I),PMUDST(I),I=1,NS)
        WRITE(6,820)
        WRITE (6,821)(LXST(I),LYST(I),DXST(I),DYST(I),I=1,NS)
400     CONTINUE
        WRITE(6,891)
        WRITE(6,890)(BETST(I),PDST(I),PDOMST(I),I=1,NS)
        READ (1,901) END
        IF(.NOT.END) GO TO 150
        STOP
        END
```

```
      PROGRAM GRID1
      DIMENSION XST(80,26),YST(80,26),PHIST(80,26)
      DIMENSION PMINS(80),PMAXS(80),XG(240),YG(240),NGRS(20)
      DIMENSION SRS(26),KGT(160),PHICST(20),KM(80),IVECS(20)
      COMMON/BX/XG,YG,KGT,IG,NGR
      LOGICAL LHIGH,LMOD
      READ(9,8800) ICOUNT,KST
      IF(KST.EQ.0) GO TO 1234
      READ(18,8810) (IVECS(I),I=1,KST)
1234  CONTINUE
8800  FORMAT(3X,2I2)
8810  FORMAT(1X,5I5)
      LTI=0
      READ (3,900)((XST(I,J),YST(I,J),PHIST(I,J)
     *,I=1,80),J=1,26)
      READ (3,902) NPHIC,LMOD
      READ (3,901) (PHICST(I),I=1,NPHIC)
      READ(3,915)(SRS(J),J=1,26),BH,DB
915   FORMAT(1X,2E13.6)
C     FIND MAX & MIN OF PHI ON ANY RADIAL NORMAL LINE
C     MODIFICATION FOR CIRCULATION
      IF(.NOT.LMOD) GO TO 61
      READ(3,901)GAMA
      PI=3.1418
      ROL=0.5/SIN(PI/8.)
      C1= GAMA/(4.*PI)
      C2=-GAMA/(2.*PI)*ALOG(ROL)
      DO 60 J=1,26
      SRS1=SRS(J)**2
      DO 60 I=1,80
      PHIMOD=C1*ALOG(SRS1)+C2
60    PHIST(I,J)=PHIST(I,J)+PHIMOD
61    CONTINUE
      DO 1 I=1,80
      PMIN=PHIST(I,1)
      PMAX=PMIN
      DO 2 J=2,26
      IF(KST.EQ.0) GO TO 255
      IVEC=(J-1)*80+I
      DO 326 KI=1,KST
      IF(IVECS(KI).NE.IVEC) GO TO 326
      GO TO 2
326   CONTINUE
255   CONTINUE
      PHIT=PHIST(I,J)
      IF(PHIT.GE.PMIN) GO TO 2
      PMIN=PHIT
2     CONTINUE
      PMINS(I)=PMIN
      DO 3 J=2,26
      IF(KST.EQ.0) GO TO 355
      IVEC=(J-1)*80+I
      DO 426 KI=1,KST
```

```
      IF(IVECS(KI).NE.IVEC) GO TO 426
      GO TO 3
426   CONTINUE
355   CONTINUE
      PHIT=PHIST(I,J)
      IF(PHIT.LE.PMAX) GO TO 3
      PMAX=PHIT
3     CONTINUE
      PMAXS(I)=PMAX
1     CONTINUE
      DO 10 IPHI=1,NPHIC
      PHIC=PHICST(IPHI)
      KN=0
      KSUM=0
      NGR=1
      IS=1
      KNS=1
      B=BH-DB
      DO 15 I=1,80
      B=B+DB
      IF(PHIC.LT.PMINS(I)) GO TO 15
      IF(PHIC.GT.PMAXS(I)) GO TO 15
      K=0
      KN=KN+1
      IF((I-IS).EQ.(KN-KNS)) GO TO 50
      IF(KSUM.EQ.0) GO TO 52
      NGR=NGR+1
      KSUM=0
      KN1=KN-1
      WRITE (4,850) PHIC
      WRITE (4,810)KN1,(KM(IX), IX=KNS,KN1)
      WRITE (4,805)IG
      WRITE (4,850) (XG(IX),YG(IX),IX=1,IG)
      CALL BRGRID
      WRITE (6,889)IG
      WRITE (6,888)(XG(IX),YG(IX),IX=1,IG)
52    IS=I
      KNS=KN
50    CONTINUE
      LHIGH=PHIST(I,1).GT.PHIC
      DO 20 J=2,26
      IF(KST.EQ.0) GO TO 455
      IVEC=(J-1)*80+I
      DO 526 KI=1,KST
      IF(IVECS(KI).NE.IVEC) GO TO 526
      GO TO 20
526   CONTINUE
455   CONTINUE
      IF(LHIGH) GO TO 21
      IF(PHIST(I,J).LT.PHIC) GO TO 20
      LHIGH=.TRUE.
      JH=J
      JL=J-1
```

```
      GO TO 22
21    IF(PHIST(I,J).GT.PHIC) GO TO 20
      LHIGH=.FALSE.
      JL=J
      JH=J-1
22    K=K+1
      IG=KSUM+K
C     KGT VALUES INDICATE BRANCH. OF MULT. INT. STR. LINES
      KGT(IG)=K
      IF(K.LE.3) GO TO 30
      WRITE(4,860)I,J
      KN=KN-1
      IG=IG-1
      GO TO 15
30    PHIL=PHIST(I,JL)
      PHIH=PHIST(I,JH)
      IF(LHIGH) GO TO 31
      JINT=JH
      JH=JL
      JL=JINT
      PHINT=PHIH
      PHIH=PHIL
      PHIL=PHINT
31    IF(PHIL.GT.-999.) GO TO 32
      JL=JL-1
      IF(JL.GE.1) GO TO 34
      JL=JH+1
      PHIL=PHIST(I,JL)
      GO TO 33
34    PHIL=PHIST(I,JL)
      GO TO 31
32    IF(PHIH.GT.-999.) GO TO 33
      JH=JH+1
      IF(JH.LE.26) GO TO 35
      JH=JL-1
      PHIH=PHIST(I,JH)
      GO TO 33
35    PHIH=PHIST(I,JH)
      GO TO 32
33    CONTINUE
      RATIO=(PHIC-PHIL)/(PHIH-PHIL)
      SRL=SRS(JL)
      SRH=SRS(JH)
      SR=SRL+RATIO*(SRH-SRL)
      XG(IG)=SR*COS(B)
      YG(IG)=SR*SIN(B)
20    CONTINUE
      KM(KN)=K
      KSUM=IG
15    CONTINUE
      WRITE (4,850) PHIC
      WRITE (4,810)KN,(KM(I),I=1,KN)
      WRITE (4,805) IG
```

```
      WRITE (4,850)(XG(I),YG(I),I=1,IG)
      CALL BRGRID
      WRITE(6,889) IG
      WRITE(6,888)(XG(I),YG(I),I=1,IG)
      NGRS(IPHI)=NGR
10    CONTINUE
      WRITE(4,815)(NGRS(I),I=1,NPHIC)
      WRITE(7,889)NPHIC
      WRITE(7,889)(NGRS(I),I=1,NPHIC)
      STOP
888   FORMAT(1H ,2E13.6)
889   FORMAT(1H ,10I5)
900   FORMAT(1X,3E15.4)
2655  FORMAT(1H ,3E15.4)
901   FORMAT(5F10.0)
902   FORMAT(I2,L1)
860   FORMAT(' MULTIPLE POSIT. DATA SPACE EXPECTED',2I10)
810   FORMAT(1H ,'KN,KM'/1H ,I10/(1H ,10I4))
850   FORMAT(1H ,2E13.6)
805   FORMAT(' NUNMBER OF POINTS ON A STREAM
     *LINE',I10/'X & Y DATA')
815   FORMAT(' NGR VALUES',/1H ,10I5)
      END
      SUBROUTINE BRGRID
      COMMON/BX/XG,YG,KGT,IG,NGR
      DIMENSION XG2(120),YG2(120),XG(240),YG(240),KGT(160)
889   FORMAT(1H ,10I5)
888   FORMAT(1H ,2E13.6)
      DO 70 IGT=1,IG
      IF(KGT(IGT).EQ.1) GO TO 70
      GO TO 71
70    CONTINUE
C     MULTIPLE BRANCHES ARE NOT PRESENT
      RETURN
C     MULTIPLE BRANCHES ARE PRESENT
C     GRAPHS ARE RE ORGERNISED
71    IG1=0
      IG2=0
      DO 74 IGT=1,IG
      IF(KGT(IGT).EQ.2) GO TO 75
      IG1=IG1+1
      XG(IG1)=XG(IGT)
      YG(IG1)=YG(IGT)
      GO TO 74
75    IG2=IG2+1
      XG2(IG2)=XG(IGT)
      YG2(IG2)=YG(IGT)
74    CONTINUE
      WRITE(6,889) IG2
      WRITE(6,888)(XG2(IX),YG2(IX),IX=1,IG2)
      NGR=NGR+1
      IG=IG1
      RETURN
      END
```

```
      PROGRAM PART2
      REAL M, M1,K1,K2
      INTEGER SG(10)
      DIMENSION DELXS(8),DELYS(8),NBEGS(8),NENDS(8)
      DIMENSION XS(10), YS(10), NEST(10)
      DIMENSION PHI(92), X(185), Y(185), PHID(92)
      COMMON XM(80),YM(80),XR(80),YR(80)
      DIMENSION XMM(42),YMM(42),XRR(42),YRR(42)
      EQUIVALENCE (XMM,XM(43)),(YMM,YM(43))
      EQUIVALENCE (XRR,XR(43)),(YRR,YR(43))
C     N=SEGMENTS REFER TO NAG NOTATION
C     SIDES(=10 FOR OCTAGON  WITH JET AND SUCTION)
C     SG(1) TO SG(10) SEGMENTS FOR EACH SIDE
C     N1P1=(2N+1) COORD POINTS ON CONTOUR REF TO NAG NOTAT
C     NODAL POINTS ARE MID -POINT OF SEGMENTS= N IN NUMBER
851   FORMAT(1H , 3E15.4)
900   FORMAT(5F13.6)
901   FORMAT(10I2)
800   FORMAT('   THETAD       SHOL       CMU'/1H ,3E13.6)
801   FORMAT('SG(1) SG(2) SG(3) SG(4) SG(5) SG(6) SG(7)
     *SG(8) SG(9),SG(10)'/1H ,10I4)
850   FORMAT(1H ,2E13.6)
      F(S)=-K1*K2*(S**M1)
      G(S)=-2*K1*K2*((SHOL/2.)**M1)+K1*K2*(S**M1)
      READ (3,900) DELNM
      READ(3,900) THETAD, SHOL, CMU
      READ(3,901) SG
C     WRITE(4,800)THETAD, SHOL, CMU
C     WRITE(4,801) SG
      PI=3.141593
      THETA=THETAD*PI/180.
      M=1./7.
      M1=M+1.
      I23=0
      K1=8./7.*SQRT(CMU/(SHOL*SIN(PI/8.)))
C     (R/SMALL L) IS R1
      R1=1./(2.*SIN(PI/8.))
C     NON-DIMENSIONALISED WRT SIDE OF OCTAGON(L)
      R1R2=0.5*R1*SQRT(2.)
      CT=COS(THETA)
      ST=SIN(THETA)
      K2=((2./SHOL)**M)/M1
C     COORDINATES OF A
      XS(1)=R1*CT
      YS(1)=R1*ST
C     CORDINATES OF B
      XS(2)=(R1-SHOL)*CT
      YS(2)=(R1-SHOL)*ST
C     COORDINATES OF C
      XS(3)=R1R2*(ST+CT)
      YS(3)=R1R2*(ST-CT)
C     CORDINATES OF D
      XS(4)=YS(1)
```

```
      YS(4)=-XS(1)
C     COORDINATES OF E
      XS(5)=YS(3)
      YS(5)=-XS(3)
C     COORDINATES OF F
      XS(6)=-XS(1)
      YS(6)=-YS(1)
C     COORDINATES OF G
      XS(7)=-XS(2)
      YS(7)=-YS(2)
C     COORDINATES OF H
      XS(8)=-XS(3)
      YS(8)=-YS(3)
C     COORDINATES OF I
      XS(9)=-XS(4)
      YS(9)=-YS(4)
C     COORDINATES OF J
      XS(10)=-XS(5)
      YS(10)=-YS(5)
      N=0
C     CALCULATE NO OF SEGMENTS =NODAL POINTS
      DO 1 I=1,10
1     N=N+SG(I)
C     CALCULATE M P FOR DO3EAF
      N1P1=2*N+1
      NE=0
C     SETS PHID VALUES=0 FOR DIRICH. INTER. PROB.
      DO 100 J=1,N
100   PHID(J)=0.
C     EVALUATE THE COORD. OF ALL THE POINTS USE DO L-10
      DO 10 I=1,10
      NB=NE+1
      NBP1=NB+1
C     NO OF INTERVALS IN THE SEGMENT (I)
      NIS=SG(I)
      NE=2*NIS+NB-1
      NEST(I)=NE
C     NE DENOTES END POINT -1.
      X(NB)=XS(I)
      Y(NB)=YS(I)
      IP1=I+1
      IF(IP1.EQ.11) IP1=1
C     DELX,DELY =0.5*DISTANCE BETWEEN NODAL POINTS
      DELX=0.5*(XS(IP1)-XS(I))/FLOAT(NIS)
      DELY=0.5*(YS(IP1)-YS(I))/FLOAT(NIS)
      IF(I.EQ.1.OR.I.EQ.6) GO TO 13
C     DELX DELY FOR OCTAGON SIDES ONLY, STORED (1-8)
      I23=I23+1
      DELXS(I23)=DELX
      DELYS(I23)=DELY
13    CONTINUE
      DO 11 J=NBP1,NE
      X(J)=X(J-1)+ DELX
```

```
11      Y(J)=Y(J-1)+ DELY
10      CONTINUE
C       THE CONTOUR IS COMPLETED BY REPEAT. START.
        X(N1P1)=X(1)
        Y(N1P1)=Y(1)
C       CALCULATION OF THE COORD. OF M
C       HERE ONLY OCTAGON SIDESS CONSIDERS FOR M POINTS
        IS=0
        DO 50 I=1,10
        IF(I.EQ.1.OR.I.EQ.6) GO TO 50
        IS=IS+1
        NBEGS(IS)=NEST(I-1)+2
        NENDS(IS)=NEST(I)
50      CONTINUE
        NS=0
        DO 15 I=1,8
        DELX=DELXS(I)
        DELY=DELYS(I)
        DELN=2.*SQRT(DELX**2+DELY**2)
        RATIO=2.*DELNM/DELN
        DELMX=RATIO*DELY
        DELMY=RATIO*DELX
         NBEG=NBEGS(I)
        NEND=NENDS(I)
        DO 16 J=NBEG,NEND,2
        XJ=X(J)
        YJ=Y(J)
        NS=NS+1
        XM(NS)=XJ-DELMX
16      YM(NS)=YJ+DELMY
15      CONTINUE
C       PROG. FOR FINDING PHI VALUES FOR NODAL POINTS
C       NBD= THE POINT CORRRESPONDS MID POINT OF SEG.1
        NBD=1+SG(1)
        J=0
        DO 25 I=2,N1P1,2
        J=J+1
        IF(I.GT.NBD) GO TO 35
        S=SQRT((XS(1)-X(I))**2+(YS(1)-Y(I))**2)
        PHI(J)=F(S)
        GO TO 25
35      IF(I.GT.NEST(1)) GO TO 37
        S=SQRT((XS(2)-X(I))**2+(YS(2)-Y(I))**2)
        PHI(J)=G(S)
        IF(I.NE.NEST(1)) GO TO 25
        PHIB=-2.*K1*K2*((SHOL/2.)**M1)
        GO TO 25
37      IF(I.GT.NEST(5)) GO TO 38
        PHI(J)=PHIB
        GO TO 25
C       PHI IS MADE CONSTANT =PHIB UP TO POINT F
        PHI(J)=PHIB*(XS(7)-X(I))/(XS(7)-XS(6))
        GO TO 25
```

```
39      PHI(J)=0.
25      CONTINUE
        IX=12
        DO 444 I=7,N
        IX=IX+2
        IF(I.GT.46.AND.I.LT.53) GO TO 444
444     CONTINUE
        FIRST TWO WRITE STATEMENTS ARE FOR CHECKING ONLY
        WRITE(4,850)(X(J),Y(J),J=14,92,2)
        WRITE(4,850)(X(J),Y(J),J=106,184,2)
        WRITE(7,850)(XM(I),YM(I),I=1,80)
        WRITE(4,851)(X(J),Y(J),PHI(J),J=14,92,2)
        WRITE(4,851)(X(J),Y(J),PHI(J),J=106,184,2)
        WRITE(4,850)(DELXS(I),DELYS(I),I=1,8)
        WRITE (9,850)(XS(I),YS(I),I=1,10)
        WRITE (4,850)(X(J),Y(J),J=1,N1P1)
        WRITE (8,850)(PHI(J),PHID(J),J=1,N)
        WRITE(6,850)(X(JT),Y(JT),JT=2,N1P1,2)
        END
```

```
      PROGRAM PART3
      INTEGER SG(4)
      DIMENSION XS(4), YS(4), NEST(4)
      DIMENSION PHI(24),PHID(24),X(49),Y(49)
850   FORMAT (1H ,2E13.6)
900   FORMAT (5F13.6)
950   FORMAT (4I2)
      READ(3,900) D
      READ(3,950) SG
C     COORDINATES OF K
      XS(1)=D
      YS(1)=D
C     COORDINATES OF R
      XS(2)=-D
      YS(2)=D
C     COORDINATES OF P
      XS(3)=-D
      YS(3)=-D
C     COORDINATES OF M
      XS(4)=D
      YS(4)=-D
      N=0
C     CALCULATE NO OF SEG.=NOD POINTS
      DO 1 I=1,4
1     N=N+SG(I)
C     CALCULATE M POINT FOR NAG ROUT.
      N1P1=2*N+1
C     SETS PHID VALUES =0 FOR INT. DIRCH. PROBLEM
      DO 100 J=1,N
100   PHID(J)=0.
C     CALCULATE THE COORDINATES OF ALL POINTS DO L-10
      NE=0
      DO 10 I=1,4
      NB=NE+1
      NBP1=NB+1
C     NO OF INTERVALES IN THE SECTION(I)
      NIS=SG(I)
      NE=2.*NIS+NB-1.
      NEST(I)=NE
C     NE DENOTES THE END POINT -1.
      X(NB)=XS(I)
      Y(NB)=YS(I)
      IP1=I+1
      IF(IP1.EQ.5) IP1=1
      DELX=0.5*(XS(IP1)-XS(I))/FLOAT(NIS)
      DELY=0.5*(YS(IP1)-YS(I))/FLOAT(NIS)
      DO 11 J=NBP1,NE
      X(J)=X(J-1)+DELX
11    Y(J)=Y(J-1)+DELY
10    CONTINUE
C     CONTOUR IS COMPLETED BY REPEATING START POINT
      X(N1P1)=X(1)
      Y(N1P1)=Y(1)
```

```
C       FINDING PHI VALUES FOR NODAL POINTS
        J=0
        DO 25 I=2,N1P1,2
        J=J+1
C       SECTION K-R HAS A CONST STREAM FUNCTION
        IF(I.GT.NEST(1)) GO TO 35
        PHI(J)=D
        GO TO 25
C       AT THE ENTRANCE FLOW IS UNIFORM
35      IF(I.GT.NEST(2)) GO TO 37
        PHI(J)=Y(I)
        GO TO 25
C       SECTION P-M HAS A CONST STREAM FUNCTION
37      IF(I.GT.NEST(3)) GO TO 39
        PHI(J)=-D
        GO TO 25
C       AT THE EXIT THE FLOW IS UNIFORM
39      PHI(J)=Y(I)
25      CONTINUE
        WRITE (4,850)(X(J),Y(J),J=1,N1P1)
        WRITE (4,850)(X(1),Y(1))
        WRITE (6,850)(PHI(J),PHID(J),J=1,N)
        STOP
        END
```

```
      PROGRAM CPMAX
      REAL KS(20),K,KMXVAL
      DIMENSION YS(20,20), XLS(20,20),XHS(20,20),ELS(20,20)
      DIMENSION EL1S(20), ELMS(20),KMXVAL(20),EHS(20,20)
      DIMENSION YMOXMS(20), Y1OX1S(20), YMINS(20), YLMS(20)
C     EL, EH ARE EFFICIENCIES FOR LOW AND HIGH LEGS
C     ELM IS EFFICIENCY MAXIMUM OF LOWER LEG
C     EL1 IS EFFICIENCY FOR Y=1
C     YMOXM IS (Y/X) FOR MAX EFFICIENCY POSS. OF LOWER LEG
C     Y1OX1 IS Y/X FOR LOWER LEG WHEN Y=1
C     Y IS V'/V(INFINITY) =(A INFT/A')
C     X IS V (M)/V(INFT) = (A INFT/A (M))
      LOGICAL LSIGN
      PHI(YD) = 4.*BET*YD**3-(ALF*YD-1.)**2
      DATA ER/0.000001/
C     IKM -NUMBER OF K VALUES MAX =20
C     INPUT REQUIRED IS K VALUES
C     K MUST BE IN THE RANGE OF 0 TO1 1
C     K=0 CORRESPOND TO THE TRADITIONAL BETZ'S LIMIT
      READ (7,900) IKM
      READ (7,901)(KS(I),I=1,IKM)
900   FORMAT (I2)
901   FORMAT (5F10.0)
      KMAX=0
      IK=1
100   K=KS(IK)
      ALF=(4.-K)/(2.-K)
      BET=K/(2.-K)
      WRITE (6,800)K,ALF,BET
800   FORMAT(' K,ALF,BET',3E15.8)
C     DETERMINE Y MIN VALUES
      YTR=0.5
      IF(KS(IK).EQ.0.) GO TO 25
      DY=0.1
      PHI1=PHI(YTR)
      LSIGN=PHI1.GT.0.
20    YTR=YTR+DY
      IF(ABS(DY).LT.ER) GO TO 25
      PHI2=PHI(YTR)
      IF(LSIGN) GO TO 10
      IF(PHI2) 20,25,30
30    LSIGN=.NOT.LSIGN
      DY=-0.5*DY
      GO TO 20
10    IF(PHI2) 35,25,20
35    DY=-0.5*DY
      LSIGN=.NOT.LSIGN
      GO TO 20
25    CONTINUE
      YMIN=YTR+(ER)
      WRITE(6,8010)YMIN
8010  FORMAT(' YMIN',E15.8)
C     DECIDE DY STEP, INITIALY
```

```
      DY=(1.-YMIN)/19.
      Y=YMIN
      DO 150 I=1,20
C     DETERMINE XL,XH
      XT=(ALF*Y-1.)
      DISC=SQRT(XT**2-4.*BET*Y**3)
      XH=(XT+DISC)*0.5
      XL=(XT-DISC)*0.5
      EH=Y*(1.-XL**2)
      EL=Y*(1.-XH**2)
C     NOTE I=20  CORRESPOND TO Y=1
      YS(I,IK)=Y
      XHS(I,IK)=XH
      XLS(I,IK)=XL
      EHS(I,IK)=EH
      ELS(I,IK)=EL
150   Y=Y+DY
C     LOCATE THE ELMAX POSITION
      ELMX=ELS(20,IK)
      DO 50 I=2,20
      IB=21-I
      IF(ELS(IB,IK).GT.ELMX) GO TO 52
      GO TO 55
52    ELMX=ELS(IB,IK)
50    CONTINUE
      GO TO 85
55    IF(IB.LT.19) GO TO 70
85    WRITE(6,8050)K
8050  FORMAT(' THIS K HAS NO EL MAX',E15.8)
      GO TO 75
C     LOCATE MAX POSITION
70    IB1=IB+1
      IB2=IB+2
      KMAX=KMAX+1
      EL0=ELS(IB,IK)
      EL1=ELS(IB1,IK)
      EL2=ELS(IB2,IK)
      Y0=YS(IB,IK)
      Y1=YS(IB1,IK)
      Y2=YS(IB2,IK)
      C=(EL2+EL0-2.*EL1)/(2.*DY**2)
      B=(EL1-EL0)/DY-C*(Y1+Y0)
      A=EL0-B*Y0-C*Y0**2
      YLMS(KMAX)=-B/(2.*C)
      ELMS(KMAX)=A+B*YLMS(KMAX)+C*YLMS(KMAX)**2
      KMXVAL(KMAX)=KS(IK)
C     DETERMINE XMAX CORRES. TO YMAX=YLMS(KMAX)
      YMAX=YLMS(KMAX)
      XT=ALF*YMAX-1.
      DISC=SQRT(XT**2-4.*BET*YMAX**3)
      XMAX=(XT-DISC)*0.5
      YMOXMS(KMAX)=YMAX/XMAX
75    CONTINUE
      EL1S(IK)=ELS(20,IK)
```

```
      YMINS(IK)=YMIN
      Y1OX1S(IK)=1./XLS(20,IK)
      IK=IK+1
      IF(IK.LE.IKM) GO TO 100
      DO 301 IK=1,IKM
      WRITE(6,831)KS(IK)
831   FORMAT(' K VALUE-GRAPH1 EL VS Y',1H ,E15.8)
      WRITE(6,851)(ELS(IG,IK),YS(IG,IK),IG=1,20)
851   FORMAT(1H ,2E15.8)
301   CONTINUE
C     WRITING FOR GRAPH 2
      DO 302 IK=1,IKM
      WRITE(6,832) KS(IK)
832   FORMAT(' KVALUE-GRAPH 2 EH VS Y',1H ,E15.8)
      WRITE(6,851)(EHS(IG,IK),YS(IG,IK),IG=1,20)
302   CONTINUE
C     WRITING FOR GRAPH 3
      DO 303 IK=1,IKM
      WRITE(6,833)KS(IK)
833   FORMAT(' K VALUES -GRAPH 3 XL VS Y',1H ,E15.8)
      WRITE(6,851)(XLS(IG,IK),YS(IG,IK),IG=1,20)
303   CONTINUE
C     WRITING FOR GRAPH 4
      DO 304 IK=1,IKM
      WRITE(6,834)KS(IK)
834   FORMAT(' K VALUES -GRAPH 4 XH VS Y',1H ,E15.8)
      WRITE(6,851)(XHS(IG,IK),YS(IG,IK),IG=1,20)
304   CONTINUE
C     WRITING FOR GRAPH 5
      WRITE(6,835)
835   FORMAT(' GRAPH-5 EL(Y=1)VS K')
      WRITE(6,851)(EL1S(IK),KS(IK),IK=1,IKM)
C     WRITING FOR GRAPH 6
      WRITE(6,836)
836   FORMAT(' GRAPH-6 EL(MAX)VS K')
      WRITE(6,851)(ELMS(IK),KMXVAL(IK),IK=1,KMAX)
C     WRITING FOR THE GRAPH 7
      WRITE(6,837)
837   FORMAT(' GRAPH-7 Y(MAX)/X(MAX) VS K')
      WRITE(6,851)(YMOXMS(IK),KMXVAL(IK),IK=1,KMAX)
C     WRITING FOR THE GRAPH 8
      WRITE(6,838)
838   FORMAT(' GRAPH-8 1/(X AT Y=1) VS K')
      WRITE(6,851)(Y1OX1S(IK),KS(IK),IK=1,IKM)
C     WRITING FORTHE GRAPH 9
      WRITE(6,839)
839   FORMAT(' GRAPH-9 Y MIN VS K')
      WRITE(6,851)(YMINS(IK),KS(IK),IK=1,IKM)
C     WRITING FOR THE GRAPH-10
      WRITE(6,840)
840   FORMAT(' GRAPH-10 Y(AT EL MAX) VS K')
      WRITE(6,851)(YLMS(IK),KMXVAL(IK),IK=1,KMAX)
      STOP
      END
```